

bradscholars

Raman spectroscopic application for the analysis of organic compounds and minerals of astrobiological significance. The detection and discrimination of organic compounds and mineral analogues in pure and mixed samples of astrobiological significance using raman spectroscopy, XRD and scanning electron microscopy

| | |
|---------------|---|
| Item Type | Thesis |
| Authors | Alajtal, Adel I. |
| Rights | The University of Bradford theses are licenced under a Creative Commons Licence. |
| Download date | 2026-03-09 17:44:09 |
| Link to Item | http://hdl.handle.net/10454/4425 |



University of Bradford eThesis

This thesis is hosted in [Bradford Scholars](#) – The University of Bradford Open Access repository. Visit the repository for full metadata or to contact the repository team



© University of Bradford. This work is licenced for reuse under a [Creative Commons Licence](#).

**Raman Spectroscopic Application for the Analysis of Organic
Compounds and Minerals of Astrobiological Significance**

**The detection and discrimination of organic compounds and mineral
analogues in pure and mixed samples of astrobiological significance
using Raman spectroscopy, XRD and scanning electron microscopy**

ADEL IMHEMED ALAJTAL

BSc, MSc

A Thesis submitted to the University of Bradford for the Degree of Doctor of
Philosophy

**Division of Chemical and Forensic Sciences
School of Life Sciences
University of Bradford
Bradford
UK**

2010

Abstract

Raman spectroscopy has been used to characterise both organic and geological samples in order to build a database for the future characterization of biomarker molecules that are of astrobiological relevance.

Characteristic geological features and hydrated minerals recently found on the surface of Mars by the NASA planetary rovers Spirit and Opportunity suggest that a possible biosphere could have once existed there. Analytical instrumentation protocols for the unequivocal detection of biomarkers in suitable geological matrices are critical for future unmanned explorations, including the forthcoming ESA ExoMars mission scheduled for 2018.

Several geological features found on the surface of Mars by planetary rovers suggest that a possible extinct biosphere could exist based on similar sources of energy as occurred on Earth. For this reason, analytical instrumental protocols for the detection of isolated biomarkers preserved in suitable geological matrices unequivocally and non-destructively have to be evaluated for future unmanned missions. Raman spectroscopy is currently part of the Pasteur instrumentation suite of the ExoMars mission for the remote detection of extant or extinct life signatures in the Martian surface and subsurface. Terrestrial analogues of Martian sites have been identified and the biogeological modifications resulting from extremophilic survival activity have been studied.

Here we present the Raman spectral characterization of several examples of organic compounds which have been recorded using 785 nm, 633 nm and 514 nm laser excitation -polycyclic aromatic hydrocarbons (PAHs), organic acids, chlorophyll and carotenoids. Experimental mixtures of β -carotene in usnic acid, PAHs in usnic acid and PAHs in mineral matrices have also been investigated. Organic compounds and PAHs located under crystalline minerals samples were identified using a 5x objective lens and 785 nm

excitation. The pure compounds and compound mixtures were also analysed using X-ray powder diffraction and scanning electron microscopy (SEM).

The results of this study indicate that near infrared laser at 785 nm provided the clearest and the most informative spectra due to the reduction of fluorescence emission. Higher energy lasers operating in the visible region have resulted in the emission of significant background fluorescence. Few samples fluoresce even with the use of 785 nm excitation and FT-Raman spectroscopy remains the instrument of choice for the analysis of these samples.

Key words: Raman spectroscopy; Mars analogues; Minerals; PAHs, organic compounds, astrobiology

List of sections of this work have been published or reported in the following forms:

Papers:

* A.I. Alajtal, H.G.M. Edwards, M.A. Elbagerma and I.J. Scowen, The effect of laser wavelength on the Raman Spectra of phenanthrene, chrysene, and tetracene: Implications for extra-terrestrial detection of polyaromatic hydrocarbons, *Spectrochimica Acta Part A*, **2010**, 76, 1–5

* A. I. Alajtal, H. G. M. Edwards and I. J. Scowen, Raman spectroscopic analysis of minerals and organic molecules of relevance to astrobiology, *Analytical and Bioanalytical Chemistry*, **2010**, 397,215–221

* A. I. Alajtal, H. G. M. Edwards and I. J. Scowen, The effect of spectral resolution on the Raman spectra of polyaromatic hydrocarbons and beta-carotene mixtures, *journal of Raman spectroscopy*, **2010**, doi: 10.1002/jrs.2681, Accepted for publication: 16 March 2010

* A. I. Alajtal, H. G. M. Edwards and I. J. Scowen, Raman spectroscopic identification of beta-carotene in usnic acid and PAHs as a potential Martian analogue, *Vibrational spectroscopy*, **2010**, submitted for publication

* A. I. Alajtal, H. G. M. Edwards and I. J. Scowen, Identification of polyaromatic hydrocarbons and minerals of relevance to Mars, **2010**, submitted for publication

Conference poster presentations and abstracts:

1) Proceedings of the International Conference on Raman Spectroscopy (ICORS XXI) 17 – 22 August 2008, Uxbridge, West London.

* “Evaluation of simulants for the Raman spectroscopic characterisation of biomolecular degradation products in geological matrices: Polyaromatic Hydrocarbons (PAHs) under calcite and gypsum”

A.I.Alajtal, H.G.M.Edwards, M.D.Hargreaves and I.J.Scowen (abstract and poster 107)

2) Proceedings of the Euroanalysis XV, 6 – 10 September 2009, Innsbruck, Austria.

* “Raman spectroscopic analysis of minerals and PAHs of relevance to Astrobiology”

A.I.Alajtal, H.G.M.Edwards, and I.J.Scowen (abstract and poster: P 149-B2)

* “The Effect of Spectral Resolution on the Raman Spectra of Polyaromatic Hydrocarbons and Beta-Carotene Mixtures”

A.I.Alajtal, H.G.M.Edwards, and I.J.Scowen (abstract and poster: P 150-B2)

3) School of Life sciences Research open day, University of Bradford, 2 April 2009

* “Evaluation of simulates for the Raman spectroscopic characterisation of biomolecular degradation products in geological matrices: Polyaromatic Hydrocarbons (PAHs) under calcite and gypsum”

A.I.Alajtal, H.G.M.Edwards, M.D.Hargreaves and I.J.Scowen (abstract and poster: 6.1)

4) School of Life sciences Research open day, University of Bradford, 23 March 2010

* “Raman spectroscopic analysis of minerals and PAHs of relevance to Astrobiology”

A.I.Alajtal, H.G.M.Edwards, and I.J.Scowen (abstract and poster: 6.20)

Acknowledgement

Firstly, I am very grateful to my Lord Almighty ALLAH who helped me and guided me throughout my life and made it possible. I could never have done it by myself.

I would like to take this opportunity to thank my supervisors, Professor Howell Edwards and Dr Ian Scowen for their expert guidance, help and patience.

I am thankful to Dr Mike Hargreaves and Dr Tas Munshi for their help, and direction through this intricate subject matter.

Dennis Farwell and Stuart Fox are thanked for giving me their help in selecting relevant spectra for this project.

I would like also to thank my fellow doctoral students Mohamed, Esam, Kristian Page, Alex and Darren for their support and advice

Finally, my thanks to my family and friends in Libya for their great support and forgiveness for being absent when they need me. The best thanks goes to my wife and my (6) children Nowara, Emhemed, Abdulrhman, Abdulaziz, Kadeja and Noordeen for their unceasing support and encouragement with this project.

Table of Contents

| | |
|--|-------------|
| Abstract | II |
| List of sections of this work have been published | IV |
| Acknowledgement | VII |
| Table of Contents | VIII |
| CHAPTER 1 | 1 |
| Introduction | 1 |
| 1.1 Introduction | 2 |
| 1.2 Why PAHs, organic compounds and minerals? | 2 |
| 1.3 Aims and objectives | 3 |
| 1.4 Structure of the thesis | 4 |
| 1.5 References | 5 |
| CHAPTER 2 | 6 |
| Raman spectroscopy and X-ray diffraction | 6 |
| 2.1 Raman spectroscopy | 7 |
| 2.2 History of Raman spectroscopy | 7 |
| 2.3 Vibrational spectroscopy | 10 |
| 2.4 Molecular motion | 10 |
| 2.5 The theory of Raman spectroscopy | 11 |
| 2.6 Selection Rules for Raman spectroscopy | 15 |
| 2.7 Use of Raman Spectroscopy | 18 |
| 2.8 Raman intensity | 18 |
| 2.9 Comparison of infrared and Raman spectroscopy | 19 |
| 2.10 Advantages of Raman Spectroscopy | 19 |
| 2.11 Disadvantages of Raman Spectroscopy | 20 |
| 2.12 Charge-Coupled Device Detection | 21 |
| 2.13 Theory of X-ray powder diffraction | 21 |

| | |
|--|-----------|
| 2.14 References | 23 |
| CHAPTER 3 | 26 |
| Instrumentation | 26 |
| 3.0 Raman Instrumentation | 27 |
| 3.1 Dispersive Spectrometers | 27 |
| 3.1.1 Renishaw In Via Raman Microscope | 28 |
| 3.1.2 Renishaw Portable Raman RX210 analyser (RIAS) | 30 |
| 3.2 Non Dispersive FT-Spectrometers | 31 |
| 3.2.1 Fourier-transform (FT) Raman spectrometer | 31 |
| 3.3 X-ray powder diffractometry (XRD) | 33 |
| 3.4 Scanning Electron Microscopy | 34 |
| 3.5 Data processing | 34 |
| 3.5.1 Baseline correction | 35 |
| 3.5.2 Normalisation | 35 |
| 3.5.3 Smoothing | 35 |
| 3.5.4 Deconvolution | 35 |
| 3.5.5 Integration of peak area and width | 36 |
| 3.6 References | 36 |
| CHAPTER 4 | 38 |
| Astrobiology | 38 |
| 4.1 Introduction to astrobiology | 39 |
| 4.2 The origin and evolution of life | 40 |
| 4.3 Life outside the Earth | 41 |
| 4.4 Mars | 42 |
| 4.5 Extant Life | 45 |
| 4.6 Extinct Life | 45 |
| 4.7 Terrestrial analogues of Mars | 46 |

| | |
|--|-----------|
| 4.8 Protective Biomolecules | 47 |
| 4.8.1 Polyaromatic hydrocarbons | 47 |
| 4.8.2 Carotenoids | 52 |
| 4.8.3 Chlorophyll | 53 |
| 4.8.4 Scytonemin | 54 |
| 4.8.5 Usnic acid | 55 |
| 4.9 Minerals | 56 |
| 4.9.1 Quartz | 56 |
| 4.9.2 Carbonate (Calcite) | 56 |
| 4.9.3 Gypsum | 57 |
| 4.10 References | 57 |
| CHAPTER 5 | 62 |
| Effect of Raman spectrometer on the appearance of the Raman spectra | 62 |
| 5.0 Pure compound samples | 63 |
| 5.1 Renishaw Raman Spectrometer. | 63 |
| 5.2 RIAS Raman Spectrometer | 64 |
| 5.3 Bruker FT Spectrometer | 65 |
| 5.4 Influence of Raman Spectrometer on the Raman spectra produced | 67 |
| 5.5 Assignment of Raman spectra | 68 |
| 5.5.1 Naphthalene | 69 |
| 5.5.2 Anthracene | 70 |
| 5.5.3 Phenanthrene | 71 |
| 5.5.4 Tetracene | 73 |
| 5.5.5 Chrysene | 75 |
| 5.5.6 Triphenylene | 76 |
| 5.5.7 Pyrene | 77 |
| 5.5.8 Perylene | 79 |

| | |
|---|------------|
| 5.5.9 Beta-carotene | 80 |
| 5.5.10 Usnic acid | 81 |
| 5.5.11 Chlorophyll a | 83 |
| 5.6 Conclusions | 84 |
| 5.7 References | 84 |
| CHAPTER 6 | 87 |
| Evaluation of simulates for the Raman spectroscopic characterization of biomolecular degradation products in geological matrices: organic compounds under calcite and gypsum | 87 |
| 6.1 Introduction | 88 |
| 6.2 Experimental | 91 |
| 6.2.1 Compound Samples | 91 |
| 6.2.2 Compounds Mixture | 91 |
| 6.2.3 Dispersive Raman microscopy | 91 |
| 6.3 Result and Discussion | 94 |
| 6.3.1 Calcite and gypsum | 94 |
| 6.3.2 PAHs under calcite and gypsum crystalline | 96 |
| 6.3.3 PAH Mixtures | 100 |
| 6.3.4 PAH Mixtures under Calcite and Gypsum crystalline | 101 |
| 6.3.5 Usnic acid under calcite and gypsum crystalline | 102 |
| 6.4 Conclusion | 103 |
| 6.7 References | 103 |
| CHAPTER 7 | 105 |
| Identification of polyaromatic hydrocarbons and minerals of relevance to Mars using Raman spectroscopy and other techniques | 105 |
| 7.1 Introduction | 106 |
| 7.2 Experimental | 107 |
| 7.2.1 Materials | 107 |

| | |
|---|------------|
| 7.2.2 Raman spectroscopy | 107 |
| 7.2.2.1 FT Raman spectroscopy | 107 |
| 7.2.2.2 Dispersive Raman microscopy | 108 |
| 7.2.2.3 RIAS Raman Spectrometer | 108 |
| 7.2.3 Scanning Electron Microscopy (SEM) | 109 |
| 7.2.4 Powder X-Ray Diffraction | 110 |
| 7.3 Results and discussion | 110 |
| 7.3.1 Compound Mixtures | 110 |
| 7.3.1.1 Anthracene and matrices (calcite, gypsum and quartz) in 50-50 mixtures | 111 |
| 7.3.1.2 Pyrene and matrices (calcite, gypsum and quartz) in 50-50 mixtures | 117 |
| 7.3.1.3 Perylene and matrices (calcite, gypsum and quartz) in 50-50 mixtures | 123 |
| 7.4 Scanning Electron Microscopy (SEM) and Powder X-Ray Diffraction | 129 |
| 7.5 Conclusions | 136 |
| 7.6 References | 136 |
| CHAPTER8 Part 1 | 138 |
| The effect of spectral resolution on the Raman spectra of polyaromatic hydrocarbons and beta-carotene mixtures | 138 |
| 8.1.1 Introduction | 139 |
| 8.1.2 Experimental | 141 |
| 8.1.3 Results and discussion | 142 |
| 8.1.3.1 Beta-carotene | 142 |
| 8.1.3.2 Pyrene | 146 |
| 8.1.3.3 Anthracene | 146 |
| 8.1.3.4 Naphthalene | 149 |
| 8.1.3.5 Beta-carotene (5-95) pyrene mixture | 150 |
| 8.1.3.6 Beta-carotene (5-95) anthracene mixture | 153 |
| 8.1.3.7 Beta-carotene (5-95) naphthalene mixture | 155 |

| | |
|--|------------|
| 8.1.4 Conclusions | 157 |
| 8.1.5 References | 158 |
| CHAPTER 8 Part 2 | 161 |
| The Effect of Laser wavelength on The Raman spectra of Phenanthrene, chrysene and Tetracene: Implication for extra-Terrestrial detection of Polyaromatic hydrocarbons | 161 |
| 8.2.1 Introduction | 162 |
| 8.2.2. Experimental | 164 |
| 8.2.2.1. Materials | 164 |
| 8.2.2.2. X-ray powder diffractometry | 164 |
| 8.2.2.3 Raman spectroscopy | 164 |
| 8.2.2.3.1 1064 nm excitation | 164 |
| 8.2.2.3.2 785, 633 and 514 nm excitations | 165 |
| 8.2.3 Results and Discussion | 165 |
| 8.2.4 Conclusions | 167 |
| 8.2.5 References | 175 |
| CHEPTER 9 Part 1 | 177 |
| Raman spectroscopic analysis of minerals and organic molecules of relevance to astrobiology | 177 |
| 9.1 Introduction: | 178 |
| 9.1.2 Experimental | 179 |
| 9.1.2.1 Materials | 179 |
| 9.1.2.2 Raman spectroscopy | 180 |
| 9.1.3 Results and discussion | 180 |
| 9.1.3.1 Naphthalene in matrices | 180 |
| 9.1.3.2 Phenanthrene in matrices | 184 |
| 9.1.3.3 Triphenylene in matrices | 187 |
| 9.1.4 Conclusion | 189 |

| | |
|---|------------|
| 9.1.5 References | 190 |
| CHEPTER 9 Part 2 | 192 |
| Raman spectroscopic identification of beta-carotene in usnic acid and PAHs as a potential Martian analogue | 192 |
| 9.2.1 Introduction | 193 |
| 9.2.2 Experimental | 195 |
| 9.2.2.1 Materials | 195 |
| 9.2.2.2 Raman spectroscopy | 196 |
| 9.2.3 Results and discussion | 196 |
| 9.2.3.1 Calculations of I/ σ ratio | 196 |
| 9.2.3.2 Beta-carotene in organic acid and PAHs | 198 |
| 9.2.3.3 Beta-carotene in usnic acid | 199 |
| 9.2.3.4 Beta-carotene in phenanthrene | 201 |
| 9.2.3.5 Beta-carotene in triphenylene | 203 |
| 9.2.4 Conclusions | 204 |
| 9.2.5 References | 204 |
| CHAPTER10 | 207 |
| Conclusions and Further Work | 207 |
| 10.1 Conclusions | 208 |
| 10.2 Further Work | 210 |
| 10.3 References | 211 |
| CHAPTER 11 | 212 |
| Appendices | 212 |
| Appendix I: Structural formulae of molecules | 213 |
| Appendix II: Spectra of the pure compounds on all three instruments. | 216 |
| Appendix III: Diffraction patterns of the pure polyaromatic hydrocarbons | 222 |
| Appendix IV: SEM of the pure compounds | 226 |

CHAPTER 1

Introduction

1.1 Introduction

The Raman spectrometer is one of a number of instruments that will be deployed on Mars on future robotic landing missions. The goal of these missions will include characterizing the mineralogy of the rocks and soils, in addition to determining if the planet may be or may have been habitable for life. The astrobiology questions are linked to an understanding of the aqueous and biogeochemical history of Mars. Polyaromatic hydrocarbons, minerals and organic compounds are studied here because if they are found on Mars they may provide information about the geochemistry of the primary rocks and the aqueous history of the planet.

1.2 Why PAHs, organic compounds and minerals?

Polyaromatic hydrocarbons (PAHs), organic compounds and minerals have been found extraterrestrially and as a result they can act as probes of conditions in distant regions. These molecules have been detected in comet and asteroidal dust and are common in meteorites. It is believed that these molecules form in the outflows of dying carbon rich stars from which they are ejected into the space between the stars. These compounds are of importance for the search for life in the Solar System, because on Earth these molecules are used as biomarkers (i.e. chemicals that indicate life).

The analysis of polycyclic aromatic hydrocarbons (PAHs), organic compounds and minerals in terrestrial and extraterrestrial environments is particularly pertinent because of their resistance to oxidative and photochemical degradation [1]. Terrestrial PAHs are predominantly formed via the pyrolysis, dehydrogenation, and incomplete combustion of

biogenic material [1]. PAHs can also be produced via abiotic reactions, both in space and through planetary geological activity [1, 2]. PAHs have been found throughout the universe, specifically in carbonaceous chondrite meteorites [3], Martian meteorites, [4, 5] and interplanetary dust particles [6], and radioastronomers have observed PAHs in interstellar matter [2].

1.3 Aims and objectives

The aim of this study was to evaluate Raman spectroscopy as a viable technique for the analysis of PAHs and related materials alone and in admixture with key biological compounds and mineralogical environments relevant to inter-planetary science. From this aim, several key objectives for the project were identified.

- (1) To achieve spectral assignments for the Raman bands of organic minerals and to demonstrate the reliability of their spectral identification in admixture with one another.
- (2) The preparation and characterisation of controlled mixtures of organic and inorganic minerals in the solid state. Characterisation of these materials was undertaken with powder X-ray diffraction prior to study with Raman spectroscopy.
- (3) The evaluation of the influence of Raman experimental data collection parameters on the Raman spectra of PAHs, organic compounds, minerals and these materials in admixture; parameters varied included laser excitation wavelength and data collection parameters included exposure time and number of spectral accumulations.
- (4) To evaluate the importance of potential interfaces when organic minerals were measured in the context of an inorganic host matrix.

In this study several polyaromatic hydrocarbons (PAHs), minerals, and organic compounds alone and in admixture with minerals have been analysed using three different Raman spectrometers. Powder X-ray diffraction and scanning electron microscopy (SEM) were then used in conjunction with the Raman spectra to give support the conclusions that were obtained.

The results have important implications for the construction and evaluation of miniaturised Raman spectrometers for space flight missions and incorporation into instrumentation for landers and rovers being proposed for missions to Mars in the next two decades.

1.4 Structure of the thesis

This thesis has been structured in 10 Chapters. Chapter One provides the context and aims of this project. Chapters Two and Three introduce Raman spectroscopy and Raman instrumentation, respectively. Chapter Four gives a comprehensive review of astrobiology. Chapters Five to Nine present a comprehensive study of the Raman spectroscopy for the characterisation of selected compounds that are used in this study. Finally, Chapter 10 draws together the conclusion of this study and considers areas suitable for further study.

1.5 References

- [1] M. Zolotov, E .J. Shock, Geophys. Res, **1999**, 104,14033.
- [2] E. Herbst, Angew. Chem., Int. Ed. Engl, **1990**, 29,595.
- [3] M.A. Sephton, Nat. Prod. Rep, **2002**, 19, 292.
- [4] L.Becker, B.Popp, T.Rust, J.L.Bada, Earth Planet. Sci. Lett, **1999**, 167, 71.
- [5] D.S.McKay, E.K.Gibson, K.L.Thomas-Keptra, H.Vali, C.S.Romanek,
S.J.Clemett, X.D.F.Chillier, C.R.Maechling, R.N.Zare, Science,**1996**, 273, 924.
- [6] S.J. Clemett, C.R.Maechling, R.N. Zare, P.D. Swan, R.M. Walker, Science, **1993**,
262, 721.

CHAPTER 2

Raman spectroscopy and X-ray diffraction

2.1 Raman spectroscopy

Raman spectroscopy has become widespread in its applications because it is non-destructive and samples require little or no preparation. It is also rapid and provides both qualitative and quantitative data in physics and chemistry relevant to molecular vibration frequencies. The latter can be obtained from either Raman spectroscopy or Infrared (IR) spectroscopy. However, in a centrosymmetric molecule, the Rule of Mutual Exclusion states that in a molecule possessing a centre of symmetry no vibration can be both IR and Raman active [1]. While IR spectroscopy requires a molecule to have a permanent dipole moment or dipole change during the molecular vibration concerned, Raman spectroscopy makes no such requirement. Instead, it is the polarisability of the bond which is important. This means that Raman spectroscopy provides a means by which molecules or bonds which might be inactive, or only weakly absorbing in IR spectroscopy, can be analysed to obtain information which, otherwise, would be unavailable [1,2].

2.2 History of Raman spectroscopy

Although theoretically predicted at an earlier date (1923) by the Austrian quantum physicist A. Smekal, the phenomenon of inelastic scattered light was first observed and documented in 1928 by Sir C.V Raman [3]. He noted that when monochromatic light hits a material, the radiation which was scattered contained not only photons with an identical frequency to that of the incident radiation, but also a small percentage (approximately 0.0001%) with a slightly different frequency. This shifting of frequencies was to become known as the Raman effect and the radiation made up of the photons with these

frequencies as Raman radiation. In 1930, Sir C.V Raman won the Nobel prize in physics for his discovery of the Raman effect [3].

In the earliest experiments carried out by Raman and his co-worker Krishnan, filtered sunlight was used as a radiation source, but as their work and that of contemporaries continued, attention was directed to improving the radiation sources used. During the 1930s, the mercury lamp became the standard choice. Through use of appropriate glass filters and solutions it was possible to obtain effectively monochromatic radiation at 435.8 nm. The most successful example of such a source was a mercury lamp (Toronto arc) developed by Welsh et al,[4] but other types of sources were used, including annular electrodeless lamps powered by microwaves[1].

At this time Raman spectroscopy became the most popular form of non-destructive chemical analysis. The equipment used, although time consuming, was relatively simple, and those working on IR absorption spectroscopy often used the collection of extensive Raman data reference material which had been built up [1]. However, with later technical advances contemporary IR replaced Raman spectroscopy as the primary vibrational spectroscopic method. In general, IR spectroscopy was looked on as an easier and more accurate, method which could be used in a number of situations where Raman spectroscopy simply was not suitable. The calibration and alignment of a Raman system based on dispersive gratings simply was a very time-consuming method. The spectra were often ruined by the presence of a fluorescence background from the sample which swamped the Raman signal and made identification of the Raman bands difficult, if not impossible. Although the instrumentation required was still relatively simple, advances in IR spectroscopy had made the Raman technique far less attractive and interest in the previously popular method dwindled [1].

The invention of the laser in 1960 brought a renaissance to Raman spectroscopy [5]. A laser produces a beam of high-intensity coherent monochromatic radiation through the process of stimulated emission; the emission of a photon as an atomic electron falls in energy, causes the emission of another photon of the same frequency [5].

Laser illumination required a much smaller sample size than the Toronto arc, which was a great advantage and the capability to select a variety of wavelengths of radiation to use, was also very important. In some cases this selective capability enabled Raman spectroscopy to avoid, or at least minimise the problems with fluorescence and absorption which had been encountered hitherto so improving the quality of the results obtained.

Despite these advantages, however, the durability and reliability of lasers was questionable. It was not until some time later, around the mid-1980s, when Raman spectroscopy really became a popular vibrational spectroscopic method again. At this time, the use of a NIR (near IR) source of radiation created renewed interest in the technique.

A lower excitation energy would be of great help in reducing the amount of fluorescence observed, and therefore cleaning up the spectra obtained from the Raman instrument. It was also advantageous in that it allowed longer illumination times and spectral accumulation without causing decomposition of the sample and so a stronger signal could be obtained [3].

This new development led to resurgence in the popularity of Raman spectroscopy and renewed interest resulting in development of laser Fourier-Transform instruments which were first seen in 1986. More modern and advanced versions of these, combined with computers, continue to be used to the present day. A wide range of possible visible and near infrared laser wavelengths for dispersive instrument is available for Raman spectroscopy.

With these sensitive, modern instruments, a variety of different types of sample forms (e.g. powders, organic liquids and other solid materials), it is possible to perform analysis on very small amounts of material, covering an extensive range of frequencies in a limited time period. It is perhaps because of these practical aspects that the method today is so popular and is used extensively in many different areas of chemistry and physics as an analytical tool.

2.3 Vibrational spectroscopy

Raman and infrared spectroscopies are techniques that yield complementary information in order to characterize and identify the molecular structure of materials. These vibrational spectroscopic techniques, however, are governed by different selection rules [6]. An overview of the origins of both the Raman effect and infrared absorption will now be provided.

2.4 Molecular motion

Molecular motion consists of translations, rotations, vibrations and combinations of all three. In vibrational spectroscopy, pure rotations and translations are not relevant the reason for which is explained below.

To describe the exact position of a molecule in three-dimensional space, each atom is given an x, y and z co-ordinate. The motions of the atoms can then be described by changes in these co-ordinates. Therefore, if a molecule has n atoms, it will require 3n co-ordinates (degrees of freedom) to describe all the possible motions. Three of these degrees describe a translational motion that involves moving all the atoms simultaneously in the same direction, hence not altering any bond lengths. Another three involve rotations

around the principal axes of the molecule, again not changing any distances between the atoms (except for linear molecules, which only have two distinct rotations). The remaining degrees of freedom describe the molecular internal motions, which all involve vibration. Hence a non-linear molecule has $3n-6$ vibrational degrees of freedom and each linear molecule possesses $3n-5$, giving rise to the fundamental vibrations of the molecule [1, 7].

2.5 The theory of Raman spectroscopy

Electromagnetic radiation has been shown to have a dual nature, displaying both wave-like and particle properties. When looked on as waves, it is considered that electromagnetic radiation is made up of an electric and a magnetic field, which oscillate with time and distance, resulting in a fluctuation of the electric field strength of the wave. When interaction with matter is involved, the particle properties of the radiation can be considered as discrete packets of energy, called photons, which have an energy related to the frequency of the radiation by the relationship:

$$E = h \nu$$

Where, h = Planck's constant, and ν = frequency

When electromagnetic radiation is used to irradiate a molecule several possibilities can occur:

1. transmission;
2. absorption;

3. scattering.

The scattering of radiation can be further broken down into three types as shown in figure

2.1:

1. Rayleigh scattering
2. Anti -Stokes Raman scattering
3. Stokes Raman scattering

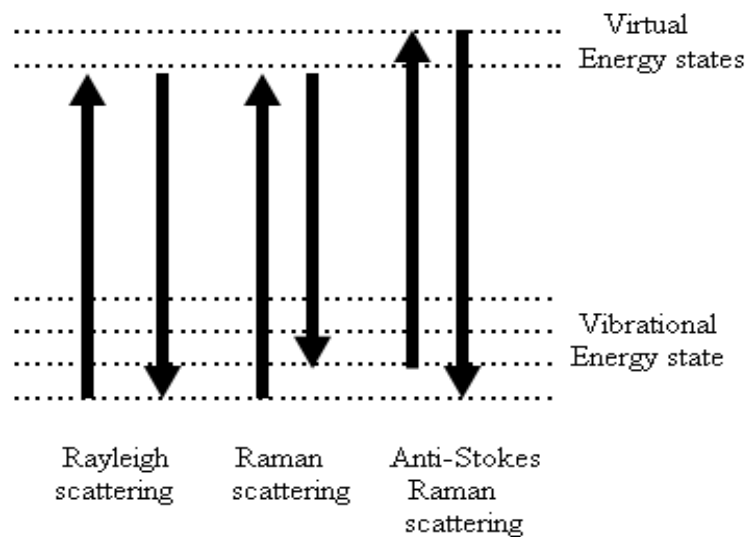


Figure 2.1 Diagram showing the excitation of a molecular vibration by Raman scattering

Rayleigh scattering involves the scattering of radiation, by particles and molecules respectively, with no change in wavelength of individual photons; this accounts for the vast majority of the scattered radiation. The second and third types of scattering in contrast, account for a relatively small amount of the scattered radiation observed. It is nonetheless very important analytically because there is a shift in frequency, and therefore

wavelength, corresponding to a change in motion of the molecule. This shift in frequency can be recorded and analysed.

While Rayleigh scattering is modelled as an elastic collision between molecule and incident photon, the Raman effect is conversely modelled as an inelastic collision between molecule and an incident photon. Some energy is removed from the incident photon by the molecule; resulting in a change in energy:

$$\Delta E = h \nu_i - h \nu_s$$

Where $h\nu_i$ = energy of the incident photon and $h\nu_s$ = energy of the scattered photon

It can be seen that ΔE can be either positive, or negative, depending on the relative values of $h\nu_i$ and $h\nu_s$, leading to a classification of two types of scattering within the Raman effect.

These are:

- a) Stokes, involving a gain in energy of the molecule and therefore a negative value of ΔE
- b) Anti-Stokes, involving a loss in energy of the molecule and therefore a positive value of ΔE

The second of these requires that a molecule is initially in an excited state before collision, and therefore under normal circumstances is far less likely to occur. Consequently, the former, Stokes scattering is more common.

ΔE is in fact equal to the change in rotational and/or vibrational energy of the target molecule; this is called the Raman shift and different functional groups give rise to different Raman shifts.

As mentioned above, the change in energy can be related to a change in wavelength using the wave equation:

$$\lambda = c / \nu$$

Where λ = wavelength, c = speed of light and ν = frequency

This allows a second expression for ΔE to be derived:

$$\Delta E = 1/\lambda_{\text{incident}} - 1/\lambda_{\text{scattered}} = \tilde{\nu}$$

Where $\lambda_{\text{incident}}$ wavelength of the incident radiation, $\lambda_{\text{scattered}}$ wavelength of the scattered radiation, and $\tilde{\nu}$ is the wavenumber

This expression introduces $\tilde{\nu}$, which is called the wavenumber, and has units of cm^{-1} . In general, Raman shifts are measured in these units, rather than the frequencies mentioned above.

While both rotational and vibrational Raman spectroscopy are possible, the energy source used to excite the molecule is generally selected to ensure that vibrational transitions take place within the molecule rather than rotational transitions. The main reason for this is that rotational transitions occur at smaller wavenumber shifts than their vibrational counterparts.

Whether or not a molecule will show Raman activity will depend on its polarisability. The electric field associated with the incident photons will produce an induced dipole within the molecule, leading to the relationship:

$$\mu = \alpha E$$

Where μ = induced dipole moment, α = polarisability and E = electric field strength.

In order to be Raman active, there must be a change in polarisability associated with the molecular vibration taking place; for a normal bond coordinate Q (bond length or bond angle) a change in polarisability, dx/dQ , is required for Raman scattering to be produced.

The Raman spectrometer provides a way to record the Raman scattering which takes place from a sample, recording the Raman intensity as a function of the Raman shift in reciprocal centimetres (wavenumber). The radiation source used is a laser, and the detector can be positioned orthogonally to the source to ensure that it only collects those photons which have been scattered at 90° to the incident laser beam. The detector output produced is in the form of an interferogram, which then undergoes Fourier transformation to produce the spectrum which is displayed on the computer and can be saved on disk and printed out for use. Computer programs can then be used to facilitate the precise labelling of the position of bands.

2.6 Selection Rules for Raman spectroscopy

Polarisability plays an important role in Raman spectroscopy; when the sample is placed in an electric field (a laser beam) its electron cloud suffers distortion. The ease with which an electron cloud can be distorted by an external electric field may be described by the term 'polarisability'.

Distortion results from the attraction of the positively charged nuclei towards the negative pole, and the electrons move towards the positive pole. This gives a charge separation

which produces an induced dipole moment. Due to its connection with the electrons, polarizability depends on how tightly the electrons are bound to the nuclei.

Quantum mechanics can be used to determine whether a vibration is infrared (IR) or Raman active by detecting what changes occur during the vibration. If the dipole moment is changed during the vibration then it is IR-active, whereas if the polarizability changes then the vibration is Raman-active [8]. If both change during a molecular vibration then the vibration is both Raman and IR active.

An example of Raman active and inactive vibrations is given by a molecule of carbon disulphide (CS_2). Carbon disulphide is a linear molecule that contains a centre of symmetry and no permanent dipole moment. Vibrational theory states that a linear molecule containing n atoms has $3n-5$ vibrational modes, therefore it would be expected that carbon disulphide has $3 \times 3 - 5 = 4$ modes [9]. (Figure 2.2)

The ν_2' vibration occurs in the plane of the paper and ν_2'' also occurs but in the plane at right angles to the paper. These two modes are indistinguishable in wavenumber and are considered as one vibration called 'doubly degenerate' (of the same energy). Sulphur has a higher electron density than carbon and hence a slightly higher negative charge. Therefore, in the vibrational modes ν_2 and ν_3 a change in dipole moment occurs. This is because during the vibration, the centres of positive and negative charge move and create a situation where the electrical centre of the molecule is displaced from the carbon atom. As this vibration involves a change in dipole moment it is seen to be infrared-active.

The ν_1 vibrational mode is a symmetric stretching mode and no change in dipole moment occurs. This is because the two negative centres move in equal distances in opposite directions from the positive centre (carbon atom). The electron cloud present around the molecule expands and contracts with nuclear motion; resulting in a change in polarizability, thus this vibration is Raman-active [6].

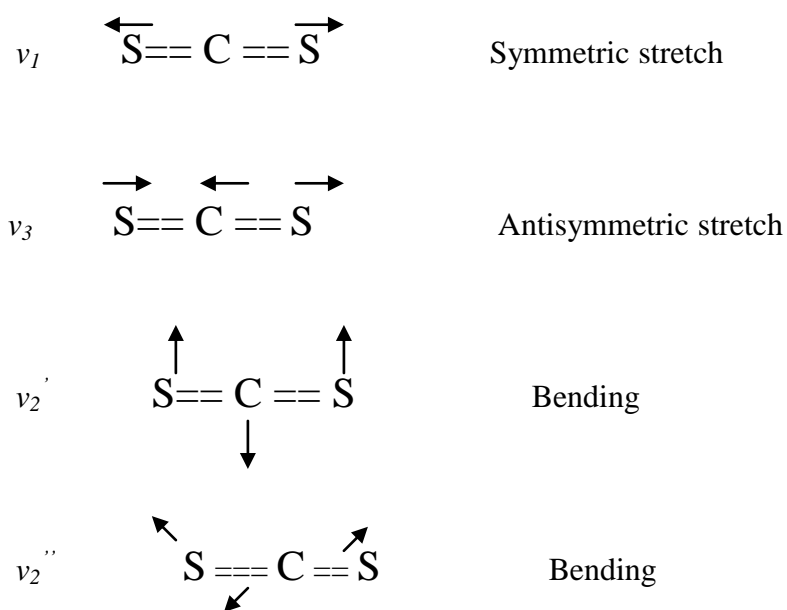


Figure 2.2 The vibrational modes of carbon disulphide [10]

The antisymmetric stretch contains two types of 'bond' in any given instant one of which compresses and the other expands. The electrons contained in the bond which expands are more easily polarized, whereas the electrons in the bond that is compressed are polarized less easily. Therefore there is no overall change in the polarizability and this asymmetric stretch is termed Raman-inactive [11].

Some vibrations may be active or inactive in both IR and Raman, this transpires from the fact that there are different selection rules for Raman scattering and IR absorption. Raman and infrared spectroscopy only yield partial descriptions of the internal vibrational motion of a molecule with respect to the normal vibrations of the constituent atoms. It is because of this fact that Raman and infrared spectroscopy should be seen to be complementary techniques rather than alternative [7].

2.7 Use of Raman Spectroscopy

Raman spectroscopy is commonly used in chemistry, since vibrational information is very specific for the chemical bonds in molecules. The position of the Raman band in the spectrum is dependent upon the chemical and physical environment of the chemical bond. It therefore provides information about the molecular structure of a compound and can be used to identify unknown compounds and the technique can therefore be used to study changes in chemical bonding.

Raman spectroscopy was first used in the context of planetary sciences to analyse lunar mineral samples returned by the Apollo missions [12, 13]. The majority studies still concentrate on the analysis of minerals that might be found on planetary surfaces and subsurface, but more recent studies have been reported to consider the use of Raman spectroscopy to detect extinct and extant biological signatures [14]. This has many advantages over IR as it is non-destructive and does not suffer from interference by water.

2.8 Raman intensity

Raman band intensities are given by the expression:

$$I \propto \nu^4 \sigma_{\nu} I C$$

Where ν is the frequency of the incident radiation, σ_{ν} is the Raman cross-section, I is the irradiance (W m^{-2}) of the incident radiation and C is the sample concentration.

Therefore, a more intense spectrum will be produced by increasing the laser power, or decreasing the wavelength (increasing the frequency) of the incident laser. The Raman intensity is also dependent on the magnitude of the polarisability change occurring in the molecular vibration [15].

2.9 Comparison of infrared and Raman spectroscopy

Both Raman and infrared spectroscopic techniques are complementary because of their different selection rules. Since infrared activity requires a change in the dipole moment of a molecule, those bonds which are highly polar will absorb most strongly, for example C=O and O-H. However, diatomic molecules, such as H₂, will not be infrared active [16]. In Raman spectroscopy it is the change in polarizability which is important, and so bonds such as C=C are the most intense.

Raman spectroscopy has certain advantages over infrared, particularly for biological studies. It is a non-destructive and non-invasive technique, which requires little or no sample preparation. It is possible to study aqueous solutions and hydrated specimens since water is a very weak Raman scatterer, whereas infrared spectroscopy usually requires desiccation of the sample. Glass is another weak Raman scatterer and so analyses can often be carried out through glass containers.

2.10 Advantages of Raman Spectroscopy

The non-destructive nature of the technique means that specimens can be analysed without permanent damage to or loss of the sample; additionally, in most cases, the sample does not need to be pre-treated chemically or mechanically prepared. Also, any size of sample can be studied from pg to kg quantities, which makes Raman spectroscopy ideal for both forensic and astrobiological use, where samples can be found in different situations.

The main advantage of Raman spectroscopy is the ease of examining difficult-to-handle small samples and being able to analyse a sample in a relatively short period of time.

Another advantage of the technique is that water produces a weak Raman spectrum, so molecules in aqueous solution can be analysed without the resulting spectra being

swamped by a water band and the presence of hydrates in geological specimens does not interfere in the interrogation of specimens.

2.11 Disadvantages of Raman Spectroscopy

There are several processes by which excess energy may be lost after a molecule has undergone an electronic transition into an excited state; the most important of these is fluorescence.

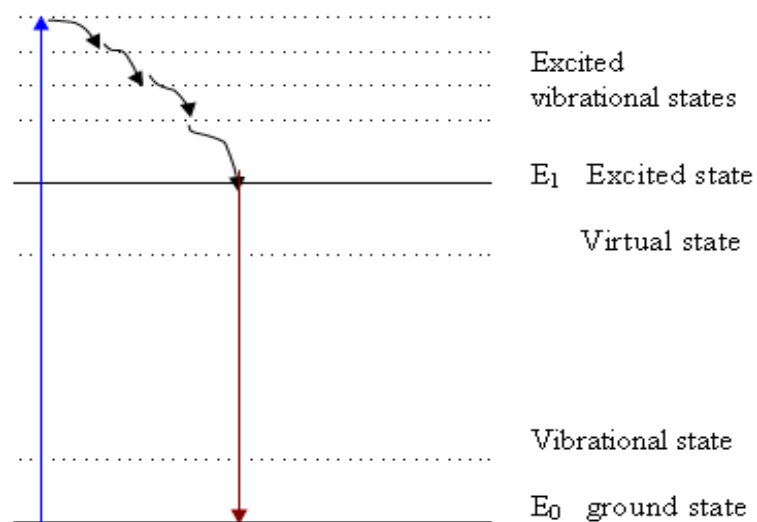


Figure 2.3 Energy level diagram showing fluorescence emission

Fluorescence occurs when the molecule is excited into the first excited electronic state by the absorption of a photon and relaxes to the ground electronic energy state through

broad-band emission. Since Raman scattering is a weak phenomenon, any background fluorescence emission (Figure 2.3) will swamp the Raman signals.

Another disadvantage is related to the use of higher power laser excitation as this can also cause sample degradation especially if molecular absorption occurs at or near the laser excitation wavelength.

2.12 Charge-Coupled Device Detection

In the early 1990s the charge-coupled device (CCD) detector was created [17]. This development greatly increased the speed at which a complete Raman spectrum could be collected but CCD detectors are most suited for lasers with wavelengths of less than 1000 nm, due to the silicon being essentially transparent above 1100 nm. The detector is made up of thousands of pixels, each of which stores charge proportional to the number of photons that hit it. Each pixel can only take a limited charge so sometimes the charge overflows, creating peak shape distortion in the spectrum.

2.13 Theory of X-ray powder diffraction

The main characteristic of a crystalline state is the periodic arrangement of units from which the crystal is formed. This structural pattern is repeated by 3-D translational repetition and it is this structure that is analysed in X-ray diffraction. The incident X-ray can interact with the electrons in the matter and be diffracted. The resultant diffraction is measured by a detector and this produces a powder pattern. This powder pattern can then be compared against known data in a database for identification of the crystal phases in

the sample. For the analysis of the diffraction pattern there is one thing that must be understood which is the atoms in the crystal are separated by distances similar to the wavelength of the incident wavelength used (1.5418 Å). This means that if the path difference is $n\lambda$ then there will be constructive interference and a peak will be seen and if the path difference is $\lambda/2$ then there will be destructive interference and no peak will appear. Figure 2.4 shows the diffraction of X-rays [18].

The Bragg equation can then be applied to determine where the peaks will appear:

$$n\lambda = 2d\sin \Theta$$

Thus, values of d , the distance between the planes, and Θ , the angle of incident radiation that produce integral values of n , will produce peaks in the pattern. The diffraction from the sample is in fact a cone of diffraction, so a detector can simply cut through these cones to collect a full pattern, however due to the importance of Θ in the equation a flat surface on the specimen is crucial to good data being produced. It is also crucial that the sample is homogenous and the crystals are randomly orientated and this random orientation will allow full cones of diffraction to be produced.

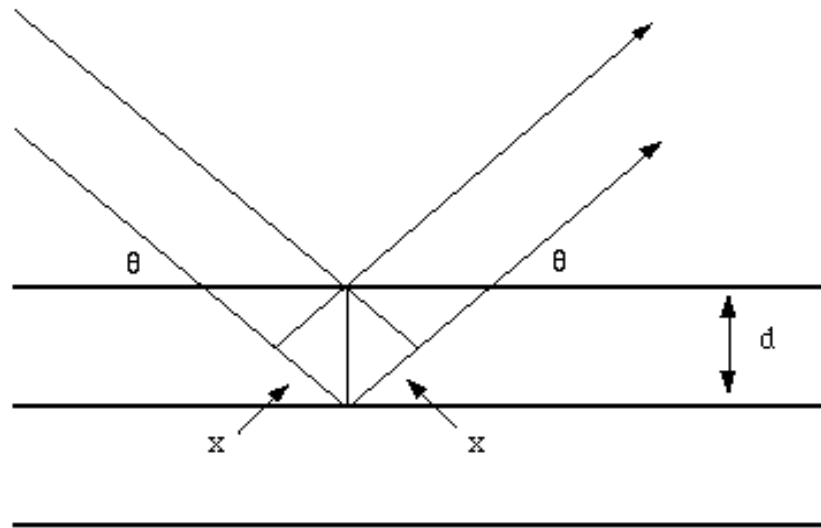


Figure 2.4 Diagram of Bragg theory of x-ray diffraction.

2.14 References

- [1].B.Colthup, E.Wiberley, H.Lawrence, Introduction to Infrared and Raman Spectroscopy, Academic Press , New York, San Francisco and London, **1975**
- [2] D. H. Whiffen, Spectroscopy, Longman Group Limited, London, **1972**, 12, 109
- [3] <http://www.optics.rochester.edu:8080/workgroups/berger/history.html>
- [4] H. L. Welsh, J. Stansburye, Romankoj, N. Feldmat, J. Opt. Soc. Amer, **1955** ,45,338
- [5] Webster's Family Encyclopedia, Laser, **1991**, 6, 1480

- [6] J. G. Grasselli, M. K. Sanavely, B. J. Bulkin, Chemical Applications of Raman Spectroscopy, New York, Wiley, **1981**
- [7] P. Hendra, C. Jones, G. Warnes, Fourier-Transform Raman Spectroscopy: Instrumentation and Chemical Application. New York and London, Ellis Horwood Press **1991**.
- [8] J. R. Ferraro, K. Nakamoto. Introductory Raman Spectroscopy. Academic Press, San Diego, **1994**.
- [9] J. Loader . Basic Laser Raman Spectroscopy. London: Heyden and Son **1970**.
- [10] D. A. Long, Raman Spectroscopy, McGraw Hill International Book Company **1977**.
- [11] M. J. Pelletier, Analytical Applications of Raman Spectroscopy. Oxford. Blackwell Science Ltd, **1999**.
- [12] G. W. Fabel, W. B. White, E. W. White, R. Roy, 'Structure of lunar glasses by Raman and soft X-ray spectroscopy.' Proceedings of the 3rd Lunar Science conference , volume I, Geochimica et Cosmochimica Acta Supplement **1972**, 1, 939
- [13] C. H. Perry, D. K. Agrawal, E. Anastassakis, R. P. Lowndes, N. E. Tornberg, 'Far infrared and Raman spectroscopic investigation of lunar materials from Apollo 11, 12, 14, 15.' Proceedings of the 3rd Lunar Science Conference, Geochimica et Cosmochimica Acta (suppl.), **1972**, 3, 3077.
- [14] H.G.M. Edwards, E.M. Newton, in J. A. Hiscox (ed.), The search for life on Mars, British Interplanetary Society, London, **1999**, 83.
- [15] B. Schrader, Ed. Weinheim, 'General Survey of Vibrational Spectroscopy' Infrared and Raman Spectroscopy, VCH: **1995**, 7.
- [16] D. L. Pavia, G. L. Lampman, G. S. Kriz, Saunders College Publishing, Florida, USA. **1996**, 14.
- [17] G. Osinski, New Scientist, **2003**, 40.

[18] R. E. Van Grieken, A. A. Markowicz, Handbook of X-Ray Spectrometry: Methods and Techniques, Marcel Dekker, New York, NY, USA, **1993**.

CHAPTER 3
Instrumentation

3.0 Raman Instrumentation

In the course of this study two dispersive and one non- dispersive Raman instruments were used. The first dispersive Raman was a Renishaw *In Via* confocal Raman microscope, the second one was a Renishaw portable Raman analyser (RX210) and the non- dispersive was a Fourier-transform Raman spectrometer (Bruker Spectrometer). Furthermore, an X-Ray powder diffractometer (a Bruker D8 diffractometer) and Scanning Electron Microscopy (SEM Quanta 400, FEI Company, Cambridge, UK) were also used.

3.1 Dispersive Spectrometers [1-4]

In a dispersive spectrometer the instrument spatially separates the Raman scattered radiation into constituent wavelengths before it reaches the detector. Early dispersive spectrometers used a diffraction grating to remove Rayleigh scattering and produce a spectrum. However, this reduces the radiation throughput of the instrument and makes it difficult to detect weaker Raman bands. In modern instruments holographic notch filters or edge filters are used for selective Rayleigh scatter rejection. Another development is the low-noise sensitive detectors called charged coupled devices (CCD)

The 2D charged coupled device (CCD) consists of a large number of closely spaced electrodes on an oxide covered silicon substrate. Photons from the dispersive grating pass through the electrodes into the silicon and cause electron hole pairs to be formed. Each group of electrodes form a potential well (1 potential well equals 1 pixel) and these wells collect the electrons. The charge on each pixel is proportional to the number of incident photons and this charge can be read off the chip after the correct exposure time. These low noise detectors are very useful but their quantum efficiency (percentage of

incident photons that result in a detected electron) depends on the wavelength. For very short wavelengths in the visible spectrum the electrodes will absorb all the radiation, causing no electron holes to be formed in the silicon layer as no photons will reach it. At higher wavelengths the electron holes are formed too deep in the silicon layer and will not be detected. The upper limit of the silicon-based CCD detector is about 1000 nm. The main advantage of the array detector is that all frequencies are analysed Simultaneously as they have been separated by the holographic notch. This means that each frequency is scanned for n times longer than if the range of frequencies was scanned (n = the number of simultaneously recorded spectral elements). This also means that the signal-noise is increased by $n^{1/2}$; this is known as the multi-channel advantage.

3.1.1 Renishaw In Via Raman Microscope [5]

The Renishaw In Via microscope is a spectrometer with several different laser excitation wavelengths that can be focussed through a modified Olympus metallurgical microscope onto a sample stage. The wavelengths that were used during this study were from the argon ion (Ar^+) gas laser which produces two useable wavelengths at 488 nm and 515 nm, a helium-neon gas laser (He-Ne) produceing radiation at 633 nm and the gallium-aluminium-arsenide diode laser (GaAlAs) which produces radiation at 785 nm.

The instrument is always calibrated by running a spectrum of a silicon wafer. A spectrum should be produced with a peak at $520.5 \text{ cm}^{-1} \pm 1$. Raman spectra were acquired at 2 cm^{-1} spectral resolution and recorded normally over the range 3200 – 100 cm^{-1} .

A diagram of the In Via instrument can be seen in figure 3.1. Laser radiation enters via fibre optic cables at the bottom right of the diagram marked with an arrow. The radiation

passes through a filter wheel (1), which can be used to reduce laser power. The beam is then spectrally (2) and spatially (3) filtered. The beam is directed to the microscope via mirrors (4 and 5) and then directed into the microscope via one of two holographic notch filter (both labelled 6). The incident radiation is directed through the microscope via mirrors and hits the sample via the objective lens (5x was used in this study) the scattered radiation is collected by the objective lens (180° backscattering geometry) and passed back to the holographic notch filter (6), which rejects any Rayleigh scattering. The backscattered Raman radiation is filtered through the spectrograph entrance slit (7) and passed via a reflecting prism (8) to a diffraction grating (9) which separates the radiation into its constituent wavelengths before reflecting them back to the prism (8) and then onto the CCD detector (10).

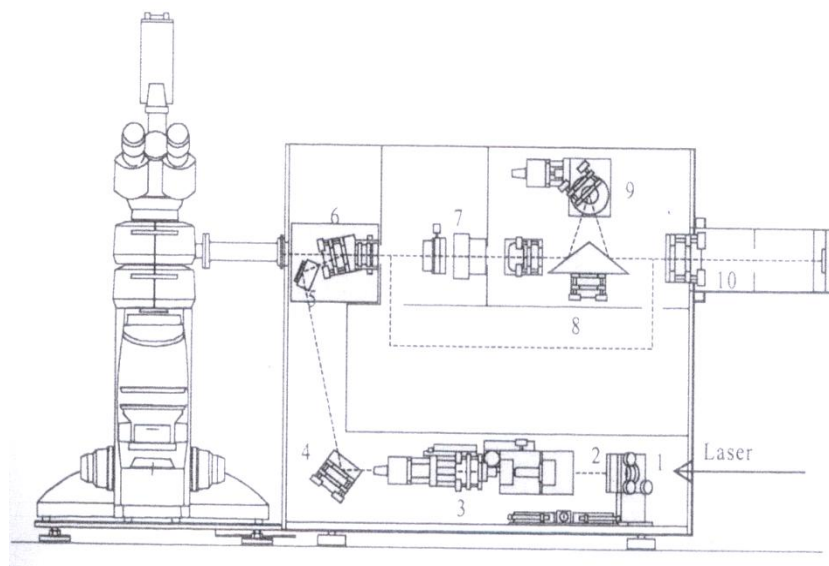


Figure 3.1 Diagram of the Renishaw In Via confocal Raman microscope [1]

3.1.2 Renishaw Portable Raman RX210 analyser (RIAS)

The Renishaw RX 210 spectrometer (Figure 3.2) uses a diode laser operating at 785 nm and a thermoelectrically cooled CCD detector. The instrument is equipped with a fiber optic probe with a 20x objective lens and a diffraction grating with 1000 lines/mm which limits the observable spectral range to 2100-100 cm^{-1} . The output power of the diode laser is 500 mW at the source and 40 mW at the sample. Daily calibration of the instrument was carried out by recording the Raman spectra of silicon (1 accumulation, 10 second exposure, in static mode). If necessary, an offset correction was formed to ensure the position of the silicon band was at $520.5 \pm 0.1 \text{ cm}^{-1}$. The spectrometer was controlled by a portable PC using the instrument control software, Renishaw WiRE 2TM.

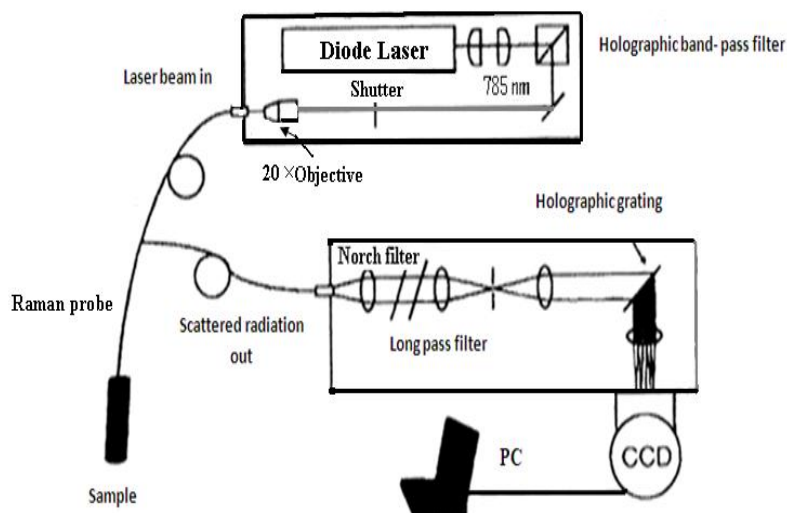


Figure 3.2 Diagram of Renishaw Portable Raman analyser RX210 (RIAS)

3.2 Non Dispersive FT-Spectrometers [1, 5, 7]

In non-dispersive spectrometers the scattered radiation is not spatially separated, but enters an interferometer through an aperture known as a Jacquinot stop. Here the beam is split into 2 equal components by a silicon-coated copper fluoride beam splitter and the two beams are reflected off mirrors that have a controllable separation. The two beams can interfere constructively (their path length = $n \lambda$) or destructively (their path length = $\frac{1}{2} n \lambda$)

The polychromatic radiation that enters the interferometer comes out as a sum of cosine waves, the amplitude of which depends on the intensity of all the component parts, i.e. the Raman scattering. This interferogram is really a plot of intensity versus optical delay. It is resolved into its constituent cosine waves and then a Fourier-Transform operation is applied to obtain a plot of intensity versus frequency, which is the Raman spectrum. The sample data acquisition rate can be a controlled rate and the detector frequency monitored by a He-Ne laser which acts as an internal standard.

3.2.1 Fourier-transform (FT) Raman spectrometer

The model of Fourier-transform Raman spectrometer used in this work is a Bruker IFS 66 FT-IR optical bench with an FRA 106 FT-Raman accessory. This accessory has several different stages that can be used to accommodate different types of sample. These stages can also be removed entirely to allow the spectrometer to be connected to a microscope. It has air-cooled Nd⁺³/YAG laser excitation (1064 nm). A Nikon microscope attachment was also used to obtain spectra of very precise sample areas.

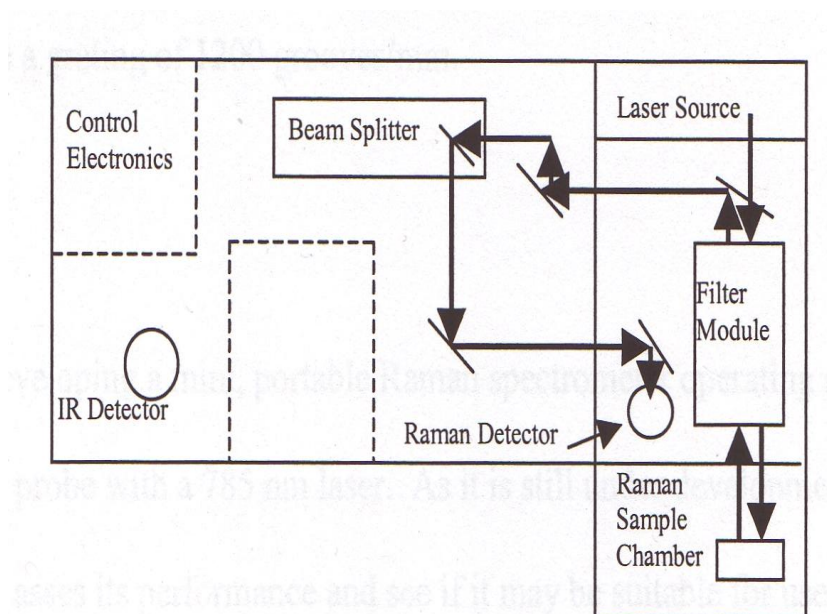


Figure 3.3 Diagram of the Bruker IFS 66 FT-IR with a FRA 106 FT-Raman module

The filter module is necessary as the scattered light is not of the same intensity in all directions. The filter is set to collect at a specific direction (such as 90° or 180°) from the direction of the incident light.

Samples that are in powder form of less than ~ 2 mm in size are placed in the sample cups and placed on the standard stage which is accurately aligned with the laser at the correct focal distance. Larger samples are placed on a different stage; a microscope option is available but the laser power at the spectrum is greatly reduced by the transfer optics used.

3.3 X-ray powder diffractometry (XRD)

Powder X-ray diffractograms were recorded with a Bruker D8 diffractometer (Figure 3.4). The wavelength of the X-rays was 0.154 nm using a copper source, at a voltage of 40 kV and with filament emission current of 30 mA. Each sample was scanned from 5-90° (2θ) using a step width of 0.01° and a 1 second time count. The receiving slit was 1° and the scatter slit of 0.2°. The software used to read the data was EVA, which comprises both a means by which the data can be presented and manipulated and also a database with which to compare the data with spectra of known materials.

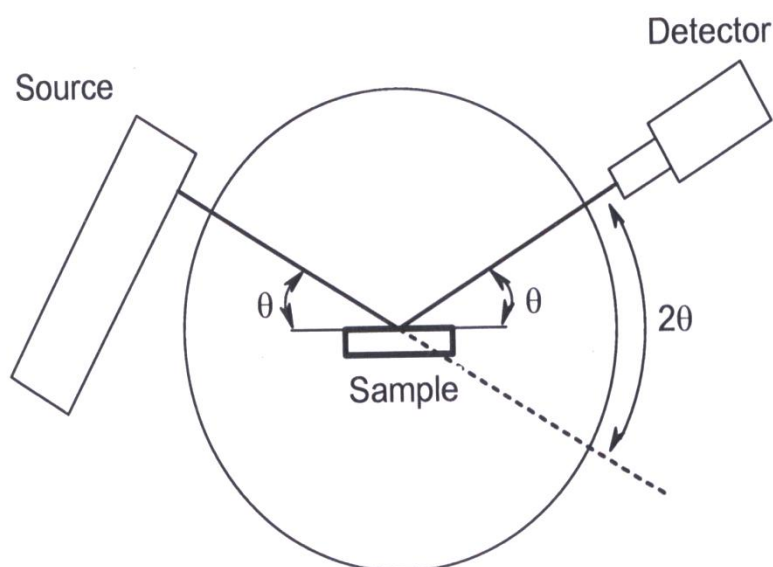


Figure 3.4 Diagram of a typical X-ray powder diffractometer.

3.4 Scanning Electron Microscopy

The SEM instrument is an FEI Quanta 400. The source of the emission is a tungsten filament and there is an accelerating voltage of 20000 volts and an emission current of approximately 100 amps. Samples can be analysed in different conditions. Samples were used either alone or coated in carbon or gold and the stubs onto which the samples were fixed are made of aluminium with a double-sided self-adhesive carbon disc for mounting.

The detection equipment (EDX) consists of the Oxford Instruments Micro Analysis detector with a rubidium window. The required working distance from the sample under examination is 11 mm using a spot size of approximately 6. For the acquisition of data, the instrument rate is about 4000 counts per second and the deadtime must be less than 50%. The deadtime can be corrected by changing the spot size. The SEM instrument utilises cobalt for calibration and the software employed is INCA.

3.5 Data processing [6]

Five main data manipulation programmes were undertaken using Galactic*. SPC format using GRAMS AI (Galactic Industries, Salem, NH, Version 8.0), these were:

- Baseline correction
- Normalisation
- Smoothing
- Deconvolution
- Integration of peak area and width

3.5.1 Baseline correction [6, 7]

The baseline correction was set as a baseline containing multiple points, which were set flat, at approximately zero. When applying this baseline, peaks were emphasised slightly, allowing weaker peaks in highly fluorescent spectra to appear more strongly. The effect however, was only slight and there was not much change in data.

3.5.2 Normalisation

The Raman technique is not based on an absolute intensity due to differences in laser power and detector response which are not uniform across the spectra range. Normalisation was used in this research to display stack-plotted spectra, which relative intensities of peaks in the spectra can be clearly compared.

3.5.3 Smoothing

A smoothing function is basically a convolution between the spectrum and a vector whose points are determined by the degree of smoothing applied.

The Savitzky-Golay smoothing algorithm was used in this research with seven smoothing points using a second order polynomial. The algorithm is based on performing a least squares linear regression fit of a polynomial around each point in the spectrum to smooth the data.

3.5.4 Deconvolution

Deconvolution is the process of compensating for the intrinsic line widths of bands in order to resolve overlapping bands [8]. This technique yields spectra that have much

narrower bands and is able to distinguish closely spaced features. The instrumental resolution is not increased, but the ability to differentiate spectral features in composite can be significantly improved.

3.5.5 Integration of peak area and width

Band area integration is performed using the trapezoidal rules. The area under the peak is separated into trapezoids which the ends are made equal by the use of baseline correction.

The peak width at half height is the distance between each side of a peak measured at half the peak height.

3.6 References

- [1] P. Hendra, C. Jones, G. Warnes, Fourier - Transform Raman Spectroscopy: Instrumentation and Chemical Application. New York and London, Ellis Horwood Press **1991**.
- [2] J. G. Grasselli, M. K. Snavely, B.J. Bulkin, 'Chemical Application of Raman Spectroscopy' Wiley, New York, **1981**.
- [3] P.R. Carey, Biochemical Application of Resonance Raman Spectroscopies, Academic Press, New York, **1982**.
- [4] M. J. Pelletier, Analytical Application of Raman Microscopy, Blackwell Science, Malden, MA , **1999**.
- [5] S. Webster, Raman Microscopy and Optical Spectroscopy of Conjugated Polymers at High Pressure, PhD Thesis, University of Leeds, **1994**, ch, 2, 20.

- [6] J. M. Shaver, Chemometrics For Raman Spectroscopy. Handbook of Raman Spectroscopy: Practical Spectroscopy Series. Marcel Dekker Inc, New York **2001**.
- [7] H. G. M. Edwards, Encyclopaedia of Analytical Chemistry-Fourier Transform Raman Instrumentation (John Wiley and Sons Ltd, Chichester), **2000**.
- [8] J. K. Kauppinen, D. J. Moffat, H. H. Mantsch, D. G. Cameron, Applied Spectroscopy, **1981**, 35, 271.

CHAPTER 4

Astrobiology

4.1 Introduction to astrobiology

Astrobiology is a multidisciplinary topic concerning studies into the origins of life in the universe and its evolution. Research topics include the areas of biology, palaeontology, geology and geochemistry. Astrobiological studies can be placed into two main groupings, namely, those concerned with the origins and subsequent evolution of life on Earth and those studies that explore the Solar system for habitats that could support life. Such environments are those that have a rich supply of liquid water as well as a high abundance of elements essential for life (C, H, N, O, P and S). The environment must also provide an energy source and be stable enough to maintain life, or its precursors, once it originates [1, 2].

One theory as to where life on Earth is thought to have begun is in areas of geothermal activity such as marine beds or in subterranean hydrothermal systems. Research is currently under way to study whether the first organic compounds were proteins or nucleic acids. Proteins are favoured due to their active nature, but crystals present in naturally occurring clay compounds can catalyse the formation of nucleic acids [2].

Environments similar to early Earth are also thought to exist, or have once existed elsewhere in our Solar system. This means that it is possible that life has evolved on other planets. As previously mentioned, due to its close similarities to Earth, Mars is viewed as the most likely planet to have once supported life [1, 3].

Astrobiology has become an important part of national and international space programmes, with many missions involving the search for evidence of past or present extraterrestrial life.

4.2 The origin and evolution of life

There are several theories as to how life originated, both terrestrial and extraterrestrial. The extraterrestrial theories incorporate the concept of panspermia, first suggested by Arrhenius (1908), who speculated that spores from another planetary system propelled by the pressure of sunlight could have seeded the Earth. Related to this is the suggestion that life may have been purposely spread through space from another planet through the action of intelligent beings [1, 2].

The primary constraints on panspermia are that the organisms survive the journey through space to Earth and that the surface of the Earth be suitable for their subsequent growth. Experiments cannot rule out the possibility that bacteria and their spores could survive long transits in space [3].

Terrestrial theories vary from those which postulate that the structure of the first organism was organic and others which postulate an inorganic origin. The inorganic postulate claim that early life evolved from clay crystal compounds [58, 59]. Laboratory experiments have shown that clay minerals catalyse the formation of RNA oligomers [60, 61], RNA being the first genetic macromolecule.

The majority of theories for the origin of life presume organic origins. On Earth it is assumed that through a series of steps, referred to as chemical evolution, organic matter assembled into the first living cell. Because of the strong experimental and observational support for a biotic production of biochemically relevant organics, this theory for the origin of life on Earth by the self-assembly of organic material produced on Earth is referred to as the Standard Theory. The affinity of biochemistry for liquid water suggests that the chemical evolution phase occurred in an aquatic environment [4].

The most important parameter is the presence of liquid water, plus reasonable concentration of essential elements (C, H, N, O, P, and S), mineral particulates for

adsorption and a suitable energy source [5]. Experiments have demonstrated that simple organic molecules, including several amino acids found in living systems, can be synthesized by biotic processes driven by exogenous energy sources [6]. Many simple organic molecules are also abundant in space and are delivered to the Earth's surface by meteorites and interstellar particles [2]. It is also possible that life arose at hydrothermal vents or hot springs in a developing Earth, using geothermal energy. Conditions for redox reactions are generated at hydrothermal vents [7] and iron-sulphide membranes broaden the requisite spatial structure, energy transfer and organic synthesis [8].

4.3 Life outside the Earth

In the search for extraterrestrial life the closest environments to analyse are those on the other planets in our solar system. Studies have found Mars to be the candidate most likely to have once harboured life. This is mainly due to its reasonable distance from the Sun and the planet's similar geological history to Earth.

The early development of both planets followed a similar pattern; both had high rates of meteoric impact, volcanism, an abundance of liquid water and an atmosphere that contained N_2 , H_2 and CO_2 . As these conditions developed organisms on Earth, it seems logical that Mars too could have once supported life. One major difference between the two planets is Mars's smaller size. This would have caused Mars to cool faster than the Earth, meaning that life could actually have developed sooner than it did on Earth.

4.4 Mars

Mars is the fourth planet in the solar system; it is the second closest planet to Earth and is commonly referred to as the Red Planet, largely because of the large amount of iron (III) oxide on its surface. It has highly varied terrain, including Olympus Mons, a volcano which is 24 km in height and has a base diameter of more than 500 km. Another major feature is Valles Marineris, a system of canyons 4000 km long and from 2 to 7 km in depth [7].

Much of the Martian surface is ancient and highly cratered, although there are younger plains and other features, mainly in the lower-lying northern hemisphere.

There are permanent polar ice caps, composed mainly of carbon dioxide layered with dark-coloured dust. During the northern summer the carbon dioxide sublimates and reveals a residual layer of water ice. It is not known if the southern ice cap contains water ice as the carbon dioxide layer is permanent [7].

It is accepted that conditions on early Mars were very different to those we see today. Studies of the SNC (Three rare groups of achondritic (stony) meteorites: shergottites, nakhlites and chassignites) Martian meteorite known as ALH84001 indicate that it formed on Mars about 4.5 billion years ago (Gya) under warm, reducing conditions [9]. These findings support the theory that although the Martian surface is strongly oxidizing today, it was once a reducing environment capable of supporting organic material.

The low atmospheric pressures on Mars today (0.06-0.1 atm) mean that there is no stable liquid water at the surface. The triple point of water is 0.061 atm, below this pressure water cannot exist in a liquid state. For a pressure slightly above the triple point the liquid is still unstable because the freezing and boiling points are very close; for example, at a

pressure of 0.1 atm water will boil at 7 °C [10]. However, hydrological features on the planet's surface indicate the past presence of significant amounts of water, which were continuous over a considerable time scale. The existence of large volcanoes is further evidence that Mars has had a more active geological past.

Although it is possible that Mars was warmer during this time period, evidence indicates that the mean temperature was still well below freezing.

Greenhouse models for Mars imply that even a thick CO₂ atmosphere would not have brought the temperature past freezing, under the weaker isolation some 3.5-4.0 Gya [11]. The valley networks are not uniformly distributed; indicating regions of local heating [12]. There is little erosion on the ancient cratered terrain, indicating that a water cycle was not active for a significant period after the end of the late bombardment [13]. Therefore, Mars is thought to have been quite cold, despite having a thick atmosphere, even during its ' warm and wet ' period after the end of the late bombardment (3.8 Gya). For this reason, the study of Earth's Polar Regions is particularly suitable as analogues for early Mars.

It is still uncertain exactly how much water existed on the surface of early Mars, with estimates ranging from depths of just a few meters to almost a kilometer [10]. More important, however, for the formation of life is the availability and longevity of liquid water [7]. Carbonate formation on Mars is also important from an astrobiological perspective. Although there is no direct evidence for the existence of carbonates on Mars, it is thought that they would be stable under the current Martian environment [14]. Carbonates have been found in meteorites believed to originate on Mars [15, 16].

The major problem for life on Mars is the high level of ultraviolet radiation reaching the surface of the planet. Radiation below 190 nm is attenuated by the high amount of CO₂ in the Martian atmosphere (see Table 4.1), but there is only approximately 2 % of the ozone

content of Earth's atmosphere and so there is little shielding of high energy radiation below 300 nm.

Davis and McKay [17] have compared the theories of the origins of life with regard to Mars and have concluded that all the major habitats and microenvironments of early Earth would also be expected on early Mars. It is therefore considered reasonable to assume that whatever led to the origin of life on Earth also led to the possible origin of life on Mars, provided that the conditions remained stable for an adequate duration of time.

| | Mars | Earth |
|---------------------|---|---|
| Day | 24 hr 37 min | 24 hr |
| Year | 687 Earth days | 365 days |
| Atmosphere | 95% carbon dioxide 2.7% nitrogen 2.3% other gases | 78% nitrogen 21% oxygen 1% other gases |
| Atmosphere pressure | 0.7% of Earth pressure | |
| Gravity | 35% the gravity on Earth | |
| Diameter | 4217 miles | 7,926 miles |
| Land Surface Area | ~56 million square miles | ~57 million square miles (Total surface ~196.9 million square miles) |
| Distance from Sun | 141.6 million miles | 93 million miles |
| Moons | 2(Phobos and Deimos) | 1(Moon Lunar) |

Table 4.1 shows the difference between Earth and Mars [18]

4.5 Extant Life

Although the conditional changes described would have eliminated all surface-borne life on Mars, it is theoretically possible for life to still exist within subsurface environments. These habitats would be heated by the planets core and thus could contain liquid water. This is, however, purely theoretical as there is currently no physical, biochemical or spectroscopic evidence to prove life does or has ever existed on Mars.

The identification of life on Mars will rely on the ability to recognize so-called biomarkers. Raman spectroscopy is suitable for such a role due to its ability to analyse molecules non-destructively and *in-situ* for biological systems and for organic molecules in the geological record [19, 20]. The suitability of this technique for identifying a number of biomarkers, potentially applicable to life systems on Mars, has been shown in a number of terrestrial applications [21]. This may provide a database of terrestrial biomarkers that will be very useful for comparison with any data that can be gained from a Martian sample; this database construction is ongoing.

4.6 Extinct Life

Finding carbon in the form of kerogen is a firm indicator of extinct life. This is a substance that is formed after the death of an organism. Upon death, the bulk of organisms carbon are demineralised as CO₂; some, however, is buried within newly formed sediments. The primary biopolymers undergo a large-scale reconstruction that results in the formation of the final product, kerogen, a chemically inert polycondensed aggregate of aromatic and aliphatic hydrocarbons. The composition of this fossilized

material tends to be very resistant to chemical or biological attack. Hence, the presence of kerogen is a chemical record evident of the former existence of microorganisms.

As life on Mars is thought unlikely to have evolved in the form of surface dwelling organisms it becomes necessary for us to look deeper into the regolith for signs of life. For this reason the Beagle 2 Mars Lander was equipped with both a corer and a “mole” drill. These devices would have allowed the sampling of the substratum facilitating the investigation of the planet for any fossilized endolithic organisms [22].

4.7 Terrestrial analogues of Mars

Terrestrial Mars analogues are sites on Earth that approximate some features of the geological, environmental and putative biological conditions, either at the present-day or where they have applied sometime in the past. Analogue studies are driven by the need to understand processes on Earth in order to interpret data accessed by unmanned orbiters and rovers in extra-terrestrial environments. The definition and characterization of a hostile planetary biosphere is of critical importance for future human missions into our Solar System and for planned landing missions on planetary surfaces and moons.

The study of terrestrial analogues of possible extraterrestrial life is a prerequisite before planetary exploration can be envisaged [23]. Knowledge as to where and how life survives in the most extreme conditions on Earth, what analytical signals can be correlated with life and how we can recognize those markers as life, either extant or extinct, is vital to the success of these extra-planetary missions.

4.8 Protective Biomolecules

In order to survive in an inhospitable environment there is a need to develop survival mechanisms. If the biomolecules or their derivatives are present in a rock sample as fossils they can be indicative of past life and occasionally identification may be made, as certain molecules are specific to certain life forms. These compounds are known as biomarkers and some of the more important and common ones are listed below.

4.8.1 Polyaromatic hydrocarbons

Raman spectroscopy has been proposed as a valuable analytical technique for environmental and planetary exploration because it is sensitive to organic and inorganic compounds and it is able to identify key spectral markers in mixtures of biological and geological compounds.

Polycyclic aromatic hydrocarbons (PAHs) are chemical compounds that consist of fused aromatic rings. PAHs containing up to six fused aromatic rings are often known as small PAHs and those which containing more than six aromatic rings are called large PAHs. They have relatively low solubilities in water. Polycyclic aromatic hydrocarbons (PAHs) have been the subject of many studies because of their carcinogenic effect, involvement in widespread environmental pollution and they have a well-documented toxicity. They are produced by the incomplete combustion or degradation of carbonaceous materials. Significant efforts have been expended to devise techniques for the identification and quantification of PAHs in water and they are common constituents of complex mixtures such as automobile exhaust gases, crude oil, cigarettes smoke and coal [24]. They have

been found at significant concentration levels in the atmosphere, waterways and food chains [25].

Raman spectroscopy is sensitive to molecular skeletal characteristic frequencies showing multiple bond orders, branching of chains, saturated and aromatic rings, and their substitution patterns [26].

Raman spectral data have been reported for several polycyclic aromatic hydrocarbons, results are obtainable for naphthalene [27, 2], anthracene [28] , phenanthrene [4] , chrysene [29], triphenylene [30] and pyrene [4, 5]. While these studies were concerned with the assignment of the vibrational modes for the molecules in question, no systematic studies have been undertaken hitherto to characterize these materials in admixture with themselves, with other biomarker or with geological minerals.

Asher [5] has investigated resonance enhanced Raman methods for the identification and detection at low levels of polyaromatic hydrocarbons. The method was found to be highly sensitive, rapid and precise, but the technique does require the use of special spectrometric equipment and tuneable lasers operating in the ultraviolet and visible region.

Our understanding of the evolution of organic molecules, and their progress from molecular clouds in the early Solar System and Earth has changed dramatically. Incorporating recent observational results from the ground and space, as well as laboratory simulation experiments and new methods for theoretical modelling, this review describes the inventory and distribution of organic molecules in different environments. The evolution, survival, transportation, and transformation of organics are monitored from molecular clouds and the diffuse interstellar medium to their incorporation into Solar System material such as comets and meteorites [31].

In the Solar System, space missions to Halley's Comet and observations of the bright comets Hyakutake and Hale-Bopp have recently allowed a reexamination of the organic chemistry of dust and volatiles in long-period comets [7, 17]. Ehrenfreund and Charnley [31] have reviewed the advances in this area and also discussed progress being made in elucidating the complex organic inventory of carbonaceous meteorites. The knowledge of organic chemistry in molecular clouds, comets, and meteorites and their common link provides constraints for the processes that lead to the origin, evolution, and distribution of life in the Galaxy [31].

Polycyclic aromatic hydrocarbons (PAHs) have been found in meteorites, interplanetary dust particles, and interstellar matter and thus are an attractive target in the search for organic molecules on Mars.

PAHs are believed to be the most abundant free organic molecules in space [32, 33]. Electron delocalization over their carbon skeleton makes them remarkably stable. PAHs represent one of the principal forms of complex molecular carbon in space. They are thought to be initially produced in the outflows of late type carbon stars forming protoplanetary and planetary nebulae [34]. These molecules are produced partly in the outer atmospheres of carbon stars or formed by shock fragmentation of carbonaceous solid material. PAHs may eventually also form in the diffuse interstellar gas by neutral-neutral reactions [35] or by the energetic processing of specific ices in dense clouds [36, 37]. They play a central role in gas phase chemistry [38]. The environmental conditions and the local ultraviolet radiation fields determine their charge and hydrogenation state.

PAHs are ubiquitously distributed in the interstellar medium and are also seen in traces in Solar System matter

Several critics [39,40] argue that the PAHs reported in ALH84001 are not diagnostic of life because PAHs form at high-temperatures and also because the PAHs are almost

identical to those in the carbonaceous chondrite Murchison [41], which is thought to have come from the asteroid belt, not Mars. In addition, a study [42] has suggested that the PAHs in ALH84001 are probably contamination products from the Antarctic ice field. In their original paper, McKay et al [43] did not claim that the PAHs were directly of biogenic origin but suggested that the PAHs might be products of the decay and fossilization of bacteria. The PAHs in ALH84001 are actually not identical to those in Murchison or any other carbonaceous chondrite [44], differing in the presence or absence of some of the attached side chains and in the relative type and abundance of each major compound. Furthermore, Clemett et al [44] demonstrated in their study that micrometeorites collected from the Antarctic ice are characterized by their own unique PAH fingerprints, which are specific to each particle. The carbon abundances within micrometeorites have been shown to be variable [40, 45] and these particles range in carbon concentrations from 0.1 to 50 wt% C. The micrometeorites are highly porous and have unusually large surface areas onto which organics within the ice or melt water could have been readily adsorbed. If all the PAHs in these micrometeorites were contaminants from the ice, then all particles would have similar concentrations and types of PAHs. Also, they have presented strong evidence that Martian polycyclic aromatic hydrocarbons (PAHs) are present in ALH84001 [40] and it was demonstrated Antarctic environment does not in fact contribute to the introduction of PAHs into ALH84001. As control samples, they measured concentrations of PAHs in numerous ordinary chondrite meteorites that resided longer in the Antarctic ice than ALH84001; the concentrations of PAHs did not increase as a function of exposure or residence time in the Antarctic environment and that the ice from Antarctica did not contain measureable PAHs. As additional evidence for the Martian origin of the PAHs, the PAH profile of ALH84001

was reanalyzed from the exterior fusion crust to the interior and it was found, again, that the abundance always increases from the exterior of the meteorite to the interior [40].

In another study it has been suggested that PAHs have a homogenous distribution and are not specifically concentrated in the carbonate globules [46]; they are to be found in the centres of the igneous mineral grains and are even apparently depleted in the carbonate globule. These analyses were made on polished thin sections of the meteorite, whereas the analyses of previous studies were made on freshly broken surfaces. Most polishing procedures use organic solvents or organic diamond paste and require considerable handling in less than clean conditions. It could be argued that the thin section making process have introduced PAH contamination? Or could it even have smeared out existing PAHs over the polished surface so that they no longer reflect their original location and abundance? It is perceived opinion [47, 48] that the results reported really represent contamination and do not provide meaningful information about the true state of reduced carbon components within ALH84001 [42].

Possible organic biomarkers are present within ALH84001 in the form of PAHs associated with the rims of the carbonate globules, some of which may be a unique product of bacterial decay. The PAH data combined with the recent amino acid data, show that a portion of the detected PAHs are most likely to be indigenous to ALH84001, whereas all the detected amino acids are most likely to be Antarctic contamination [40]. Exhaustive data must be collected before either component can be used as a biomarker for a specific sample. Recent studies of fossilized bacteria in terrestrial rocks have shown that PAHs are, indeed, a decay product of the bacterial systems and may represent a new biomarker. Recent studies [45, 49] have documented the presence of reduced carbon species within the clay-filled fractures of the Nakhla meteorite and investigations have shown that organic components appear to be indigenous to Nakhla. This observation

corresponds with the Nakhla carbon-14 which indicates that 80% of the carbon is not modern-day but Martian carbon [50].

4.8.2 Carotenoids

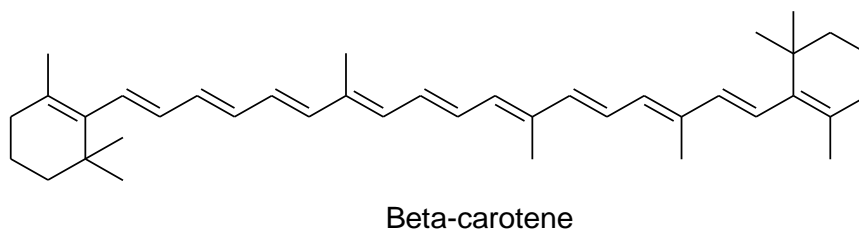


Figure 4.1 Structural formula for beta-carotene used in this study [51]

The main structural characteristic of carotenoids is the long, conjugated hydrocarbon chain. Due to this chain, there is extensive π -electron delocalisation, which leads to intense visible absorption bands [52] due to the relatively small amount of energy required for the $\pi - \pi^*$ transition. A common member of this group is Beta-carotene (Figure 4.1), which is a red, yellow or brown pigment and is thought to absorb the radiations that are not absorbed by chlorophyll [53]. The longevity of preservation of carotenoids is very poor due to the large number of double bonds, where intact carotenoids have not been found in rocks older than 20 Ma. However, the detection of the carbon skeleton in modified carotenoids has been made in rocks as old as 450 Ma [54].

4.8.3 Chlorophyll

This green pigment is perhaps the best known of the observed pigments. The function of this substance is to absorb photons and transport them to reaction centres where the chemical aspect of photosynthesis occurs [55, 35]. Chlorophyll (Figure 4.2) is found in two forms, b and a; of these two type are the most commonly found. The activity of chlorophyll is dependent on a tetrapyrrolic structure. This formation acts as a molecular biomarker that can be found in sediments and living organisms.

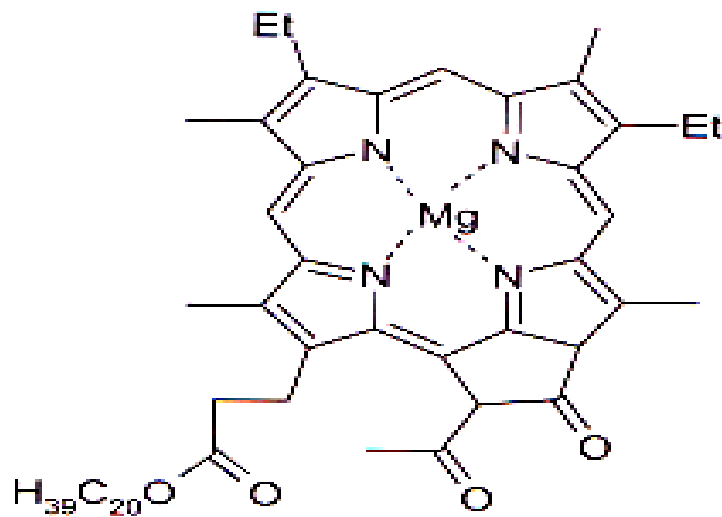


Figure 4.2 Structural formula of chlorophyll

4.8.4 Scytonemin

Scytonemin is yellow- brown and lipid-soluble [56]. It is found in the sheaths of cyanobacteria where it acts as a UV radiation protectant, allowing the organism to survive in areas of high exposure to radiation. Its presence in bacteria acts to screen out up to 90% of incident UVA radiation irradiation. This prevents the harmful energy from entering the organism where it could slow the photo-bleaching effect of chlorophyll. It also absorbs significant amounts in both the UVB and UVC regions. It is a valuable biomarker as it does not photo-degrade and has a long-term survival in sediments. The structure is also temperature resistant and able to remain intact in thermal conditions [39, 57] exceeding 325 °C.

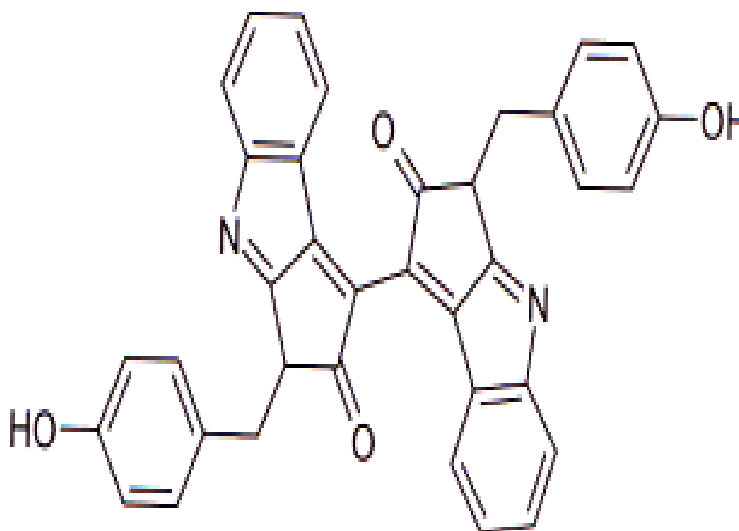


Figure 4.3 Structural formula of scytonemin [41]

4.8.5 Usnic acid

Usnic acid is a naturally occurring dibenzofuran derivative found in several lichen species [37]. The molecule contains intramolecular bonds and has the molecular formula $C_{18}H_{16}O_7$. Its structure can be seen in figure 4.4

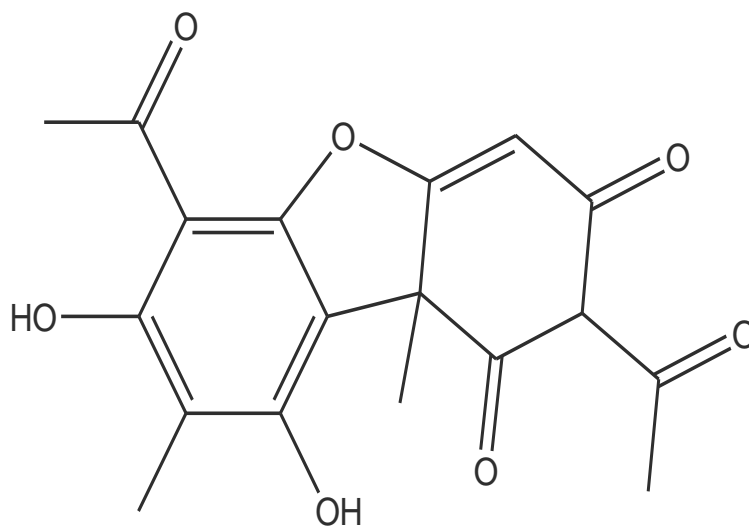


Figure 4.4 Structural formula of usnic acid

4.9 Minerals

Minerals are naturally occurring chemical compounds or elements found in the earth's crust and are the building blocks of rocks. Rocks may contain only a single mineral, but usually they contain a mixture of many minerals.

Rock forming minerals come in all colours, size and chemical compositions. The size of the crystals depends on environmental factors such as space for growth and the rate of cooling. The colour is often formed by the presence of an impurity.

4.9.1 Quartz

Quartz (crystalline silica or SiO_2) is the most common single mineral of the continental crust. Quartz is a glassy, transparent or translucent mineral which varies in colour from white and grey to smoky. It is so common in coarse-grained igneous rocks and metamorphic rocks that its absence may be more noteworthy than its presence. Most sandstone is made up solely of quartz. It has an excellent Raman scattering factor with a very intense band at 463 cm^{-1} [21].

4.9.2 Carbonate (Calcite)

There are many different carbonate minerals. The most common is probably calcium carbonate which has two common forms: calcite and aragonite. Calcite is a very common mineral in sedimentary rocks. It is commonly white to grey in colour. Individual crystals are generally clear and transparent. In a rock, calcite grains are often irregular to rhomb-like in shape.

4.9.3 Gypsum

Gypsum is a soft mineral, hydrous calcium sulfate or $\text{CaSO}_4 \cdot 2\text{H}_2\text{O}$. Sulfate minerals are delicate and occur near the Earth's surface in sedimentary rocks such as limestone, gypsum rock and rock salt. Sulfates tend to occur where there is oxygen and water and whole communities of bacteria survive by reducing sulfate to sulfide where oxygen is absent. Gypsum forms seawater becomes concentrated from evaporation, and it is associated with rock salt and anhydrite in evaporite rocks. Gypsum forms bladed concretions called desert roses or sand roses, growing in sediments that are subjected to concentrated brines. It is the most common of the approximately 150 sulfate minerals.

4.10 References

- [1] Arrhenius, Svante, *Worlds in the Making*, Harper, London, **1908**.
- [2] F. Crick, *Life Itself: Its Origin and Nature* (New York: Simon & Schuster), **1981**.
- [3] P. Weber, J. M. Greenberg, , *Nature*, **1985**, 316, 403
- [4] L.Wanda, Davis, P. Christopher, Mc Kay, *Origins of Life and Evolution of the Biosphere*, **1996**, 61
- [5] S. A. Asher, *Analyt Chemistry*, **1984**, 56,720
- [6] J. N. Miller, J. C. Miller, *Statistics and Chemometrics for Analytical Chemistry*. Harlow, Prentice Hall, **2000**.
- [7] G. R. Bock, J. A. Good, Eds, *Evolution of Hydrothermal Ecosystems on Earth and Mars*. Chichester, John Wiley & Sons, 1996.
- [8] M. J. Russell, R. M. Daniel, A. J. Hall, J. A. Sherringham, *J. Mol. Evol*, **1994**, 39, 231.

- [9] C. S. Romanek, M. M. Grady, I. P. Wright, R. A. Mittlefehldt Socki, C. T. Pillinger, E. K. Gibson, *Nature*, **1994**, 372,655.
- [10] C. P. McKay, *Origins of Life and Evolution of the Biosphere* **1997**, 27,263.
- [11] R. M. Haberle, D. Tyler, C. P. McKay, W. L. Davis, 'A model for the evolution of CO₂ on Mars.' *Icarus* **1994**,109, 102.
- [12] V.A.Gulick, *Geomorphology*, **2001**,37,241.
- [13] M. H. Carr, *Water on Mars*. New York, Oxford University Press **1996**.
- [14] J.A. Gooding, 'Chemical weathering on Mars.' *Icarus* **1978**, 33,483.
- [15] J.A. Gooding, S.J.Wentworth, M.E. Zolensky, *Geochimica et Cosmochimical Acta*, **1988**, 52, 909.
- [16] D.S. McKay, E.K.Gibson, K.L.Thomas-Keprta, H.Vali, C.S. Romanel, S.J.Clemett, X.D.F.Chillier, C.R.Maechling, R.N.Zare., *Science* **1996**,273, 924.
- [17] W.L. Davis, C.P. McKay, *Origins of Life and Evolution of the Biosphere*, **1996**. 26,61.
- [18] <http://www.lpi.usra.edu/publications/slidesets/marslife/>
- [19] D. D. Wynn-Williams, H. G. M. Edwards, *Icarus*, **2000**, 144 (2),486.
- [20] S. K. Sharma , S. M. Angel, M. Ghosh H. W. Hubble , P. G. Lucey, *Appl. Spectrosc* , **2002**,56 (6),699.
- [21] S.E .Jorge Villar, H.G.M Edwards, *Anal. Bioanal. Chem*, **2006**, 384, 100.
- [22] .M. R. Sims. et al, *Beagle 2: A proposed Exobiology Lander for ESA's 2003 Mars Express Mission*, *SPIE Proceedings Series*, **1998**, 3441, 15-29
- [23] H. J. Cleaves , J.H. Chalmers , *Astrobiology*, **2004**,4(1),1.
- [24] J. S. Sinninghe Damste , J. W. De Leeuw , *Org. Geochem*, **1990**,16, 1077
- [25] H.P. Chiang , R. Song, Mou B; K.P.Chiang, P. Li, D.Wang ,W. S. Tse, L.T. Ho *Journal Raman spectrosc*, **1999**, 30, 551.

- [26] B. Schrader (Verlag Chemic Wemhelm), 4th ed, **1980**.
- [27] N. J. Bridge , D. Vincent , J. Chem. Soc., Faraday Trans, **1972**, 2 (68),152.
- [28] Bernhard Schrader , Appl. Spectrosc, **1991** , 45 (8), 1230
- [29] B. N. Cyvin , P. Klaeboe , J. C. Whitmer , S. J. Cyvin, Z. Naturforsch, **1982**, 37A. 251.
- [30] R. Mecke , K.Witt, Z. Naturforsch, **1966**, 21A, 1899 .
- [31] P. Ehrenfreund, S. P. Charnley , Annu.Rev.Astronphys, **2000**,38,427
- [32] L. d'Hendecourt, P. Ehrenfreund , Adv. Space Res, **1997**, 19,1023.
- [33] J. L. Puget , A. L'eger, Annu. Rev. Astron. Astrophys, **1989**, 27,161.
- [34] L.J.Allamandola, A. G. G. M. Tielens, J. R. Barker, AP. J. Suppl. Ser, **1989**, 71, 733
- [35] R.P.Bettens, E. Herbst, Astrophysical Journal. **1996**, 468,686.
- [36] R. I. Kaiser, K.Roessler, Astrophysical Journal. **1998**, 503,959.
- [37] E. L. O. Bakes, A. G. G. M. Tielens, Astrophysical Journal.**1994**, 427,822.
- [38] E. L. O. Bakes, A. G. G. M. Tielens , Astrophysical Journal.**1998**,499,258.
- [39] L. Becker, D. P. Glavin, J. L. Bada, Geochim. Cosmochim. Acta, **1997**, 61, 475.
- [40] J. Oro,BioAstronomy News, **1998**,10 (2), 1.
- [41] L. Becker, B. Popp, T. Rust, J. L. Bada, Earth Planet. Sci. Lett, **1999**, 167, 71.
- [42] J. L. Bada, D. P. Glavin, G. D. McDonald, L. Becker, Science, **1998**, 279, 362.
- [43] D.S. McKay, E.K. Gibson, K. L. Thomas-Keprta, H. Vali, C. S. Romanek, S. J. Clemett, Science , **1996**,273, 924.
- [44] S. J. Clemett, M. T. Dulay, J. S. Gillette, S.D.F.Chillier, T. B. Mahajan, R.N.Zare, Faraday Discuss, **1998**, 109,417.
- [45] S. J. Clemett, C. R. Maechling, R. N. Zare, P. D. Swan, R. M. Walker, Science, **1993**, 262, 721.

- [46] T. Stephan, D. Rost, E. K. Jessberger, A. Greshake, *Meteoritics Planet. Sci.*, **1998**, 33,A149.
- [47] E. K. Gibson, D. S. McKay, K. L. Thomas-Keprta, C. S. Romanek, *Scient. Am* , **1997**, 277, 58.
- [48] E. K. Gibson, D. S. McKay, K.L. Thomas-Keprta, *BioAstronomy News*, **1998**, 10 (3), 1.
- [49] G. J. Flynn, L. P. Keller, M. A. Miller, C. Jacobsen, S. Wirick, *Sci.*, XXIX , **1998**, 367.
- [50] A. J. T. Jull, J. W. Beck, G. S. Burr, I. A. Gilmour, M. A. Sephton, C. T. Pillinger, 62nd Meteoritical Society Meeting, Cape Town, South Africa, **1999**, 11.
- [51] P. R. Carey, *Biochemical Applications of Resonance Raman Spectroscopies*, Academic press **1982**.
- [52] R. L. McCreery, *Chemical Analysis: 'Raman Spectroscopy for Chemical Analysis'*, **2000**, 157
- [53] E. M. Newton, H. G. M. Edwards, D. W. Farwell, D. D. Wynn-Williams, *Proceedings of GeoRaman 99, 4th international Conference on Raman Spectroscopy Applied to the Earth Sciences, June 1999*, edited by F. Rull Perez, University of Valladolid press, [Imprenta Calatrava, Valladolid, Spain, **1999**, 69.
- [54] J. S. S. Damste, M. P. Koopmans, *Pure and applied chemistry*, **1997**, 69,2067.
- [55] D. D. Wynn-Williams, H. G. M. Edwards, E. M. Newton, J. M. Holder, *International Journal of Astrobiology*, **2002**, 1(1) ,39.
- [56] R. P. Sinha, M. Klisch, A. Groniger, D. P. Hader, *Journal of Photochemistry and Photobiology B: Biology*, **1998**, 47, 83.
- [57] H. G. M. Edwards, F. Garcia-Pichel, E. M. Newton, D. D. Wynn-Williams, *Spectrochimica Acta, Part A*, **1999**, 56,193.

[58] A.G. Cairns-Smith, *J. Theoretical Biology*, **1965**, 10, 53.

[59] A. G. Cairns-Smith and Hyman Hartman, *Clay minerals and the origin of life*
Cambridge University Press, **1986**

[60] J. P. Ferris, G. Ertem, *Science*, **1992**, 257, 1387.

[61] K. Joseph Prabakar¹, James P. Ferris, *Origins of Life and Evolution of Biospheres*,
1996, 26, 3-5, 251

CHAPTER 5

Effect of Raman spectrometer on the appearance of the Raman spectra

5.0 Pure compound samples

Raman spectra were obtained using three different spectrometers, two bench-top spectrometers and one portable spectrometer. The bench top spectrometers were a Bruker IFS 66 spectrometer with a FRA 106 FT Raman module and a Renishaw InVia Reflex dispersive Raman spectrometer. The portable spectrometer used was a Renishaw RX210 “Raman in a suitcase (RIAS)”

All the Raman spectra for the pure compounds recorded on the three instruments can be found in Appendix II of this study.

5.1 Renishaw Raman Spectrometer.

Raman spectroscopic analysis was carried out on the 11 compounds selected here ; spectra were collected using a Renishaw InVia Reflex dispersive Raman spectrometer (Renishaw plc, Wotton-under-Edge, UK). The substrates were excited with a 785 nm near-infrared diode laser. The laser beam was focused on the sample using a 5x objective lens, resulting in a laser spot of approximately 10 μm at the surface.

Spectra were obtained at 2 cm^{-1} resolution for a 10s exposure of the CCD detector in the region 100-3200 cm^{-1} using the extended scanning mode of the instrument. With 100% laser power, 5 accumulations were collected for the compounds. The total acquisition time of the spectrum of each compound was about eight minutes. Spectral acquisition, presentation, and data analysis were performed with the Renishaw WIRE 2 (Renishaw plc) and GRAMs AI version 8 (Galactic Industries, Salem, NH) software.

5.2 RIAS Raman Spectrometer

All 11 compounds were also analysed using the RIAS instrument, which has a 785 nm gallium-aluminium-arsenide (GaAlAs) diode laser. The probe was set on a stand facing directly down onto the sample. The sample was spread on a microscope slide and this was placed underneath the laser on a black surface. A shroud to prevent exterior light entering the experiment was then placed over the entire system. Samples were run for 5 accumulations of 5 seconds each. The power used was 1-100 mW with a spectral resolution of around 10 cm^{-1} .

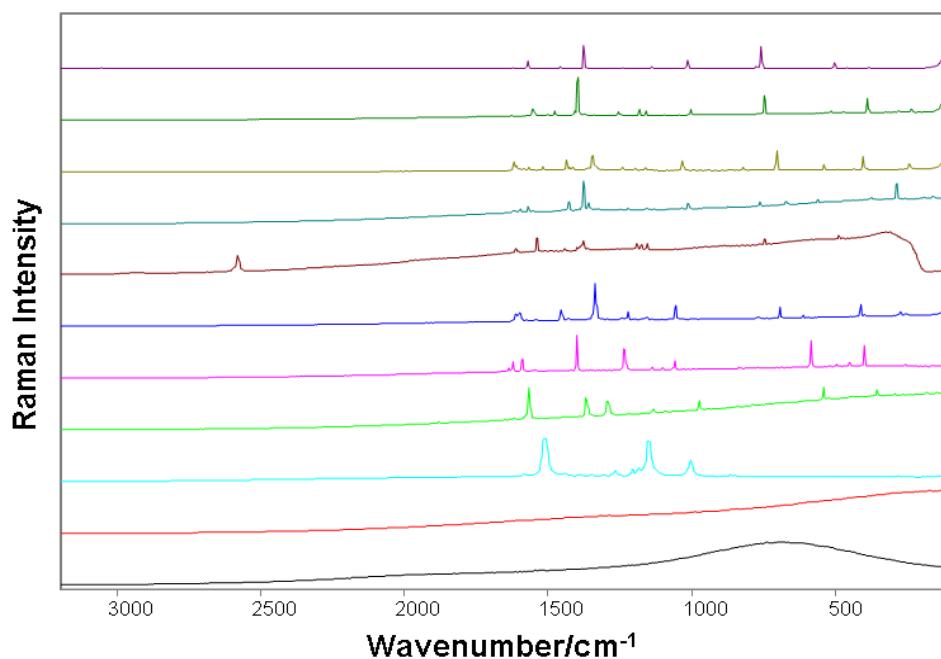


Figure 5.1 The 11 pure organic compounds run on the In Via Renishaw Raman spectrometer. Compounds from top to bottom are naphthalene, anthracene, phenanthrene, chrysene, tetracene, triphenylene, pyrene, and perylene, beta-carotene, usnic acid and chlorophyll a

5.3 Bruker FT Spectrometer

Raman spectra were recorded using a Bruker IFS 66/FRA 106 instrument with a Nd³⁺/YAG laser operating at 1064 nm and liquid nitrogen cooled InGaAs detector. Samples were held in an aluminium cup and placed in the sample holder facing the incident laser beam. 500 scans were accumulated at a spectral resolution of 4 cm⁻¹ with a spectral footprint of approximately 100 microns. The spectral wavenumber range was 3500-80 cm⁻¹. Daily checks of the interferometer, wavenumber and intensity calibration were undertaken by recording the Raman spectra of sulphur. The spectra were controlled by a PC using the instrument control software Bruker OpusTM.

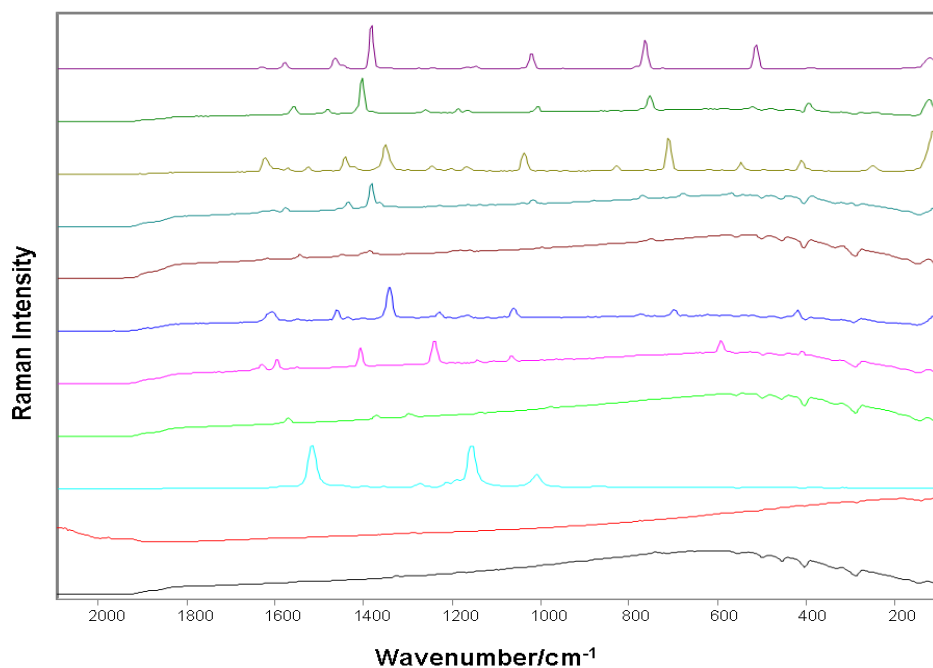


Figure 5.2 The 11 pure organic compounds run on the RIAS Raman spectrometer. Compounds from top to bottom are naphthalene, anthracene, phenanthrene, chrysene, tetracene, triphenylene, pyrene, and perylene, beta-carotene, usnic acid and chlorophyll a

Eleven pure compounds were run on the three machines. These compounds were:

- * Naphthalene 99%
- * Anthracene 99%
- * Phenanthrene 98%
- * Chrysene 98%
- * Tetracene 98%
- * Triphenylene 97%
- * Pyrene 99%
- * Perylene 99%
- * Beta carotene 97%
- * Usnic acid 98%
- * Chlorophyll a 96%

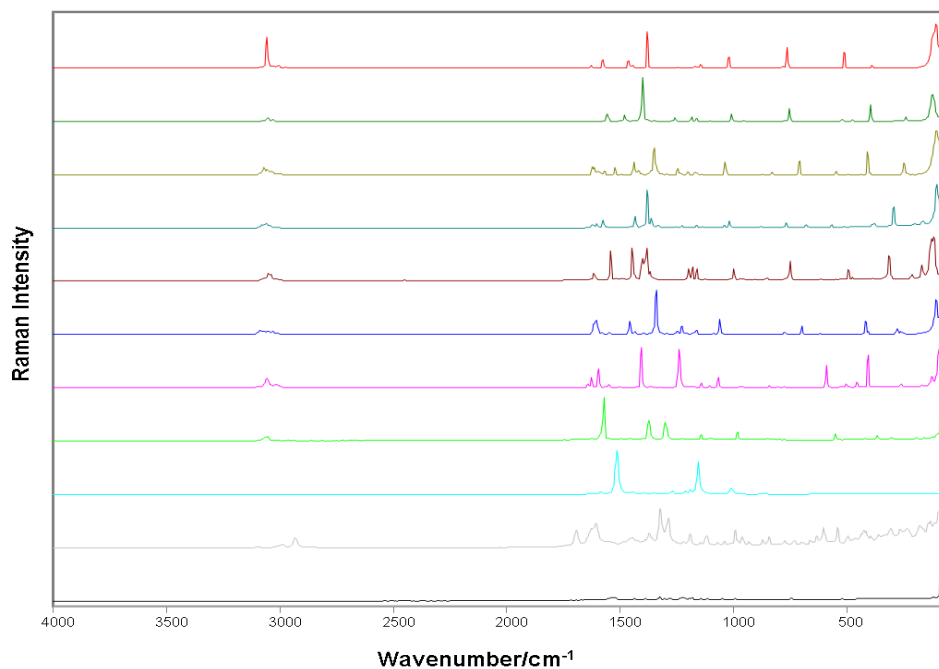


Figure 5.3 The 9 pure organic compounds run on the Bruker Raman spectrometer. Compounds from top to bottom are naphthalene, anthracene, phenanthrene, chrysene, tetracene, triphenylene, pyrene, and perylene, beta-carotene, usnic acid and chlorophyll a

The Raman spectra obtained from organic samples show that each compound has its own characteristic spectrum of vibrational Raman bands. This spectrum allows each compound to be distinguished from another and this forms the basis of the identification of key structural biomarkers for the discrimination between the Raman spectra of different materials (Figures 5.1-5.3). The Raman spectra of PAHs are similar as they have very similar fused benzene ring structures however; pyrene, tetracene and perylene fluoresce significantly whereas usnic acid and chlorophyll have but little fluorescence emission.

The compounds were run on all three instruments. It was observed that at 785 nm and 1064 nm, less fluorescence occurred with the PAH samples whereas lower wavelengths of excitation at 633 nm and 514 nm caused more fluorescence in the samples (see Chapter 8, part two).

5.4 Influence of Raman Spectrometer on the Raman spectra produced

The spectra from the three instruments have many similarities for most of the compounds studied here but the significant spectral features of each compound can be recorded on all three instruments. The peak values for all the spectra are shown in the next section of this chapter. The problem of fluorescence, compromising the spectra of usnic acid, chlorophyll, triphenylene, tetracene and perylene. A possible problem is noted in the lower resolution of the portable RIAS instrument where peaks often merge to produce broader features and the actual peak wavenumber value is then rather different compared with that given by the Bruker or the Renishaw instrument. It has been noted already that the Bruker detector seems to be much more sensitive to the region around 3000 cm^{-1} , than

either the Renishaw or RIAS, meaning that the C-H stretching peaks are much clearer on the spectra from the Bruker.

One of the major problems in identification of the compounds is sample fluorescence. Naphthalene and beta-carotene showed no fluorescence emission on any of the instruments. All the other compounds however fluoresced at least slightly on the RIAS, such as phenanthrene.

Fluorescence was minimized on the Bruker instrument at 1064 nm with the possible exception of usnic acid, chlorophyll, tetracene and perylene; this seems to be the best wavelength to avoid fluorescent interference [1]. Other methods of reducing fluorescence have been used, in the literature including UV-excitation [2] which allows the observation of resonance and photobleaching [3, 4] which is where the sample is lased for a period of time before the spectrum is run. Anthracene and triphenylene showed little if no fluorescence using the Renishaw at 785 nm. Pyrene, perylene and tetracene fluoresced but the spectra were still easy to analyse and identify.

5.5 Assignment of Raman spectra

Tentative assignments of the Raman spectra of the pure compounds are shown in the tables 5.1-5.11. The Raman shifts and relative intensities of the bands recorded with all three instruments are shown in the tables. In most cases, peaks match up in all three spectra. Spectral bands can sometimes merge in the others in the same spectra to give broader peaks. This is due to the different resolutions operating on the three instruments and applies particularly to the RIAS, which has a relatively poorer resolution. However, it has been shown from these spectra that the main identifying peaks for each compound can still be determined. The assignments of naphthalene, anthracene, phenanthrene,

tetracene, chrysene, triphenylene, pyrene, perylene, beta carotene, chlorophyll a and usnic acid have been made from previously reported assignments [5-24]

5.5.1 Naphthalene

The structure of naphthalene is shown in appendix I. It is a crystalline, aromatic, white, solid hydrocarbon with formula $C_{10}H_8$ (M.W 128.17052 g/mol) and has a structure comprising two fused benzene rings.

| Bruker | | Renishaw | | RIAS | | Assignment |
|-------------------------|-----|-------------------------|-----|-------------------------|-----|-------------------------------------|
| Wavenumber cm^{-1} | I | Wavenumber cm^{-1} | I | Wavenumber cm^{-1} | I | |
| 3055 | st | 3055 | w | | | CH stretching |
| 3036 | w | | | | | |
| 1628 | w | 1625 | w | 1626 | w | C=C stretching |
| 1576 | st | 1573 | st | 1578 | m | C=C stretching |
| 1463 | m | 1461 | m | 1464 | m | |
| 1381 | vst | 1379 | vst | 1383 | vst | C=C in plane vibration |
| 1238 | w | 1241 | w | 1238 | w | CCH deformation |
| 1146 | m | 1143 | m | 1146 | w | |
| 1020 | st | 1017 | st | 1021 | st | =C-H in plane deformation vibration |
| 763 | m | 760 | vst | 764 | st | CCC in-plane bending modes |
| 727 | w | 722 | vw | 726 | vw | |
| 512 | st | 505 | st | 514 | st | C-C ring deformations |
| 471 | w | 461 | w | 463 | w | |
| 391 | m | 388 | w | 390 | w | |
| | | | | | | |

* I = intensity, vst = very strong; st = strong; m = medium; w = weak and vw = very weak

Table 5.1 Raman spectral wavenumber (cm^{-1}) and band vibrational assignments for naphthalene from the Bruker, Renishaw and RIAS

The characteristic bands of this spectrum are those of CH stretching, C=C stretching, C=C in-plane vibration and C-H in-plane deformation vibration at 3055, 1576, 1381, and 1020 cm^{-1}

5.5.2 Anthracene

The structure of anthracene is shown in appendix I; it is a crystalline, aromatic, Colorless, solid hydrocarbon with formula $\text{C}_{14}\text{H}_{10}$ (M.W 178.23 g/mol) and consisting of three fused benzene rings.

| Bruker | | Renishaw | | RIAS | | |
|--------------------------------|-----|--------------------------------|-----|--------------------------------|-----|-------------------------------------|
| Wavenumber cm^{-1} | I | Wavenumber cm^{-1} | I | Wavenumber cm^{-1} | I | Assignment |
| | | | | | | |
| 3050 | m | 3053 | vw | | | C-H stretching |
| 3028 | m | 3026 | vw | | | C-H stretching |
| | | | | | | C=C stretching |
| 1557 | m | 1554 | m | 1559 | m | C=C stretching |
| | | 1502 | w | 1502 | w | |
| | | 1409 | w | | | |
| 1480 | m | | | 1482 | m | C=C stretching |
| | | | | | | |
| 1401 | vst | 1399 | vst | 1403 | vst | C=C in plane vibration |
| | | 1373 | w | | | |
| 1259 | m | 1256 | m | 1260 | m | =C-H in plane deformation vibration |
| 1186 | m | 1183 | m | 1187 | m | =C-H in plane deformation vibration |
| 1163 | m | 1160 | m | 1161 | m | =C-H in plane deformation vibration |
| 1007 | m | 1004 | m | 1007 | m | =C-H in plane deformation vibration |
| 955 | w | 952 | w | 953 | w | |
| 771 | w | 766 | w | | | |
| 752 | m | 749 | st | 753 | st | C-H out of plane |

| | | | | | | deformation vibration |
|-----|----|-----|----|-----|----|-----------------------|
| 520 | m | 516 | w | 522 | w | CCC bending |
| 477 | w | 473 | w | 481 | w | |
| 394 | st | 391 | st | 394 | st | CCC bending |
| 285 | w | 281 | w | | | |
| 242 | m | 238 | m | | | |
| | | | | | | |

* I = intensity, vst = very strong; st = strong; m = medium; w = weak and vw = very weak

Table 5.2 Raman spectral wavenumber (cm^{-1}) and band vibrational assignments for anthracene from the Bruker, Renishaw and RIAS

The characteristic bands of this spectrum are those of C-H stretching at 3050 cm^{-1} , C=C stretching at 1557 cm^{-1} , C=C in-plane vibration at 1401 cm^{-1} , C-H in-plane deformation vibration at 1007 cm^{-1} and C-H out-of-plane deformation vibration at 752 cm^{-1}

5.5.3 Phenanthrene

Phenanthrene is a tricyclic aromatic hydrocarbon (isomeric with anthracene). It is a white crystalline compound with formula $\text{C}_{14}\text{H}_{10}$ (M.W 178.23 g/mol) composed of three fused benzene rings. It is very similar to anthracene. The structure of phenanthrene is shown in appendix I

| Bruker | | Renishaw | | RIAS | | Assignment |
|--------------------------------|------|--------------------------------|------|--------------------------------|------|---------------------------------|
| Wavenumber cm ⁻¹ | I | Wavenumber cm ⁻¹ | I | Wavenumber cm ⁻¹ | I | |
| 3071 | st | 3071 | St | | | CH stretching |
| 3055 | m | 3055 | M | | | CH stretching |
| 3035 | m | 3035 | M | | | CH stretching |
| | | 1748 | W | | | |
| 1622 | m | 1620 | M | 1620 | m | C=C stretching vibration |
| 1613 | m,sh | 1613 | m,sh | 1608 | m,sh | C-C stretching |
| 1599 | w,sh | 1599 | w,sh | | | |
| 1569 | m | 1569 | W | 1570 | w | C-C stretching |
| 1523 | st | 1523 | M | 1523 | m | C-C stretching |
| 1440 | st | 1437 | St | 1439 | st | C-C stretching , HCC bending |
| 1429 | w,sh | 1429 | w,sh | 1429 | w,sh | C-C stretching , HCC bending |
| 1418 | m,sh | 1418 | m,sh | | | |
| 1349 | st | 1349 | St | 1348 | vst | C-C stretching , HCC bending |
| 1318 | w | 1318 | W | | | |
| 1245 | st | 1242 | St | 1244 | m | HCC bending |
| 1200 | m | 1200 | M | 1200 | w | C-C stretching , HCC bending |
| 1168 | m | 1168 | M | 1167 | w | C-C stretching |
| 1161 | w | 1161 | W | | | |
| 1036 | st | 1033 | St | 1035 | st | C-C stretching, HCC bending |
| 828 | m | 825 | M | 827 | m | |
| 710 | st | 706 | St | 709 | vst | HCCC out of plane bending |
| 547 | m | 543 | M | 546 | m | CCC bending |
| 498 | vw | 498 | Vw | | | |
| 442 | w | 442 | W | | | |
| 410 | st | 406 | St | 409 | st | CCC bending |
| 249 | m | 246 | M | 249 | m | |

* I = intensity, vst = very strong; st = strong; m = medium; w = weak; vw = very weak; sh = shoulder; w,sh = weak shoulder and m, sh = medium shoulder

Table5. 3 Raman spectral wavenumber (cm⁻¹) and band vibrational assignments for phenanthrene from the Bruker, Renishaw and RIAS

The characteristic bands of this spectrum are those of CH stretching at 3071 cm^{-1} , C-C stretching, HCC bending at 1440 cm^{-1} , 1349 and 1036 cm^{-1} , HCC bending at 1245 cm^{-1} and HCCC out-of-plane bending at 710 cm^{-1}

5.5.4 Tetracene

The structure of tetracene is shown in appendix I. Tetracene is a polycyclic hydrocarbon with four fused benzene rings in a rectilinear arrangement. It is yellow to orange hydrocarbon with formula $\text{C}_{18}\text{H}_{12}$ (M.W 228.29 g/mol).

| Bruker | | Renishaw | | RIAS | | Assignment |
|-----------------------------|------|-----------------------------|------|-----------------------------|----|--------------------------------------|
| Wavenumber cm^{-1} | I | Wavenumber cm^{-1} | I | Wavenumber cm^{-1} | I | |
| 3050 | m | | | | | =C-H stretching |
| 1630 | w,sh | | | | | |
| 1616 | m | 1614 | M | 1618 | m | C=C stretching |
| 1606 | w,sh | 1605 | w,sh | | | |
| 1542 | st | 1540 | St | 1542 | st | C-C or ring stretching |
| 1517 | w | 1517 | W | | | |
| 1490 | w | | | | | |
| 1447 | st | 1445 | St | 1449 | st | C-C stretching vibrations |
| 1403 | m | 1400 | M | | | Skeletal ring vibration |
| 1384 | st | 1381 | St | 1386 | st | C=C in plane vibration |
| 1368 | w | 1364 | W | | | |
| 1197 | m | 1194 | M | 1198 | m | C-H in plane |
| 1180 | m | 1181 | M | 1181 | m | = C-H in plane deformation vibration |
| 1160 | m | 1157 | M | 1161 | m | = C-H in plane deformation vibration |

| | | | | | | |
|-----|----|-----|---|-----|---|--|
| 997 | m | 994 | m | 997 | w | = C-H in plane deformation vibration |
| 973 | w | | | | | |
| 960 | w | | | | | |
| 851 | w | | | | | C-H out of plane deformation vibration |
| 751 | m | 748 | M | 751 | m | CCC ring deformations |
| 494 | m | 491 | M | | | C-C deformation vibration |
| 314 | st | 311 | M | | | CCC ring deformations |
| 213 | w | | | | | |

* I = intensity, st = strong; m = medium; w = weak and w, sh = weak shoulder

Table 5.4 Raman spectral wavenumber (cm^{-1}) and band vibrational assignments for tetracene from the Bruker, Renishaw and RIAS

The characteristic bands of this spectrum are those of a C-C stretching at 1542 and 1447 cm^{-1} , C=C in-plane vibration at 1384 cm^{-1} , CCC ring deformations at 751 cm^{-1} and C-H in-plane deformation at 1197 cm^{-1} .

5.5.5 Chrysene

The structure of chrysene is shown in appendix I. Chrysene is a polycyclic aromatic hydrocarbon (PAH) with the molecular formula $C_{18}H_{12}$ (M.W 228.28 g/mol) and consists of four fused benzene rings.

| Bruker | | Renishaw | | RIAS | | Assignment |
|-------------------------|----|-------------------------|----|-------------------------|----|--------------------------|
| Wavenumber cm^{-1} | I | Wavenumber cm^{-1} | I | Wavenumber cm^{-1} | I | |
| 3078 | w | | | | | C-H stretching |
| 3062 | w | 3063 | vw | | | C-H stretching |
| 1621 | w | 1621 | vw | 1624 | w | C-C stretching |
| 1601 | w | 1599 | w | 1603 | w | |
| 1574 | m | 1573 | m | 1576 | w | C-C stretching |
| 1432 | m | 1430 | m | 1435 | m | C-C stretching |
| 1381 | st | 1379 | st | 1383 | st | C-C stretching |
| 1363 | m | 1361 | m | 1365 | m | C-C stretching |
| 1331 | w | 1330 | w | 1330 | w | |
| 1228 | w | 1226 | w | 1229 | w | |
| 1162 | w | 1159 | w | 1163 | w | C-C stretching |
| 1137 | w | 1134 | w | 1137 | w | |
| 1041 | w | 1039 | w | 1041 | w | |
| 1017 | m | 1015 | m | 1018 | m | C-H in plane bending |
| 878 | w | 875 | w | 878 | w | C-H Out of plane bending |
| 769 | w | 766 | w | 770 | m | |
| 678 | w | 675 | w | 678 | m | |
| 567 | w | 563 | w | 569 | w | |
| 381 | w | 376 | w | | | |
| 294 | m | 289 | st | | | CCC out of plane bending |

* I = intensity, st = strong; m = medium; w = weak and vw = very weak

Table 5.5 Raman spectral wavenumber (cm^{-1}) and band vibrational assignments for chrysene from the Bruker, Renishaw and RIAS

The characteristic bands of this spectrum are those of C-C stretching at 1574 and 1381 cm^{-1} , C-H in-plane bending at 1017 cm^{-1} and C-H out-of-plane bending at 878 cm^{-1} .

5.5.6 Triphenylene

The structure of triphenylene is shown in appendix I. Triphenylene is a flat polycyclic aromatic hydrocarbon (PAH) consisting of four fused benzene rings with the molecular formula $\text{C}_{18}\text{H}_{12}$ (M.W 228.3 g/mol). The structure of triphenylene is composed only of full benzene rings interconnected by carbon-carbon single bonds. The three benzene rings can be drawn as the three outer rings, with the central ring formed by one face of each and the three carbon-carbon single bonds.

| Bruker | | Renishaw | | RIAS | | |
|--------------------------------|----|--------------------------------|----|--------------------------------|----|-------------------------|
| Wavenumber cm^{-1} | I | Wavenumber cm^{-1} | I | Wavenumber cm^{-1} | I | Assignment |
| 3085 | w | | | | | C-H stretching |
| 3050 | w | | | | | C-H stretching |
| 3030 | w | | | | | C-H stretching |
| 1615 | m | 1614 | M | | | C-C stretching |
| 1604 | m | 1602 | M | 1607 | m | C-C stretching |
| 1579 | w | 1577 | W | 1577 | w | |
| 1547 | w | 1544 | W | 1545 | w | |
| 1458 | m | 1456 | M | 1460 | m | C-C stretching |
| 1434 | w | 1431 | W | 1434 | w | |
| 1394 | vw | 1393 | Vw | | | |
| 1340 | st | 1337 | St | 1340 | st | C-C stretching |
| 1298 | w | 1296 | W | 1298 | w | |
| 1246 | w | 1244 | W | | | |
| 1228 | m | 1226 | M | 1229 | m | C-H in plane bending |

| | | | | | | |
|------|------|------|------|------|---|----------------------------|
| 1162 | w | 1160 | W | 1162 | w | |
| 1061 | m | 1058 | St | 106 | m | C-H in plane bending |
| 775 | w | 773 | W | 772 | w | |
| 698 | m | 695 | St | 696 | m | C-H out of plane bending |
| 619 | w | 615 | W | | | |
| 418 | m | 414 | St | 419 | m | C-C-C out of plane bending |
| 407 | w,sh | 403 | w,sh | | | |
| 281 | w | 277 | M | | | |
| 263 | w,sh | 259 | w,sh | | | |

* I = intensity, st = strong; m = medium; w = weak; vw = very weak and w,sh = weak shoulder

Table 5.6 Raman spectral wavenumber ν (cm^{-1}) and band vibrational assignments for triphenylene from the Bruker, Renishaw and RIAS

The characteristic bands of this spectrum are those of C-C stretching at 1604 and 1340 cm^{-1} , C-H in-plane bending at 1061 cm^{-1} and C-H out-of-plane bending at 698 cm^{-1} .

5.5.7 Pyrene

The structure of pyrene is shown in appendix I .Pyrene is a colourless solid polycyclic aromatic hydrocarbon that consists of four fused benzene rings, resulting in a flat aromatic system with the molecular formula $\text{C}_{16}\text{H}_{10}$ (M.W 202.25 g/mol). It is the smallest peri-fused polycyclic aromatic hydrocarbon i.e. one where the rings are fused through more than one face.

| Bruker | | Renishaw | | RIAS | | Assignment |
|--------------------------------|----|--------------------------------|----|--------------------------------|----|---|
| Wavenumber cm ⁻¹ | I | Wavenumber cm ⁻¹ | I | Wavenumber cm ⁻¹ | I | |
| 3054 | m | 3057 | vw | | | CH stretching |
| 3014 | w | | | | | |
| 1642 | w | 1641 | w | | | CC stretching |
| 1627 | m | 1625 | m | 1629 | m | CCH stretching |
| 1594 | m | 1591 | m | 1596 | m | CCH stretching |
| 1549 | w | 1547 | w | 1550 | w | |
| 1406 | st | 1403 | st | 1407 | st | C=C in plane vibration, Skeletal ring vibrations |
| 1240 | st | 1238 | st | 1240 | st | CH bending |
| 1142 | m | 1140 | w | 1143 | w | CH bending |
| 1107 | w | 1104 | w | 1105 | w | |
| 1065 | w | 1063 | m | 1066 | m | CH bending |
| 840 | w | 838 | w | | | |
| 804 | w | 801 | vw | | | |
| 592 | m | 588 | st | 592 | st | CCC ring deformation |
| 503 | w | 500 | w | | | |
| 457 | w | 453 | w | | | |
| 407 | st | 403 | st | 409 | m | |
| 262 | w | 257 | w | | | |
| | | | | | | |

* I = intensity st = strong; m = medium; w = weak and vw = very weak

Table 5. 7 Raman spectral wavenumber ν (cm⁻¹) and band vibrational assignments for pyrene from the Bruker, Renishaw and RIAS

The characteristic bands of this spectrum are those of CCH stretching at 1627 cm⁻¹, C=C in-plane vibration, skeletal ring vibrations at 1406 cm⁻¹ and CH bending at 1240 cm⁻¹.

5.5.8 Perylene

The chemical structure of Perylene is shown in appendix I. Perylene is a polycyclic aromatic hydrocarbon (PAH) with the molecular formula $C_{20}H_{12}$ (M.W 252.31 g/mol) consisting of five fused benzene rings and occurring as a brown solid.

| Bruker | | Renishaw | | RIAS | | |
|-------------------------|------|-------------------------|-----|-------------------------|----|----------------------------|
| Wavenumber cm^{-1} | I | Wavenumber cm^{-1} | I | Wavenumber cm^{-1} | I | Assignment |
| 3062 | m | | | | | C-H stretching |
| 3052 | m | | | | | C-H stretching |
| 3008 | w,sh | | | | | |
| | | 1882 | W | | | |
| 1622 | w | 1620 | W | 1620 | vw | |
| 1569 | vst | 1567 | Vst | 1570 | st | C-C stretching |
| 1494 | w | | | | | |
| 1446 | w | 1450 | W | | | |
| 1372 | st | 1371 | St | 1371 | st | C-C stretching |
| 1297 | st | 1295 | St | 1297 | st | C-C stretching |
| 1222 | w | 1220 | W | | | |
| 1140 | m | 1138 | M | 1140 | w | C-H in plane bending |
| 1101 | w | 1099 | W | | | |
| 1046 | vw | 1036 | Vw | | | |
| 979 | st | 976 | St | 976 | m | C-H out of plane bending |
| 845 | w | 842 | W | | | |
| 795 | w | 791 | W | | | |
| 549 | st | 545 | St | 545 | w | C-C-C out of plane bending |
| 532 | w | 527 | W | | | |
| 450 | w | 446 | W | | | |
| 418 | w | 413 | W | | | |
| 363 | st | 359 | St | 366 | w | C-C-C out of plane bending |
| 301 | w | 296 | W | | | |
| 192 | w | 187 | W | | | |

* I = intensity, vst = very strong; st = strong; m = medium; w = weak; vw = very weak and w, sh =weak shoulder

Table 5.8 Raman spectral wavenumber (cm^{-1}) and band vibrational assignments for perylene from the Bruker, Renishaw and RIAS

The characteristic bands of this spectrum are those of C-C stretching at 1569 cm^{-1} , C-C stretching at 1372 cm^{-1} , C-H in-plane bending at 1140 cm^{-1} and C-H out-of-plane bending at 979 cm^{-1} .

5.5.9 Beta-carotene

The chemical structure of beta-carotene is shown in appendix I. Beta-carotene is the molecule that gives carrots their orange colour. It is part of a family of chemicals called the carotenoids and has the molecular formula $\text{C}_{40}\text{H}_{56}$ (M.W 536.87g/mol).

| Bruker | | Renishaw | | RIAS | | Assignment |
|-----------------------------|-----|-----------------------------|-----|-----------------------------|-----|--|
| Wavenumber cm^{-1} | I | Wavenumber cm^{-1} | I | Wavenumber cm^{-1} | I | |
| 1586 | w | 1584 | w | 1586 | w | |
| 1513 | vst | 1516 | vst | 1516 | vst | in-phase ν (C=C) |
| 1353 | w | 1351 | w | 1353 | w | |
| 1270 | w | 1272 | w | 1274 | w | |
| 1210 | w | 1212 | w | 1214 | w | |
| 1190 | w | 1188 | w | 1189 | w | |
| 1156 | st | 1157 | vst | 1161 | vst | ν (C-C) Stretching vibrations |
| 1008 | m | 1005 | m | 1008 | m | in-plane rocking modes of (C-CH ₃) |
| | | | | | | |

* I = intensity, vst = very strong, m = medium and w = weak

Table 5.9 Raman spectral wavenumber (cm^{-1}) and band vibrational assignments for beta carotene from the Bruker, Renishaw and RIAS

The characteristic bands of this spectrum are those of ν (C=C) at 1513 cm^{-1} , ν (C-C) at 1156 cm^{-1} and δ (C-CH₃) modes at 1008 cm^{-1}

5.5.10 Usnic acid

The structure of usnic acid is shown in appendix I. Usnic acid is a bitter, yellow, solid substance with formula C₁₈H₁₆O₇ (M.W 344.315 g/mol).

| Bruker | | Renishaw | | RIAS | | |
|--------------------------------|-----|--------------------------------|-----|--------------------------------|----|--|
| Wavenumber cm^{-1} | I | Wavenumber cm^{-1} | I | Wavenumber cm^{-1} | I | Assignment |
| 3002 | w | - | - | - | - | ν (CH) aromatic |
| 3091 | w | - | - | - | - | ν (CH) aromatic |
| 3012 | w | - | - | - | - | |
| 2985 | w | - | - | - | - | ν (CH ₃) asymmetric |
| 2931 | m | - | - | - | - | ν (CH ₃) asymmetric |
| 2869 | w | - | - | - | - | ν (CH ₃) symmetric |
| 1694 | m | 1693 | w | 1692 | vw | ν (C=O) conjugated cyclic ketone |
| 1626 | msh | 1629 | wsh | - | - | ν (C=O) aromatic ketone |
| 1607 | st | 1608 | w | 1607 | vw | Quadrant ring stretch |
| 1553 | vw | - | - | - | - | ν (C=C) aromatic |
| 1486 | vw | - | - | - | - | |
| 1457 | wsh | - | - | - | - | δ (CH ₂ ,CH ₃) |
| 1444 | w | - | - | - | - | |
| 1422 | w | - | - | - | - | |
| 1390 | wsh | - | - | - | - | |

| | | | | | | |
|------|-----|------|----|------|----|-------------------------------|
| 1372 | w | - | - | - | - | |
| 1358 | wsh | - | - | - | - | |
| 1322 | st | 1322 | w | 1323 | w | Ring stretch |
| 1289 | st | 1287 | w | 1289 | w | v (COC) as aryl alkyl ether |
| 1220 | w | - | - | - | - | |
| 1192 | w | 1191 | vw | 1191 | w | δ (OH) phenyl in plane |
| 1144 | w | - | - | - | - | |
| 1119 | w | 1117 | w | - | - | |
| 1071 | w | - | - | - | - | v (COC) as aryl alkyl ether |
| 1040 | w | - | - | - | vw | |
| 992 | w | 991 | vw | 990 | - | |
| 959 | w | 956 | vw | - | - | |
| 845 | w | 843 | vw | 842 | w | |
| 773 | w | - | - | - | - | |
| 602 | w | 600 | w | - | - | |
| 541 | w | 540 | w | - | -- | |
| 498 | w | 495 | w | - | - | |
| 415 | w | 416 | w | 415 | w | |
| | | | | | | |

* I = intensity, w = weak; vw = very weak; sh = shoulder; w,sh = weak shoulder

Table 5.11 Raman spectral wavenumber (cm^{-1}) and band vibrational assignments for usnic acid from the Bruker, Renishaw and RIAS

The characteristic bands of this spectrum are those of a v (C=O) conjugated cyclic ketone at 1694 cm^{-1} , quadrant ring stretch at 1607 cm^{-1} , ring stretch at 1322 cm^{-1} and 1289 cm^{-1} , due to v (COC) as an aryl alkyl ether.

5.5.11 Chlorophyll a

The chemical structure of chlorophyll a is shown in appendix I. Chlorophyll absorbs light most strongly in the blue and red but poorly in the green portions of the electromagnetic spectrum, hence the green colour of chlorophyll. It has the molecular formula $C_{55}H_{72}MgN_4O_5$ (M.W 893.49 g/mol).

| Bruker | | Renishaw | | RIAS | | Assignment |
|----------------------|---|----------------------|----|----------------------|---|----------------|
| Wavenumber cm^{-1} | I | Wavenumber cm^{-1} | I | Wavenumber cm^{-1} | I | |
| | | | | | - | |
| 1601 | w | - | | - | - | |
| 1530 | w | 1537 | w | 1532 | w | ν (C-C) |
| 1385 | w | 1355 | w | - | - | |
| 1324 | w | 1320 | vw | 1323 | w | ν (C-N) |
| 1227 | w | - | - | - | - | |
| 1219 | w | - | - | - | - | Ring vibration |
| 1183 | w | - | - | 1184 | w | Ring breathing |
| 1140 | w | 1141 | vw | - | - | |
| 1117 | w | - | - | - | - | |
| 743 | w | 741 | w | 741 | w | Ring breathing |
| 522 | w | - | - | - | - | |
| | | | | | | |

* I = intensity, w = weak, vw = very weak

Table 5.11 Raman spectral wavenumber (cm^{-1}) and band vibrational assignments for chlorophyll a from the Bruker, Renishaw and RIAS

The characteristic bands of this spectrum are those of a ν (C-C) at 1530 cm^{-1} , ν (C-N) at 1324 cm^{-1} and ring breathing at 743 cm^{-1} .

5.6 Conclusions

All the pure compounds analysed have different spectra, although in several cases there are similarities, they can all be distinguished from each other in Raman spectra. The choice of excitation wavelength is important, especially when fluorescence can interfere. The use of the Bruker spectrometer would be recommended if the analysis of the C-H stretch region is important due to the increased intensity of these peaks on the Bruker compared to the other two spectrometers. However, if speed is of greater importance then both Renishaw spectrometers seem useful, the RIAS being much faster but at the expense of peak resolution.

5.7 References

- [1] C. M. Hodges, P. J. Hendra, H. A. Willis, T. Farley, *Journal of Raman Spectroscopy*, **1989**, 20,745.
- [2] W. Vincent, Couling, Peer Fischer, David Klenerman, and Walter Huber, *Biophysical Journal*, **1998**, 75 (2),1097.
- [3] J. S. Day, H. G. M. Edwards, S. A. Dobrowski, A. M. Voice, *Spectrochimica Acta Part A*, **2004**, 60,563.
- [4] J. S. Day, H. G. M. Edwards, S. A. Dobrowski, A. M. Voice, *Spectrochimica Acta Part A*, **2004**, 60 (8-9),1725.
- [5] M. Z. Tabrizi, S. F. Tayyari, F. Tayyari, M. Behforouz, *Spectrochimica Acta part A*, **2004**,60(1-2),111.
- [6] J. Godec, L. Colombo, *Journal of Chemical physics*, **1976**, 66 (11), 4693 .

- [7] H. G. M. Edwards, S. E. Jorge Villar, J. Jehlicka, T. Munshi, *Spectrochim Acta A*, **2005**, 61, 2273.
- [8] R. L. McCreery, *Raman Spectroscopy for Chemical Analysis*. John Wiley & Sons: New York, **2000**
- [9] I. B. Berlman, *Handbook of Fluorescence Spectra of Aromatic Molecules*, Academic Press, New York, **1971**.
- [10] M. Delhaye, J. Barbillat, J. Aubard, M. Bridoux, E. Da Silva, in: Turrell G Corset.J (Ed.), *Raman Microscopy: Developments and Applications*, Academic Press, London, **1996**.
- [11] D. Lin-Vien, J. G. Grasselli, N. B. Colthup, W. G. Fateley, *The Handbook of Infrared and Raman Characteristic Frequencies of Organic Molecules*, chapter 11, Academic Press, **1991**
- [12] G. Socrates, *Infrared Characteristic Group Frequencies: Tables and Charts* (Third ed.), John Wiley & Sons Ltd., New York, **2001**.
- [13] J. Jehlicka, H. G. M. Edwards, S. E. Jorge Villar, O. Frank, *Journal of Raman Spectroscopy*, **2006**, 37,220 .
- [14] J.Jehlicka, H.G.M.Edwards, *Organic Geochemistry*, **2008**, 39,371.
- [15] J. Jehlicka, H. G. M. Edwards, P. Vitek, *Planetary and space Science*, **2009**, 57 606.
- [16] Yek Tann Chua and Peter C. Stair. *Journal of Catalysis*, **2003**,213, 39 .
- [17] W. Charles , Jr.,Bauschlicher, R. Stephen , Langhoff, A. Scott , Sandford. *Journal of Chemical physics. A* ,**1997**,101, 2414.
- [18]L. J. Allamandola, A. G. G. M. Tielens, J. R. Barker, *The Astrophysical Journal Supplement Series*, **1989**,71, 733.
- [19] D. Gill, R.G. Kilponen ,L. Rimai, *Nature*,**1970**, 227, 743.
- [20] J.C. Merlin, *Pure Appl. Chem*, **1985**,57,785.

- [21] L. J. Allamandola, in IAU Symposium 135, Interstellar Dust, eds. L. J. Allamandola, A. G. G. M. Tielens (Kluwer, Dordrecht), **1989**, 129.
- [22] M. Veronelli, G. Zerbi, Journal of Raman Spectroscopy, **1995**, 26, 683.
- [23] R. J. Weesie, J. C. Merlin, J. Lugtenburg, G. Britton, F. J. H. M. Jansen, J. P. Cornard, Biospectroscopy, **1999**, 5, 19.
- [24] H. G. M. Edwards, E. M. Newton, D. D. Wynn-Williams, J. Mol. Struct., **2003**, 27, 651.

CHAPTER 6

Evaluation of simulates for the Raman spectroscopic characterization of biomolecular degradation products in geological matrices: organic compounds under calcite and gypsum

6.1 Introduction

Raman spectroscopy is currently part of the instrumentation suite of the ESA Exomars mission for the remote detection of life signatures in the Martian surface and subsurface. Terrestrial analogues of Martian sites have been identified and the biogeological modifications incurred as a result of extremophilic activity have been studied. Raman spectroscopy has been proposed as a valuable analytical technique for environmental and planetary exploration because it is sensitive to organic and inorganic compounds and able to clearly identify key spectral markers in a mixture of biological and geological compounds; also, sample manipulation is not required and any size of sample can be studied without chemical or mechanical preparation [1, 2].

Astrobiology aims at identifying the pathways through which life arose, evolved, and may have been distributed throughout the universe. With the ability to expose microorganisms to the space environment in a controlled manner [1] the opportunity has arisen to explore questions related to the hypothesis of interplanetary transfer of life [2]. Possible mechanisms of interplanetary transfer include spacecraft, or natural mechanisms such as meteorites, comets or interplanetary dust particles. Interplanetary transfer of life is particularly relevant with regard to Mars and Earth because it is thought that the meteorites traveled from Mars to Earth, and possibly meteorites from Earth traveled to Mars, providing a pathway for the transport of biological material between these two planets [3, 4].

Polycyclic aromatic hydrocarbons (PAHs) have been the subject of well-documented study because of their carcinogenic effect, widespread environmental pollution. They are produced daily in great quantities by incomplete combustion of carbonaceous materials. Significant efforts have been expended to devise techniques for the identification and quantification of PAHs in water, and they are common constituents of complex mixtures

such as automobile exhausts, crude oil, cigarettes, coal, and have been found at significant levels in the atmosphere, waterways and food chains [5].

Polycyclic aromatic hydrocarbons are found to be a component of organic matter in space [6]. Their contribution is invoked in a broad spectrum of astronomical observations that range from the ultraviolet to the far-infrared and cover a wide variety of objects and environments from meteorites and interplanetary dust particles to outer Solar System bodies and to the interstellar medium in the local Milky Way.

Polycyclic aromatic hydrocarbons are believed to be the most abundant free organic molecules in space [7, 8]. Electron delocalization over their carbon skeleton makes them remarkably stable. PAH molecules are produced partly in the outer atmospheres of carbon stars or formed by shock fragmentation of carbonaceous solid material. PAHs may eventually also form in the diffuse interstellar gas by neutral-neutral atom reactions [9] or by the energetic processing of specific ices in dense clouds [10]. PAHs play a central role in the gas phase chemistry [11, 12]. The environmental conditions and the local ultraviolet radiation field determine their charge and hydrogenation state [13].

The need to identify and determine these compounds has led to the establishment of methods that allow for the simultaneous determination of as many PAHs as possible.

In secondary lichen metabolites, the dibenzofuran derivative usnic acid has been without a doubt the most extensively studied. Lichens are formed through the symbiosis between fungi and algae.

Usnic acid is widely distributed in species of *Cladonia* (Cladoniaceae), *Usnea* (Usneaceae), *Lecanora* (Lecanoraceae), *Ramalina* (Ramalinaceae), *Evernia*, *Parmelia* (Parmeliaceae) and other lichen genera. *Alectoria* (Alectoriaceae) species are often rich sources of usnic acid, and yields of up to 6% have been reported [14]. In the literature,

usnic acid has been quoted as being present in *Cetraria islandica* (Parmeliaceae), commonly known as Iceland moss or *Lichen islandicus*.

Although usnic acid has only been identified in lichens, closely related compounds have been found in fungi, e.g. the phytotoxin mycousnine and similar compounds in *Mycosphaerella nawae* [15] and cercosporamide and usnic acid amide in *Cercosporidium henningsii* [16].

Raman spectroscopy is sensitive to molecular skeletal structures: characteristic wavenumber indicate bond orders, branching of chains, saturated and aromatic rings, and their substitution pattern [17]. However, fluorescence emission is frequently observed from impurities and common by-products and often even of the main components.

The present work reports a Raman spectroscopic study of several pure fused ring organic aromatic compounds observed under crystalline calcite and gypsum, in the solid state, using confocal microspectroscopy for the detection and identification of features which are important in environmental chemistry and astrobiology. A similar study was undertaken of mixtures of relevant PAH material to assess the potential of Raman for the discrimination between specific molecular structure.

The capability of Raman spectroscopy for the detection of minerals and organic compounds in mixtures has led to adoption by the European Space Agency (ESA) as part of a life-detection instrumental suite to be sent to Mars for the ExoMars project.

6.2 Experimental

6.2.1 Compound Samples

Anthracene, phenanthrene, naphthalene, tetracene, chrysene, pyrene, triphenylene and usnic acid were supplied by Sigma-Aldrich (UK) and ALFA AESAR (UK). All the compounds were used as received.

Samples of crystalline calcite (calcium carbonate, CaCO_3) and crystalline gypsum (calcium sulphate, $\text{CaSO}_4 \cdot 2\text{H}_2\text{O}$) were kindly supplied by Prof Howell Edwards from a geological mineral collection.

6.2.2 Compounds Mixture

Anthracene, phenanthrene and naphthalene were mixed together similar tetracene, chrysene, pyrene and triphenylene were mixed together. Sample mixtures were made up by mixing known amounts of the compounds, followed by grinding in an agate mortar and pestle to ensure sample homogeneity by thorough mixing of components.

6.2.3 Dispersive Raman microscopy

Raman spectra were collected using a Renishaw InVia Reflex dispersive Raman spectrometer (Renishaw plc, Wotton-under-Edge, UK). Excitation was effected using a 785 nm near-infrared diode laser. The laser beam was focused on the sample by a 5x objective lens, resulting in a laser spot of approximately 10 μm at the surface.

Spectra were obtained at 2 cm^{-1} resolution for 10s exposure of the CCD detector in the region 100-3200 cm^{-1} using the extended scanning mode of the instrument with 100% laser power and 5 accumulations were collected for the compounds. The total acquisition

time of each spectrum was therefore about eight minutes. Spectral acquisition, presentation, and analysis were performed with the Renishaw WIRE 2 (Renishaw plc) and GRAM AI version 8 (Galactic Industries, Salem, NH) software.

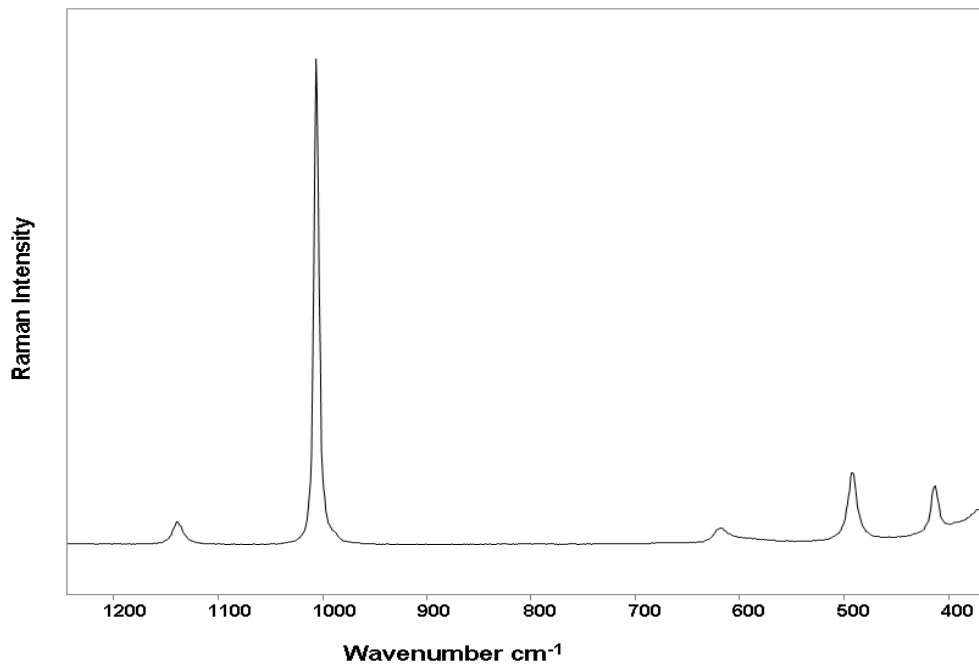


Figure 6.1 The Raman spectra of gypsum obtained with 785 nm excitation

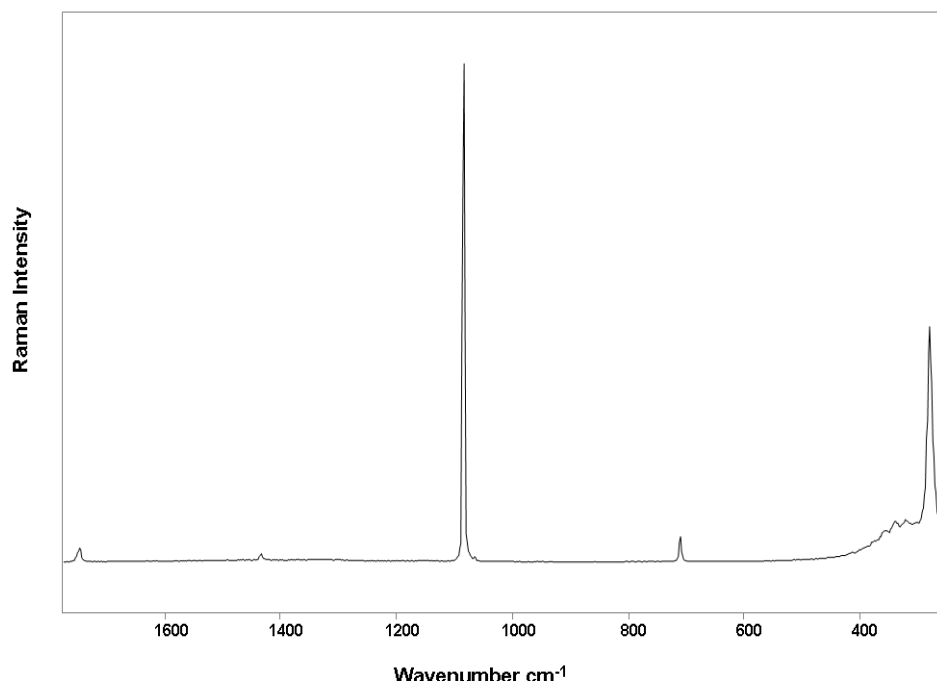


Figure 6.2 The Raman spectra of calcite obtained with 785 nm excitation

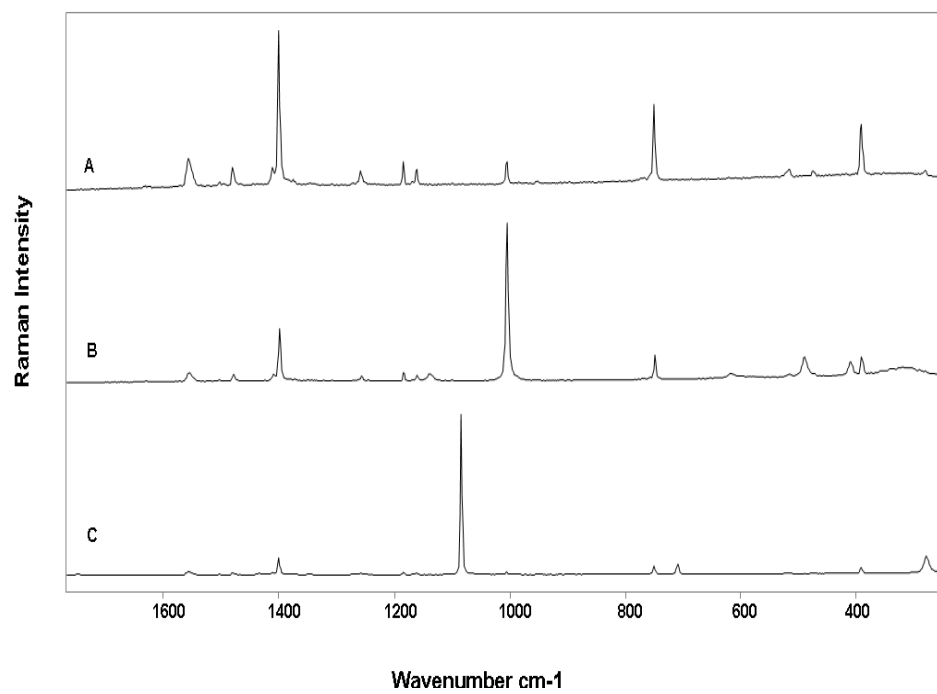


Figure 6.3 Raman spectra of (a) pure anthracene, (b) anthracene under gypsum and (c) anthracene under calcite

6.3 Result and Discussion

6.3.1 Calcite and gypsum

The Raman spectrum of calcite presents two strong bands at 1086 cm^{-1} assigned to the $\nu(\text{CO}_3)^{2-}$ Stretch and 278 cm^{-1} (Lattice mode) and two medium sharp bands at 1747 and 708 cm^{-1} (bending mode). Also, the gypsum spectrum contains one strong peak at 1002 cm^{-1} assigned to the symmetric sulfate stretching [$\nu(\text{SO}_4)^{2-}$] and four weaker peaks at 1138 cm^{-1} which is asymmetric sulfate stretching, 615 cm^{-1} [symmetric deformation], 488 cm^{-1} [symmetric deformation] and 410 cm^{-1} as shown in figure 6. 1 and 6.2. [18, 19].

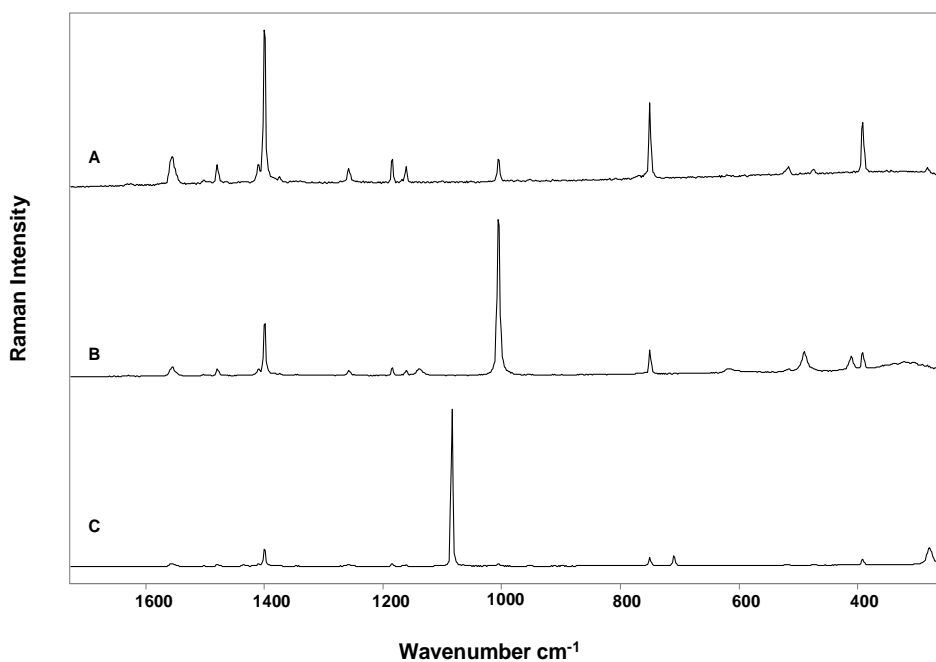


Figure 6.4 Raman spectra of (a) pure phenanthrene, (b) phenanthrene under gypsum and (c) phenanthrene under calcite

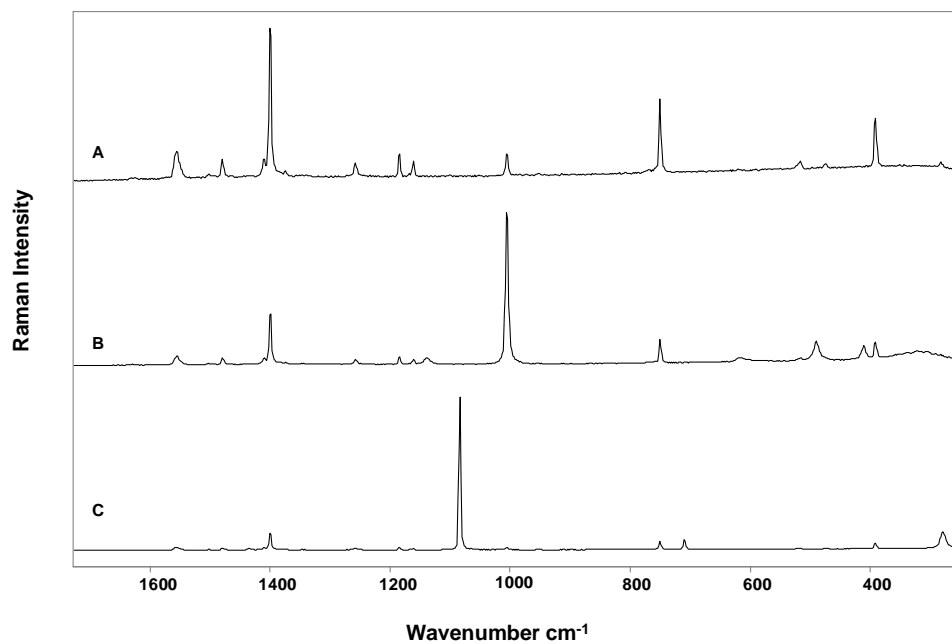


Figure 6.5 Raman spectra of (a) pure naphthalene, (b) naphthalene under gypsum and (c) naphthalene under calcite

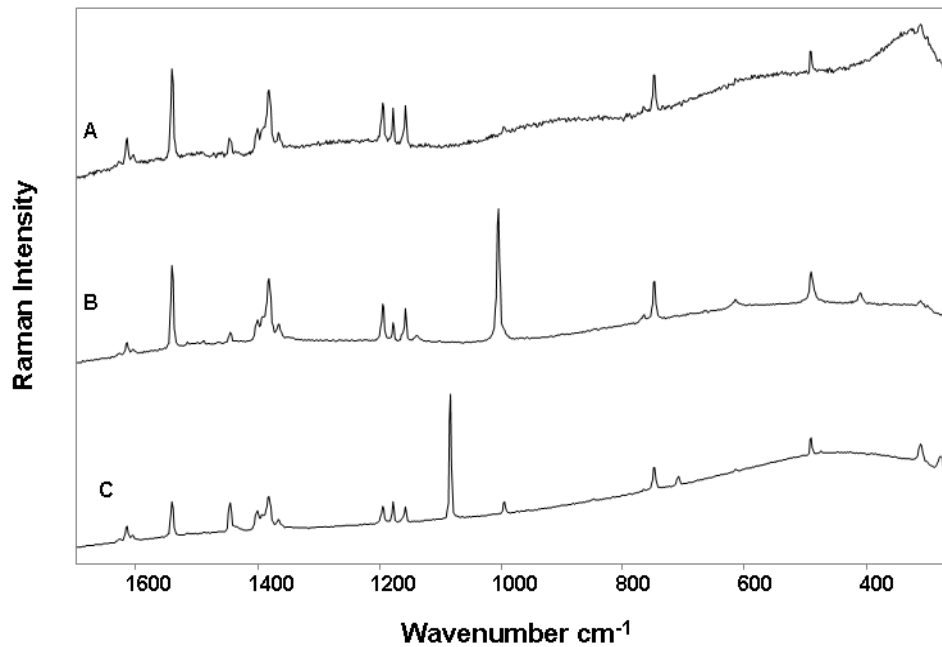


Figure 6.6 Raman spectra of (a) pure tetracene, (b) tetracene under gypsum and (c) tetracene under calcite

6.3.2 PAHS under calcite and gypsum crystalline

The spectra obtained from anthracene, phenanthrene, naphthalene, tetracene, chrysene, pyrene and triphenylene crystals under calcite and gypsum are shown in figures 6.3 -6.11. Comparison of these spectra with the reference spectra of the compounds shows that the compounds could still be easily identified using characteristic bands in their Raman spectra. Anthracene can be identified by several characteristic bands, such as one strong band at 1399 cm^{-1} due to C=C in-plane vibration and three medium bands at 1004 (C-H in-plane deformation vibration), 749 (C-H out-of-plane deformation vibration) and 391 cm^{-1} (CCC bending) as depicted in figure (6.3 A).

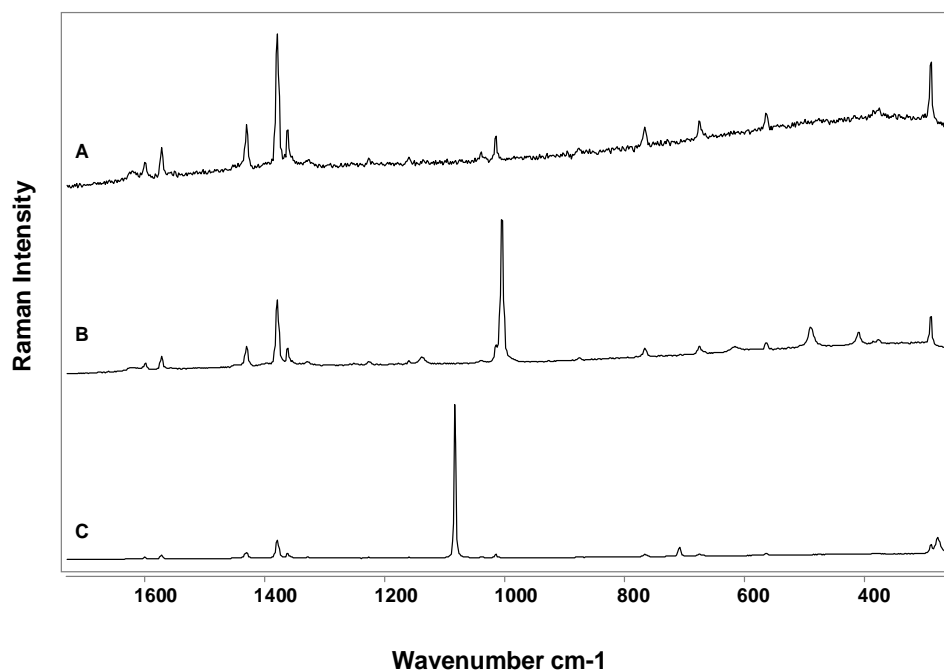


Figure 6.7 Raman spectra of (a) pure chrysene, (b) chrysene under gypsum and (c) chrysene under calcite

The phenanthrene spectrum contains three strong peaks at 1346, 708, 407 cm^{-1} due to C-C stretching, HCC bending, HCCC out-of-plane bending and CCC bending respectively and three medium sharp features at 1438, 1034, 543 cm^{-1} assigned to C-C stretching, HCC bending, C-C stretching, HCC bending and CCC bending, respectively, as depicted in figure (6.4 A).

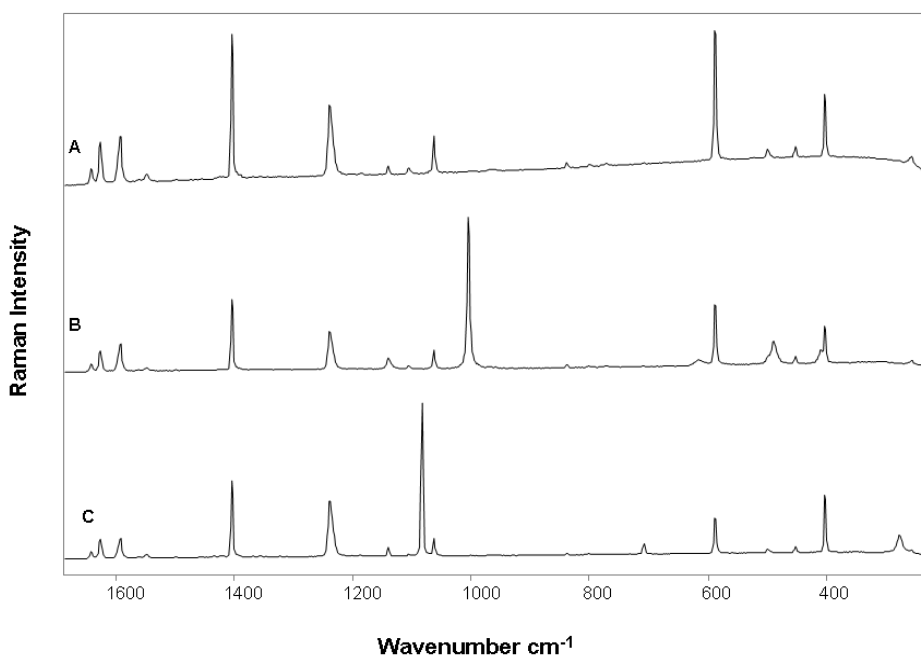


Figure 6.8 Raman spectra of (a) pure pyrene, (b) pyrene under gypsum and (c) pyrene under calcite

Similarly, the naphthalene spectrum has several characteristic bands that can be used to identify the compound, for example the two strong bands $1378, 759 \text{ cm}^{-1}$ (C=C in-plane vibration and CCC in-plane bending modes) and three medium bands at $1461, 1018$ (C-H in-plane deformation vibration) and 509 (C-C ring deformation) cm^{-1} depicted in figure (6.5 A). Also, tetracene can be identified by its three strong Raman bands at $1540, 1381, 750 \text{ cm}^{-1}$ due to C-C stretching, C=C in-plane vibration and CCC ring deformations, respectively, and three medium intensity Raman bands at $1194, 1177$ and 1157 cm^{-1} assigned to C-H in-plane deformation vibrations as depicted in figure (6.6 A).

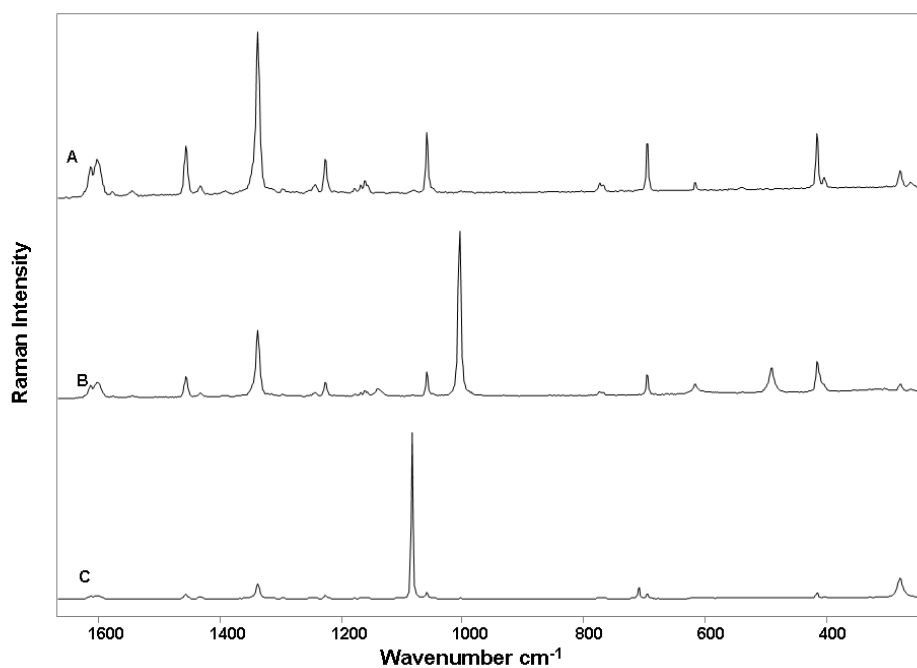


Figure 6.9 Raman spectra of (a) pure triphenylene, (b) triphenylene under gypsum and (c) triphenylene under calcite

The chrysene spectrum contains one strong Raman band at 1378 cm^{-1} (C-C stretching) and four medium sharp Raman bands at $1571, 1430, 1361$ and 1014 cm^{-1} assigned to C-C

stretching, C-C stretching, C-C stretching and C-H in-plane bending respectively that can be used to identify the compounds as shown in figure (6.7 A). The pyrene spectrum has two strong Raman bands at 1403 and 589 cm^{-1} (C=C in-plane vibration, skeletal ring vibrations, CCC ring deformation) and three medium sharp Raman bands at 1238, 1063 and 403 cm^{-1} due to CH bending which can be used to identify it as depicted in figure (6.8 A). Similarly, the triphenylene spectrum has several characteristic bands that can be used to identify the compound, namely, one strong band at 1336 cm^{-1} (C-C stretching) and three medium-sharp features at 1455, 1058 and 695 cm^{-1} assigned to C-C stretching, C-H in-plane bending and C-H out-of-plane bending respectively shown in figure (6.9 A). Although Raman spectra of anthracene, phenanthrene, naphthalene, tetracene, chrysene, pyrene and triphenylene have been recorded under calcite and gypsum, the characteristic bands of each compound are still observable and are in agreement with the reference spectra of the pure compounds. Although the spectra have several bands assigned to the calcite or gypsum, these bands do not overlap with the characteristic bands of the PAHs.

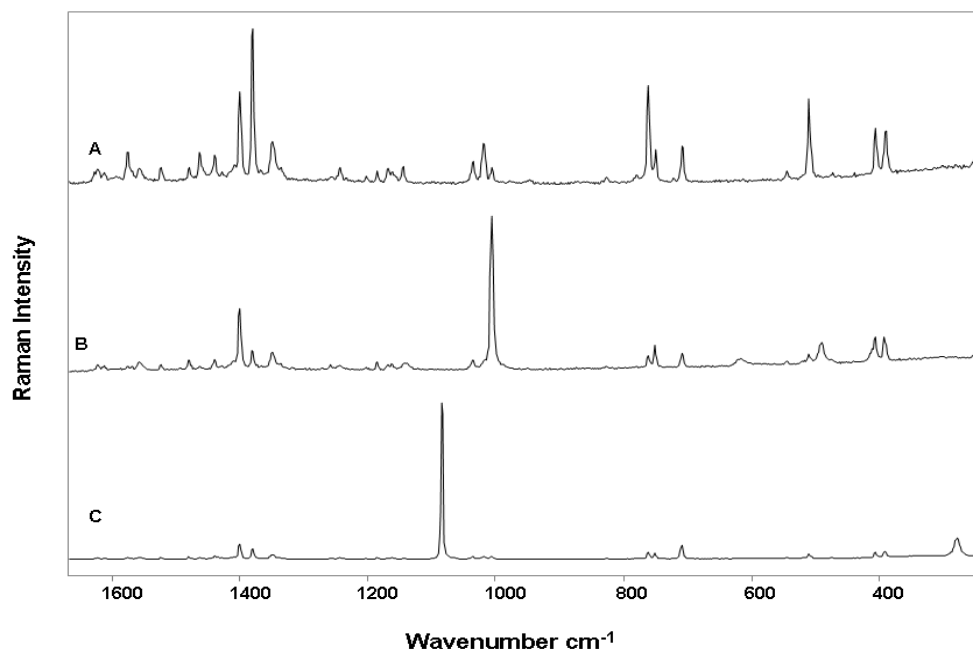


Figure 6.10 Raman spectra of (a) pure Mixture 1, (b) Mixture 1 under gypsum and (c) Mixture 1 under calcite

6.3.3 PAH Mixtures

Figure (6.10 A) shows the Raman spectra of a mixture of anthracene, phenanthrene, and naphthalene (Mixture 1) and figure (6.11 A) shows the Raman spectra of a mixture of tetracene, chrysene, pyrene and triphenylene (Mixture 2). All the compounds in each mixture can be clearly identified by their characteristic bands with no band overlap being observed. Although the spectra of the mixtures have several bands due to the different compounds these bands do not overlap with the characteristic bands of each compound.

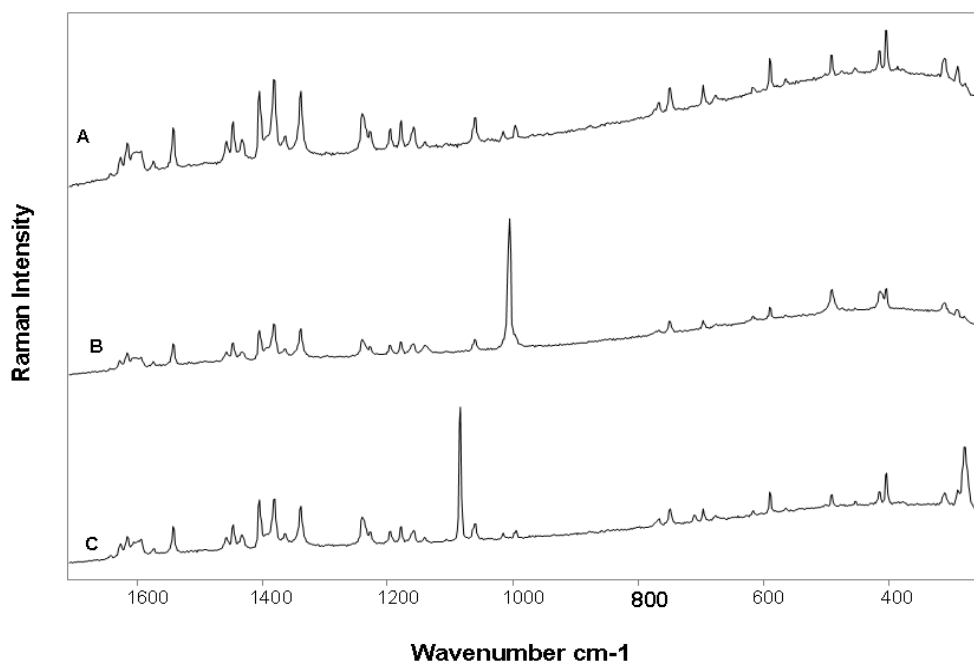


Figure 6.11 Raman spectra of (a) pure Mixture 2, (b) Mixture 2 under gypsum and (c) Mixture 2 under calcite

6.3.4 PAH Mixtures under Calcite and Gypsum crystalline

Figure (6.10 B, C), shows the Raman spectra of Mixture 1 (anthracene, phenanthrene and naphthalene) under calcite and gypsum also Figure (6.11 B, C) shows the Raman spectra of Mixture 2 (tetracene, chrysene, pyrene and triphenylene) under calcite and gypsum. The characteristic bands of each compound are still observable in the mixture under calcite and gypsum despite the presence of the calcite and gypsum bands.

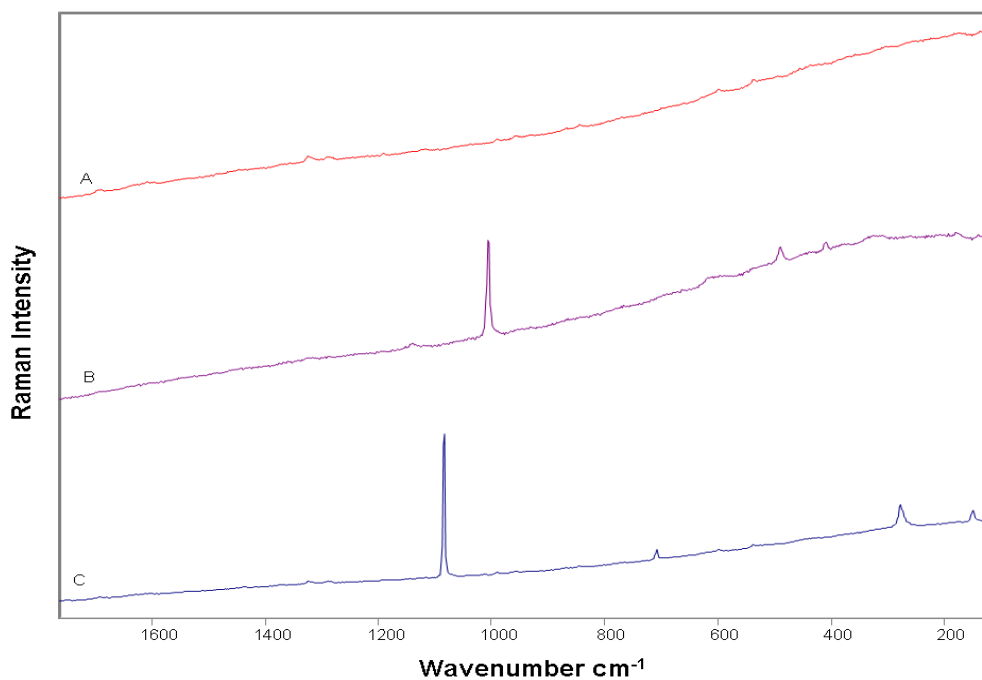


Figure 6.12 Raman spectra of (a) pure usnic acid, (b) usnic acid under gypsum and (c) usnic acid under calcite

6.3.5 Usnic acid under calcite and gypsum crystalline

The spectra obtained from usnic acid under calcite and gypsum are shown in figure 6.12. Comparison of these spectra with the reference spectrum of the compound shows that usnic acid could be identified using its Raman spectrum. Usnic acid can be identified by several characteristic bands which can be used to identify it such as three bands at 1322 cm^{-1} assigned to ring stretch, 1288 cm^{-1} due to ν (COC) of the aryl alkyl ether and 539 cm^{-1} depicted in figure (6.11 A). The usnic acid could still be identified by its characteristic Raman bands under calcite and gypsum, although bands due to the mineral can also be identified.

6.4 Conclusion

Raman spectroscopy provides an efficient way for detection and identification of pure and mixed organic compounds through crystals of calcite and gypsum. The presence of spectral bands arising from the calcite or gypsum did not interfere with the identification of the organic compounds. The significances of which can be discriminated alone and in admixture, using confocal Raman spectroscopy.

It is clear that the observation of two or more characteristic bands for each species is necessary for the identification of the individual compound or organic mixtures.

6.5 References

- [1] G. Horneck, *Adv. Space Res*, **1999**. 23. 381.
- [2] S. Arrhenius, *Die Verbreitung des Lebens im Weltenraum Die Umschau*, **1903**. 7. 481.
- [3] H.J. Melosh, *Nature*, **1988**. 332. 687.
- [4] C. Mileikowsky , F. A. Cucinotta , J. W. Wilson , B. Gladman , G. Horneck , L. Lindegren, H. J. Melosh, H. Rickman , M.Valtonen , J. Q. Zheng, *Natural transfer of viable microbes in space. Part 1: from Mars to Earth and Earth to Mars. Icarus*, **2000** .145. 391.
- [5] H. P. Chiang, R. Song, B. Mou, K. P.Li, P. Chiang, D. Wang, W. S. Tse, L. T. Ho. *Raman spectrosc*, **1999**.30.551
- [6] S. J. Clemett, C. R.Maechling, R. N. Zare, P. D. Swan, R. M. Walker, *Science*, **1993**. 262 .721.
- [7] J. L. Puget, A. Leger. *Annu. Rev. Astron. Astrophys*, **1989**. 27.161
- [8] L .d'Hendecourt, P .Ehrenfreund. *Adv. Space Res*, **1997**. 19.1023.

- [9] R.P. Bettens, E .Herbst. *Astrophysical Journal*, **1996**. 468.686.
- [10] R.I .Kaiser, K .Roessler. *Astrophysical Journal*, **1998**. 503.959.
- [11] E.L.O .Bakes, A.G.G.M. Tielens. *Astrophysical Journal*, **1994**. 427.822.
- [12] E.L.O Bakes, A.G.G.M. Tielens. *Astrophysical Journal*, **1998**. 499.258.
- [13] S.J.Clemett, C.R .Maechling, R.N .Zare, P.D .Swan, R.M.Walker. *Science*, **1993**. 262.721.
- [14] B.Proksa, M.Sturdi kova , N.Pro nayova , T .Liptaj. *Pharmazie*, **1996**.51.195.
- [15] T.Sassa, , M.Igarashi, .*Agr. Biol. Chem*, **1990**. 54.2231.
- [16] M. A .Conover , R . Mierzwa , A . King , D . Loebenberg , W. R . Bishop , M . Puar, M. Patel, S. J. Coval, J. Hershenhorn, G. A. Strobel, *Phytochemistry*, **1992**. 31.2999.
- [17] B. Schrader, (Verlag Chemic Wemhelm, 4th ed., **1980**.V. 303.
- [18] H. G. M. Edwards, S. E. J. Villar, J. Jehlicka, T. Munshi. *Spectrochimica Acta Part A*, **2005**. 61(10).2273.
- [19] H. G. M. Edwards, S. E. Jorge-Villar, J. Parnell., S .Charles, Cockell, P. Lee. *Analyst*, **2005**.130. 917.

CHAPTER 7

Identification of polycyclic aromatic hydrocarbons and minerals of relevance to Mars using Raman spectroscopy and other techniques

7.1 Introduction

A combination of analytical techniques is extremely valuable for obtaining complementary information about complex biogeological systems [1-6]. Raman spectroscopic instrumentation is currently being evaluated for the adoption of miniaturized versions as part of life detection analytical suites on future Mars missions [7-10], including the ESA ExoMars mission as part of the Aurora programme.

Biological markers (biomarkers) is a term used to describe the wide variety of organic compounds that are derived from living organisms that can be found in sediments in rocks and in the geological record. Such compounds have also been termed ‘‘chemical fossils’’ but the most commonly-used term is that of biomarker [11-13]. Those biomarkers which show little or no change in structure from those of the original biochemical compounds are easily recognised in extracts from their mineral hosts but compounds with strongly diagenetic or catagenetic altered structures carry carbon skeletons which differ from those of the original biological compounds yet can still carry sufficient residual portions of their original structures to facilitate their identification.

Since the beginning of space exploration, most of the probes sent to investigate other planetary atmospheres and surfaces have carried instruments to determine their elemental, isotopic and molecular (inorganic and organic) compositions. Space appears to be a potential chemical reactor that can provide a broad range of organic molecules, including biological building blocks and their chemical precursors. Lists of chemical compounds found in space is not exhaustive but is established from data provided by observations of atmospheres and the interstellar medium, analyses of meteorites and from laboratory simulation experiments. Organic compounds identified in the interstellar medium and in Solar System bodies are of particular importance for revealing the chemistry that may

have led to the interaction and evaluation of life on Earth. More than 120 molecules containing up to 11 atoms have been detected in interstellar space [14]. The organic fraction contains many precursors for biological molecules. Intensive studies of the chemical composition of meteorite samples also have been carried out; studies of the Murchison meteorite revealed the presence of more than 500 organic compounds [15-19].

7.2 Experimental

7.2.1 Materials

Anthracene, pyrene, perylene (PAHs), quartz, calcite and gypsum were supplied by Sigma-Aldrich (UK) and AA pin Chemicals Limited (UK), and were used as received. Anthracene, pyrene and perylene were mixed separately with calcite, gypsum and quartz (mineral hosts) in 50:50 concentration and the mixtures were ground in an agate mortar. Solid state mixtures of the PAHs in calcite, gypsum and quartz matrices were prepared representing 50 - 50 concentrations between them.

7.2.2 Raman spectroscopy

7.2.2.1 FT Raman spectroscopy

The synthetic mixtures were analysed using FT-Raman spectroscopy at 4 cm⁻¹ spectral resolution and 500 scans and 30 mW laser power were used to collect spectra in the 2000–0 cm⁻¹ wavenumber region in each case using an FT-Raman Bruker IFS66 spectrometer with FRA 106 Raman module attachment and a Nd³⁺/YAG laser source operating at 1064 nm.

7.2.2.2 Dispersive Raman microscopy

Raman spectra were collected using a Renishaw InVia Reflex dispersive Raman spectrometer (Renishaw plc, Wotton-under-Edge, UK). The substrates were excited with a 785 nm near-infrared diode laser. The laser beam was focused on the sample using a 5x objective lens, resulting in a laser spot footprint of approximately 10 μm diameter. Spectra were obtained for 5 accumulations, each of 10s exposure of the CCD detector in the wavenumber range 100-3200 cm^{-1} using the extended scanning mode of the instrument. Spectral acquisition, presentation, and analyses were performed with the Renishaw WIRE 2 (Renishaw plc) and GRAM AI version 8 (Galactic Industries, Salem, NH) software.

Powder mixtures have an inherent heterogeneity on the micron scale. This has a major implication for sampling using Raman microscopy. To address these issues, we have adopted the lowest magnification available to us namely, a 5 x objective which gives ~ 10 μm footprint, and each specimen was analysed at seven random positions, with each point sampled twice. On this basis, the spectral data quoted represent the most reproducible available from our experiments; adequate reproducibility was attached to an observation for at least 6/14 measurements for each sample.

7.2.2.3 RIAS Raman Spectrometer

The RIAS (Wotton-under-Edge, UK) is equipped with a diode laser emitting at 785 nm and a thermoelectrically cooled (400 x 575 pixels) CCD detector, with a coupled Renishaw compact fibre optic probe, equipped with a 20x (NA 0.35) Olympus objective lens. The diffraction grating (1000 lines/mm) covers the spectral range 2100 – 100 cm^{-1} with a spectral resolution of 10 cm^{-1} . The power of the diode laser is 49 mW at the

sample. Daily calibration of the wavenumber axis is achieved by recording the Raman spectrum of a silicon wafer (1 accumulation, 10 second exposure) for static modes. If necessary, an offset correction is performed to ensure that the position of the silicon band is $520.5 \pm 0.1 \text{ cm}^{-1}$. Spectra were recorded with the accumulation of 1 scan, 10 s exposures. Spectra were not corrected for instrument response. The spectrometer was controlled by portable PC with instrument control software (Renishaw WiRE 2 Service pack 8).

7.2.3 Scanning Electron Microscopy (SEM)

SEM was accomplished using a FEI Quanta 400 instrument equipped with an INCA EDX detector. The Scanning Electron Microscope (SEM) used in a low-vacuum mode in which samples need no coating with a conductive film of gold or graphite to avoid any possible damage of the samples. Also, such uncoated samples remained suitable for further or repeat investigations. The backscattered electron (BSE) detector was used which provided the topographical and compositional information in one image. The acquisition time for EDS qualitative and quantitative analyses was approximately 100 s, while for mapping analyses the acquisition time was between 500 and 600 s. Self-calibration of the EDS was made before testing with a cobalt standard.

7.2.4 Powder X-Ray Diffraction

Powder X-ray diffractograms were recorded with a Bruker D8 diffractometer. The wavelength of the X-rays was 0.154 nm using a copper source, at a voltage of 40 kV and with filament emission of 30 mA. Each sample was scanned from 5-90° (2 θ) using a step width of 0.01° and a 1 second time count. The receiving slit was 1° and the scatter slit of 0.2°. The software used to read the data was EVA, which comprises both a means by which the data can be presented and manipulated and also a database with which to compare the data with spectra of known materials.

7.3 Results and discussion

7.3.1 Compound Mixtures

As can be seen from Chapter Five, the Raman spectra of the polyaromatic hydrocarbons analysed in this project are all distinguishable from each other individually. The question that needs to be answered now is, can the identity of all these compounds in admixtures be confirmed? Here, nine compound mixtures were analysed containing a combination of three polyaromatic hydrocarbons, namely anthracene, pyrene and perylene and three geological samples (inorganic compounds), namely calcite, gypsum and quartz. These three polyaromatic hydrocarbons could be mixed with geological samples and found together and with their inorganic hosts in space. The three polyaromatic hydrocarbons have very similar dominant bands as all three of them contain two fused benzene rings or more (anthracene, pyrene and perylene contain three, four and five fused benzene rings, respectively) and the Raman bands could overlap with other features from the host minerals. There is also a problem of possible fluorescence emission interference with the

mixtures at 785 nm excitation. However, if the compounds in the mixtures can be identified even though they have many similar bands then Raman spectroscopy has good potential for the identification of organic biomarkers in their inorganic mineral hosts in an astrobiological measurement.

The Raman spectra of the compound mixtures (polyaromatic hydrocarbons in mineral matrices) have been obtained and assignments of the Raman spectra are shown in figures 7.1-7.9 and tables 7.1-7.9.

7.3.1.1 Anthracene and matrices (calcite, gypsum and quartz) in 50-50 mixtures

It can be seen from figures 7.1-7.3 that on all three instruments the spectra of the mixtures differ from those of the pure compounds. It is quite obvious at a glance that anthracene is present in its mixtures from its strong bands around 1401, 1006 and 752 cm^{-1} , which are clearly present in the mixtures, and other bands near 1084 cm^{-1} due to calcite, two peaks around 1135, and 619 cm^{-1} assigned to gypsum, only one due to quartz at 464 cm^{-1} and several bands for the both compounds (Anthracene and minerals) such as 280, 1006, 490, 1160 and 392 cm^{-1} as seen in tables 7.1-7.3. However, it is less easy to prove that the secondary compounds of the mixtures which are calcite, gypsum and quartz as most of their main peaks are obscured by anthracene peaks. The spectra show that all but a couple of the peaks can be assigned to anthracene, the last matrices or both compounds and that peaks that cannot be identified are of very low intensities and can be regarded as noise. Some peaks are hard to define because of differences in spectral resolution and the number of peaks will vary because some peaks have become broader due to a combination of band intensity from more than one of the compound in admixtures.

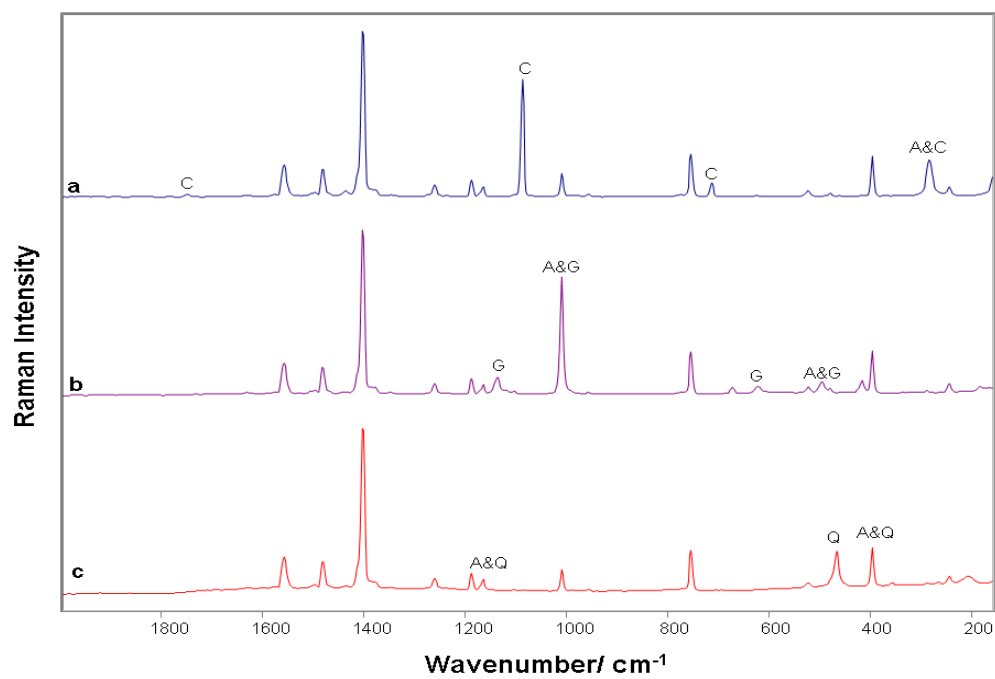


Figure 7.1 Raman spectra of (a) anthracene and calcite, (b) anthracene and gypsum and (c) anthracene and quartz in 50-50 mixtures run on the Bruker spectrometer

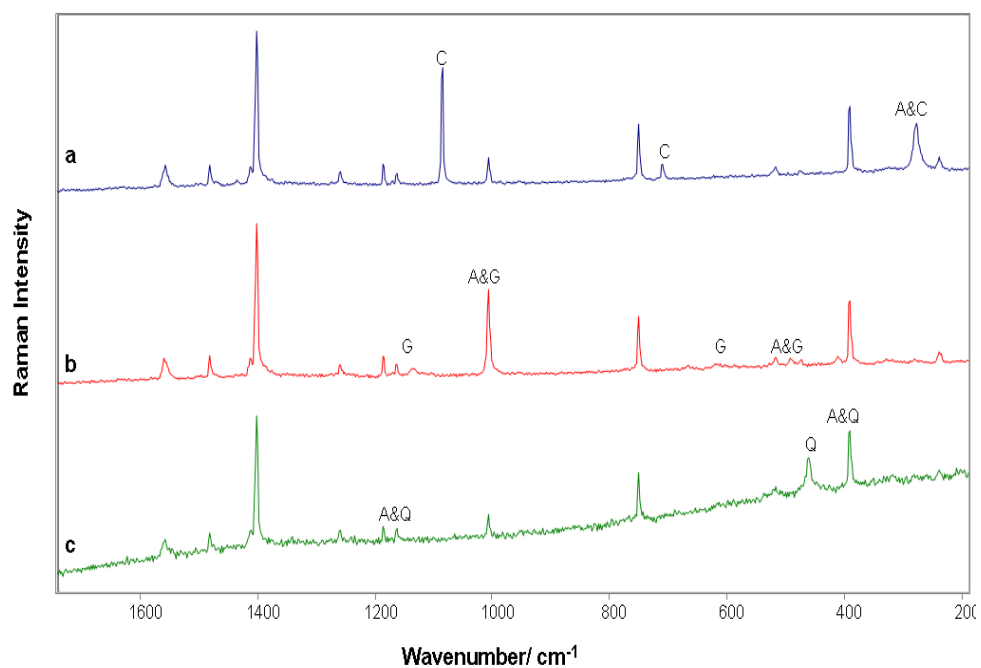


Figure 7.2 Raman spectra of (a) anthracene and calcite, (b) anthracene and gypsum and (c) anthracene and quartz in 50-50 mixtures run on the Renishaw In Via spectrometer

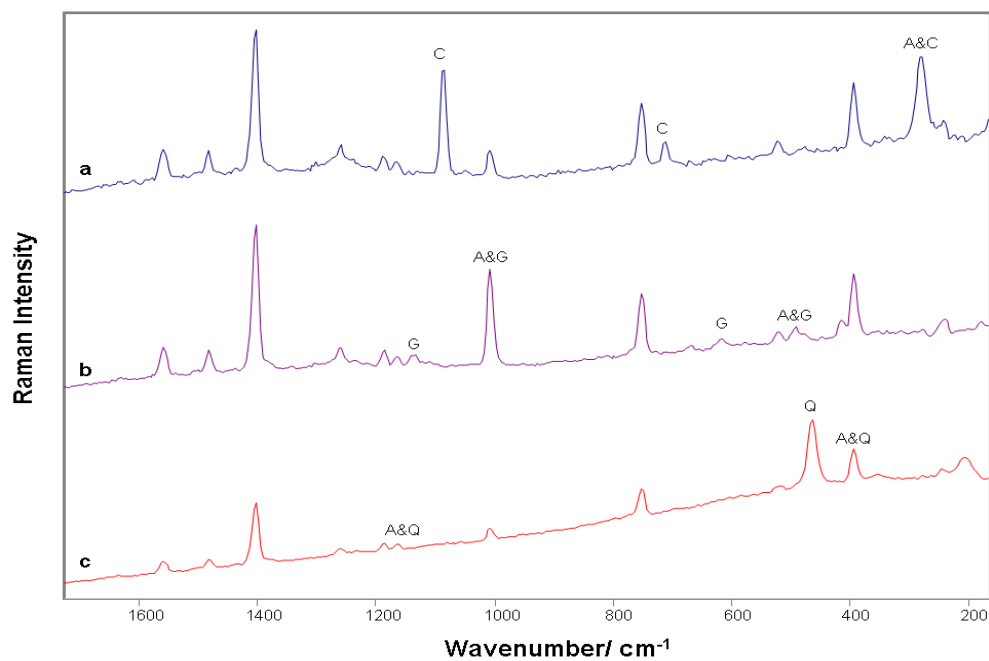


Figure 7.3 Raman spectra of (a) anthracene and calcite, (b) anthracene and gypsum and (c) anthracene and quartz in 50-50 mixtures run on the RIAS

| Bruker | | Renishaw | | RIAS | | |
|--------------------------------|-----|--------------------------------|-----|--------------------------------|-----|-----|
| Wavenumber cm ⁻¹ | I | Wavenumber cm ⁻¹ | I | Wavenumber cm ⁻¹ | I | Com |
| 3072 | wsh | - | - | | - | A |
| 3051 | M | 3050 | vw | - | - | A |
| 3028 | W | 3030 | vw | - | - | A |
| 1750 | W | - | - | - | - | C |
| 1557 | M | 1556 | w | 1558 | w | A |
| 1480 | W | 1479 | w | 1481 | w | A |
| 1401 | vst | 1400 | vst | 1402 | vst | A |
| 1259 | W | 1257 | w | 1259 | w | A |
| 1186 | W | 1184 | w | 1186 | w | A |
| 1163 | W | 1161 | w | 1163 | w | A |
| 1084 | W | 1083 | vw | 1086 | vw | C |
| 1005 | M | 1005 | m | 1008 | m | A |
| 955 | Vw | 955 | w | 955 | w | A |
| 752 | M | 752 | m | 752 | m | A |
| 708 | Vw | 708 | w | - | - | A |
| 520 | W | 519 | w | 521 | w | A |
| 477 | W | 477 | w | 481 | w | A |
| 395 | M | 391 | st | 393 | m | A |
| 280 | W | 279 | w | 279 | w | A&C |
| 242 | W | 239 | w | 241 | w | A |

* I = intensity, Com = compound, vst = very strong; st = strong; m = medium; w = weak; vw = very weak; sh = shoulder; w, sh = weak shoulder and m, sh = medium shoulder

Table 7.1 Raman spectral wavenumber (cm⁻¹) and band vibrational assignments for the Raman spectrum of a 50:50 mixture of anthracene (A) and calcite(C) from the Bruker, Renishaw and RIAS

| Bruker | | Renishaw | | RIAS | | |
|--------------------------------|-----|--------------------------------|-----|--------------------------------|----|-----|
| Wavenumber cm ⁻¹ | I | Wavenumber cm ⁻¹ | I | Wavenumber cm ⁻¹ | I | Com |
| 3072 | w | | | - | | A |
| 3050 | m | 3051 | vw | - | | A |
| 3028 | m | 3029 | w | - | | A |
| 1557 | m | 1555 | w | 1559 | w | A |
| 1480 | m | 1479 | m | 1482 | m | A |
| 1401 | vst | 1399 | vst | 1402 | st | A |
| 1259 | w | 1257 | w | 1261 | w | A |
| 1186 | m | 1184 | m | 1186 d | w | A |
| 1163 | w | 1161 | m | 1165 d | w | A |
| 1138 | w | 1136 | w | 1136 | w | G |
| 1006 | m | 1005 | m | 1007 | m | A&G |
| 954 | w | 953 | w | 955 | w | A |
| 752 | m | 749 | m | 754 | m | A |
| 617 | vw | 619 | w | 619 | w | G |
| 520 | w | 517 | w | 522 | w | |
| 490 | w | 489 | w | 489 | w | A&G |
| 394 | m | 391 | st | 396 | m | A |
| 284 | w | 282 | w | - | | A |
| 242 | m | 239 | m | 244 | w | A |
| | | | | | | |

* I = intensity, Com = compound, vst = very strong; st = strong; m = medium; w = weak; vw = very weak; sh = shoulder; w, sh = weak shoulder and m, sh = medium shoulder

Table 7.2 Raman spectral wavenumber (cm⁻¹) and band vibrational assignments for the Raman spectrum of a 50:50 mixture of anthracene (A) and gypsum (G) from the Bruker,

Renishaw and RIAS

| Bruker | | Renishaw | | RIAS | | |
|--------------------------------|-----|---------------------------------|-----|---------------------------------|----|-----|
| Wavenumber cm ⁻¹ | I | Wavenum ber cm ⁻¹ | I | Wavenumbe r cm ⁻¹ | I | Com |
| | | | | | - | A |
| 3050 | m | - | - | - | - | A |
| 3028 | w | - | - | - | - | A |
| 1557 | w | 1556 | w | 1558 | w | A |
| 1480 | w | 1479 | w | 1481 | w | A |
| 1401 | vst | 1400 | vst | 1402 | st | A |
| 1259 | w | 1257 | w | 1259 | w | A |
| 1186 | w | 1184 | w | 1186 | w | A |
| 1160 | w | 1162 | w | 1162 | w | A&Q |
| 1007 | w | 1005 | w | 1007 | w | A |
| 955 | w | 954 | w | - | - | A |
| 752 | m | 749 | m | 752 | m | A |
| 520 | w | 517 | w | 520 | w | A |
| 477 | w | 473 | w | 477 | w | A |
| 464 | w | 462 | w | - | - | Q |
| 392 | m | 392 | m | 392 | m | A&Q |
| 242 | w | 239 | w | 243 | w | A |
| | | | | | | |

* I = intensity, Com = compound, vst = very strong; st = strong; m = medium; w = weak; vw = very weak; sh = shoulder; w, sh = weak shoulder and m, sh = medium shoulder

Table 7.3 Raman spectral wavenumber (cm⁻¹) and band vibrational assignments for the Raman spectrum of a 50:50 mixture of anthracene (A) and quartz (Q) from the Bruker, Renishaw and RIAS

7.3.1.2 Pyrene and matrices (calcite, gypsum and quartz) in 50-50 mixtures

As with the mixtures of anthracene and minerals, vibrational features of both compounds can be seen in the spectra obtained from all three instruments (figures 7.4-7.6) with bands of weaker intensity observed from calcite, gypsum and quartz. Pyrene can be seen with its characteristic strong and medium intensity bands around 1627, 1594, 1406, 1240 and 592 cm^{-1} . In tables 7.4-7.6 a more in-depth inspection of the spectra is shown with tentative assignments for most of the bands. Further analysis shows that many pyrene peaks dominate the spectra and there are few peaks in the spectra produced by the calcite, gypsum and quartz host minerals, namely calcite at 1086 and 279 cm^{-1} , three bands due to gypsum at 1006, 617 and 490 cm^{-1} . It could be noted that the 617 and 490 cm^{-1} bands were observed just with 1064 nm excitation and two overlapping peaks around 1141 and 410 cm^{-1} were noted for gypsum and only one peak at 464 cm^{-1} for quartz was seen with 785 nm excitation. It should be noted that weak peaks in the minerals disappeared and that strong peaks become medium to weak in intensity as observed with anthracene and minerals mixtures.

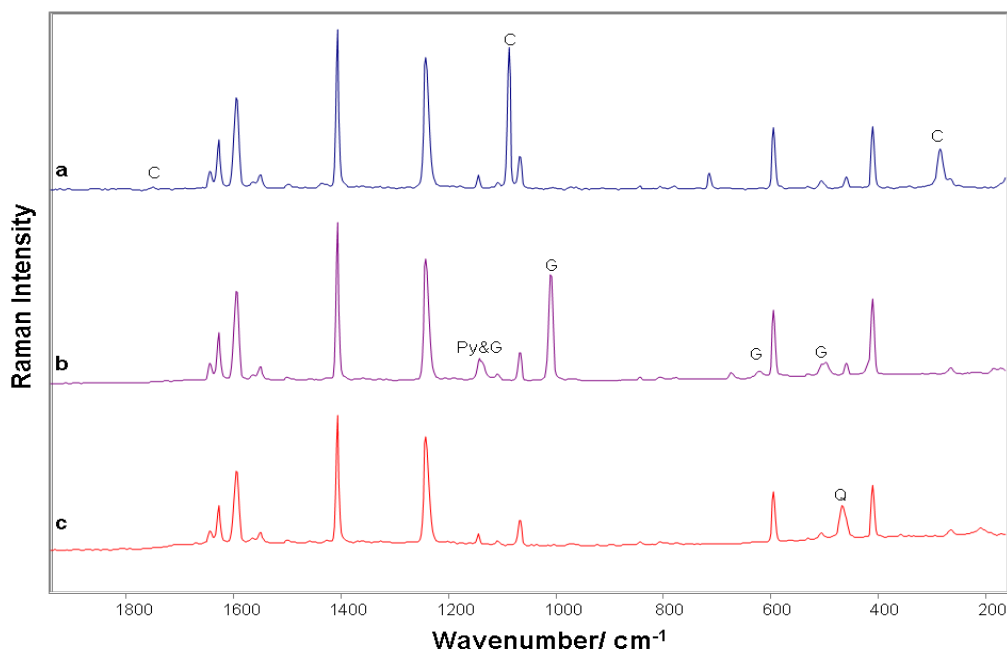


Figure 7.4 Raman spectra of (a) pyrene and calcite, (b) pyrene and gypsum and (c) pyrene and quartz in 50-50 mixtures run on the Bruker spectrometer

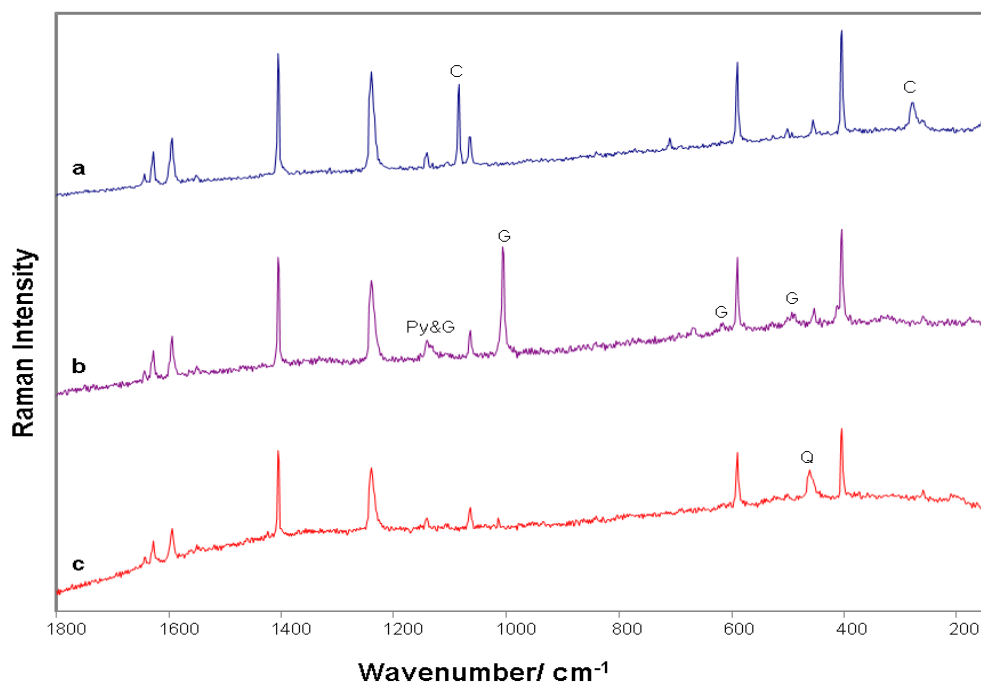


Figure 7.5 Raman spectra of (a) pyrene and calcite, (b) pyrene and gypsum and (c) pyrene and quartz in 50-50 mixtures run on the Renishaw In Via spectrometer

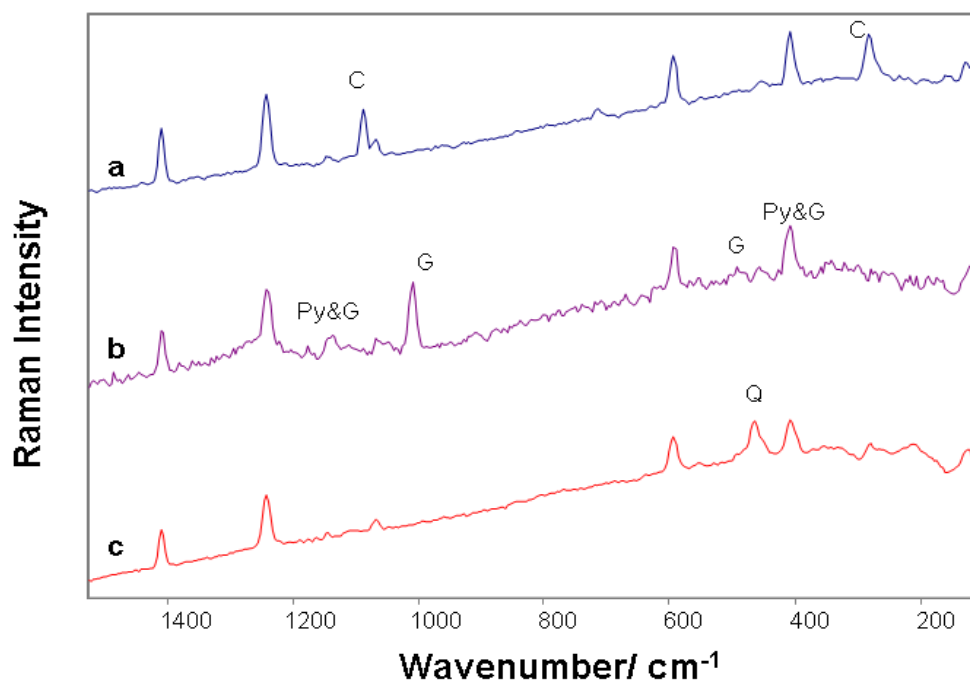


Figure 7.6 Raman spectra of (a) pyrene and calcite, (b) pyrene and gypsum and (c) pyrene and quartz in 50-50 mixtures run on the RIAS

| Bruker | | Renishaw | | RIAS | | |
|--------------------------------|-----|--------------------------------|-----|--------------------------------|-----|-----|
| Wavenumber cm ⁻¹ | I | Wavenumber cm ⁻¹ | I | Wavenumber cm ⁻¹ | I | Com |
| 3054 | m | 3057 | vw | - | - | Py |
| 3022 | w | - | - | - | - | Py |
| 1642 | w | 1642 | w | 1644 | wsh | Py |
| 1627 | m | 1626 | m | 1629 | m | Py |
| 1594 | m | 1592 | m | 1596 | m | Py |
| 1549 | w | 1548 | w | 1552 | vw | Py |
| 1406 | vst | 1404 | vst | 1405 | st | Py |
| 1240 | vst | 1239 | vst | 1242 | st | Py |
| 1143 | w | 1141 | w | 1145 | w | Py |
| 1107 | w | 1105 | vw | 1108 | vw | Py |
| 1086 | w | 1084 | w | 1087 | w | C |
| 1065 | w | 1063 | w | 1067 | w | Py |
| 841 | vw | 841 | w | 843 | w | Py |
| 709 | w | 708 | w | - | - | Py |
| 592 | m | 590 | m | 594 | m | Py |
| 503 | w | 502 | w | - | - | Py |
| 457 | w | 455 | w | - | - | Py |
| 407 | m | 405 | m | 410 | w | Py |
| 279 | w | 278 | vw | 277 | w | C |
| 261 | w | 259 | w | - | - | Py |

* I = intensity, Com = compound, vst = very strong; st = strong; m = medium; w = weak; vw = very weak; sh = shoulder; w,sh = weak shoulder and m, sh = medium shoulder

Table 7.4 Raman spectral wavenumber (cm⁻¹) and band vibrational assignments for the Raman spectrum of a 50:50 mixture of pyrene (Py) and calcite(C) from the Bruker,

Renishaw and RIAS

| Bruker | | Renishaw | | RIAS | | |
|--------------------------------|-----|--------------------------------|-----|--------------------------------|-----|------|
| Wavenumber cm ⁻¹ | I | Wavenumber cm ⁻¹ | I | Wavenumber cm ⁻¹ | I | Com |
| | | | | - | - | |
| 3054 | m | 3055 | vw | - | - | Py |
| 3011 | w | - | - | - | - | Py |
| 1642 | w | 1642 | w | 1643 | wsh | Py |
| 1627 | m | 1626 | m | 1629 | m | Py |
| 1594 | m | 1592 | m | 1596 | m | Py |
| 1550 | w | 1548 | w | 1551 | w | Py |
| 1406 | vst | 1404 | vst | 1407 | vst | Py |
| 1240 | vst | 1239 | vst | 1241 | vst | Py |
| 1141 | w | 1140 | w | 1141 | w | Py&G |
| 1107 | w | 1105 | w | 1105 | w | Py |
| 1065 | m | 1063 | m | 1066 | m | Py |
| 1006 | w | 1005 | w | 1006 | w | G |
| 842 | w | 839 | w | 842 | w | Py |
| 803 | w | 801 | w | 803 | w | Py |
| 617 | w | 618 | w | - | - | G |
| 592 | m | 591 | m | 592 | m | Py |
| 526 | w | 523 | w | 522 | w | Py |
| 503 | w | 502 | w | 504 | w | Py |
| 490 | w | 490 | w | 490 | vw | G |
| 457 | w | 453 | w | 456 | | Py |
| 410 | m | 405 | m | 408 | m | Py&G |
| 261 | w | 257 | w | 261 | w | Py |
| | | | | | | |

* I = intensity, Com = compound, vst = very strong; st = strong; m = medium; w = weak; vw = very weak; sh = shoulder; w, sh = weak shoulder and m, sh = medium shoulder

Table 7.5 Raman spectral wavenumber (cm⁻¹) and band vibrational assignments for the Raman spectrum of a 50:50 mixture of Pyrene (Py) and gypsum (G) from the Bruker, Renishaw and RIAS

| Bruker | | Renishaw | | RIAS | | |
|--------------------------------|-----|--------------------------------|-----|--------------------------------|-----|-----|
| Wavenumber cm ⁻¹ | I | Wavenumber cm ⁻¹ | I | Wavenumber cm ⁻¹ | I | Com |
| | | | | | | |
| 3054 | m | | | | | Py |
| 3021 | w | | | | | Py |
| 1642 | w | 1642 | w | | | Py |
| 1627 | m | 1626 | m | 1629 | w | Py |
| 1594 | m | 1593 | m | 1596 | m | Py |
| 1549 | w | 1548 | w | 1548 | w | Py |
| 1499 | vw | 1499 | vw | - | | Py |
| 1406 | vst | 1404 | vst | 1406 | vst | Py |
| 1240 | vst | 1239 | vst | 1240 | vst | Py |
| 1143 | w | 1141 | w | 1142 | w | Py |
| 1107 | w | 1105 | w | - | | Py |
| 1065 | w | 1063 | m | 1065 | m | Py |
| 841 | w | 839 | vw | 841 | vw | Py |
| 592 | m | 590 | st | 592 | st | Py |
| 503 | w | 501 | w | - | | Py |
| 456 | w | 454 | w | - | | Py |
| 464 | m | 464 | m | 463 | m | Q |
| 407 | m | 405 | st | 410 | m | Py |
| 261 | w | 259 | w | - | | Py |
| | | | | | | |

* I = intensity, Com = compound, vst = very strong; st = strong; m = medium; w = weak; vw = very weak; sh = shoulder; w, sh = weak shoulder and m, sh = medium shoulder

Table 7.6 Raman spectral wavenumber (cm⁻¹) and band vibrational assignments for the Raman spectrum of a 50:50 mixture of Pyrene (Py) and quartz (Q) from the Bruker, Renishaw and RIAS

7.3.1.3 Perylene and matrices (calcite, gypsum and quartz) in 50-50 mixtures

Figures 7.7-7.9 show spectra obtained from perylene, with calcite, gypsum and quartz, respectively. Perylene is highly fluorescent using 785 nm excitation and this caused a problem in the identification of the compound as several bands are obscured by the fluorescent emission background. Fluorescence caused problems with both the Renishaw and RIAS spectrometers using 785 nm excitation. Spectra obtained from the RIAS instrument show but few bands. However, the Bruker instrument, using 1064 nm excitation, gave little or no fluorescence emission background.

Tables 7.7-7.9 show that perylene is present in the mixture from its strong and medium bands around 1569, 1372, 1297, 979 and 549 cm^{-1} , which are clearly present in the mixtures. Peaks that are present from calcite, gypsum and quartz are those at 1085 and 279 cm^{-1} for calcite, two peaks at 1006 and 619 cm^{-1} and two overlapped peaks around 1140 and 418 cm^{-1} for gypsum and one peak at 463 cm^{-1} due to quartz. Also, as with the previous mixtures, weak peaks disappeared and stronger peaks were observed of lower intensity compared with the pure isolated materials.

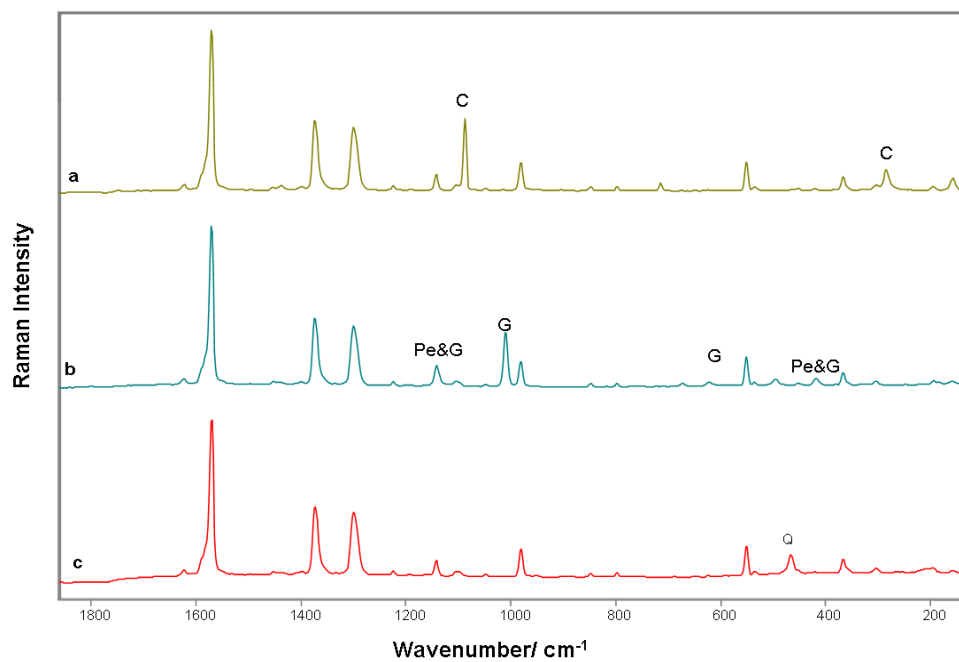


Figure 7.7 Raman spectra of (a) perylene and calcite, (b) perylene and gypsum and (c) perylene and quartz in 50-50 mixtures run on the Bruker spectrometer

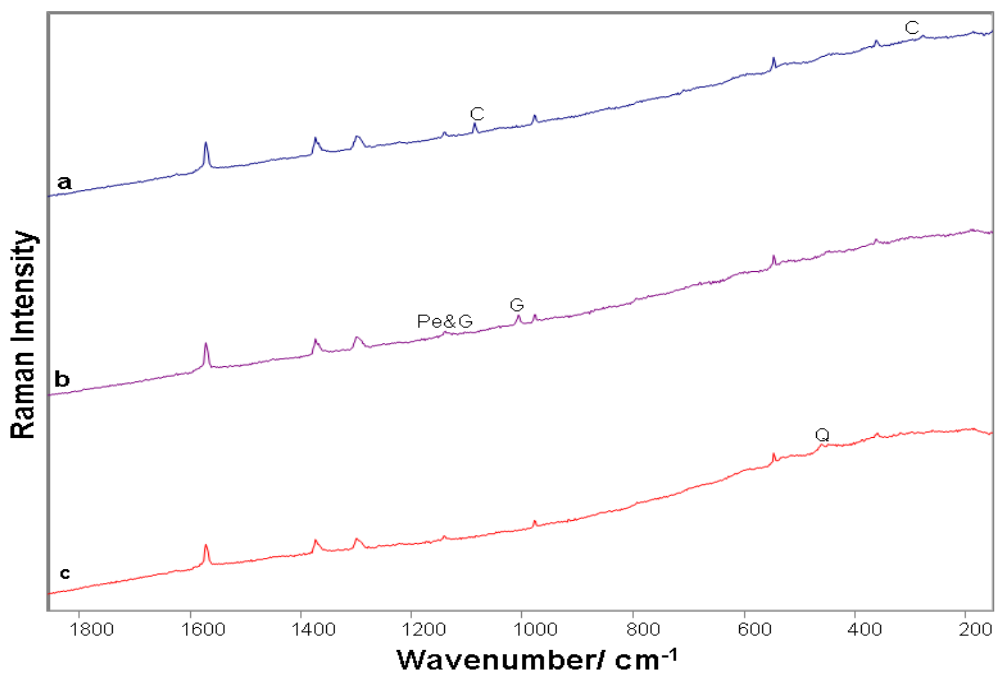


Figure 7.8 Raman spectra of (a) perylene and calcite, (b) perylene and gypsum and (c) perylene and quartz in 50-50 mixtures run on the Renishaw In Via spectrometer

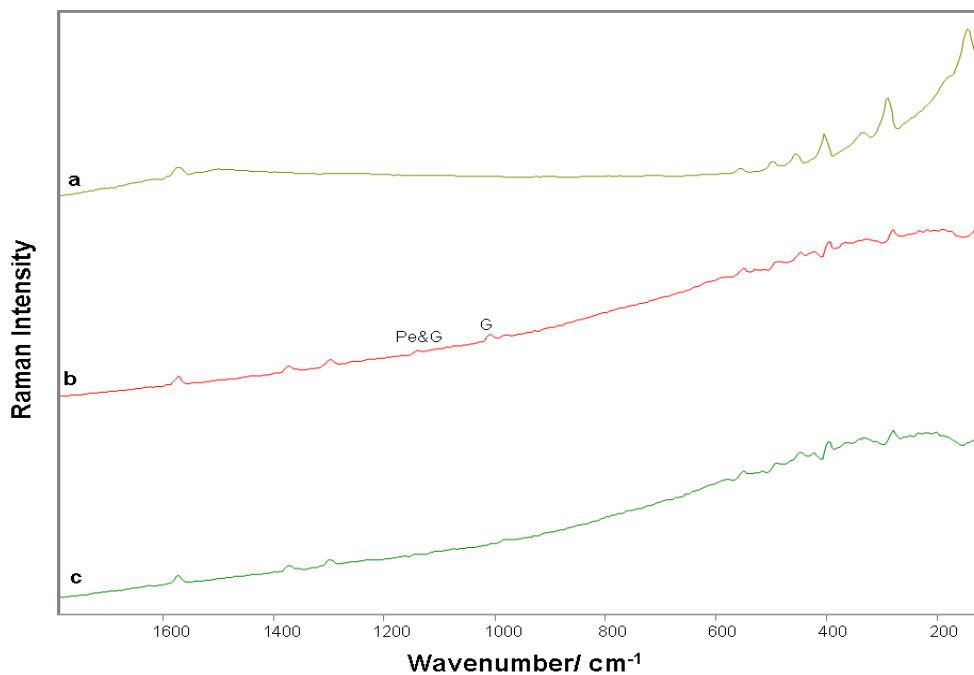


Figure 7.9 Raman spectra of (a) perylene and calcite, (b) perylene and gypsum and (c) perylene and quartz in 50-50 mixtures run on the RIAS

| Bruker | | Renishaw | | RIAS | | |
|--------------------------------|----|--------------------------------|----|--------------------------------|----|-----|
| Wavenumber cm ⁻¹ | I | Wavenumber cm ⁻¹ | I | Wavenumber cm ⁻¹ | I | Com |
| 3063 | w | - | - | - | - | Pe |
| 3052 | w | - | - | - | - | Pe |
| 3010 | vw | - | - | - | - | Pe |
| 1621 | vw | - | - | - | - | Pe |
| 1569 | st | 1569 | st | 1572 | st | Pe |
| 1372 | st | 1371 | st | - | - | Pe |
| 1297 | st | 1296 | st | 1298 | st | Pe |
| 1222 | vw | 1220 | vw | - | - | Pe |
| 1140 | w | 1140 | m | 1138 | vw | Pe |
| 1085 | w | 1084 | w | - | - | C |
| 1045 | vw | - | - | - | - | Pe |
| 979 | m | 976 | m | - | - | Pe |
| 845 | vw | 843 | w | - | - | Pe |
| 795 | vw | 793 | vw | - | - | Pe |
| 549 | st | 545 | m | - | - | Pe |
| 532 | w | 533 | vw | 533 | vw | Pe |
| 450 | vw | 451 | w | 453 | w | Pe |
| 411 | vw | 409 | w | 408 | w | Pe |
| 363 | m | 361 | m | - | - | Pe |
| 301 | vw | 298 | vw | 298 | w | Pe |
| 279 | w | 278 | w | - | - | C |

* I = intensity, Com= compound, vst = very strong; st = strong; m = medium; w = weak; vw = very weak; sh = shoulder; w, sh = weak shoulder and m, sh = medium shoulder

Table 7.7 Raman spectral wavenumber (cm⁻¹) and band vibrational assignments for the Raman spectrum of a 50:50 mixture of perylene (Pe) and calcite (C) from the Bruker,

Renishaw and RIAS

| Bruker | | Renishaw | | RIAS | | |
|--------------------------------|-----|--------------------------------|----|--------------------------------|----|------|
| Wavenumber cm ⁻¹ | I | Wavenumber cm ⁻¹ | I | Wavenumber cm ⁻¹ | I | Com |
| | | - | - | | - | Pe |
| 3062 | w | - | - | - | - | Pe |
| 3052 | w | - | - | - | - | Pe |
| 1621 | w | - | - | - | - | Pe |
| 1569 | vst | 1567 | st | 1570 | w | Pe |
| 1451 | vw | 1451 | vw | - | - | Pe |
| 1372 | m | 1371 | st | 1372 | w | Pe |
| 1297 | m | 1298 | st | 1295 | w | Pe |
| 1222 | vw | | | - | - | Pe |
| 1140 | w | 1139 | w | 1139 | vw | Pe&G |
| 1100 | W | - | - | - | - | Pe&G |
| 1045 | vw | - | - | - | - | Pe |
| 1006 | w | 1006 | w | 1007 | vw | G |
| 979 | st | 976 | m | - | - | Pe |
| 845 | vw | - | - | - | - | Pe |
| 795 | vw | - | - | - | - | Pe |
| 619 | vw | - | - | - | - | G |
| 549 | st | 546 | m | 551 | w | Pe |
| 532 | w | 534 | w | 535 | w | Pe |
| 490 | vw | - | - | - | - | G |
| 450 | vw | - | - | - | - | Pe |
| 418 | W | - | - | - | - | Pe&G |
| 363 | m | - | - | - | - | Pe |
| 301 | w | 299 | w | 298 | w | Pe |
| 192 | w | - | - | - | - | Pe |
| | | | | | | |

* I = intensity, Com = compound, vst = very strong; st = strong; m = medium; w = weak; vw = very weak; sh = shoulder; w, sh = weak shoulder and m, sh = medium shoulder

Table 7.8 Raman spectral wavenumber (cm⁻¹) and band vibrational assignments for the Raman spectrum of a 50:50 mixture of perylene (Pe) and gypsum (G) from the Bruker,

Renishaw and RIAS

| Bruker | | Renishaw | | RIAS | | |
|--------------------------------|----|--------------------------------|----|--------------------------------|---|------|
| Wavenumber cm ⁻¹ | I | Wavenumber cm ⁻¹ | I | Wavenumber cm ⁻¹ | I | Com |
| | | | | | | Pe |
| 3062 | w | - | | | | Pe |
| 3052 | w | - | | | | Pe |
| 3009 | vw | - | | | | Pe |
| 1621 | vw | - | | | | Pe |
| 1570 | st | 1571 | w | 1572 | w | Pe |
| | | 1504 | w | | | Pe |
| 1453 | vw | - | | | | Pe |
| 1372 | m | 1371 | w | 1373 | w | Pe |
| 1297 | m | 1297 | w | 1295 | w | Pe |
| 1222 | vw | - | | | | Pe |
| 1140 | w | - | | | | Pe |
| 1100 | vw | - | | | | Pe |
| 1045 | vw | - | | | | Pe |
| 979 | wm | 978 | vw | 980 | w | Pe |
| 845 | vw | - | | | | Pe |
| 795 | vw | - | | | | Pe |
| 549 | wm | - | | | | Pe |
| 532 | w | - | | | | Pe |
| 463 | w | 464 | w | - | - | Q |
| 450 | w | - | | | | Pe |
| 363 | w | 361 | w | | | Pe&Q |
| 301 | w | 298 | w | 298 | w | Pe |
| 192 | w | - | | | | Pe |
| | | | | | | |

* I = intensity, Com = compound, vst = very strong; st = strong; m = medium; w = weak; vw = very weak; sh = shoulder; w, sh = weak shoulder and m, sh = medium shoulder

Table 7.9 Raman spectral wavenumber (cm^{-1}) and band vibrational assignments for the Raman spectrum of a 50:50 mixture of perylene (Pe) and quartz (Q) from the Bruker, Renishaw and RIAS

7.4 Scanning Electron Microscopy (SEM) and Powder X-Ray Diffraction

The SEM images of the mixtures clearly show the presence of two distinct compounds (Figs. 7.10–7.18) and the powder XRD diffractograms from individual compounds and mixtures (figures 7.19- 7.21) show significant differences between the diffraction patterns of the individual compounds and their mixtures.

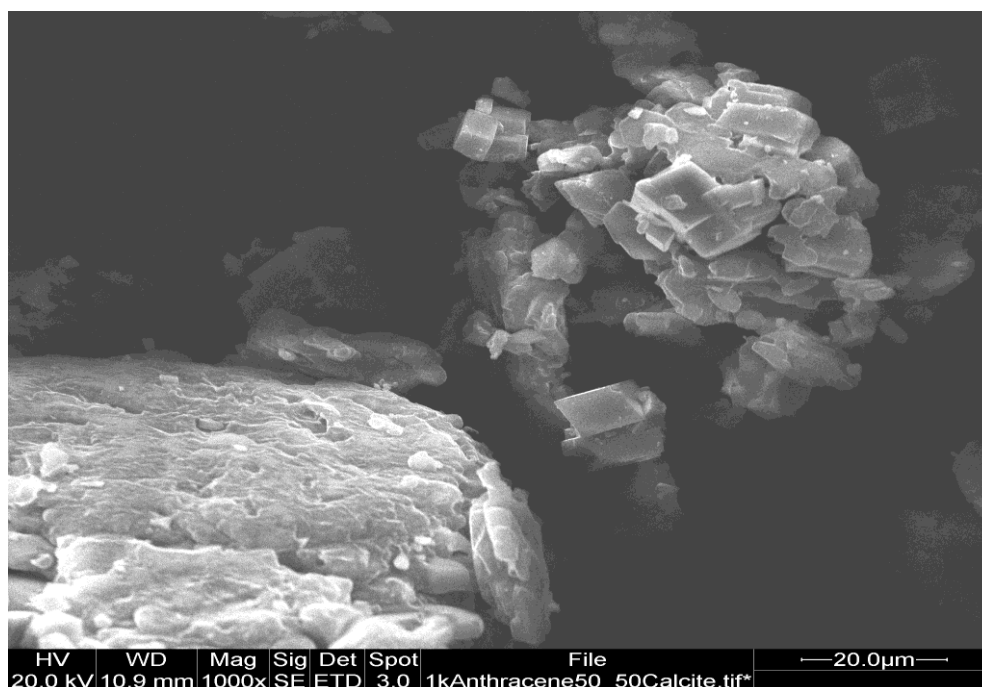


Figure 7.10 SEM of anthracene 50-50 calcite mixture

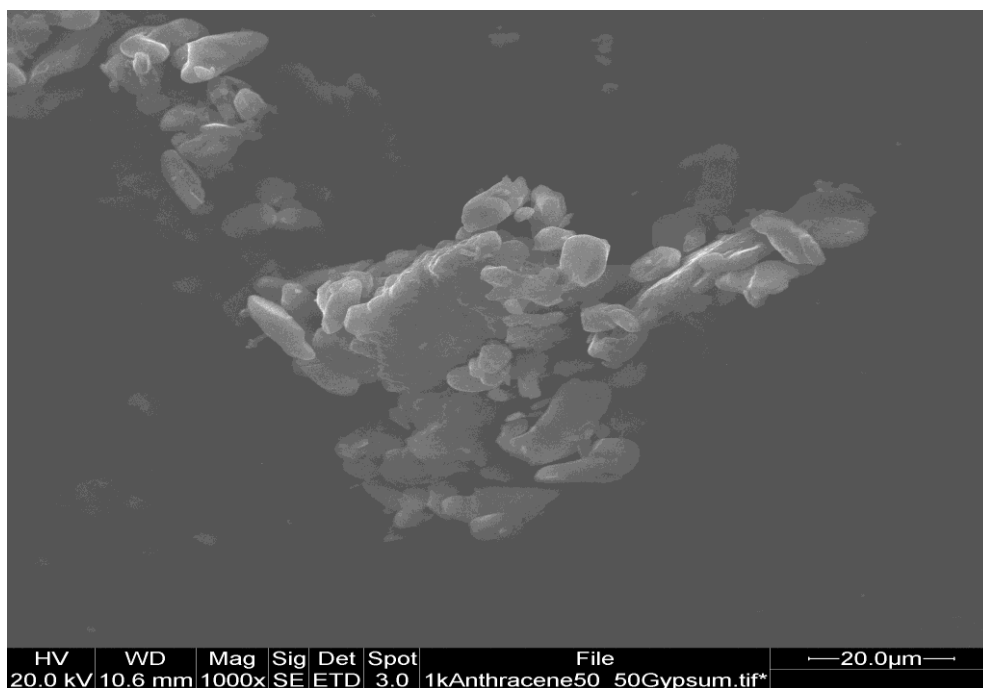


Figure 7.11 SEM of anthracene 50-50 gypsum

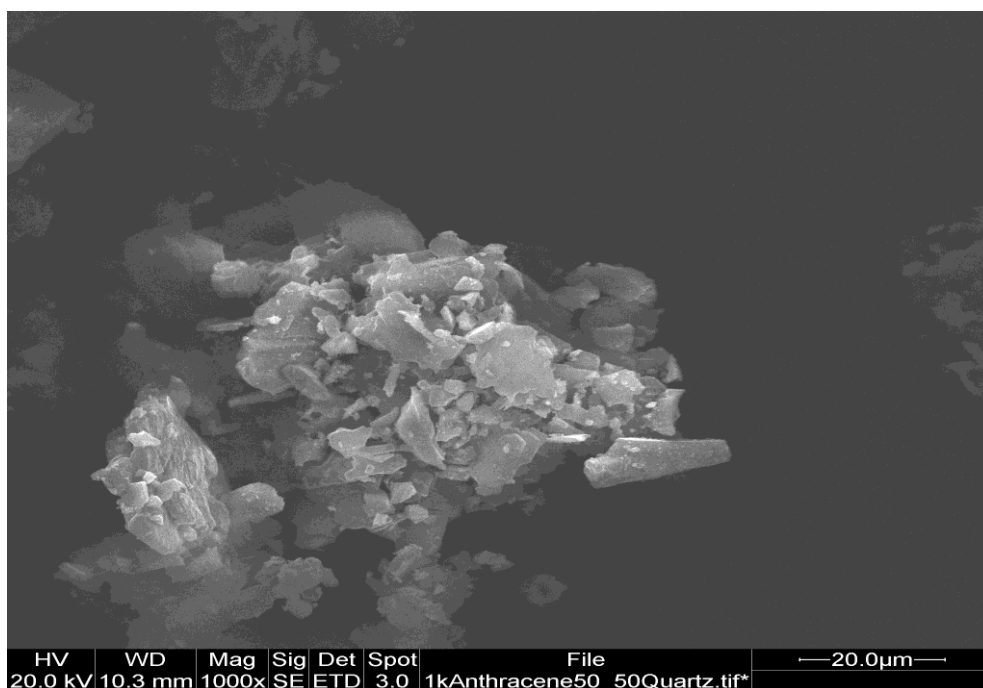


Figure 7.12 SEM of anthracene 50-50 quartz mixture

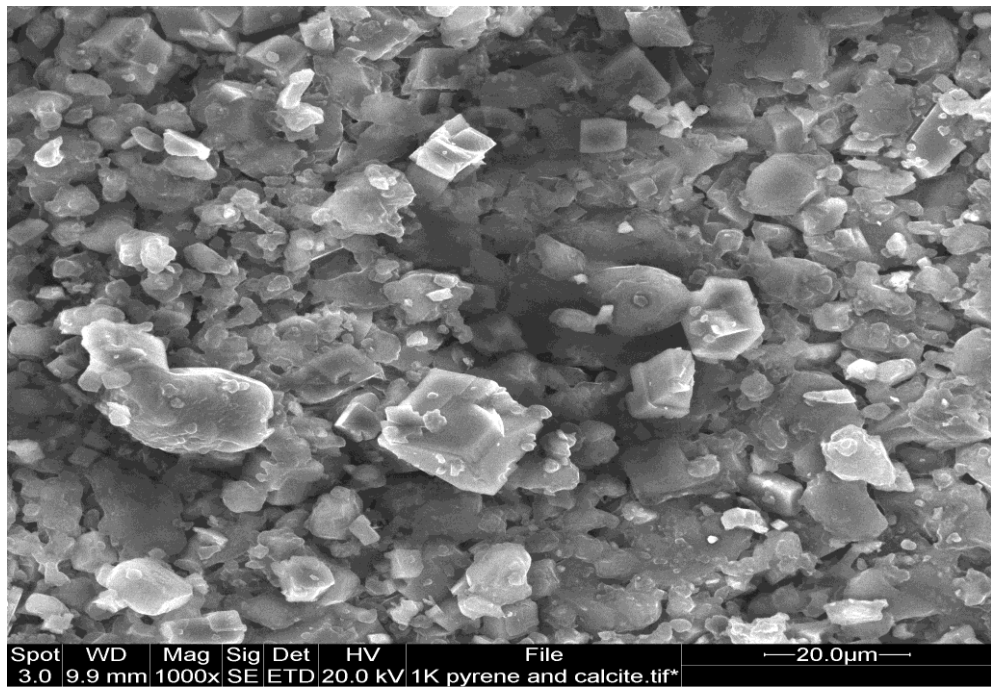


Figure 7.13 SEM of pyrene 50-50 calcite mixture

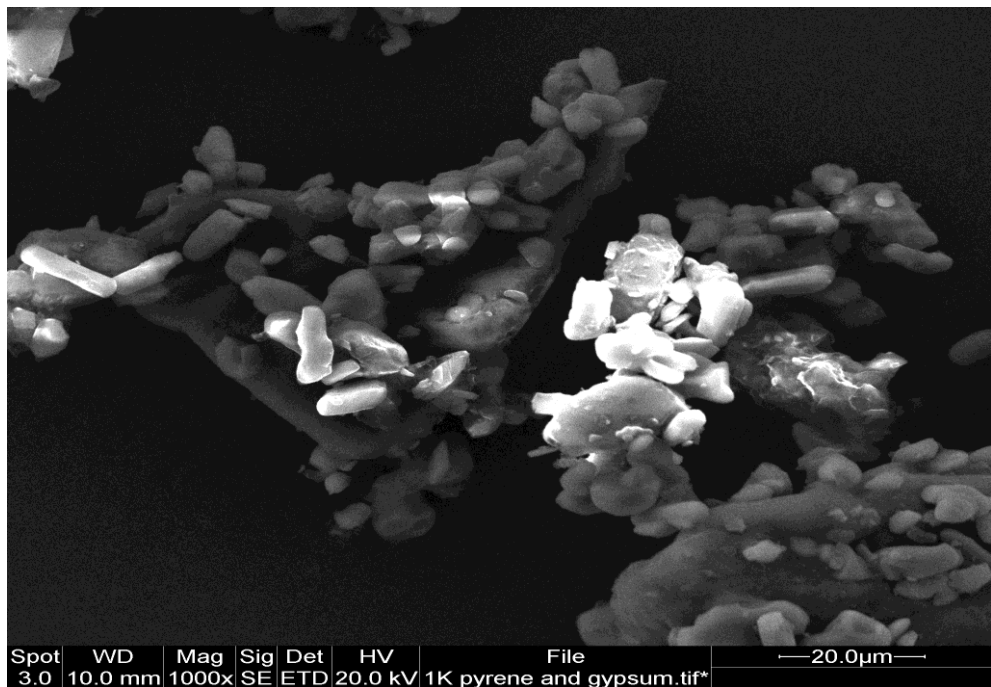


Figure 7.14 SEM of pyrene 50-50 gypsum mixture

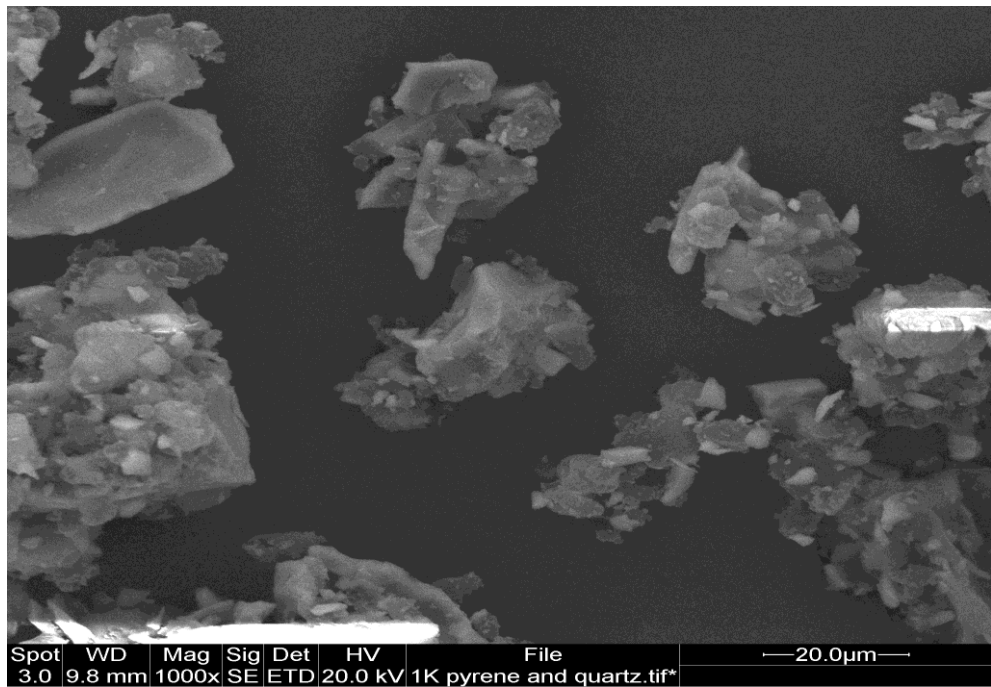


Figure 7.15 SEM of pyrene 50-50 quartz mixture

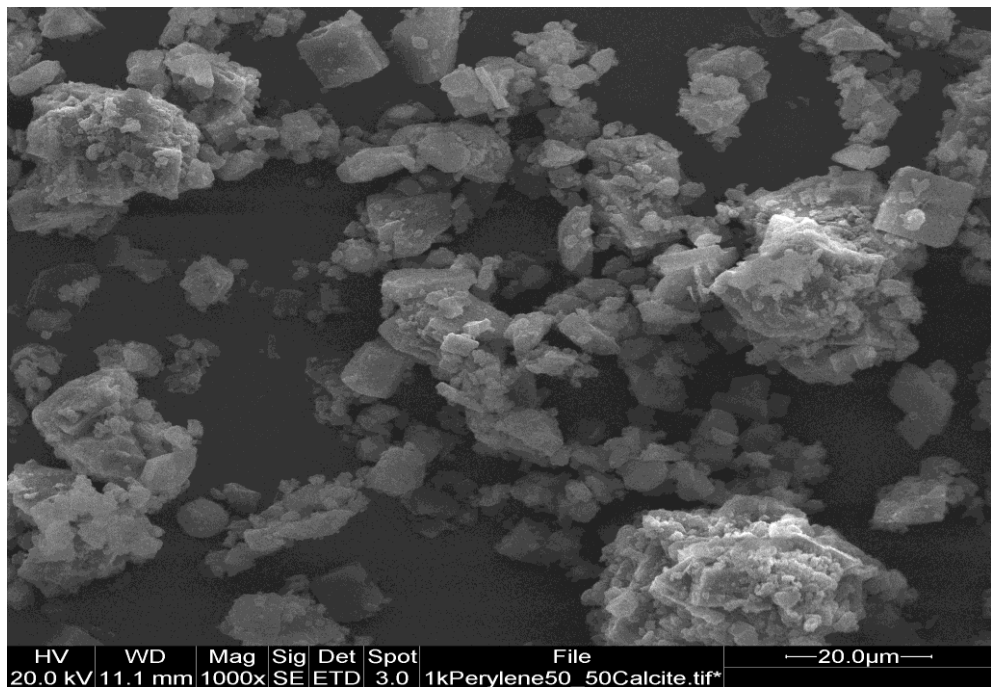


Figure 7.16 SEM of perylene 50-50 calcite mixture

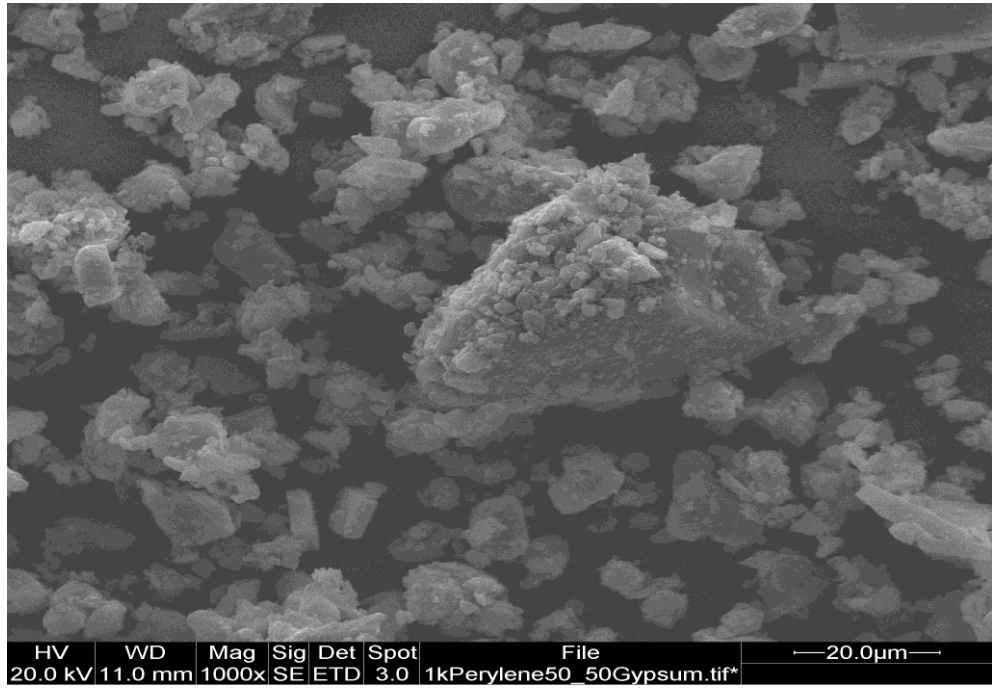


Figure 7.17 SEM of perylene 50-50 gypsum mixture

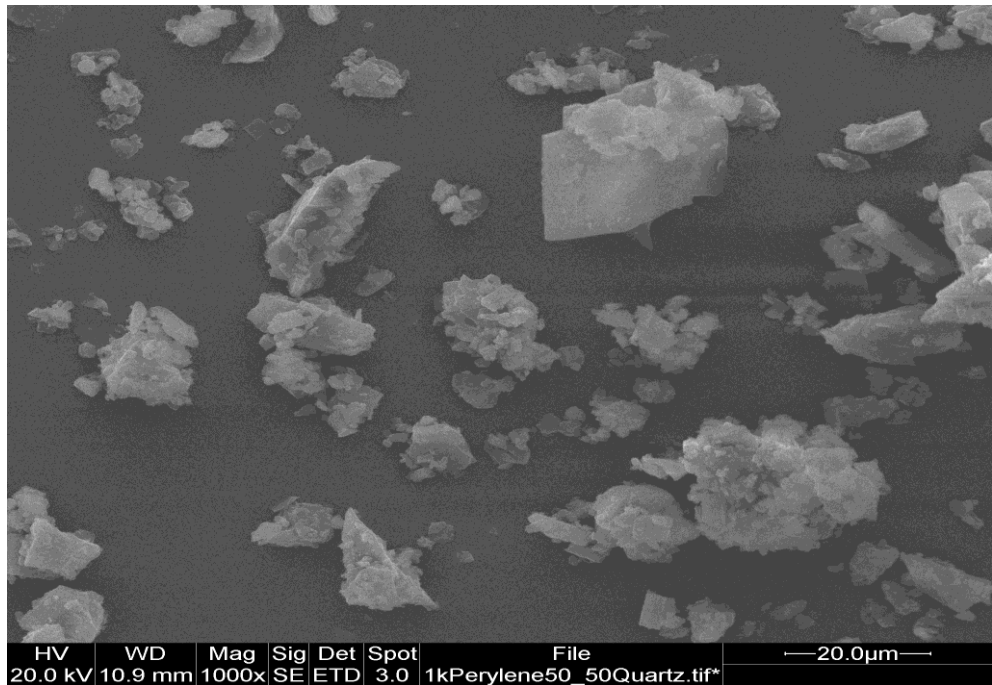


Figure 7.18 SEM of perylene 50-50 quartz mixture

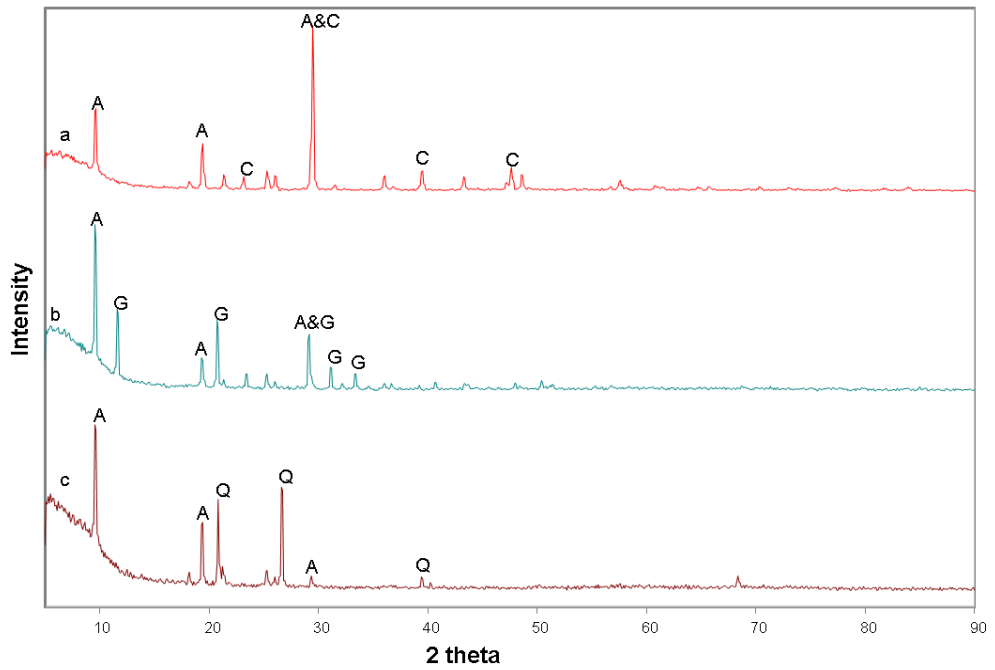


Figure 7.19 XRD pattern of (a) anthracene (A) and calcite (C), (b) anthracene (A) and gypsum (G) and (c) anthracene (A) and quartz (Q) in 50-50 mixtures

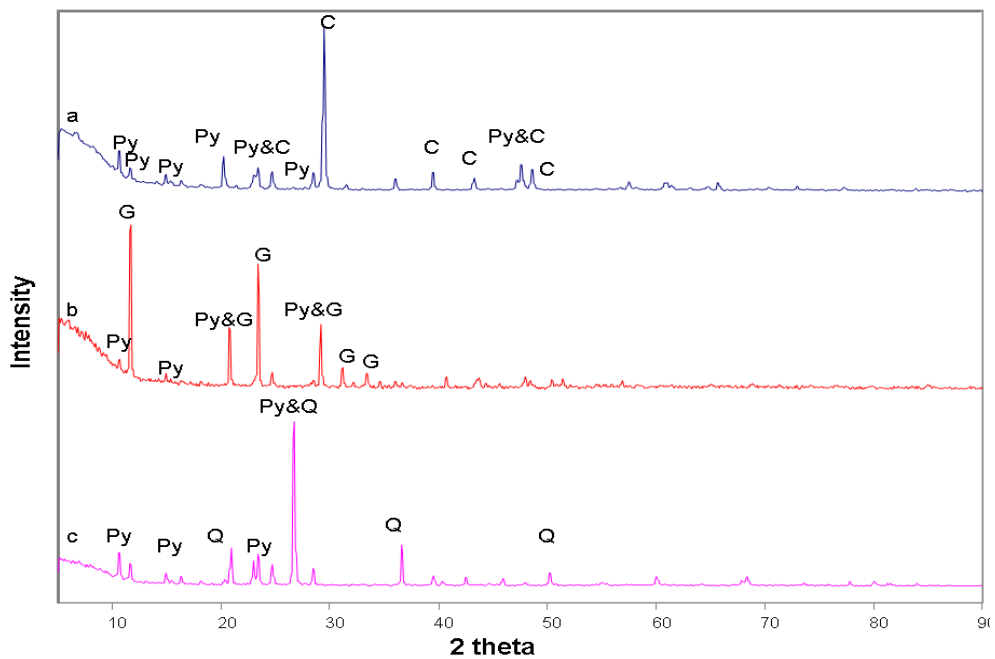


Figure 7.20 XRD pattern of (a) pyrene (Py) and calcite (C), (b) pyrene (Py) and gypsum (G) and (c) pyrene (Py) and quartz (Q) in 50-50 mixtures

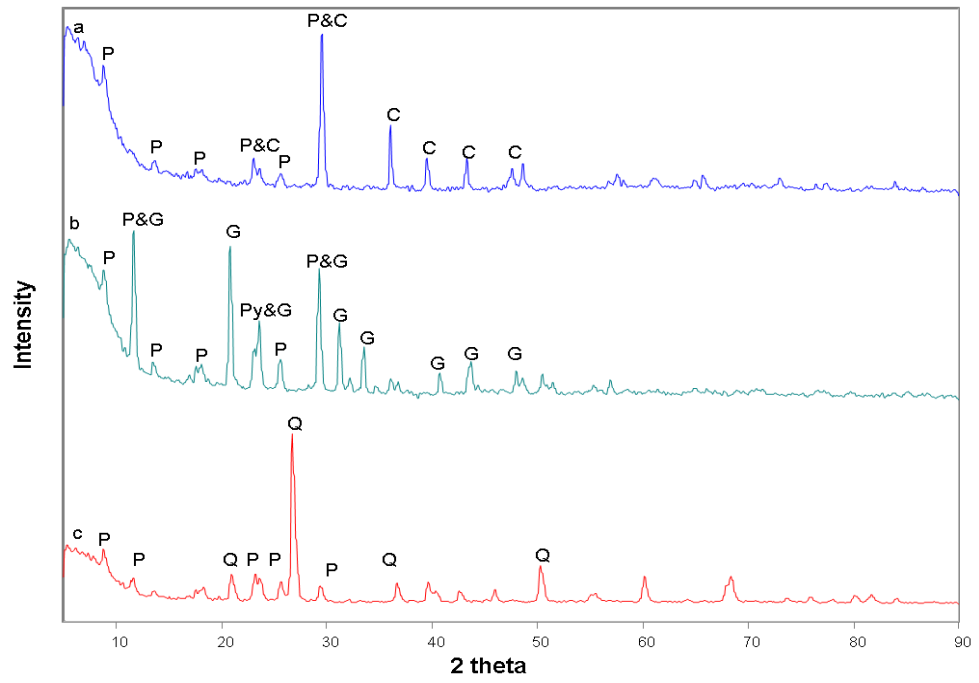


Figure 7.21 XRD pattern of (a) perylene (P) and calcite (C), (b) perylene (P) and gypsum (G) and (c) perylene (P) and quartz (Q) in 50-50 mixtures

7.5 Conclusions

The ability to identify organic molecular components and minerals present in admixture in a specimen at the same time is another advantage of the Raman analytical technique applied to astrobiology.

The three polyaromatic hydrocarbons, anthracene, pyrene and perylene of all nine mixtures have been identified using at least two of the three instruments if not all three. The most difficult mixture to analyse was that of perylene and its matrix mixtures due to its high fluorescence when 785 nm excitation was used. The RIAS instrument did have some problem with the mixtures, but it was still possible to identify the compounds in admixture. It is important to note that it was more difficult to identify the mineral components of the mixtures and that only the strongest mineral bands were seen in the Raman spectra of the mixtures, although they were very clearly observed in XRD pattern. A detailed knowledge of the different chemical strategies adopted by terrestrial extremophiles, which are considered potential Martian analogues, is a prerequisite for planetary exploration and the study of geo and bio-markers together to provide an understanding of the adaptation abilities of the organisms is considered essential.

7.6 References

- [1] R. F. Knacke, *Astrobiology*, **2003**, 3 (3), 531.
- [2] J. Vago, B. Gardini, G. Kminek, P. Baglioni, G. Gianfiglio, A. Santovincenzo, A. Bayon, M. Van Winnendael: *Esa Bulletin-European Space Agency*, **2006**,16.
- [3]J. L. Bada, M. A. Sephton, P. Ehrenfreund, R. A. Mathies, A. M. Skelley, F. J. Grunthaner, A. P. Zent, R. C. Quinn, J. L. Josset, F. Robert, O. Botta, D. G. Glavin, *Astronom Geophys*, **2005**,46 (6),26.

- [4] G. Kminek, J. L. Bada, O. Botta, D. P. Glavin, F. Grunthaner, *Planet Space Sci*, **2000**, 48 (11), 1087.
- [5] D. Schulze-Makuch, L. N. Irwin, *Astrobiology*, **2003**, 3 (3), 487.
- [6] A. Ellery, A. J. Ball, C. Cockell, D. Dickensheets, H. G. M. Edwards, C. Kolb, H. Lammer, M. Patel, L. Richter, *Acta Astronautica*, **2005**, 56 (3), 397.
- [7] A. Ellery, D. D. Wynn-Williams, *Astrobiology*, **2003**, 3 (3), 565.
- [8] A. Ellery, D. D. Wynn-Williams, J. Parnell, H.G.M. Edwards, D. Dickensheets, *Journal of Raman Spectroscopy*, **2004**, 35(6), 441.
- [9] S. E. J. Villar, H. G. M. Edwards, *Anal. Bioanal. Chem*, **2006**, 384 (1), 100.
- [10] D. L. Dickensheets, D. D. Wynn-Williams, H. G. M. Edwards, C. Schoen, C. Crowder, E. M. Newton, *Journal of Raman Spectroscopy*, **2000**, 31(7), 633
- [11] J. R. Cronin, S. Pizzarello, *Adv. Space Res*, **1983**, 3, 3.
- [12] M. H. Engel, S. A. Macko, *Organic Chemistry*, Plenum Press, New York, USA, **1983**
- [13] S. D. Killops, V. J. Killops, *An introduction to Organic Geochemistry*, Longman, UK, **1993**
- [14] K. E. Peters, J. M. Moldowan, *Naturwissenschaften*, **1978**, 65, 611.
- [15] G. Winnewisser, *J. Mol. Struct*, **1997**, 408, 1.
- [16] M. A. Sephton, *Nat. Prod. Rep*, **2002**, 19, 292.
- [17] U. Meierhenrich, G. M. Munoz Caro, J. H. Bredehoft, E. K. Jessberger, W. H. P. Thiemann, *PNAS*, **2004**, 101, 9182.
- [18] J. R. Cronin, S. Pizzarello, *Adv. Space Res*, **1983**, 3, 5.
- [19] J. R. Cronin, S. Pizzarello, *Organic matter in carbonaceous chondrites, planetary satellites, asteroids and comets*. In: Kerridge, J.F., Matthews, M.S. (Eds.), *Meteorites and the Early Solar System*. University of Arizona Press, Tucson, **1988**.

CHAPTER 8 Part 1

The effect of spectral resolution on the Raman spectra of polycyclic aromatic hydrocarbons and beta-carotene mixtures

8.1.1 Introduction

Raman spectroscopy has been proposed as part of an instrumentation suite for the remote detection of materials using robotic landers for planetary surface exploration [1] (ESA, ExoMars mission 2018) because of the ability to identify key organic biomaterials in their host mineralogical matrices as has already been demonstrated for extremophiles in terrestrial niche scenarios [2]. A fundamental process in the remote detection of extant or extinct life biomolecules using Raman spectroscopy is the detection of the changes in the band signatures [3] accompanied by molecular interactions in mixtures due to the different molecular environments that are created in the samples under investigation.

Polycyclic aromatic hydrocarbons (PAHs) are believed to be the most abundant free organic molecules in deep space [4, 5]. PAH molecules are produced partly in the outer atmospheres of carbon stars or formed by shock fragmentation of carbonaceous solid material. PAHs may also form eventually in the diffuse interstellar gas by neutral-neutral reactions [6] or by energetic processing of specific ices in dense clouds [7,8] and they play a central role in interstellar gas phase chemistry [9]. The environmental conditions and local ultraviolet radiation fields determine their charge and hydrogenation state. PAHs are ubiquitously distributed in the interstellar medium and are also seen in traces in solar system matter. Terrestrially, PAHs occur in the partial degradation processes of plant material en route to the formation of carbon and graphitic deposits.

Carotenoids are common in nature occurring, in fruit, vegetables, flowers, leaves and seeds [10] (e.g. bixin, the main pigment extract from the seed of the annatto tree) and animals, from molluscs [11] and lichens [12] to higher life forms. They have strong colours due to the high electric dipole transition moment of the $\pi - \pi^*$ ($S_0 - S_2$) electronic

absorption transition [13], the observed colour depending upon the extent of conjugation of the double bonds in the main polyene chain.

The search for evidence of life, whether extant and extinct, is one of the most challenging objectives of future Mars exploration. In addition to modified geosignatures such as morphological features, erosion consistent with biological processes and the presence of geosignatures such as aragonite and whewellite life can leave traces biosignatures (e.g., organic macromolecules) that can be explained only by biological activity [14] allowing us to detect its past and present occurrence. On Earth, molecular biomarkers derive from biochemical precursors through reduction or oxidation process and generally include lipids and pigments, their derivatives and diverse degradation products [15, 16]. Within the payload of the forthcoming instruments currently being developed by ESA and NASA for future missions on Mars, Raman spectroscopy is considered as a fundamental instrument for characterizing mineralogical and organic material. Therefore, it is necessary to perform a series of Earth-based analyses on terrestrial Martian-analogs to evaluate the possibilities of Raman spectroscopy in this context and subsequently to facilitate future in-situ measurements on planetary surfaces and subsurfaces.

The Raman spectra of a suite of geological mineral specimens which are relevant to Martian planetary exploration under different conditions of spectral resolution have been previously reported using a laser excitation wavelength of 1064 nm [17].

In previous studies beta-carotene was investigated as biomarker in the experimentally prepared mixtures with three powdered evaporitic matrices gypsum, epsomite, and halite in various proportions and the results demonstrated that it was possible to identify the characteristic Raman signals of beta-carotene at low levels [18].

In this study, we have investigated the effect of spectral resolution on the Raman spectra of beta-carotene (5-95) naphthalene, beta-carotene (5-95) anthracene, beta-carotene (5-95) pyrene, naphthalene, anthracene and pyrene. These results will provide useful information to build up a database of simulated systems which can be used for the remote detection of possible life signatures in planetary exploration arising from PAHs and other biomolecules in crystalline mineral matrices [19] and to assess the reliability of Raman spectral diagnostic interpretation under different experimental conditions

8.1.2 Experimental

Anthracene, naphthalene, pyrene and beta-carotene were supplied by Sigma-Aldrich (UK) and ALFA AESAR (UK). All the compounds were used as received.

Three mixtures of polyaromatic hydrocarbons and beta-carotene, two groups of key biomaterials identified for detection on Mars, were analysed using Fourier-transform Raman spectroscopy was undertaken using a Bruker IFS 66 instrument with an FRA 106 Raman module attachment and a Nd³⁺ /YAG laser operating at 1064 nm laser excitation. The laser power was set at about 10 μ W at the sample and the samples run for co-accumulations of 500 scans with spectral resolutions of 4, 6, 8, 16, 32 cm^{-1} , the total time required for each co-added spectral data set was about 30s. Initial experiments indicated that the molecular scattering factors for the carotenoids were about 20:1 compared with the PAHs, hence the three mixtures selected were of the following composition: beta-carotene (5-95) naphthalene mixture, beta-carotene (5-95) anthracene mixture and beta-carotene (5-95) pyrene mixture. Each PAH compound was mixed separately with beta-carotene and the mixtures were ground and homogenized manually in an agate mortar.

Solid state mixtures of the beta-carotene in PAHs were prepared representing 5-95 PAH to beta-carotene.

The assignments of anthracene, naphthalene, pyrene and beta-carotene have been made from previous assignments [3 and 19-30].

8.1.3 Results and discussion

8.1.3.1 Beta-carotene

The beta-carotene spectrum recorded at 4 cm^{-1} spectral resolution contains two strong Raman band at $1513, 1156\text{ cm}^{-1}$ and one medium Raman band at 1008 cm^{-1} and several weak Raman bands at $1584, 1353, 1270, 1211$ and 1190 cm^{-1} (Fig 8.1.1).

When the spectrum is collected using 6 and 8 cm^{-1} spectral resolution, some of these weaker bands disappear.

No significant changes were visible between the spectra collected at 16 or 32 cm^{-1} spectral resolution except that the bands become broader and some weaker bands disappear (Table 8.1.1).

| 4 cm⁻¹ | P.W | 6 cm⁻¹ | P.W | 8 cm⁻¹ | P.W | 16 cm⁻¹ | P.W | 32 cm⁻¹ | P.W | Assignment |
|------------------------------|-------|------------------------------|-------|------------------------------|-------|-------------------------------|------------|-------------------------------|-------|--|
| 1584 w | 0.139 | - | - | - | - | - | - | - | - | |
| 1513 st | 3.022 | 1513 st | 3.272 | 1513 st | 5.507 | 1514 st | 22.63 9 | 1514 st | 0.854 | in-phase v (C=C) |
| 1353 w | 0.069 | 1355 w | - | - | - | - | - | - | - | |
| 1270 w | 0.036 | 1270 w | 0.185 | 1271 w | 0.298 | 1273 w | 0.379 | - | - | |
| 1211 w | 0.072 | - | - | - | - | - | - | - | - | |
| 1190 w | 0.140 | 1189 w | 0.068 | 1189 w | 0.085 | - | - | - | - | |
| 1156 st | 2.478 | 1155 st | 1.523 | 1155 st | 2.339 | 1155 st | 5.225 | 1157 st | 2.521 | v (C-C) stretching vibrations |
| 1008 m | 0.766 | 1008 st | 0.650 | 1008 st | 1.006 | 1009 st | 1.081 | 1009 st | 0.525 | in-plane rocking modes of (C-CH ₃) |

* P.W = peak width; vst = very strong; st = strong; m = medium; w = weak; vw = very weak; sh = shoulder; w sh = weak shoulder

Table 8.1.1 Raman signatures from beta-carotene recorded at different spectral resolutions

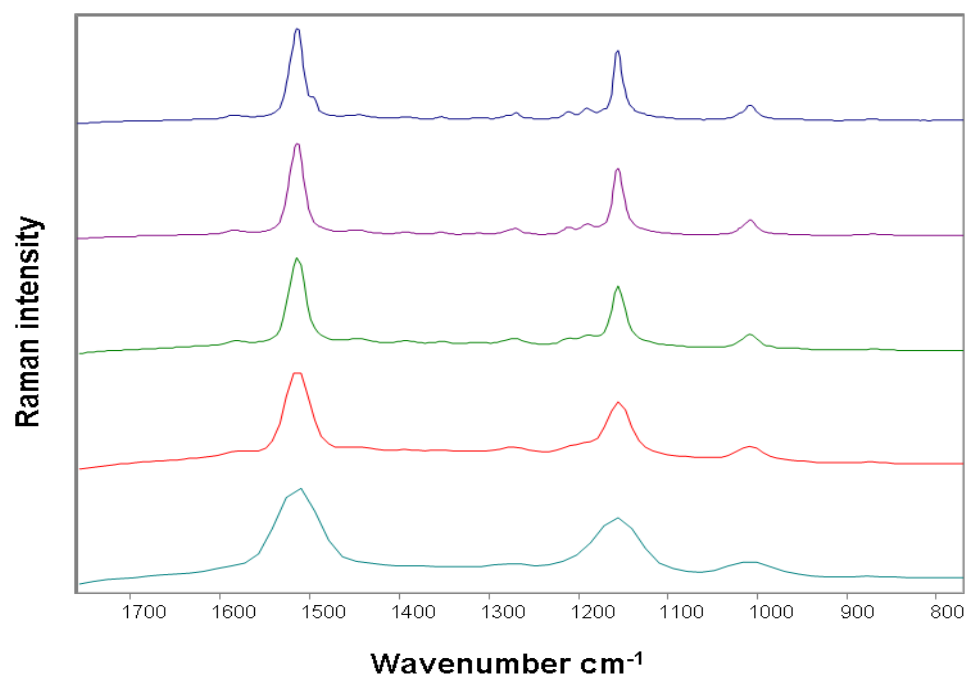


Fig. 8.1.1. Raman spectra of beta-carotene recorded at different spectral resolutions (from top 4, 6,8,16 and 32 cm⁻¹)

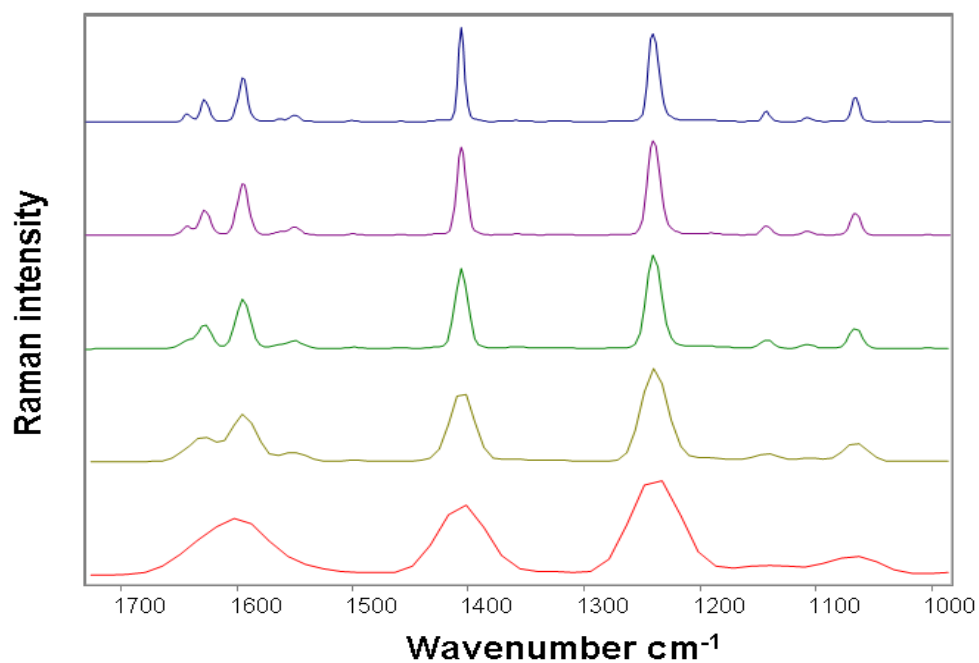


Fig. 8.1.2. Raman spectra of pyrene recorded at different spectral resolutions (from top 4, 6,8,16 and 32 cm⁻¹)

| 4 cm ⁻¹ | P.W | 6 cm ⁻¹ | P.W | 8 cm ⁻¹ | P.W | 16 cm ⁻¹ | P.W | 32 cm ⁻¹ | P.W | Assign- ment |
|-----------------------|-------|-----------------------|------------|-----------------------|------------|------------------------|------------|---------------------|------------|---|
| 3054 m | 5.290 | 3054 m | 6.708 | 3055 m | 7.020 | 3055 m | 8.403 | 3050 m | 9.073 | CH stretching |
| 3021 w | 0.056 | - | - | - | - | - | - | - | - | |
| 3010 w | 1.781 | 3011 w | 2.571 | 3013 w | 0.678 | - | - | - | - | |
| 1642 w | 0.248 | 1642 w | 3.857 | - | - | - | - | - | - | CC stretching |
| 1627 m | 2.065 | 1627 m | 10.52 9 | 1627 m | 6.004 | 1629 m | 4.839 | - | - | |
| 1594 m | 3.912 | 1594 m | 9.878 | 1594 m | 10.19 6 | 1594 m | 16.97 0 | 1599 m | 18.59 4 | CCH stretching |
| 1406 st | 6.064 | 1406 st | 14.46 4 | 1406 st | 13.75 0 | 1406 st | 13.38 | 1406 st | 14.787 | C=C in plane vibration, Skeletal ring vibrations |
| 1240 | 9.421 | 1240 | 20.85 0 | 1239 | 20.56 5 | 1239 | 19.88 3 | 1239 | 19.371 | CH bending |
| 1142 st | 0.732 | 1142 st | 1.715 | 1142 st | 1.449 | 1143 st | 0.872 | - | - | CH bending |
| 1107 w | 0.332 | 1107 w | 0.841 | 1007 w | 0.624 | - | - | - | - | |
| 1065 w | 1.760 | 1065 w | 3.847 | 1065 w | 3.445 | 1066 w | 3.140 | 1068 w | 2.621 | CH bending |
| 842 w | 0.218 | 842 w | 0.442 | 841 w | 0.432 | - | - | - | - | |
| 804 w | 0.166 | 803 w | 0.370 | 803 w | 0.356 | - | - | - | - | |
| 592 m | 3.354 | 592 m | 6.281 | 592 m | 6.174 | 591 m | 6.272 | 591 m | 6.525 | CCC ring deformati on |
| 503 w | 0.697 | 503 w | 1.401 | 502 w | 1.377 | 503 w | 1.548 | - | - | |
| 457 w | 0.764 | 457 w | 1.449 | 457 w | 1.399 | 457 w | 1.496 | - | - | |
| 407 st | 4.686 | 407 st | 8.377 | 407 st | 8.091 | 407 st | 8.532 | 407 st | 11.479 | |
| 262 w | 0.730 | 262 w | 1.216 | 262 w | 1.077 | 262 w | 1.248 | 258 w | 0.964 | |

* P.W = peak width; vst = very strong; st = strong; m = medium; w = weak; vw = very weak; sh = shoulder; w sh = weak shoulder

Table 8.1.2 Raman signatures from pyrene recorded at different spectral resolutions

8.1.3.2 Pyrene

The spectrum achieved using 4 cm^{-1} spectral resolution shows three strong bands at 1406, 1142 and 407 cm^{-1} , four medium bands at 3054, 1627, 1594 and 592 cm^{-1} and several weak bands at 3021, 3010, 1642, 1107, 1065, 842, 804, 503, 457 and 262 cm^{-1} .

No significant changes were visible between the spectra collected at 6 and 8 cm^{-1} spectral resolution except that the weak band at 3021 cm^{-1} disappears.

At 16 cm^{-1} spectral resolution some weaker bands disappear and the medium band at 1627 cm^{-1} now appears as a shoulder with its wavenumber position centred at 1629 cm^{-1} (Fig 8.1.6).

At 32 cm^{-1} spectral resolution only the strong and medium bands appear with two weak features but the compound is still clearly identifiable from the Raman spectrum (Table 8.1.6).

8.1.3.3 Anthracene

Spectra were collected at 4 cm^{-1} spectral resolution and showed bands at 3050 (weak), 3028 (weak), 1557 (weak), 1480 (weak), 1401 (strong), 1259 (weak), 1186 (weak), 1163 (weak), 1007 (weak), 752 (weak), 477 (weak), and 394 (medium) cm^{-1} .

No significant changes were visible in the spectra collected at 6 and 8 cm^{-1} , but at 16 and 32 cm^{-1} spectral resolution the bands become broader; however, most bands can still be registered, and in addition the bands at 1186 and 1164 cm^{-1} appear now as a single band centred at 1183 cm^{-1} at 16 cm^{-1} spectral resolution and 1178 cm^{-1} at 32 cm^{-1} spectral resolution (Fig 8.1.3).

Although the bands at 16 and 32 cm^{-1} spectral resolution are broader than in the previous spectral resolution setting they can still be observed and the compound is clearly identifiable from the Raman spectrum (Table 8.1.3).

| 4 cm^{-1} | P.W | 6 cm^{-1} | P.W | 8 cm^{-1} | P.W | 16 cm^{-1} | P.W | 32 cm^{-1} | P.W | Assignment |
|--------------------|-------|--------------------|--------|--------------------|--------|---------------------|--------|---------------------|--------|--|
| 3050 w | 4.609 | 3051 w | 7.543 | 3051 w | 10.075 | 3050 w | 10.761 | 3047 w | 11.379 | C-H stretching |
| 3028 w | 1.788 | 3028 w | 3.613 | 3028 w | 0.270 | - | - | - | - | |
| 1557 w | 5.202 | 1557 w | 9.586 | 1556 w | 9.915 | 1556 w | 11.161 | 1555 w | 0.133 | C=C stretching |
| 1480 w | 3.480 | 1480 w | 6.997 | 1480 w | 8.013 | 1480 w | 8.473 | 1480 w | 1.233 | C=C stretching |
| 1401 st | 23.99 | 1401 st | 44.916 | 1401 st | 46.434 | 1401 st | 46.093 | 1401 st | 63.346 | C=C in plane vibration |
| 1259 w | 2.012 | 1259 w | 3.850 | 1259 w | 3.841 | 1259 w | 4.015 | 1257 w | 3.376 | =C-H in plane deformation vibration |
| 1186 w | 1.792 | 1186 w | 3.250 | 1186 w | 3.333 | - | - | - | - | |
| 1163 w | 1.367 | 1164 w | 2.457 | 1164 w | 2.415 | 1183 w | 5.964 | 1178 w | 5.749 | =C-H in plane deformation vibration |
| 1007 w | 3.213 | 1007 w | 6.035 | 1007 w | 6.374 | 1006 w | 6.184 | 1006 w | 6.529 | =C-H in plane deformation vibration |
| 752 w | 6.193 | 753 w | 10.153 | 752 w | 9.708 | 752 w | 9.608 | 754 w | 9.615 | C-H out of plane deformation vibration |
| 477 w | 0.588 | 477 w | 0.967 | 477 w | 0.882 | 478 w | 1.066 | - | - | |
| 394 m | 7.024 | 394 m | 10.978 | 394 m | 11.05 | 395 m | 11.07 | 394 m, | 14.228 | CCC bending |

* P.W = peak width; vst = very strong; st = strong; m = medium; w = weak; vw = very weak; sh = shoulder; w sh = weak shoulder

Table 8.1.3 Raman signatures from anthracene recorded at different spectral resolutions

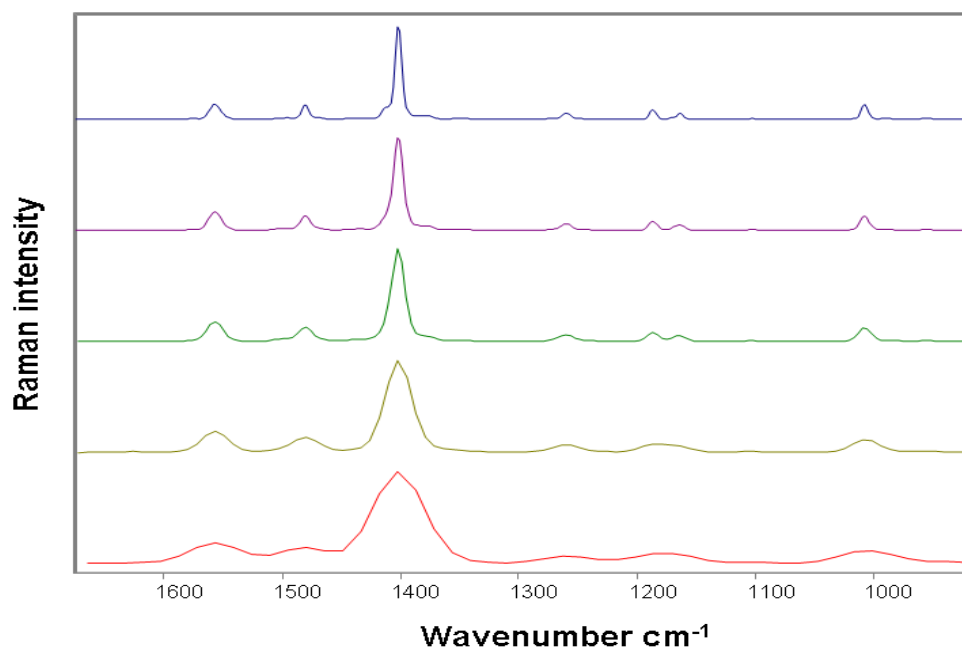


Fig. 8.1.3 Raman spectra of anthracene recorded at different spectral resolutions (from top 4, 6, 8, 16 and 32 cm^{-1})

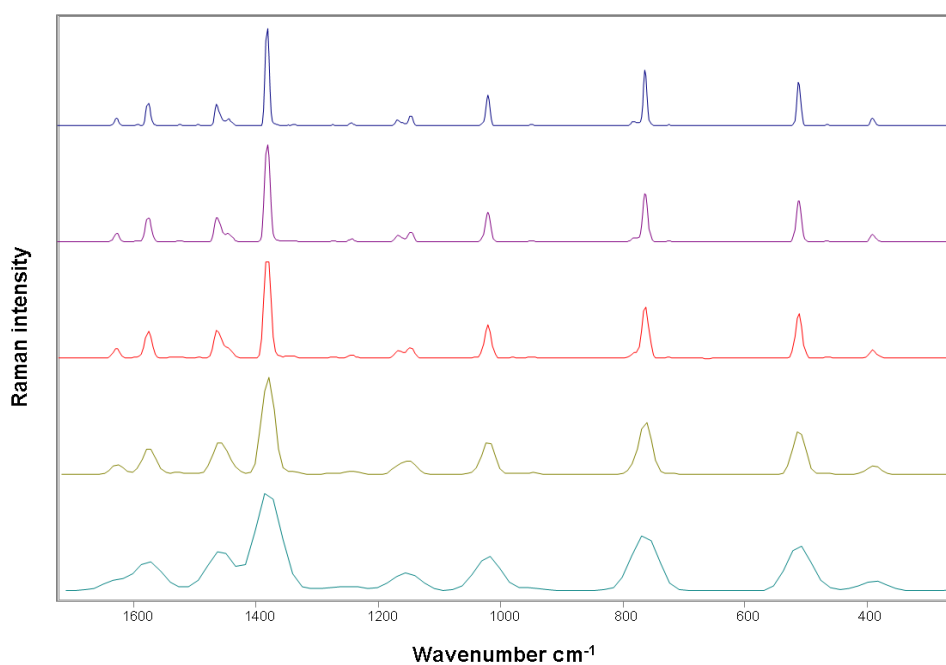


Fig. 8.1.4 Raman spectra of naphthalene recorded at different spectral resolutions (from top 4, 6, 8, 16 and 32 cm^{-1})

8.1.3.4 Naphthalene

The spectrum collected at 4 cm⁻¹ spectral resolution shows strong bands at 3055 and 1381 cm⁻¹, medium bands at 1576, 1463 and 1020 cm⁻¹ and weak bands at 3006, 1628, 1444, 1244, 1168, 1146 (doublet), 782 (shoulder), 763, 512 and 391 cm⁻¹.

No significant changes were visible in the spectrum collected at 6 and 8 cm⁻¹ spectral resolution but the same results were obtained when the spectrum is collected at either 16 or 32 cm⁻¹ spectral resolution; however, now the bands are visibly broader, the doublet at 1168, 1146 cm⁻¹ becomes a single band centred at 1152 cm⁻¹ and the weak bands at 3006 and 782 (shoulder) cm⁻¹ disappear but the main bands still appear at their characteristic Raman bands (Fig 8.1.4) (Table 8.1.4).

| 4 cm ⁻¹ | P.W | 6 cm ⁻¹ | P.W | 8 cm ⁻¹ | P.W | 16 cm ⁻¹ | P.W | 32 cm ⁻¹ | P.W | Assignment |
|--------------------|-------|--------------------|-------|--------------------|-------|---------------------|-------|---------------------|-------|---------------------------|
| 3055 st | 3.674 | 3055 st | 2.418 | 3055 st | 4.477 | 3055 st | 4.660 | 3054 st | 5.104 | CH stretching |
| 3006 w | 0.394 | 3006 w | 0.151 | 3007 w | 0.266 | - | - | - | - | |
| 1628 w | 0.272 | 1627 w | 0.861 | 1628 w | 0.842 | 1628 w | 0.068 | - | - | |
| 1576 m | 0.756 | 1575 m | 2.308 | 1575 w | 2.338 | 1575 m | 2.369 | 1577 m | 3.259 | C=C stretching |
| 1463 m | 1.117 | 1463 m | 3.779 | 1462 m | 3.570 | 1460 m | 3.422 | 1457 m | 1.406 | |
| 1444 w | 0.005 | 1445 w | 0.258 | - | - | - | - | - | - | |
| 1381 st | 2.650 | 1381 | - | 1381 | - | 1381 | - | 1381 | - | C=C in plane vibration |
| 1244 w | 0.088 | - | - | - | - | - | - | - | - | |
| 1168 w | 0.263 | 1167 w | 0.734 | 1166 w | 0.671 | - | - | - | - | |
| 1146 w | 0.295 | 1146 w | 0.912 | 1146 w | 0.921 | 1152 w | 1.571 | 1155 w | 1.411 | |
| 1020 m | 1.022 | 1020 m | 2.813 | 1020 m | 2.834 | 1020 m | 2.894 | 1021 m | 2.993 | =C-H in plane deformation |

| | | | | | | | | | | |
|-----------|-------|-----------|-------|-----------|-------|----------|-------|----------|-------|--------------------------------------|
| | | | | | | | | | | vibration |
| 782 sh | 0.030 | 781 sh | 0.080 | 779 sh | 4.705 | - | - | - | - | |
| 763 w | 1.814 | 763 w | 4.699 | - | - | 764 w | 4.781 | 763 w | 4.839 | CCC in- plane bending modes |
| 512 w | 1.369 | 512 w | 3.528 | 512 w | 3.590 | 512 w | 3.687 | 513 w | 3.817 | C-C ring deformations |
| 391 w | 0.290 | 391 w | 0.805 | 390 w | 0.836 | 390 w | 0.842 | 390 w | 0.857 | |

* P.W = peak width: vst = very strong; st = strong; m = medium; w = weak; vw = very weak; sh = shoulder; w sh = weak shoulder

Table 8.1.4 Raman signatures from naphthalene recorded at different spectral resolutions

8.1.3.5 Beta-carotene (5-95) pyrene mixture

The spectrum achieved with 4 cm^{-1} spectral resolution shows two strong bands at 1513, 1156 cm^{-1} , six medium intensity bands at 1594, 1405, 1240, 1007, 592 and 407 cm^{-1} and several weak bands, as shown in table 8.1.5.

No significant changes were visible in the spectra collected at 6 and 8 cm^{-1} spectral resolution except that the weaker bands and shoulders at 1642 and 1548 cm^{-1} respectively, disappear from the observed spectra.

At 16 and 32 cm^{-1} spectral resolution some weak bands disappear and others appear as shoulders but at a different wavenumber position (Fig 8.1.5). This latter feature is of critical concern to the construction of automatic spectral databases which require precise

wavenumber signature for the diagnostic recognition of biomarkers life-detection in complex mixtures.

| 4 cm⁻¹ | P.W | 6 cm⁻¹ | P.W | 8 cm⁻¹ | P.W | 16 cm⁻¹ | P.W | 32 cm⁻¹ | P.W |
|------------------------------|------------|------------------------------|------------|------------------------------|------------|-------------------------------|------------|-------------------------------|------------|
| 3054 w | 4.906 | 3054 w | 4.310 | 3054 w | 4.358 | 3054 w | 3.671 | 3049 w | 3.469 |
| 3010 vwsh | 0.645 | 3011 vwsh | 0.474 | 3013 vwsh | 0.395 | 3006 vwsh | 0.203 | - | - |
| 1642 vw | 1.006 | 1642 vw | 2.2078 | - | - | - | - | - | - |
| 1627 w | 4.801 | 1627 w | 4.190 | 1627 w | 3.247 | 1626 w | 1.192 | - | - |
| 1594 m | 7.018 | 1594 m | 6.100 | 1593 m | 5.668 | 1591 w | 0.058 | 1590 wsh | 0.035 |
| 1548 wsh | 0.071 | 1548 wsh | 0.075 | - | - | - | - | - | - |
| 1513 vst | 53.811 | 1513 vst | 46.225 | 1514 vst | 43.871 | 1514 vst | 51.373 | 1515 vst | 64.006 |
| 1445 vw | 1.028 | 1446 vw | 0.806 | 1446 w | 0.749 | 1450 wsh | 0.549 | - | - |
| 1405 m | 5.836 | 1405 m | 5.689 | 1405 m | 4.973 | 1405 w | 3.396 | 1408 w | 2.239 |
| 1352 w | 1.014 | 1353 w | 1.522 | 1353 w | 0.773 | 1353 w | 0.689 | - | - |
| 1312 w | 0.371 | 1312 w | 0.276 | 1311 w | 0.192 | - | - | - | - |
| 1269 w | 1.338 | 1270 w | 1.500 | 1270 w | 1.336 | - | - | - | - |
| 1240 m | 5.158 | 1240 m | 8.564 | 1239 m | 6.020 | 1239 w | 2.711 | 1228 wsh | 0.609 |
| 1210 w | 1.246 | 1210 w | 0.764 | 1210 w | 0.449 | - | - | - | - |
| 1189 w | 1.512 | 1189 w | 0.911 | 1188 w | 0.658 | - | - | - | - |
| 1156 vst | 36.595 | 1156 vst | 36.474 | 1155 vst | 34.824 | 1154 st | 39.602 | 1156 st | 51.795 |
| 1065 w | 1.293 | 1065 w | 1.856 | 1065 w | 1.562 | 1063 w | 1.287 | - | - |
| 1007 m | 9.813 | 1008 m | 9.557 | 1007 m | 8.815 | 1009 m | 6.777 | 1009 m | 15.990 |
| 871 w | 0.916 | 871 w | 0.372 | 871 w | 1.020 | 873 w | 1.103 | 869 w | 1.224 |

| | | | | | | | | | |
|-----------|-------|-----------|-------|-----------|-------|----------|-------|----------|-------|
| 592 m | 1.673 | 592 m | 1.740 | 592 m | 1.628 | 591 w | 1.507 | 590 w | 1.180 |
| 407 m | 2.042 | 407 w | 1.711 | 407 w | 1.724 | 407 w | 1.757 | 407 w | 2.638 |
| 261 vw | 4.030 | 261 vw | 2.053 | 261 vw | 0.962 | - | - | - | - |

* P.W = peak width; vst = very strong; st = strong; m = medium; w = weak; vw = very weak; sh = shoulder; w sh = weak shoulder

Table 8.1.5 Raman signatures from a beta-carotene (5-95) pyrene mixture recorded at different spectral resolutions

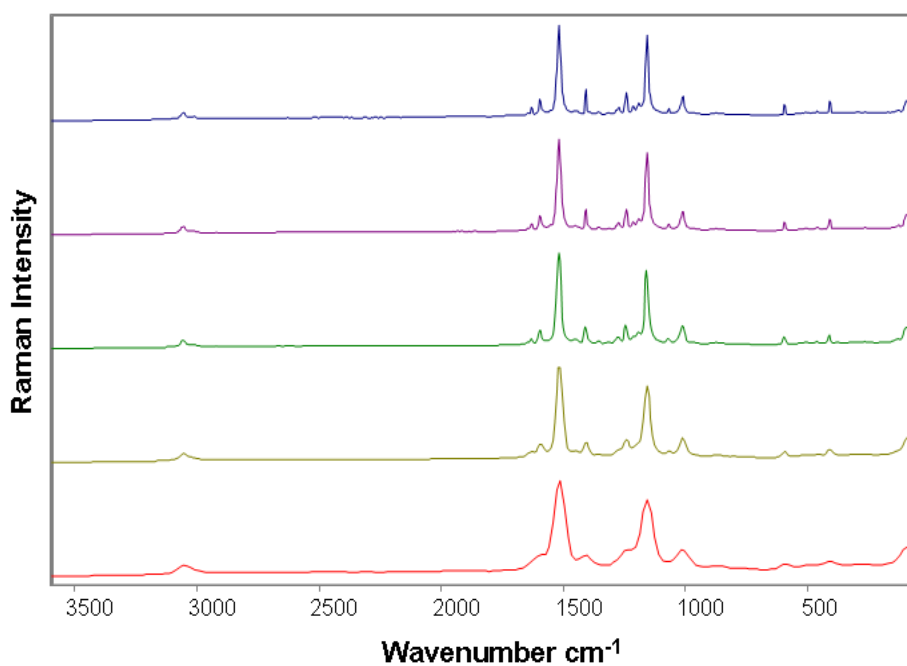


Fig. 8.1.5 Raman spectra of a beta-carotene (5-95) pyrene mixture recorded at different spectral resolutions (from top 4, 6, 8, 16 and 32 cm^{-1})

8.1.3.6 Beta-carotene (5-95) anthracene mixture

The FT-Raman spectrum of a beta-carotene (5-95) anthracene mixture collected at 4 cm⁻¹ spectral resolution shows two strong bands at 1513 and 1156 cm⁻¹, one medium band at 1007 cm⁻¹ and several weak bands as seen in table 8.1.6.

When the spectrum is collected using 6 or 8 cm⁻¹ spectral resolution, no significant changes were visible except that the two weaker intensity bands disappear.

At 16 and 32 cm⁻¹ spectral resolution, however, some weaker bands disappear and the weak band at 1270 cm⁻¹ appears as a shoulder centred at 1264 cm⁻¹ at 32 cm⁻¹ spectral resolution (Fig 8.1.6).

| 4 cm⁻¹ | P.W | 6 cm⁻¹ | P.W | 8 cm⁻¹ | P.W | 16 cm⁻¹ | P.W | 32 cm⁻¹ | P.W |
|------------------------------|-------|------------------------------|-------|------------------------------|-------|-------------------------------|-------|-------------------------------|-------|
| 3071 vw | 0.021 | 3070 vw | 0.150 | 3070 vw | 0.363 | 3061 w | 0.350 | 3057 w | 0.338 |
| 1621 w | 0.110 | 1620 w | 0.185 | 1616 w | 0.176 | - | - | - | - |
| 1613 w | 0.079 | - | - | - | - | - | - | - | - |
| 1586 w | 0.358 | 1586 w | 0.390 | 1585 w | 0.362 | 1583 w | 0.025 | - | - |
| 1513 vst | 4.698 | 1513 vst | 5.050 | 1514 vst | 4.573 | 1514 vst | 4.916 | 1515 st | 6.329 |
| 1440 w | 0.410 | 1441 w | 0.152 | 1441 w | 0.431 | 1443 w | 0.128 | - | - |
| 1393 w | 0.099 | 1393 vw | 0.149 | 1392 w | 0.046 | - | - | - | - |
| 1349 w | 0.346 | 1349 w | 0.437 | 1349 w | 0.320 | 1349 w | 0.250 | 1349 w | 0.776 |
| 1314 vw | 0.023 | 1314 vw | 0.019 | 1316 vw | 0.020 | - | - | - | - |
| 1269 w | 0.174 | 1270 w | 0.518 | 1271 w | 0.284 | 1270 w | 0.183 | 1264 wsh | 0.043 |

| | | | | | | | | | |
|-------------|-------|-------------|-------|-------------|-------|------------|-------|------------|-------|
| 1245 wsh | 0.013 | - | - | - | - | - | - | - | - |
| 1210 w | 0.249 | 1210 w | 0.065 | 1209 w | 0.142 | - | - | - | - |
| 1189 w | 0.118 | 1189 w | 0.094 | 1188 w | 0.132 | - | - | - | - |
| 1156 vst | 3.481 | 1155 vst | 4.234 | 1155 vst | 3.829 | 1154 st | 4.194 | 1156 st | 5.145 |
| 1036 wsh | 0.054 | 1035 wsh | 0.030 | 1035 wsh | 0.036 | - | - | - | - |
| 1007 m | 0.886 | 1007 m | 1.391 | 1007 m | 1.154 | 1009 m | 1.125 | 1010 m | 2.287 |
| 871 vw | 0.146 | 871 vw | 0.201 | 871 vw | 0.115 | 871 vw | 0.093 | 861 w | 0.098 |
| 828 vw | 0.028 | 828 vw | 0.025 | 828 vw | 0.027 | 828 vw | 0.298 | - | - |
| 710 w | 0.093 | 710 w | 0.101 | 710 w | 0.106 | 710 w | 0.164 | 713 w | 0.660 |
| 409 w | 0.124 | 409 w | 0.114 | 409 w | 0.105 | 409 w | 0.280 | 405 w | 1.886 |
| 248 w | 0.092 | 248 w | 0.329 | 248 w | 0.074 | 248 w | 0.107 | - | - |

* P.W = peak width; vst = very strong; st = strong; m = medium; w = weak; vw = very weak; sh = shoulder; w sh = weak shoulder

Table 8.1.6 Raman signatures from a beta-carotene (5-95) anthracene mixture recorded at different spectral resolutions

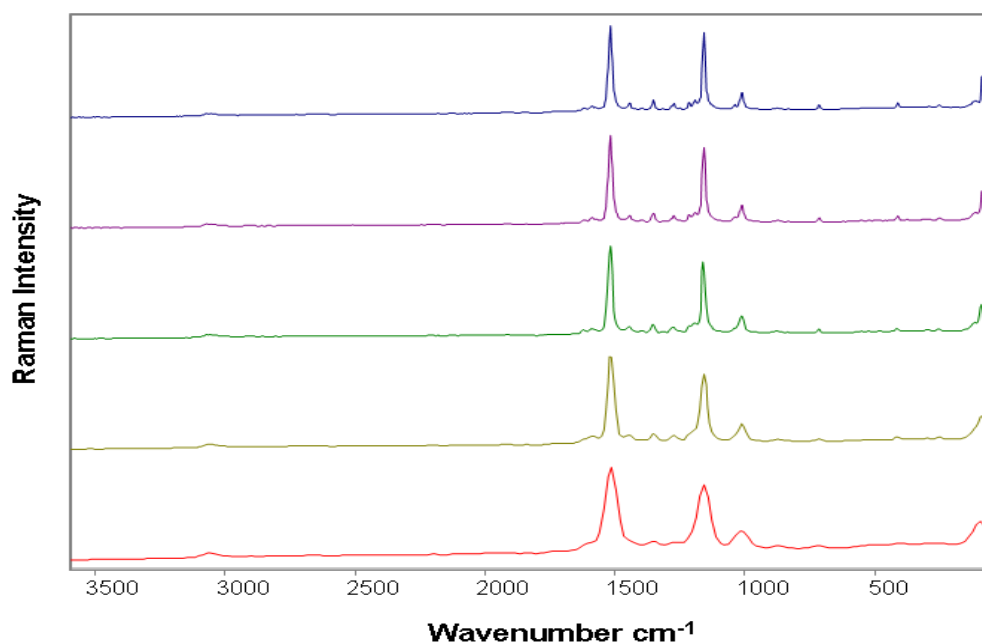


Fig. 8.1.6 Raman spectra of a beta-carotene (5-95) anthracene mixture recorded at different spectral resolutions (from top 4, 6,8,16 and 32 cm⁻¹)

8.1.3.7 Beta-carotene (5-95) naphthalene mixture

Spectra were collected from a beta carotene (5-95) naphthalene mixture at 4 cm⁻¹ spectral resolution and showed two strong bands and two medium intensity bands at 1513, 1156, 1381 and 1008 cm⁻¹, respectively, also several weak bands as shown in table 8.1.7.

No significant changes were visible in the spectra collected at 6 and 8 cm⁻¹, but at 16 and 32 cm⁻¹ spectral resolution, the bands become broader. Most bands can still be

registered, but the bands at 1461 and 1445 cm^{-1} appear now as shoulder centred at 1458 cm^{-1} at 16 cm^{-1} spectral resolution, also the band at 1381 cm^{-1} becomes a shoulder at 32 cm^{-1} spectral resolution (Fig 8.1.7).

Although the bands at 16 and 32 cm^{-1} spectral resolution are broader than at other spectral resolution settings, they can still be observed and the mixture is clearly identifiable from the Raman spectrum.

| 4 cm^{-1} | P.W | 6 cm^{-1} | P.W | 8 cm^{-1} | P.W | 16 cm^{-1} | P.W | 32 cm^{-1} | P.W |
|--------------------|--------|--------------------|--------|--------------------|--------|---------------------|--------|---------------------|--------|
| 3055 w | 0.601 | 3055 w | 0.405 | 3055 w | 1.123 | 3055 w | 0.351 | 3052 w | 1.821 |
| 1627 vw | 0.009 | 1626 w | 0.054 | 1630 w | 0.189 | - | - | - | - |
| 1576 w | 2.387 | 1577 w | 0.790 | 1578 w | 0.891 | 1578 w sh | 1.477 | - | - |
| 1513 vst | 19.230 | 1513 vst | 22.757 | 1513 vst | 23.563 | 1514 vst | 26.893 | 1514 v st | 26.257 |
| 1463 w | 0.809 | 1462 w | 0.938 | 1461 w | 0.606 | 1485 wsh | 0.357 | - | - |
| 1445 w | 1.107 | 1445 w | 1.399 | 1445 w | 1.422 | - | - | - | - |
| 1381 m | 1.404 | 1381 w | 1.686 | 1381 w | 1.883 | 1381 w | 2.446 | 1381 wsh | 0.495 |
| 1352 vw | 0.362 | 1352 vw | 0.689 | 1352 w | 0.253 | - | - | - | - |
| 1312 w | 0.105 | 1312 vw | 0.132 | 1312 vw | 0.105 | - | - | - | - |
| 1269 w | 1.059 | 1270 w | 2.182 | 1271 w | 2.040 | 1271 w | 2.411 | 1270 wsh | 0.327 |
| 1210 w | 0.356 | 1210 w | 0.517 | 1210 w | 0.512 | - | - | - | - |
| 1189 w | 0.490 | 1189 w | 0.516 | 1189 w | 0.468 | - | - | - | - |
| 1156 vst | 15.534 | 1156 vst | 18.007 | 1155 vst | 18.190 | 1154 st | 20.136 | 1156 st | 19.946 |
| 1008 m | 5.333 | 1008 m | 5.598 | 1008 m | 5.483 | 1010 m | 5.769 | 1010 m | 4.859 |
| 871 w | 0.431 | 871 w | 0.523 | 871 w | 0.511 | 872 w | 0.672 | 870 w | 0.797 |
| 763 w | 0.491 | 763 w | 0.547 | 763 w | 0.454 | 764 w | 0.487 | 764 w | 0.558 |
| 512 w | 0.630 | 512 w | 0.514 | 513 w | 0.367 | 512 w | 0.709 | 506 w | 0.600 |
| 288 w | 0.255 | 289 w | 1.651 | 289 w | 0.262 | - | - | - | - |

* P.W = peak width; vst = very strong; st = strong; m = medium; w = weak; vw = very weak; sh = shoulder; w sh = weak shoulder

Table 8.1.7 Raman signatures from beta-carotene (5-95) naphthalene mixture recorded at different spectral resolutions

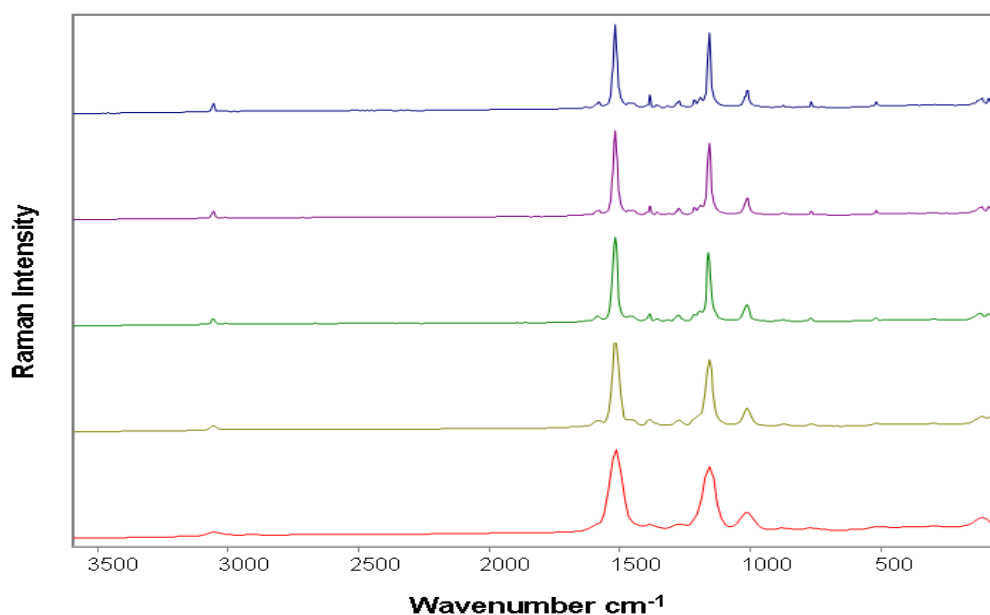


Fig. 8.1.7 Raman spectra of a beta-carotene (5-95) naphthalene mixture recorded at different spectral resolutions (from top 4, 6,8,16 and 32 cm^{-1})

8.1.4 Conclusions

PAHs and carotenoids with a few strong characteristic Raman bands, such as naphthalene, anthracene, pyrene or beta-carotene, are still clearly distinguishable at 32 cm^{-1} spectral resolution. At this spectral resolution the main bands, even those with medium intensity, appear clearly in the spectrum and act as distinctive Raman biomarkers.

While no significant changes were observed between the FT-Raman spectra of polyaromatic hydrocarbons alone and in beta-carotene collected at 4 and 6 cm^{-1} spectral resolutions, the spectra collected at 8, 16, and 32 cm^{-1} spectral resolution have a

significantly different spectral appearance. The bands in the spectra collected at 8 cm^{-1} are well-resolved whereas those collected at 16 and 32 cm^{-1} have some overlapping features which could compromise the spectral identification of biomarker in the biochemical composition.

The Raman spectra of PAHs and beta-carotene collected at 16 cm^{-1} spectral resolution show some significant bands, although not every band is observed; others are observed often wavenumber-shifted from those which appear when the spectrum is collected with higher spectral resolution, e.g. 4 cm^{-1} . These latter are the spectral data which generally appear in literature databases for PAHs and carotenoid compounds and their mixtures.

These results will provide useful information to build up a database of simulated systems which can be used for the remote detection of possible life signatures in planetary exploration arising from PAHs and other biomolecules in crystalline mineral matrices.

8.1.5 References

- [1] A. Ellery, D.D. Wynn-Williams, *Astrobiology*, **2003**,3 (3), 565.
- [2] S.E .Jorge Villar, H. G.M .Edwards and L. G. Benning, *Icarus*, **2006**,184(1),158.
- [3] H. G.M .Edwards, S.E .Jorge Villar, J .Jehlicka, T .Munshi, *spectrochim Acta A*, **2005**,61,2273.
- [4] L .d'Hendecourt, P .Ehrenfreund, *Adv. Space Res*, **1997**,19,1023.
- [5] J. L.Puget, A .L'eger, *Annu. Rev. Astron. Astrophys*, **1989**, 27,161.
- [6] R. P. Bettens, E. Herbst , *Astrophysical Journal*, **1996**,468,686.
- [7] R. I. Kaiser, K. Roessler, *Astrophysical Journal*. **1998**,503, 959.
- [8] E.L.O .Bakes, A.G.G.M. Tielens , *Astrophysical Journal*, **1994**,427,822.
- [9] E. L. O. Bakes, A. G. G. M. Tielens , *Astrophysical Journal*. **1998**,499 ,258.

- [10] L.F.C. de Oliveira, S.O. Dantas, E.S. Velozo, P.S. Santos, M.C.C Ribeiro, *J.Mol.Struct*, **1997**, 435 ,101.
- [11] A. Vershinin, *Comp. Biochem. Physiol*, **1996** ,113B, 63.
- [12] F.J. Chu, M. R. D. Seaward, H. G. M. Edwards, *Spectrochim. Acta Part A*, **1998**. 54, 967.
- [13] R.Withnall , B. Z. Chowdhry, J. Silver, H. G.M. Edwards, L. F.C. de Oliveira, *Spectrochimica Acta Part A*, 2003,59, 2207
- [14] D. Schulze-Makuch, L. N. Irwin, Springer, Berlin, Heidelberg, **2004**, 172.
- [15] C. D. Litchfield, A. Oren, *Hydrobiologia*, **2001**,466 ,81.
- [16] B.R.T.Simoneit, *Adv. Space Res*, **2004**, 33, 1255.
- [17] H. G. M .Edwards, S. E .Jorge Villar, *Vibrational Spectroscopy*, **2005**,39 ,88.
- [18] P. Víték, J. Jehlicka, H. G. M. Edwards, K. Osterrothova, *Anal. Bioanal. Chem* , **2009**, 393,1967.
- [19] J. Jehlicka, H. G. M. Edwards, P. Vitek, *Planetary and space Science*, **2009**, 57, 606.
- [20] M. Z. Tabrizi, S. F. Tayyari, F. Tayyari , M. Behforouz, *Spectrochimica Acta Part A*, **2004**, 60 (1-2), 111.
- [21] H. G. M .Edwards, S. E .Jorge Villar, J. Jehlicka , T. Munshi, *Spectrochim Acta A*, **2005**, 61,2273.
- [22] M. Delhayé, J. Barbillat, J. Aubard, M. Bridoux, E. Da Silva, in: Turrell G Corset. J (Ed.), *Raman Microscopy: Developments and Applications*, Academic Press, London, **1996**.
- [23] D. Lin-Vien, J. G. Grasselli, N. B. Colthup, W.G. Fateley, *The Handbook of Infrared and Raman Characteristic Frequencies of Organic Molecules*, Academic Press, San Diego, **1991**.

- [24] G. Socrates, *Infrared Characteristic Group Frequencies: Tables and Charts* (Third ed.), John Wiley & Sons Ltd., New York, **2001**.
- [25] J. Jehlicka, H. G. M. Edwards , S. E. JorgeVillar, O. Frank, *Journal of Raman Spectroscopy* , **2006**, 37,220.
- [26] J. Jehlicka, H. G. M. Edwards, *Organic Geochemistry*, **2008**, 39,371.
- [27] L. J .Allamandola, A. G. G. M. Tielens, J. R .Barker, *The Astrophysical Journal Supplement Series*, **1989**, 71, 733.
- [28] D. Gill, R. G. Kilponen , L. Rimai, *Nature*, **1970**, 227, 743.
- [29] M. Veronelli, G. Zerbi, *Journal of Raman Spectroscopy*, **1995**, 26,683.
- [30] R. J. Weesie, J. C. Merlin, J. Lugtenburg, G. Britton, F. J. H. M. Jansen, J. P. Cornard, *Biospectroscopy*, **1999**, 5, 19.

CHAPTER 8 Part 2

The Effect of Laser wavelength on The Raman spectra of Phenanthrene, chrysene and Tetracene: Implication for extra-Terrestrial detection of Polyaromatic hydrocarbons

8.2.1 Introduction

Polycyclic aromatic hydrocarbons (PAHs) are a group of chemical compounds with a condensed benzene ring structure that are found at different concentrations in sedimentary rocks. Generally, they are products of the diagenetic and epigenetic transformation of primary organic matter buried in marine or non-marine sediments [1]. A rich palette of aromatic hydrocarbons occurs also in petroleum, coal oil and gas [2] and as the result of biodegradation processes [3]. In the environment they occur in substituted forms and in complicated mixtures; their characterization using solid-state spectroscopic techniques in such blends is very complicated so chromatography and mass spectroscopy have been the main analytical techniques adopted for their analysis. However, polyaromatic hydrocarbons can also appear more rarely in accumulated crystalline forms, e.g. idrialite, curtisite, pendletonite, kratochvilite and ravatite. The occurrence of these organic minerals is often related to the high temperature alteration of organic precursors. Hitherto, only ravatite [4] and idrialite [5,6] have been studied by means of Raman spectroscopy; whilst the assignment of the Raman spectra of ravatite (pure phenanthrene) is straightforward [4], idrialite (and also curtisite) represents a more complex mixture of chain-type PAHs with different molecular weights [7]. Simoneit et al. [8] have also reported the presence of higher-mass thio-PAHs similar to those occurring in idrialite in hydrothermal petroleum and tars from the Guyamas Basin, Escanaba Trough and Middle Valley hydrothermal systems [8] PAHs have been found specifically in carbonaceous chondrite meteorites [9], Martian meteorites [10-12] interplanetary dust particles [13], and in interstellar matter [13]. An infall-rate of organic matter onto the Martian surface of approximately 240 tons per year [14, 15], argues for the abiotic synthesis of PAHs directly on the Martian surface [16]. It is important to probe for PAHs in any survey for

organic carbon on or near the surface of Mars the largest organic molecules found in deep space are the polyaromatic hydrocarbons,"tar- like organic compounds"[16], and the presence of these compounds has a profound implication for carbon-based life in the universe [16].

Raman spectroscopy has several important characteristics which make it a valuable technique for extraterrestrial exploration. The possibility to analyze both organic and inorganic compounds with little or no sample preparation, the determination of the structural composition of the compounds, data acquisition from macro and micro samples, the possibility of in situ analyses and the adaptability for remote analyses make Raman spectrometry a desirable technique for the potential study of planetary surfaces.

There are now several prototype portable Raman spectrometers which are in various stages of adoption or evaluation for space exploration; these have a common feature with regard to robustness and small size, but they also have a selection of operating excitation wavelengths, all are based on rapid CCD detection and diode-laser technology[13,17]. Nevertheless, there is a major draw back when analysing organic compounds with Raman spectroscopy, namely the fluorescence emission arising from either the sample itself or from a small amount of contamination in the sample. The fluorescence emission can be minimised by the selection of an appropriate laser wavelength. Furthermore, the resultant Raman spectrum is in a lower energy region of the electromagnetic spectrum than the emitted fluorescence. The Raman intensity is inversely proportional to the fourth power of the laser wavelength, so the intensity of the Raman signal is weaker with infrared excitation [18].

In this study, experiments that explore the effects of using a variety of laser wavelengths for the excitation of Raman spectra of PAHs are described.

8.2.2. Experimental

8.2.2.1. Materials

Phenanthrene, chrysene, and tetracene were supplied by Sigma-Aldrich (UK) and AA pin Chemicals Limited (UK), and were used as received.

Structures of compounds were confirmed by powder XRD as shown in figure 8.2.3.1.

8.2.2.2. X-ray powder diffractometry

Powder X-ray diffractograms were recorded with a Bruker D8 diffractometer. The wavelength of the X-rays was 0.154 nm using a copper source, at a voltage of 40 kV and with filament emission of 30 mA. Each sample was scanned from 5-90° (2 θ) using a step width of 0.01° and a 1 second time count. The receiving slit was 1° and the scatter slit of 0.2°. The software used to read the data was EVA, which comprises both a means by which the data can be presented and manipulated and also a database with which to compare the data with spectra of known materials

8.2.2.3 Raman spectroscopy

8.2.2.3.1 1064 nm excitation

Fourier-transform Raman spectroscopy was carried out using a Bruker IFS 66 instrument with an FRA 106 Raman module attachment and a Nd³⁺/YAG laser operating at 1064 nm in the near infrared with a total acquisition time of about 20 minutes. Raman spectra were recorded at 4 cm⁻¹ spectral resolution and 500 spectral scans accumulated to improve signal-to-noise ratios. The laser power was set at 30 μ W at the sample. The spectra were collected over the wavenumber range 50 – 3600 cm⁻¹.

8.2.2.3.2 785, 633 and 514 nm excitations

Raman spectra were obtained using a Raman microscope (Renishaw plc.) with 785nm stabilized diode laser excitation, 633 nm He/Ne laser, and 514 Ar⁺ laser excitation. The laser beam was focused onto the sample using a 5x objective lens, resulting in a laser spot of approximately 10 μm diameter. Spectra were obtained for 5 accumulations, each of 10s exposure, of the CCD detector in the wavenumber range 100-3200 cm^{-1} using the extended scanning mode of the instrument, with approx 50 mW laser power. The total acquisition time of the spectrum for each sample was about eight minutes. Spectral acquisition, presentation, and analysis were performed with the Renishaw WIRE 2 (Renishaw plc) and GRAMS AI version 8 (Galactic Industries, Salem, NH) software.

8.2.3 Results and Discussion

A major problem with the analysis of PAH compounds by Raman spectroscopy is the fluorescence caused by either the sample itself or by the presence of small amounts of impurity. The fluorescence emission of aromatic molecules generally occurs in the near-UV to visible region and this can interfere with the Raman signals if excitation is located near that spectral region [19]. Fluorescence can usually be avoided if the Raman signal is located in the NIR part of the spectrum. However, there are two disadvantages associated with moving to NIR excitation; the Raman scattering intensity is inversely proportional to the fourth power of the laser wavelength, so the intensity of the Raman signal is weaker than with visible excitation; hence, practically, the acquisition time must be increased. In addition, the efficiency of the typical silicon-based CCD detector decreases significantly in the NIR region [20, 21]. The benefits of avoiding the background fluorescence emission, however, often outweigh the disadvantages of NIR laser excitation.

Raman band assignments for the studied compounds have been reported [20-29].

Figure 8.2.3.2 shows the Raman spectrum of phenanthrene obtained using the four different laser excitation wavelengths, 1064, 785, 633 and 514 nm. The spectra demonstrate that all four wavelengths show a similar response and they are comparable in spectral detail. No fluorescence was observed at any wavelength with the pure samples except for a small residual spectral background with the 514 nm excitation (Table 8.2.1).

Figure 8.2.3.3 shows the Raman spectrum obtained from chrysene with the four different excitation wavelengths. The spectra are stacked with 514 nm spectrum being at the bottom and the 1064 nm spectrum at the top. The wavenumbers and proposed assignments of the Raman bands are given in table 8.2.2. The spectrum of chrysene gained from the FT instrument was very clear, giving a good signal-to-noise ratio. The strongest peak occurred at 1381 cm^{-1} and was assigned to C-C stretching. Lower intensity bands at $1574, 1432\text{ cm}^{-1}$ are assigned to C=C stretching, 1363 cm^{-1} assigned to C-C stretching, 1017 cm^{-1} which been tentatively assigned as a C-H in-plane bending and 878 assigned to C-H out-of-plane bending. Other bands occur at 3078, 1621, 1162 and 294 cm^{-1} assignable to C-H stretching, C-C stretching vibrations, C-C stretching, C-C stretching and CCC out of plane bending, respectively.

Unassigned peaks of weaker intensity also occur at 1601, 1331, 1228, 1137, 1041, 769, 678, 567, 381 cm^{-1}

The spectra obtained from the low wavelength excitation lasers vary in quality and the information they contain. All have much lower signal-to-noise ratios than those examined using the 1064 nm laser source. The spectra from the 785, 633 and 514 nm laser sources show Raman bands superimposed on the background fluorescence emission. There is a small but significant background and the most intense band occurs at 1379 cm^{-1} for 785

nm excitation, 1380 cm^{-1} for 633 nm excitation and 1381 cm^{-1} for 514 nm, excitation as shown in Table 8.2.2

The spectrum gained from the tetracene sample proves to be the most varied quality. All of the spectra acquired can be seen in figure 8.2.3.4.

Again, the best quality Raman spectrum is that obtained from the 1064 nm laser source, with the most intense peaks appearing at 1542, 1447, 1384 cm^{-1} which can be assigned as C-C or ring stretching, CC stretching vibrations and a C=C in plane vibration, respectively. Other moderately intense signals appear at 3050(C-H stretching), 1616 (C=C stretching), 1403 (skeletal ring vibration), 494 (C-C deformation vibrations) and some peaks are assignable to C-H in plane deformations at 1197, 1180, 1160 and 997 cm^{-1} . As well as these, some low intensity peaks are also present at 1630, 1606, 1517, 1490, 1368, 973, 960, 851, and 213 cm^{-1} .

The spectrum acquired using 785 nm laser excitation is only of moderately good quality; however even in this case, where the fluorescent background is high, Raman bands can be identified. The most intense of these occur at 1540, 1445 and 1381 cm^{-1} (table 8.2.3).

The spectrum from the 633 nm laser source shows only four rather weak bands. The most intense of these are 1619, 1542 and 1383 cm^{-1} with a weaker band at 1447 cm^{-1} .

However, the spectrum resulting from the 514 nm laser source exhibits very high fluorescence with no relevant Raman bands observable.

8.2.4 Conclusions

The results gained from this study indicate a clear trend in the quality of the spectra gained from each laser source; it is not unexpected that the infra-red (1064 nm) laser with the Fourier-transform instrument provided the best data for the specimens under study

here. The low energy of the near infrared laser excitation was sufficient to combat fluorescence emission, which coupled with a relatively high number of repetitive scans accumulated, gave a much improved signal- to- noise ratio. The results gained from this study indicate that the best quality spectra are gained from 1064 and 785 excitation wavelengths.

Comparisons of these spectra with those collected by the use of higher energy lasers, reveal that of the latter the near infrared (785nm) was found to be the most successful; in the analysis of PAHs it was this laser which provided the clearest and most informative spectra. This is due to the higher fluorescence background present in the spectra excited by the higher energy 633 and 514 nm lasers. In the case of the 633 nm laser this prevented a complete observation of the entire spectrum and no peaks were recorded at this wavelength for tetracene.

However, the adoption of a near infrared FT-Raman system for robotic instrumentation used in the exploration of Mars is not a practical proposition, even though the spectra collected by the use of higher energy lasers were inferior in quality. Of the diode and gas laser excitation, the near infra-red 785 nm excitation with CCD detection was found to be most successful in the provision of the clearest and most informative spectra for PAHs using a dispersive instrument. A major problem is the fluorescence caused by the higher energy 633 and 514 nm lasers which resulted in the inability of the 514 nm laser excitation system to record spectra; generally, the only spectral feature noted was of tetracene and the other spectra were rather poor. This highlights a very practical problem for current Mars research since the ExoMars Raman system is designed to operate with a laser at 532 nm.

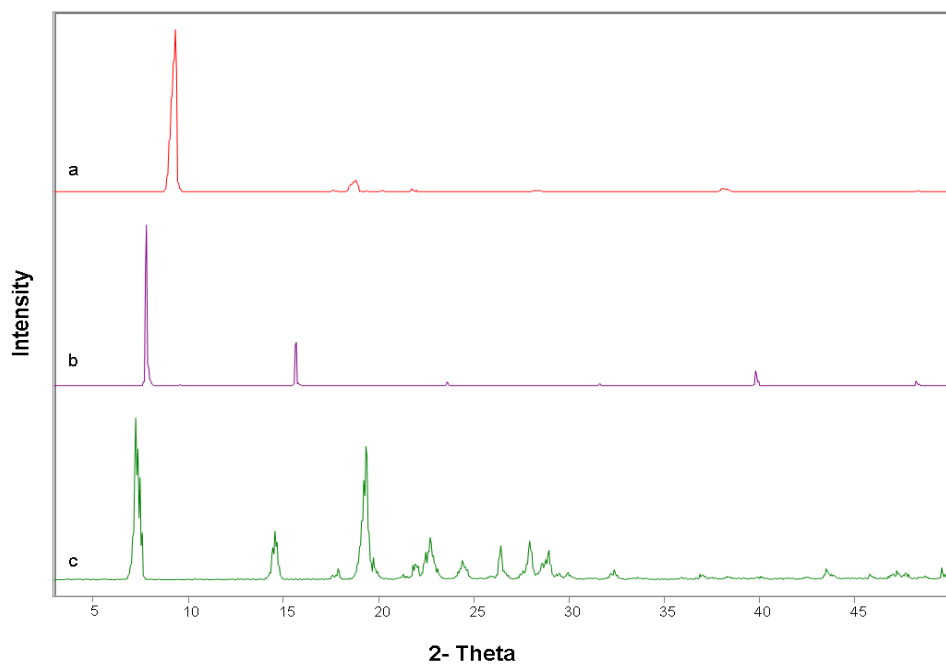


Fig. 8.2.3.1 X-ray powder diffraction patterns of (a) phenanthrene, (b) chrysene and (c) tetracene

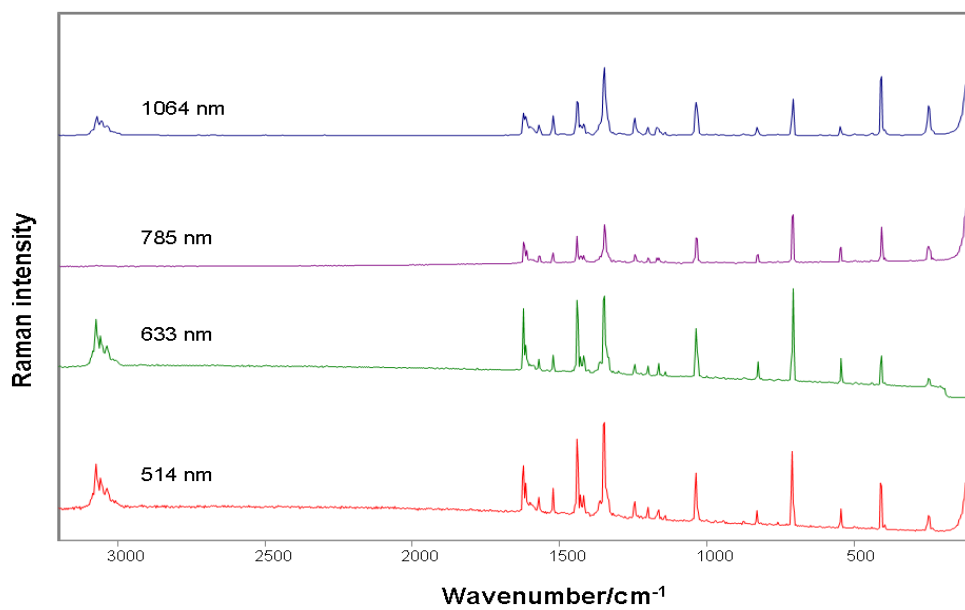


Fig. 8.2.3.2 Raman spectra of phenanthrene at 1064,785,633 and 514 nm

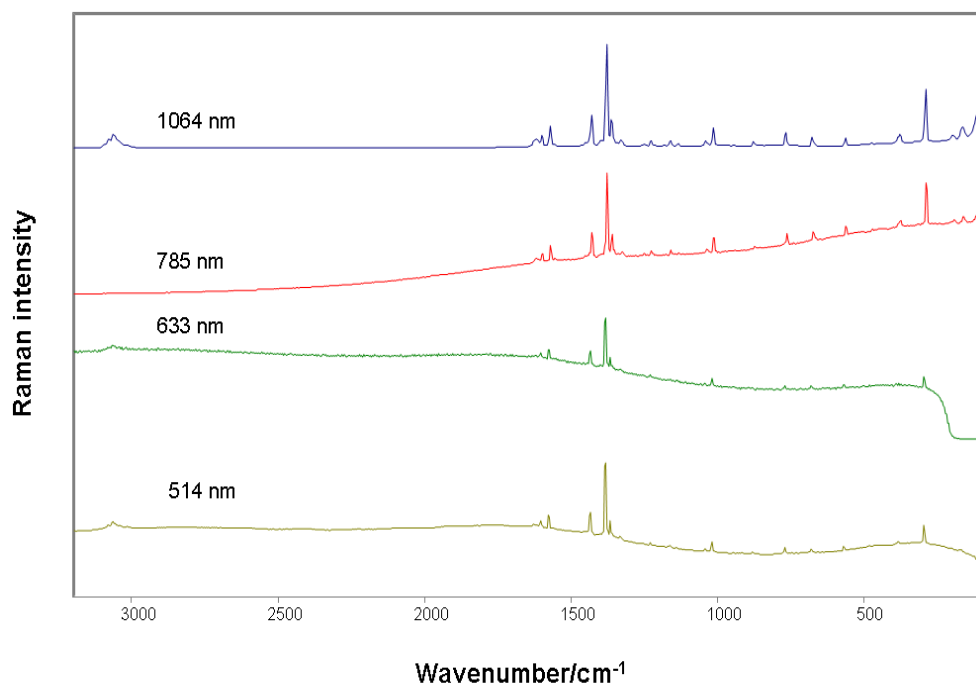


Fig. 8.2.3.3 Raman spectra of chrysene at 1064,785,633 and 514 nm

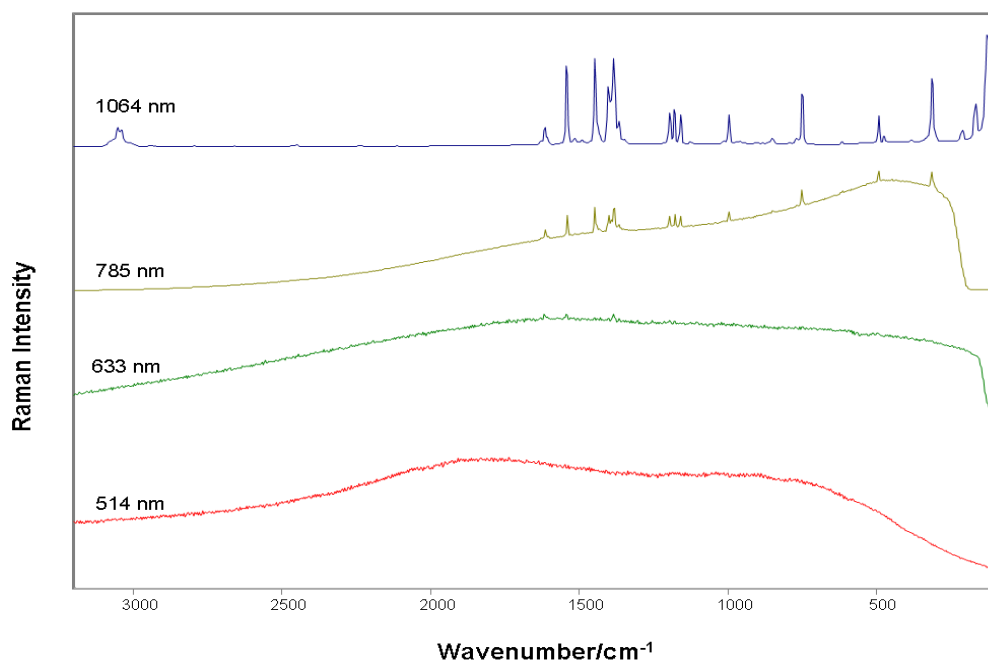


Fig. 8.2.3.4 Raman spectra of tetracene at 1064,785,633 and 514 nm

| 1064 nm | 785 nm | 633 nm | 514 nm | Assignments |
|-----------|-----------|------------|------------|-----------------------------|
| 3071 st | 3071 st | 3072 st | 3071st | CH stretching |
| 3055 m | 3055 m | 3056 m | 3057msh | |
| 3035 m | 3035 m | 3034 m | - | |
| - | 1748 w | - | - | |
| 1622 m | 1620 m | 1622 v st | 1622 st | C=C stretching vibration |
| 1613 m sh | 1613 m sh | 1613 st sh | 1613 st sh | C-C stretching |
| 1599 w sh | 1599 w sh | 1599 w | 1599 w | |
| 1569 m | 1569 w | 1569 m | 1570 m | C-C stretching |
| 1523 st | 1523 m | 1523 st | 1523 st | |
| 1440 st | 1437 st | 1439 v st | 1440 v st | C-C stretching ,HCC bending |
| 1429 w sh | 1429 w sh | 1429 st | 1429 st | C-C stretching ,HCC bending |
| 1418 m sh | 1418 m sh | 1418 st | 1418 st | |
| - | - | 1402 w sh | 1402 w sh | |
| - | - | 1362 m sh | 1362 m sh | |
| 1349 st | 1349 st | 1349 v st | 1350 v st | C-C stretching,HCC bending |
| 1318 w | 1318 w | 1320 w | 1316 w | |
| 1245 st | 1242 st | 1244 m | 1245 m | HCC bending |
| 1200 m | 1200 m | 1200 m | 1200 m | C-C stretching,HCC bending |
| 1170 m | 1170 m | 1169 m | 1169 m | |
| 1141 w | 1141 w | 1141 w | 1162 m | |
| 1036 st | 1033 st | 1035 st | 1036 st | C-C stretching,HCC bending |
| 828 m | 825 m | 828 st | 828 m | |
| 710 st | 706 st | 709 vst | 710 v st | |
| 547m | 543 m | 546 st | 546 st | CCC bending |
| 498 v w | 498 v w | 496 w | 498 w | |
| 442 w | 442 w | 441 w | 442 w | |
| 410 st | 406 st | 409 st | 409 st | CCC bending |
| 249 m | 246 m | 242 m | 250 m | |

* v st = very strong; st = strong; m = medium; w = weak; v w = very weak; sh = shoulder; w sh = weak shoulder ; m sh = medium shoulder; st sh = strong shoulder

Table 8.2.1 Raman spectral wavenumber and proposed assignments for phenanthrene

| 1064nm | 785 nm | 633 nm | 514 nm | Assignments |
|---------|----------|----------|---------|-------------------------------------|
| | | | | |
| 3078 w | - | - | 3078 w | C-H stretching |
| 3062 w | 3063 v w | 3063 w | 3063 w | |
| 1621 w | 1621 v w | - | 1601v w | C=C stretching vibration |
| 1601 w | 1599 w | - | - | |
| 1574 m | - | 1574 w | 1574 w | C=C stretching vibration |
| 1432 m | 1430 m | 1432 m | 1432 w | C=C stretching vibration |
| 1381 st | 1379 st | 1380 st | 1381 st | Skeletal ring vibrations |
| 1363 m | 1361 m | 1363 m | 1363 w | C-C stretching vibration |
| 1331 w | 1330 w | - | 1331 w | |
| 1228 w | 1226 w | 1223 v w | 1228 w | |
| 1162 w | 1159 w | 1162 v w | 1161 w | C-C stretching |
| 1137 w | 1134 w | - | - | |
| 1041 w | 1039 w | - | 1041 w | |
| 1017 m | 1015 m | 1016 w | 1017 w | C-H in plane deformation vibrations |
| 878 w | 875 w | - | 878 w | Out of plane C-H bending vibration |
| 769 w | 766 w | 770 w | 768 w | |
| 678 w | 675 w | 675 w | 678 w | |
| 567 w | 563 w | 562 w | 566 w | Out of plane of aromatic ring |
| 381 w | 376 w | 375 w | 380 w | |
| 294 m | 289 st | 292 m | 293 m | CCC ring deformations |

*st = strong; m = medium; w = weak; v w = very weak

Table 8.2.2 Raman spectral wavenumbers and proposed assignments for Chrysene

| 1064 nm | 785 nm | 633 nm | 514 nm | Assignments |
|-----------|-----------|--------|----------|--|
| 3050 m | | | No peaks | C-H stretching |
| 1630 w sh | - | - | - | |
| 1616 m | 1614 m | 1619 m | - | C=C stretching |
| 1606 w sh | 1605 w sh | - | - | |
| 1542 st | 1540 st | 1542 m | - | C-C or ring stretchings |
| 1517 w | 1517 w | - | - | |
| 1490 w | - | - | - | |
| 1447 st | 1445 st | 1447 w | - | C-C stretching vibrations |
| 1403 m | 1400 m | | - | Skeletal ring vibration |
| 1384 st | 1381 st | 1383 m | - | C=C in plane vibration |
| 1368 w | 1364 w | - | - | |
| 1197 m | 1194 m | - | - | C-H in plane |
| 1180 m | 1117 m | - | - | C-H in plane deformation vibration |
| 1160 m | 1157 m | - | - | C-H in plane deformation vibration |
| 997 m | 994 m | - | - | C-H in plane deformation vibration |
| 973 w | - | - | - | |
| 960 w | - | - | - | |
| 851 w | - | - | - | C-H out of plane deformation vibration |
| 751 m | 748 m | - | - | CCC ring deformations |
| 494 m | 491 m | - | - | C-C deformation vibration |
| 314 st | 311 m | - | - | CCC ring deformations |
| 213 w | - | - | - | |

*s = strong; m = medium; w = weak; sh = shoulder; w sh = weak shoulder

Table 8.2.3 Raman spectral wavenumber and proposed assignments for tetracene

8.2.5 References

- [1] B.P. Tissot, D.H. Welte, Petroleum Formation and Occurrence, Springer-Verlag, Berlin, **1984**.
- [2] <http://www.inchem.org/documents/ehc/ehc/ehc202.htm>.
- [3] H.P.Chiang, R.Song, B.Mou, K.P.Li, P.Chiang, D.Wang, W.S.Tse , L.T.Ho, Journal of Raman Spectroscopy, **1999**,30 , 551.
- [4] L. Nasdala, I. V. Pekov, Eur. J. Mineral, **1993**, 5, 699
- [5] J. Jehlicka, H. G. M. Edwards, S. E. J. Villar, O. Frank, Journal of Raman Spectroscopy, **2006**, 37,220.
- [6] O. Frank, J. Jehlicka, H. G. M. Edwards, Spectrochim. Acta A, **2007**,68,1065.
- [7] S. A. Wise, R. M. Cambell, W. R. West, M. L. Lee, K. D. Bartle, Chem. Geol, **1986**,54 , 339.
- [8] B. R. T. Simoneit, J. C. Fetzer, Org. Geochem, **1996**, 24 , 1065.
- [9] M. A. Sephton, Nat. Prod. Rep, **2002**, 19,292.
- [10] L. Becker, B. Popp, TRust, J. L. Bada, Earth Planet. Sci. Lett, **1999**, 167, 71.
- [11] A. J. T. Jull, C. Courtney, D. A. Jeffrey, J. W. Beck, Science, **1998**, 279, 366.
- [12] D. S. McKay, E. K. Gibson, K. L. Thomas-Keptra, H. Vali, C. S. Romanek, S. J. Clemett, X. D. F. Chillier, C. R. Maechling, R. N. Zare, Science, **1996**, 273, 924.
- [13] S. J. Clemett, C. R. Maechling, R. N. Zare, P. D. Swan, R. M. Walker, Science, **1993**, 262 , 721.
- [14] G. J. Flynn, Earth, Moon, Planets, **1996**,72, 469.
- [15] G. J. Flynn, D. S. McKay, Journal of Geophysical Research, **1990**, 95, 14497
- [16] B. E. DiGregorio, Anal. Chem, **2005**, 77 (17), 348 A.
- [17] H. G. M. Edwards, S. E. J. Villar, J. Jehlicka, T. Munshi, Spectrochim Acta A, **2005**, 61, 2273.

- [18] R. L. McCreery , Raman Spectroscopy for Chemical Analysis. JohnWiley & Sons: New York, **2000**.
- [19] I.B. Berlman, Handbook of Fluorescence Spectra of Aromatic Molecules, Academic Press, New York, **1971**.
- [20] M. Delhaye, J. Barbillat, J. Aubard, M. Bridoux, E. Da Silva, in: Turrell G Corset. (Ed.), Raman Microscopy: Developments and Applications, Academic Press, London, **1996**.
- [21] D. Lin-Vien, J. G. Grasselli, N. B. Colthup, W. G. Fateley, The Handbook of Infrared and Raman Characteristic Frequencies of Organic Molecules, Academic Press, **1991**.
- [22] Socrates,G, Infrared Characteristic Group Frequencies: Tables and Charts (Third ed.), John Wiley & Sons Ltd., New York, **2001**.
- [23] J. Jehlicka, H. G. M. Edwards, Organic Geochemistry, **2008**, 39, 371.
- [24] J. Jehlicka, H. G. M. Edwards, P. Vitek, Planetary and space Science, **2009**,57,606.
- [25] Y. T. Chua , P. C. Stair. Journal of Catalysis, **2003**.213. 39.
- [26] W.Charles. Jr.Bauschlicher, R.Stephen. Langhoff, and S. A. Sandford,J. Phys. Chem. A, **1997**. 101.2414.
- [27] J. Godec, L. Colombo, Journal of Chemical physics, **1976**, 65, 4693.
- [28] L.J.Allamandola, A.G.G.M. Tielens,J.R. Barker, The Astrophysical Journal Supplement Series, **1989**,71,733.
- [29] L. J. Allamandola, in IAU Symposium 135, Interstellar Dust,eds. L. J. Allamandola, A. G. G. M.Tielens (Kluwer, Dordrecht) ,**1989**, 129

CHAPTER 9 Part 1

**Raman spectroscopic analysis of minerals and organic molecules of relevance to
astrobiology**

9.1 Introduction:

Martian surface composition analysis needs to include multiple types of mineralogical measurements in order to maximize the analytical information to be gained; Raman spectroscopy is now being proposed as part of an instrumentation suite for the remote detection of materials using robotic landers for planetary surface exploration [1-5]

There are several good reasons for this, including the ability of Raman spectroscopic techniques to provide molecular and molecular ionic information nondestructively from microscopic and macroscopic samples, with specimen footprints of between 1 and 100 μm . Another important reason for the consideration of Raman spectroscopy for space flight missions is the wide spectral range, which covers both organic[6-8] and inorganic [9-13] molecular species and which therefore lends itself to the detection of biomolecular signatures from extant or extinct organisms and to biogeologically modified planetary materials [14-17].The provision of molecular Raman data from the same specimens in conjunction with elemental crystallographic and molecular fragmentation data from parallel Mossbauer, XRD and Mass spectra experimental is crucial for the molecular characterisation of specimens in limited supply and within restricted time frames imposed by battery power limitations for example on planetary surfaces. To this end, there has been much activity provided towards the miniaturization of Raman spectrometers for space flight assessment [18-22]; the accepted limitations of size, mass and volume of miniature Raman spectrometers now being considered for Martian exploration from 2009 and beyond (NASA-MSL; ESA-ExoMars/Pasteur) is, of course, dependent on the size of the proposed landers and rovers being evolved for these projects. The study of the organic and inorganic compounds in extreme terrestrial environments is a necessary pre-requisite for the planetary exploration. The selection of the most suitable wavelength and the

lowest concentration level of these compounds for Raman analyses are recognised as critical for the success of the search for life beyond our Planet [23], and experiments are ongoing in this direction.

The database of spectral information containing different combinations of minerals and organics will be a vital part of the mission to Mars as the data accumulated in the preliminary research on Earth will be utilised, not only by Raman spectroscopy but also by the other instruments present on the rover [24].

Modification of Raman spectrum by the geological matrix at its simplest, these will indicate areas of spectral overlap; at levels of higher complexity interactions between the analyte and the matrix are likely to modify the Raman spectrum potentially confusing automated spectral recognition. Here we address the first pass encounter of Raman spectroscopy with PAHs in geological matrices to evaluate the discriminativity and detectability issues that may arrive from the acquired data.

9.1.2 Experimental

9.1.2.1 Materials

Naphthalene, phenanthrene, triphenylene, quartz, calcite and gypsum were supplied by Sigma-Aldrich (UK) and AA pin Chemicals Limited (UK), and were used as received. Each compound was mixed separately with quartz, gypsum and calcite and the mixtures were ground in an agate mortar. Solid state mixtures of the PAHs in quartz, calcite and gypsum matrices were prepared representing 0.1, 0.25, 0.50, 1, 2, 5, 10 and 25 mg kg⁻¹.

9.1.2.2 Raman spectroscopy

Raman spectra of the mixtures were obtained using a Raman microscope (Renishaw plc.) with 785nm stabilized diode laser excitation and 633 nm He/Ne gas excitation. The laser beam was focused on the sample using a 5x objective lens, resulting in a laser spot footprint of approximately 10 μm diameter. Spectra were obtained for 5 accumulations, each of 10s exposure of the CCD detector in the wavenumber range 100-3200 cm^{-1} using the extended scanning mode of the instrument. The total acquisition time of the spectrum of each mixture was about eight minutes. Spectral acquisition, presentation, and analysis were performed with the Renishaw WIRE 2 (Renishaw plc) and GRAMS AI version 8 (Galactic Industries, Salem, NH) software.

Powder mixtures have an inherent heterogeneity on the micron scale. This has a major implication for sampling using Raman microscopy. To address these issues, we have adopted the lowest magnification available to us (namely, a5 x objective which gives ~ 10 μm footprint) and each specimen was analysed at seven random positions, with each point sampled twice. On this basis the spectral data quoted represent the most reproducible available from our experiments; reproducibility was attached to an observation for at least 6/14 measurements for each sample.

9.1.3 Results and discussion

9.1.3.1 Naphthalene in matrices

At least four naphthalene bands (C=C stretching) around 1573 cm^{-1} , (C=C in plane vibration) at 1379 cm^{-1} , (=C-H in plane deformation vibration) at 1017 cm^{-1} and (CCC in-plane bending modes) around 760 cm^{-1} were identified using both excitation sources at the 10 mg kg^{-1} concentration of naphthalene when analysed in mixtures with gypsum

and quartz. Measurements using the 633 nm excitation allowed us to detect four naphthalene bands even at the 10 mg kg⁻¹ level in quartz and calcite also two bands at 5 mg kg⁻¹ in gypsum. Even using the excitation source 785 nm excitation source at the 10 mg kg⁻¹ concentration of naphthalene in quartz, the C=C in plane vibrational band was observed in the spectra also the naphthalene bands at 1573 cm⁻¹ due to a C=C in-plane vibration and 1379 cm⁻¹ assigned to a C=C in plane vibration were observed in spectra therefore, the band at 1017 cm⁻¹ due to a C-H in plane deformation vibration appears in the spectra as a shoulder , as seen in the figure 9.1.1 and table 9.1.1. Analyses of naphthalene in calcite led to identification of all the four characteristic naphthalene bands at concentration of 10 mg kg⁻¹ at 633 and 785 nm (figure 9.1.1 and table 9.1.1) without interference from the matrix features.

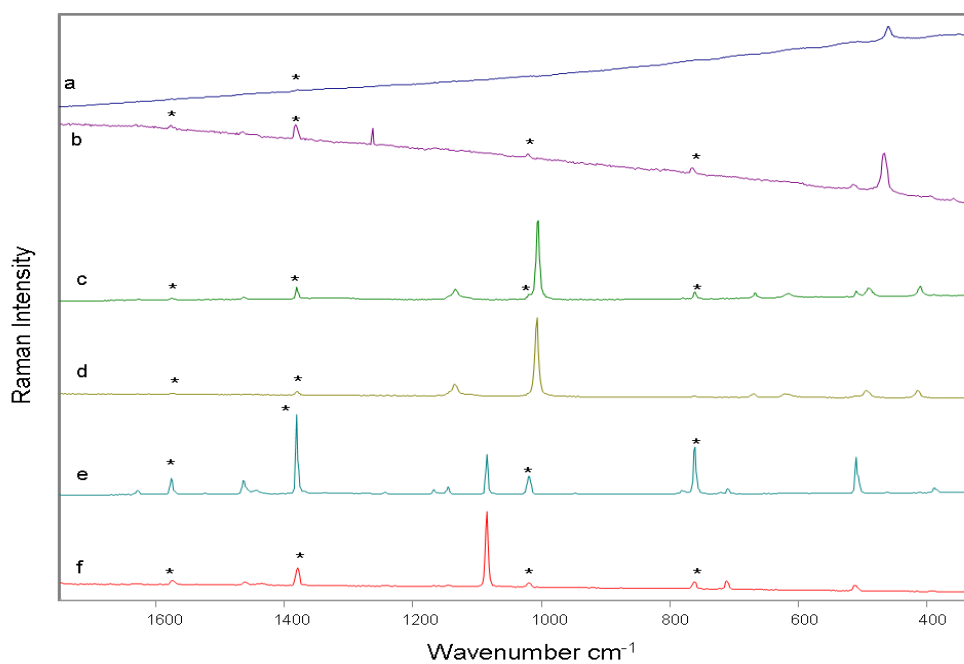


Fig. 9.1.1 Raman spectra of
 (a) Naphthalene in admixture with quartz (10 mg kg⁻¹) at 785 cm⁻¹
 (b) Naphthalene in admixture with quartz (10 mg kg⁻¹) at 633 cm⁻¹
 (c) Naphthalene in admixture with gypsum (5 mg kg⁻¹) at 785 cm⁻¹
 (d) Naphthalene in admixture with gypsum (5 mg kg⁻¹) at 633 cm⁻¹
 (e) Naphthalene in admixture with calcite (10 mg kg⁻¹) at 785 cm⁻¹
 (f) Naphthalene in admixture with calcite (10 mg kg⁻¹) at 633 cm⁻¹

| mg kg ⁻¹ | 1573 cm ⁻¹ | | 1379cm ⁻¹ | | 1017cm ⁻¹ | | 760cm ⁻¹ | | Minerals |
|---------------------|-----------------------|--------|----------------------|--------|----------------------|--------|---------------------|--------|----------|
| | Excitation sources | | | | | | | | |
| | 785 nm | 633 nm | 785 nm | 633 nm | 785 nm | 633 nm | 785 nm | 633 nm | |
| 0.10 | 2.01 | 2.19 | 2.87 | 2.89 | 2.19 | 2.23 | 2.54 | 2.65 | Quartz |
| 0.25 | 2.12 | 2.14 | 2.85 | 2.87 | 2.23 | 2.24 | 2.54 | 2.66 | |
| 0.50 | 2.09 | 2.14 | 2.89 | 2.85 | 2.22 | 2.25 | 2.59 | 2.67 | |
| 1.00 | 2.08 | 2.14 | 2.85 | 2.87 | 2.29 | 2.23 | 2.58 | 2.68 | |
| 2.00 | 2.09 | 2.15 | 2.85 | 2.89 | 2.29 | 2.24 | 2.59 | 2.61 | |
| 5.00 | 2.09 | 2.15 | 2.88 | 2.91 | 2.25 | 2.26 | 2.55 | 2.50 | |
| 10.00 | 2.50 | 14.14 | 34.98 | 25.06 | 2.22 | 16.17 | 2.57 | 24.62 | |
| 25.00 | 25.17 | 25.57 | 52.37 | 52.57 | 35.70 | 36.67 | 46.79 | 47.65 | |
| 0.10 | 1.87 | 2.60 | 2.81 | 2.40 | 2.45 | 2.68 | 2.63 | 275 | Gypsum |
| 0.25 | 1.89 | 2.61 | 2.79 | 2.39 | 2.44 | 2.67 | 2.65 | 275 | |
| 0.50 | 1.85 | 2.51 | 2.71 | 2.45 | 2.44 | 2.68 | 2.65 | 276 | |
| 1.00 | 1.85 | 2.11 | 2.77 | 2.44 | 2.45 | 2.66 | 2.64 | 275 | |
| 2.00 | 2.00 | 2.39 | 2.59 | 2.33 | 2.44 | 2.64 | 2.65 | 2.73 | |
| 5.00 | 13.45 | 13.87 | 16.23 | 13.10 | 14.77 | 2.75 | 15.16 | 2.74 | |
| 10.00 | 28.78 | 28.97 | 36.64 | 35.87 | 26.29 | 25.48 | 26.39 | 25.93 | |
| 25.00 | 40.27 | 40.59 | 47.72 | 46.71 | 37.30 | 36.23 | 42.56 | 41.06 | |
| 0.10 | 2.29 | 2.24 | 2.34 | 2.37 | 2.32 | 2.37 | 2.31 | 2.36 | Calcite |
| 0.25 | 2.29 | 2.26 | 2.35 | 2.38 | 2.37 | 2.37 | 2.39 | 2.38 | |
| 0.50 | 2.25 | 2.25 | 2.37 | 2.38 | 2.36 | 2.35 | 2.35 | 2.34 | |
| 1.00 | 2.22 | 2.28 | 2.38 | 2.39 | 2.34 | 2.37 | 2.32 | 2.35 | |
| 2.00 | 2.23 | 2.25 | 2.39 | 2.32 | 2.34 | 2.39 | 2.33 | 2.36 | |
| 5.00 | 2.22 | 2.19 | 2.31 | 2.32 | 2.32 | 2.37 | 2.34 | 2.38 | |
| 10.00 | 26.45 | 27.36 | 25.79 | 30.56 | 36.66 | 37.88 | 36.32 | 39.47 | |
| 25.00 | 28.99 | 29.54 | 51.21 | 51.07 | 39.15 | 40.11 | 44.69 | 45.72 | |

The signs in tables point to 785 nm/633 nm analysis and limit of detection at 99% confidence assigned to $I/\sigma > 3$ [25]

Table 9.1.1 I/σ ratio of Naphthalene bands at various concentrations

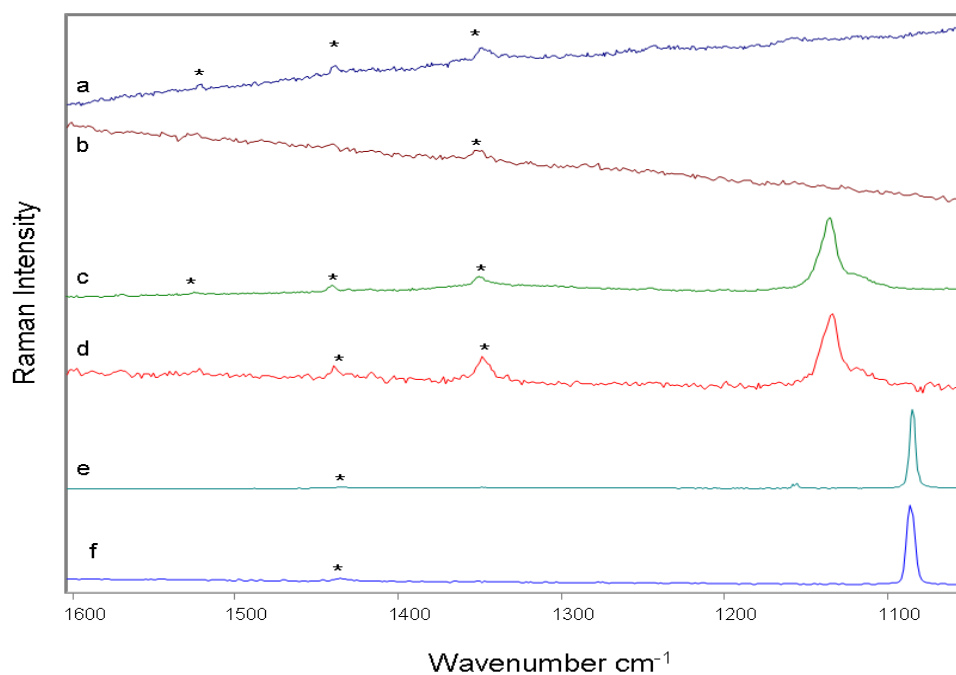


Fig. 9.1.2 Raman spectra of
 (a) Phenanthrene in admixture with quartz (1 mg kg⁻¹) at 785 cm⁻¹
 (b) Phenanthrene in admixture with quartz (1 mg kg⁻¹) at 633 cm⁻¹
 (c) Phenanthrene in admixture with gypsum (1 mg kg⁻¹) at 785 cm⁻¹
 (d) Phenanthrene in admixture with gypsum (2 mg kg⁻¹) at 633 cm⁻¹
 (e) Phenanthrene in admixture with calcite (1 mg kg⁻¹) at 785 cm⁻¹
 (f) Phenanthrene in admixture with calcite (1 mg kg⁻¹) at 633 cm⁻¹

9.1.3.2 Phenanthrene in matrices

The spectra of phenanthrene in the gypsum and quartz matrix show the phenanthrene bands at 1523 cm⁻¹ assigned to the C-C stretching vibrations and 1437, 1349 and 1033 cm⁻¹ due to C-C stretching, HCC bending all were clearly identified at the mixture with phenanthrene concentration of 2 mg kg⁻¹.

At the lower concentration level (1 mg kg⁻¹) at 785 nm the C-C stretching vibrational band at 1523 cm⁻¹ in gypsum and calcite and also 1033 cm⁻¹ in quartz disappear.

Furthermore, the other bands observed in the spectra are characteristic of quartz, gypsum and calcite.

However, the spectra recorded at 633 nm resulted in the observation of only one phenanthrene band in the limiting concentration of 1 mg kg⁻¹ in quartz (at 1349 cm⁻¹) and calcite (at 11437 cm⁻¹) but no feature was observed in gypsum at the same concentration.

The low concentrations of phenanthrene were identified in calcite is 0.25 mg kg⁻¹ using both 633 and 785 nm laser sources (Table 9.1.2 and figure. 9.1.2).

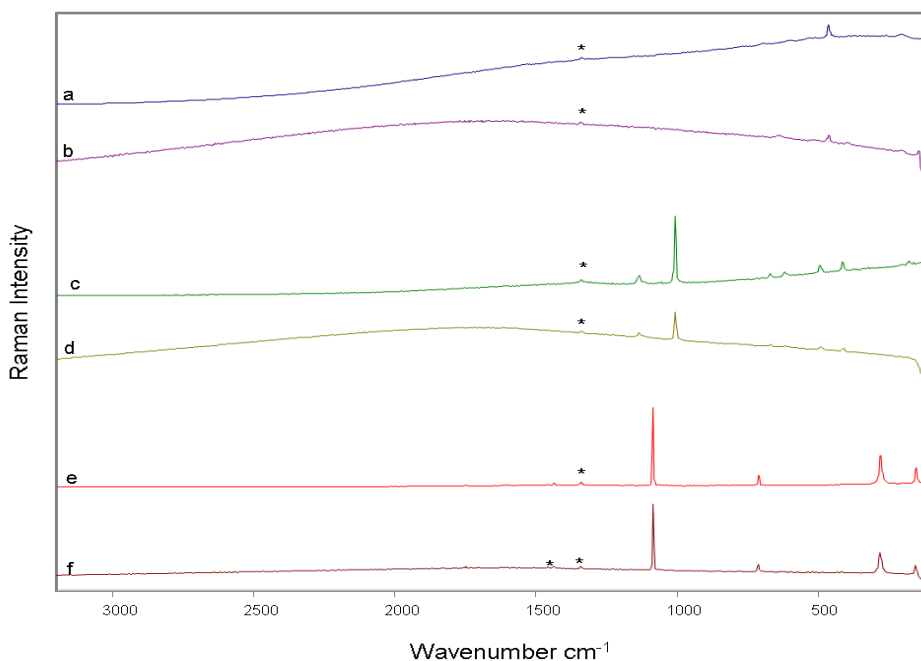


Fig. 9.1.3 Raman spectra of

- (a) Triphenylene in admixture with quartz (0.50 mg kg⁻¹) at 785 cm⁻¹
- (b) Triphenylene in admixture with quartz (0.50 mg kg⁻¹) at 633 cm⁻¹
- (c) Triphenylene in admixture with gypsum (0.50 mg kg⁻¹) at 785 cm⁻¹
- (d) Triphenylene in admixture with gypsum (1 mg kg⁻¹) at 633 cm⁻¹
- (e) Triphenylene in admixture with calcite (0.25 mg kg⁻¹) at 785 cm⁻¹
- (f) Triphenylene in admixture with calcite (0.25 mg kg⁻¹) at 633

| mg kg ⁻¹ | 1523 cm ⁻¹ | | 1437 cm ⁻¹ | | 1349 cm ⁻¹ | | 1033 cm ⁻¹ | | Minerals |
|------------------------|-----------------------|-----------|-----------------------|-----------|-----------------------|-----------|-----------------------|-----------|----------|
| | Excitation sources | | | | | | | | |
| | 785 nm | 633 nm | 785 nm | 633 nm | 785 nm | 633 nm | 785 nm | 633 nm | |
| 0.10 | 2.71 | 2.35 | 1.88 | 2.70 | 2.39 | 2.85 | 2.23 | 2.50 | Quartz |
| 0.25 | 2.70 | 2.35 | 1.89 | 2.71 | 2.44 | 2.89 | 2.22 | 2.51 | |
| 0.50 | 2.71 | 2.35 | 2.07 | 2.74 | 2.45 | 2.78 | 2.19 | 2.51 | |
| 1.00 | 2.72 | 2.77 | 70.23 | 2.19 | 53.18 | 53.97 | 17.84 | 2.60 | |
| 2.00 | 58.13 | 92.29 | 80.28 | 110.75 | 65.57 | 67.23 | 26.55 | 62.68 | |
| 5.00 | 27.26 | 106.08 | 84.50 | 130.25 | 80.73 | 91.22 | 38.57 | 77.83 | |
| 10.00 | 70.89 | 109.65 | 91.56 | 146.28 | 116.83 | 117.66 | 57.89 | 83.35 | |
| 25.00 | 87.69 | 131.44 | 120.23 | 151.91 | 125.18 | 125.87 | 64.60 | 117.35 | |
| 0.10 | 2.68 | 2.64 | 1.99 | 2.54 | 2.32 | 2.60 | 2.66 | 2.89 | Gypsum |
| 0.25 | 2.68 | 2.63 | 2.01 | 2.55 | 2.33 | 2.60 | 2.68 | 2.88 | |
| 0.50 | 2.69 | 2.64 | 2.11 | 2.54 | 2.33 | 2.59 | 2.76 | 2.86 | |
| 1.00 | 11.61 | 2.60 | 32.18 | 2.82 | 37.17 | 2.59 | 2.77 | 2.89 | |
| 2.00 | 22.46 | 2.64 | 35.75 | 66.07 | 48.39 | 37.42 | 18.91 | 2.81 | |
| 5.00 | 41.96 | 103.28 | 61.36 | 105.62 | 90.10 | 54.46 | 30.65 | 114.64 | |
| 10.00 | 71.84 | 143.35 | 76.96 | 195.82 | 182.99 | 181.11 | 71.25 | 142.92 | |
| 25.00 | 76.63 | 188.58 | 135.68 | 224.57 | 221.11 | 216.39 | 78.72 | 165.36 | |
| 0.10 | 1.42 | 2.81 | 2.48 | 2.43 | 2.22 | 2.15 | 2.63 | 2.73 | Calcite |
| 0.25 | 1.41 | 2.81 | 3.16 | 3.56 | 2.46 | 2.20 | 2.65 | 2.73 | |
| 0.50 | 1.48 | 2.83 | 5.74 | 9.16 | 2.80 | 2.15 | 2.62 | 2.75 | |
| 1.00 | 1.49 | 2.89 | 9.69 | 14.36 | 2.52 | 2.14 | 2.63 | 2.73 | |
| 2.00 | 3.34 | 9.11 | 11.54 | 19.89 | 22.12 | 6.81 | 3.32 | 6.36 | |
| 5.00 | 9.17 | 12.65 | 26.32 | 36.64 | 31.98 | 41.99 | 9.44 | 15.28 | |
| 10.00 | 15.50 | 21.25 | 33.10 | 44.57 | 47.61 | 57.66 | 18.17 | 23.51 | |
| 25.00 | 24.48 | 37.73 | 42.78 | 66.36 | 68.03 | 96.91 | 36.68 | 46.37 | |

The signs in tables point to 785 nm/633 nm analysis and limit of detection at 99% confidence assigned to $I/\sigma > 3$ [25]

Table 9.1.2 I/σ ratio of phenanthrene bands at various concentration

9.1.3.3 Triphenylene in matrices

Analyses of triphenylene in quartz led to identification of one characteristic triphenylene band at a concentration of 0.50 mg kg^{-1} and all the four bands at the 1 mg kg^{-1} triphenylene concentration at 633 and 785 nm.

However, using 633 nm excitation source three triphenylene features were identified at the $1456, 1337$ and 1058 cm^{-1} position at 2 mg kg^{-1} and only the C-C stretching band was identified at 0.50 mg kg^{-1} (figure 9.1.3 and table 9.1.3).

Measurements using 633 nm laser excitation allowed the detection of three triphenylene bands in calcite namely in the 1456 cm^{-1} band assigned to C-C stretching, 1337 cm^{-1} due to C-C stretching and 695 assigned to C-H in plane bending at the 0.50 mg kg^{-1} level in calcite. Also two bands at the 0.25 mg kg^{-1} (1456 cm^{-1} band assigned to C-C stretching and 1337 cm^{-1} due to C-C stretching) were observed. Even using laser excitation at 785 nm at the 0.50 mg kg^{-1} concentration of triphenylene in calcite, the 1456 cm^{-1} band assigned to C-C stretching, 1337 cm^{-1} due to C-C stretching and 1058 cm^{-1} assigned to C-H out of plane bending bands were observed in the spectra. Also only one band was observed at the 0.25 mg kg^{-1} concentration namely the 1337 cm^{-1} band due to C-C stretching (figure 9.1.3 and table 9.1.3).

| mg kg ⁻¹ | 1456 cm ⁻¹ | | 1337 cm ⁻¹ | | 1058 cm ⁻¹ | | 695 cm ⁻¹ | | Minerals |
|------------------------|-----------------------|-----------|-----------------------|-----------|-----------------------|-----------|----------------------|-----------|----------|
| | Excitation sources | | | | | | | | |
| | 785 nm | 633 nm | 785 nm | 633 nm | 785 nm | 633 nm | 785 nm | 633 nm | |
| 0.10 | 2.45 | 2.39 | 2.40 | 2.51 | 2.43 | 2.71 | 2.40 | 2.45 | Quartz |
| 0.25 | 2.24 | 2.45 | 2.39 | 2.50 | 2.43 | 2.73 | 2.38 | 2.40 | |
| 0.50 | 2.77 | 2.46 | 32.81 | 41.20 | 2.42 | 2.73 | 2.49 | 2.41 | |
| 1.00 | 44.75 | 63.33 | 54.22 | 66.31 | 16.86 | 30.11 | 20.91 | 61.21 | |
| 2.00 | 56.74 | 74.73 | 61.43 | 75.27 | 25.39 | 44.59 | 33.41 | 69.39 | |
| 5.00 | 68.69 | 100.48 | 91.56 | 102.43 | 37.66 | 53.04 | 46.59 | 83.79 | |
| 10.00 | 78.89 | 109.22 | 107.35 | 121.75 | 49.23 | 61.88 | 55.73 | 87.05 | |
| 25.00 | 91.57 | 154.92 | 143.82 | 154.30 | 54.56 | 87.20 | 68.51 | 99.31 | |
| 0.10 | 2.85 | 2.75 | 2.71 | 2.70 | 2.55 | 2.68 | 2.70 | 2.33 | Gypsum |
| 0.25 | 2.81 | 2.76 | 2.73 | 2.71 | 2.55 | 2.68 | 2.78 | 2.34 | |
| 0.50 | 2.88 | 2.76 | 69.72 | 2.91 | 2.51 | 2.71 | 2.79 | 2.33 | |
| 1.00 | 5.48 | 2.83 | 106.21 | 146.03 | 34.54 | 2.78 | 34.65 | 2.30 | |
| 2.00 | 19.52 | 72.37 | 160.54 | 160.05 | 39.85 | 29.72 | 63.34 | 2.31 | |
| 5.00 | 65.58 | 77.12 | 172.85 | 197.66 | 72.88 | 83.89 | 70.81 | 72.00 | |
| 10.00 | 77.24 | 100.68 | 220.03 | 225.77 | 99.15 | 126.00 | 76.63 | 77.82 | |
| 25.00 | 86.62 | 110.28 | 230.17 | 237.65 | 110.65 | 135.24 | 88.21 | 102.88 | |
| 0.10 | 2.16 | 2.66 | 2.36 | 2.41 | 2.54 | 2.39 | 2.48 | 2.56 | Calcite |
| 0.25 | 2.08 | 5.58 | 12.24 | 7.05 | 2.51 | 2.38 | 2.49 | 2.55 | |
| 0.50 | 7.72 | 10.32 | 21.40 | 15.56 | 4.12 | 2.39 | 2.55 | 5.80 | |
| 1.00 | 9.36 | 57.64 | 31.36 | 37.24 | 5.23 | 66.13 | 3.92 | 15.04 | |
| 2.00 | 22.84 | 61.48 | 41.56 | 76.92 | 41.76 | 80.64 | 4.36 | 21.68 | |
| 5.00 | 68.56 | 104.2 | 150.24 | 208.56 | 77.68 | 88.41 | 69.36 | 93.32 | |
| 10.00 | 89.64 | 140.84 | 252.24 | 287.64 | 140.84 | 238.72 | 86.12 | 142.88 | |
| 25.00 | 151.76 | 281.32 | 326.84 | 328.20 | 186.72 | 273.56 | 169.96 | 262.11 | |

The signs in tables point to 785 nm/633 nm analysis and limit of detection at 99% confidence assigned to $I/\sigma > 3$ [25]

Table 9.1.3 - I/σ ratio of triphenylene bands at various concentrations

9.1.4 Conclusion

The analytical potential of Raman microspectrometry has been demonstrated for the identification of PAHs in a two-component system comprising a biomarker in a matrix.

The number of observed Raman bands in PAHs differed depending on the particular mineral matrix, the excitation wavelength and the concentration deployed. Estimates of the relative molecular scattering factors of the PAH components were evaluated, which informed the capability of detection of the PAH using Raman spectroscopy on the surface of Mars.

This study shows the limits of detection of naphthalene, phenanthrene and triphenylene in gypsum, calcite and quartz. The lowest concentrations of naphthalene were identified in matrices, e.g. 10 mg kg^{-1} using both 633 and 785 nm laser sources. Phenanthrene concentration of 1, 2 and 0.25 mg kg^{-1} was the limit for identification of phenanthrene features, when measured in quartz, gypsum and calcite with 785 and 633 nm respectively. The low concentrations of triphenylene were identified in quartz, e.g. 1 mg kg^{-1} using both 633 and 785 nm laser sources furthermore, 1 and 2 mg kg^{-1} in gypsum with 633 and 785 nm respectively also 0.25 mg kg^{-1} in calcite with 633 and 785 nm. The results have shown that Raman spectroscopy is a suitable tool for the in-situ identification of PAHs down to a concentration of 0.25 mg kg^{-1} in selected geological matrices.

9.1.5 References

- [1] A. Ellery, D. D. Wynn-Williams, *Astrobiology*, **2003**, 3 (3), 565.
- [2] J. A. Hiscox, *Earth Moon Planets*, **2001**, 87(3), 191.
- [3] A. A. Gorbushina, W. E. Krumbein, M. Volkmann, *Astrobiology*, **2002**, 2 (2), 203.
- [4] J. L. Bishop, E. Murad, M. D. Lane, R. L. Mancinelli, *Icarus*, **2004**, 169 (2), 311.
- [5] R. C. Wiens, R. E. D.A. Arvidson, D. A. Cremers, M. J. Ferris, J. D. Blacic, F. P. Seelos, K. S. Deal, *J. Geophys. Res. Planets*, (E11), art no 8004, **2002**, 107.
- [6] H. G. M. Edwards, E. M. Newton, D. D. Wynn-Williams, R. I. Lewis-Smith, *Spectrochim. Acta Part A*, **2003**, 59 (10), 2301.
- [7] H. G. M. Edwards, E. M. Newton, D. D. Wynn-Williams, *J. Mol. Struct*, **2003**, 651. 27.
- [8] H. G. M. Edwards, E. M. Newton, D. D. Wynn-Williams, S. R. Coombes, *J. Mol. Struct*, **2003**, 648 (1–2), 49.
- [9] H. G. M. Edwards, D. W. Farwell, M. M. Grady, D. D. Wynn-Williams, *I.P. Planet, Space Sci*, **1999**, 47 (3–4), 353.
- [10] T. Mikouchi, M. Miyamoto, *Meteorit. Planet. Sci*, **2000**, 35 (1), 155.
- [11] A. Wang, J. Y. Han, L. H. Guo, J. Y. Yu, P. Zeng, *Appl. Spectrosc*, **1994**, 48 (8), 959.
- [12] A. Wang, B. L. Jolliff, L. A. Haskin, *J. Geophys. Res. Planets*, **1999**, 104 (E4), 8509.
- [13] A. Wang, K. E. Kuebler, B. L. Jolliff, L. A. Haskin, *Am. Mineral*, **2004**, 89 (5–6), 665.
- [14] H. G. M. Edwards, E. M. Newton, D. L. Dickensheets, D. D. Wynn-Williams, *Spectrochim. Acta Part A*, **2003**, 59 (10), 2277.
- [15] H. G. M. Edwards, *Biosphere*, **2004**, 34(1–2), 3.
- [16] D. D. Wynn-Williams, H. G. M. Edwards, *Icarus*, **2000**, 144 (2), 486

- [17] H. G. M. Edwards, D. D. Wynn-Williams, S. E. J. Villar, *Journal of Raman Spectroscopy*, **2004**, 35,470
- [18] D. L. Dickensheets, D. D. Wynn-Williams, H. G. M. Edwards, C. Schoen, C. Crowder, E. M. Newton, *Journal of Raman Spectroscopy*, **2000**, 31 (7) ,633.
- [19] S.K.Sharma, P. G. Lucey, M. Ghosh, H. W. Hubble, K. A. Horton, *Spectrochim. Acta A*, **2003**, 59 (10), 2391.
- [20] A. Wang, L. A. Haskin, A. L. Lane, T. T. Wdowiak, S. W. Squyres, R. J. Wilson, L. E. Hoyland, K. S. Manatt, N. Raouf, C. D. Smith, *J. Geophys. Res. Planets*, **2003**, 108 (E1), 5005.
- [21] A. Wang, L. A. Haskin *Microbeam Analysis*, *Proc. Inst. Phys.Conf. Ser*, **2000**, 165,103
- [22] A. Wang, L. A. Haskin, E. Cortez, *Appl. Spectrosc*, **1998**, 52 (4), 477.
- [23] H. G. M. Edwards, E. M. Newton, D. D. Wynn-Williams . *Intl. J. Astrobiology*, **2003**, 1,333.
- [24]H. G. M. Edwards, I. J. Scowen, M. D. Hargreaves, *ExoMars Poster*, *GeoRaman*, **2008**.
- [25]. ACS Committee on Environmental Improvement, *Anal. Chem*, **1980**, 52 ,2242

CHAPTER 9 Part 2

Raman spectroscopic identification of beta-carotene in usnic acid and PAHs as a potential Martian analogue

9.2.1 Introduction

The quest for evidence of life, both extant and extinct, especially on Mars, is a basic goal of current space exploration. In the case of Mars, the detection of extant or recent life and the search for chemical tracers left by past life have been summarized in an excellent report [1]. In addition to the geosignatures (e.g., morphological features, erosion consistent with aquifer processes) life can leave traces of biosignatures (e.g., organic macromolecules) that can be attributed to previous or current biological activity [2], allowing us to detect its past and present occurrence. On Earth, molecular biomarkers derive from biochemical precursors through reduction or oxidation processes and generally include lipids and pigments, their derivatives and degradation products [3, 4]. Within the model payload of the forthcoming instruments currently being developed by ESA and NASA for future missions on Mars, Raman spectroscopy is considered as a fundamental instrument for characterizing mineralogical and organic material (separately or in combination with LIBS or fluorescence techniques). Therefore, it is necessary to perform a series of Earth-based analyses on Martian-analogues, to evaluate the possibilities of Raman spectroscopy in this context and subsequently to facilitate future in-situ measurements. Raman spectroscopy has hitherto been proved to be a useful method for characterizing organic minerals derived from biological activity in the geological record [5-8].

The advantage of the Raman analytical method in astrobiology is its ability to identify organic molecules non-destructively, without sample preparation and on a very small scale ($\sim \mu\text{m}$).

Studies of terrestrial environments [9] show that in cases where the external conditions do not allow for the existence of surface growths, rocks become the refuge for microorganisms that need additional protection from hostile environmental conditions.

Within the Martian context, any organic matter trapped as intracrystalline inclusions within sulfates, for example would be expected to be resistant to the oxidizing conditions present on the surface of Mars [9].

Beta-carotene is one of the most widespread natural molecules, exhibiting several biological functions in a variety of organisms from bacteria and plants. Beta-carotene has two strong Raman bands at 1515 and 1157 cm^{-1} due to in-phase $\nu_1(\text{C}=\text{C})$ and $\nu_2(\text{C}-\text{C})$ stretching vibrations. A feature of medium intensity also occurs at 1008 cm^{-1} , corresponding to the in-plane rocking modes of the $(\text{C}-\text{CH}_3)$ group in phenylalanine (Fig 9.2.1) [10, 11]. Marshall et al and Withnall et al [12, 13] have reported the identification of carotenoids in halophilic archaea and in natural products by resonance Raman spectroscopy using the 514.5 nm excitation wavelength. This excitation wavelength has proved to be useful when analyzing carotenoids due to its coincidence with an electronic transition in carotenoids resulting in a resonance Raman effect, thus enhancing significantly the intensity of the Raman signal for example [10-12]. However, considering the need for other organic biomolecular species to be analyzed within astrobiological missions, other wavelengths must be considered as possible excitation sources.

In this study, Raman micro-spectroscopy was used as a non-destructive method of determining the presence of chemically pure beta-carotene in experimentally prepared mixtures with powdered usnic acid, phenanthrene and triphenylene. The aim of this work is to evaluate the discriminatory ability of the technique and to determine the lowest proportion of beta-carotene that is still possible to detect in the selected compounds—thereby simulating the analysis of beta-carotene incorporated inside organic acids and polyaromatic hydrocarbons (PAHs) as residues from extinct life. Our samples were analyzed using 785 nm excitation to test this more universal excitation source, which may be of importance from the astrobiological point of view. Various concentrations of beta-

carotene in organic acids and PAHs were investigated to determine the ability of the Raman micro-spectroscopic method to detect this biomarker species.

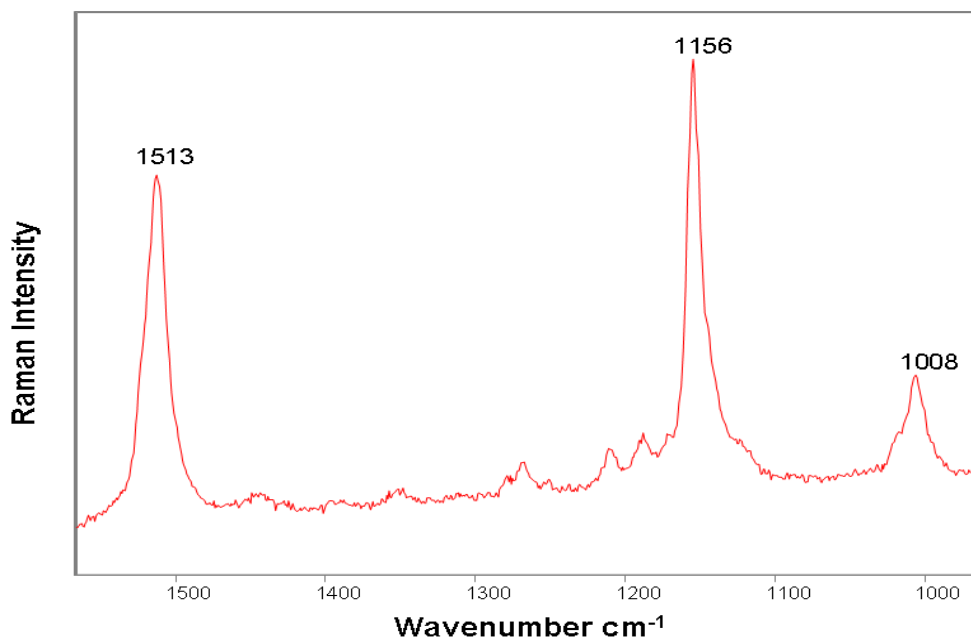


Fig.9.2.1 Raman spectrum of beta carotene with three selected key features at 785 nm , 90.8 mW , 10 s exposure and 5 accumulations.

9.2.2 Experimental

9.2.2.1 Materials

Beta-carotene, usnic acid, phenanthrene and triphenylene were supplied by Sigma-Aldrich (UK) and AA pin Chemicals Limited (UK), and were used as received. The mixtures were ground and homogenized in an agate mortar. Powders of five different concentrations of beta-carotene in usnic acid, phenanthrene and triphenylene were

prepared representing 0.25, 0.50, 1, 5 and 10 mg kg⁻¹. Spectra of the powdered mixtures were obtained directly from the surface of the specimen.

9.2.2.2 Raman spectroscopy

Raman spectra of the mixtures were obtained using an In Via Raman microscope (Renishaw plc.) with 785 nm stabilized diode laser excitation. The laser beam was focused on the sample using a 5x objective lens, resulting in a laser spot footprint of approximately 10 μm diameter. Spectra were obtained for 5 accumulations, each of 10s exposure of the CCD detector, in the wavenumber range 100-3200 cm⁻¹ using the extended scanning mode of the instrument. The total acquisition time of the spectrum of each mixture was about eight minutes. Spectral acquisition, presentation, and analysis were performed with the Renishaw WIRE 2 (Renishaw plc) and GRAMS AI version 8 (Galactic Industries, Salem, NH) software.

9.2.3 Results and discussion

9.2.3.1 Calculations of I/σ ratio

The I/σ ratios were measured for the all the Raman bands in the spectra of the compounds to differentiate between true Raman bands and noise in the spectra (where I is intensity of band and σ is the standard deviation). When this ratio is more than 3, the Raman band is considered definitive and whenever it less than 3, it is relegated to noise in the spectra [26]. The results are shown in table 9.2.2

| Beta-carotene | Usnic acid | Phenanthrene | Triphenylene |
|---|---|--|--------------------------------------|
| 1513 in-phase ν (C=C) | 1693 ν (C=O) conjugated cyclic ketone | 3071 CH stretching | 1615 C-C stretching |
| 1156 ν (C-C) Stretching vibrations | 1629 ν (C=O)aromatic ketone | 3055 CH stretching | 1604 C-C stretching |
| 1008 in-plane rocking modes of (C-CH ₃) | 1608 Quadrant ring stretch | 1622 C=C stretching vibration | 1458 C-C stretching |
| | 1322 Ring stretch | 1523 C-C stretching | 1340 C-C stretching |
| | 1289 ν (COC) as aryl alkyl ether | 1440 C-C stretching, HCC bending | 1228 C-H in plane bending |
| | | 1349 C-C stretching, HCC bending | 1162 |
| | | 1245 HCC bending | 1061 C-H in plane bending |
| | | 1200 C-C stretching, HCC bending | 698 C-H out of plane bending |
| | | 1168 C-C stretching | 418 C-C-C out of plane bending |
| | | 1161 | |
| | | 1036 C-C stretching, HCC bending | |
| | | 710 HCCC out of plane bending | |
| | | 547 CCC bending | |
| | | 410 CCC bending | |

Table 9.2.1 Raman band positions (in wavenumbers, cm^{-1}) and corresponding assignment of beta-carotene, usnic acid, phenanthrene and triphenylene

9.2.3.2 Beta-carotene in organic acid and PAHs

Beta-carotene is part of a family of chemicals called the carotenoids. It has the molecular formula $C_{40}H_{56}$ (M.W 536.87g/mol). The Raman spectrum of beta-carotene is shown in fig 9.2.1. The three vibrational signals identified above are situated in the wavenumber region between 1600 and 1050 cm^{-1} . The strong bands at 1513 and 1156 cm^{-1} correspond to the in-phase ν (C=C) and ν (C-C) stretching vibrations, respectively, and the feature at 1008 cm^{-1} is due to the in-plane rocking modes of the (C-CH₃) group.

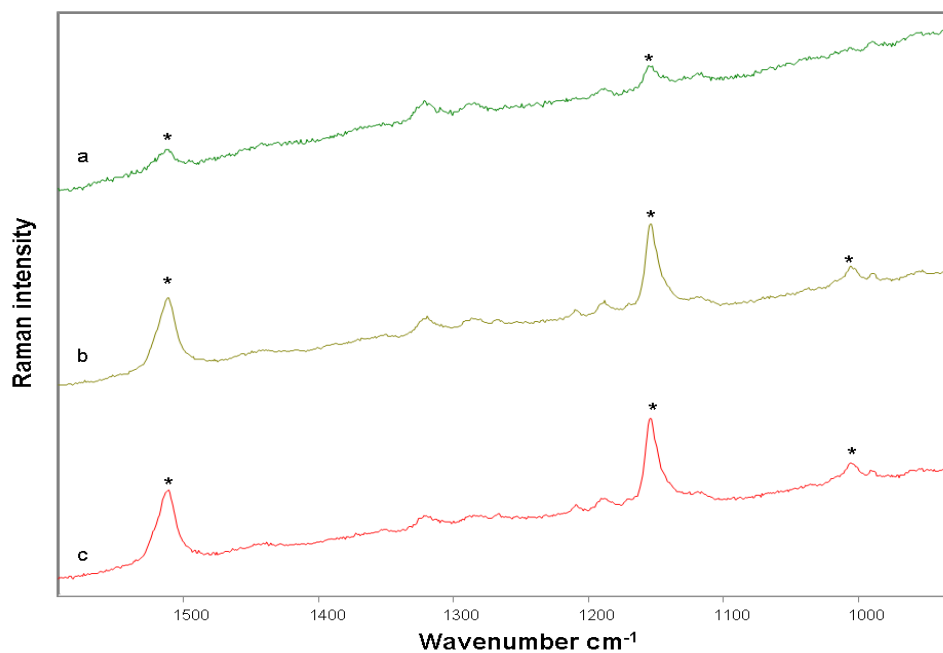


Fig.9.2.2 Raman spectra of beta-carotene in admixture with usnic acid (Asterisks indicate beta-carotene bands): (a) 0.25 $mg\ kg^{-1}$ (b) 0.50 $mg\ kg^{-1}$ (c) 1 $mg\ kg^{-1}$ beta-carotene.

Various concentrations of beta-carotene in usnic acid, phenanthrene and triphenylene have been investigated to determine the detection capability of the three selected key molecular features. The use of a 785 nm excitation wavelength was considered to be a good choice to avoid the problem of fluorescence assigned with organic molecules and visible excitation. Raman band wavenumber positions and corresponding assignments of beta-carotene, usnic acid, phenanthrene and triphenylene are listed in table 9.2.1. The assignments of phenanthrene, triphenylene, and usnic acid have been taken from previous literature assignments [7, 10, 11, 14-25].

9.2.3.3 Beta-carotene in usnic acid

The Raman spectra of beta-carotene in usnic acid at different concentrations are shown in fig. 9.2.2. At the concentration level of 0.25 mg kg^{-1} , only two weak Raman bands at 1513 and 1156 cm^{-1} assigned to the in-phase $\nu(\text{C}=\text{C})$ and $\nu(\text{C}-\text{C})$ stretching vibrations, respectively, are seen in the spectra when accumulating 5 scans of 10s each, using a 5x objective lens, resulting in a laser "footprint" of approximately $10 \text{ }\mu\text{m}$ diameter (Table 9.2.2).

Usnic acid features at 1322 and 1289 cm^{-1} which are assigned to a ring stretch and a $\nu(\text{COC})$ of an aryl alkyl ether, respectively, clearly appear in the spectra at a concentration level of beta-carotene of 1 mg kg^{-1} , as seen in fig. 9.2.3 compared with the usnic acid features.

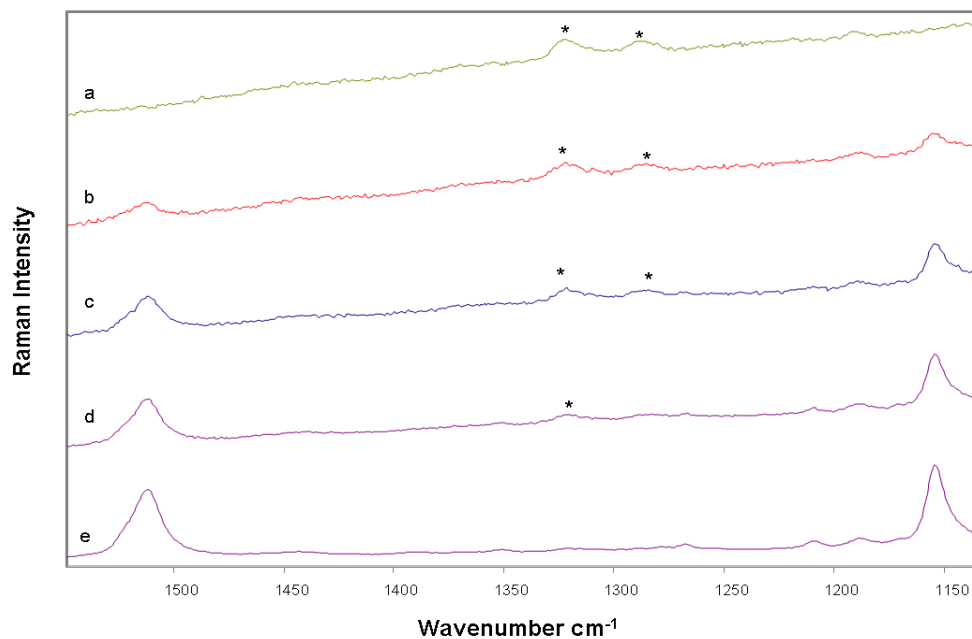


Fig.9.2.3. Raman spectra of beta-carotene in admixture with usnic acid (Asterisks indicate usnic acid bands):(a) usnic acid (b) 0.25 mg kg⁻¹ (c) 0.50 mg kg⁻¹ (d) 1 mg kg⁻¹ (e) 5 mg kg⁻¹ beta-carotene.

| mg kg ⁻¹ | 1513 cm ⁻¹ | 1156 cm ⁻¹ | 1008 cm ⁻¹ | Organic compounds |
|---------------------|-----------------------|-----------------------|-----------------------|-------------------|
| 0.25 | 13.84 | 46.09 | 2.23 | Usnic acid |
| 0.50 | 26.93 | 60.72 | 47.78 | |
| 01 | 56.42 | 95.33 | 71.60 | |
| 05 | 159.69 | 180.90 | 78.75 | |
| 10 | 164.72 | 211.69 | 106.81 | |
| 0.25 | 13.44 | 17.11 | 2.58 | Phenanthrene |
| 0.50 | 41.63 | 58.02 | 19.69 | |
| 01 | 167.30 | 187.44 | 69.36 | |
| 05 | 196.61 | 245.44 | 107.47 | |
| 10 | 217.97 | 249.91 | 117.75 | |
| 0.25 | 15.59 | 35.25 | 2.01 | Triphenylene |
| 0.50 | 29.17 | 49.34 | 1843 | |
| 01 | 61.40 | 85.65 | 28.75 | |
| 05 | 213.96 | 244.28 | 103.03 | |
| 10 | 218.25 | 249.59 | 107.38 | |

Limit of detection at 99% confidence assigned to $I/\sigma > 3$ [25]

Table 9.2.2 I/σ ratio of beta-carotene bands at various concentrations in usnic acid, phenanthrene and triphenylene mixtures.

9.2.3.4 Beta-carotene in phenanthrene

The Raman spectra of beta-carotene in phenanthrene show the beta-carotene Raman band at 1513 cm⁻¹ assigned to the in-phase ν (C=C) which appeared as a doublet bands at 0.50 mg kg⁻¹ and as a shoulder at 0.25 mg kg⁻¹ with the phenanthrene Raman band at 1523 cm⁻¹, also assigned to C-C stretching. Furthermore, the beta-carotene Raman band at 1156 cm⁻¹ assigned to the ν (C-C) stretching vibration was observed at 0.50 mg kg⁻¹ and appeared as a triplet band at 0.25 mg kg⁻¹ concentration. Also, the beta-carotene Raman band, at

1008 cm^{-1} which is assigned to the in-plane rocking modes of (C-CH₃) was observed in the spectra at the concentration level equal to or higher than 0.50 mg kg^{-1} ; however, at the concentration level of 0.25 mg kg^{-1} this band was not observed (Figure 9.2.4 and Table 9.2.2).

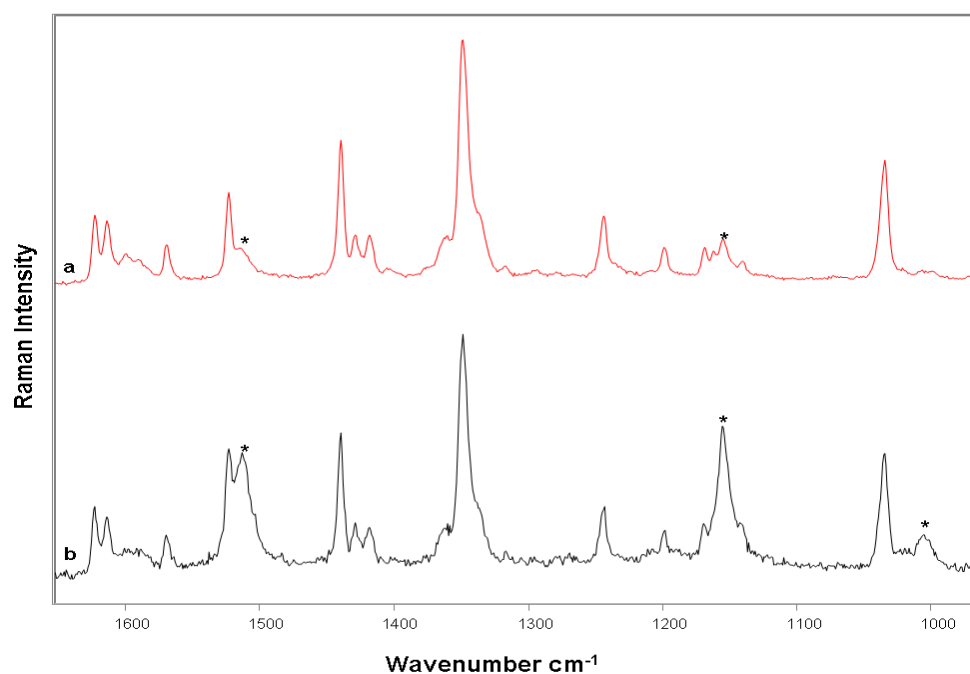


Fig.9.2.4 Raman spectra of beta-carotene with phenanthrene mixture (Asterisks indicate beta-carotene bands) :(a) 0.25 mg kg^{-1} (b) 0.50 mg kg^{-1}

9.2.3.5 Beta-carotene in triphenylene

Measurements using the 785 nm excitation wavelength allowed the detection of three characteristic bands of beta-carotene (1513, 1156 and 1008 cm^{-1}) corresponding to the in-phase ν (C=C) and ν (C-C) stretching vibrations and in-plane rocking modes of (C-CH₃), respectively) at a concentration level equal to or higher than 0.50 mg kg^{-1} (fig. 9.2.5). Only two weak Raman bands of beta-carotene are seen in the spectra at the concentration level of 0.25 mg kg^{-1} (Table 9.2.2). Therefore, the beta-carotene Raman band at 1156 cm^{-1} assigned to the ν (C-C) stretching vibration is seen as a doublet at 0.25 and 0.50 mg kg^{-1} concentration levels along with the triphenylene Raman band at 1162 cm^{-1} as shown in fig.9.2.5.

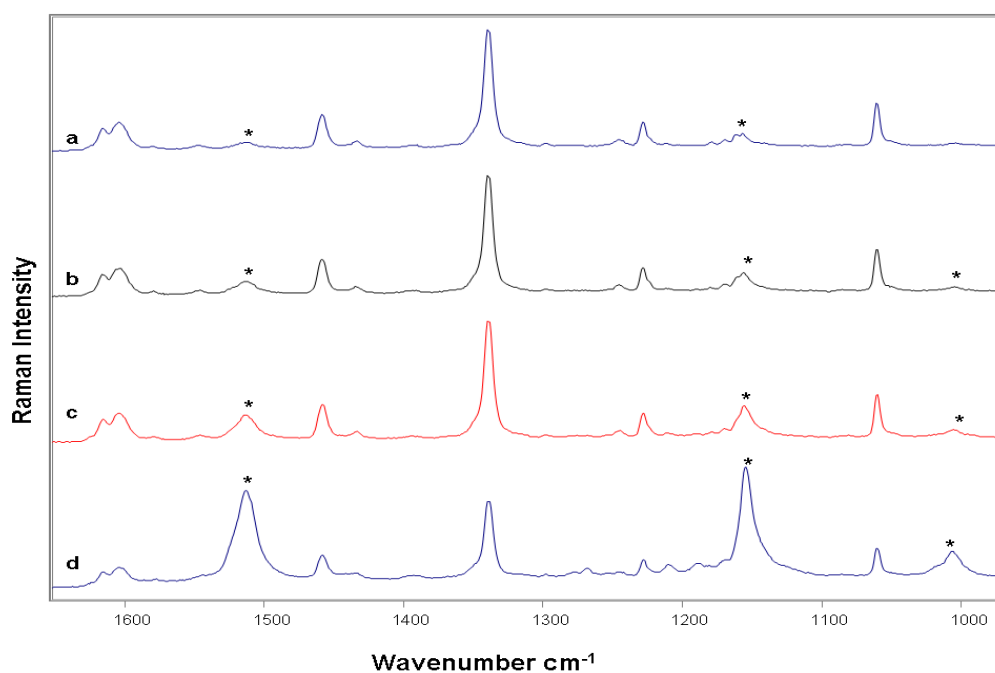


Fig. 9.2.5 Raman spectra of beta-carotene in admixture with triphenylene (Asterisks indicate beta-carotene bands):(a) 0.25 mg kg^{-1} (b) 0.50 mg kg^{-1} (c) 1 mg kg^{-1} (d) 5 mg kg^{-1}

9.2.4 Conclusions

Raman spectra obtained in this study confirm that by using a 785 nm excitation wavelength it is possible to determine the presence of beta-carotene, a potential biomarker, in experimentally prepared organic mixtures, which are considered to be potential scenarios on Mars. In addition, this potential biomarker- organic mixture system demonstrates the ability of Raman spectroscopy to detect key individual components mixture of organic compounds. In a previous study, polyaromatic hydrocarbons (PAHs) were investigated as biomarkers in a mineral matrix system, and the result demonstrated that the number of observed Raman bands in PAHs differed depending on the particular mineral, the excitation wavelength and the concentrations deployed [27]. In this study, we found that the minimum detectable concentration of beta-carotene is 0.25 mg kg^{-1} (i.e. 250 ppb) for the organic compound mixtures. The results obtained have significant implications for planned in situ robotic Raman spectroscopic measurements on Mars or elsewhere.

9.2.5 References

- [1] Committee on Planetary and Lunar Exploration, in: J.A.Wood , et al. (Eds.), *The Quarantine and Certification of Martian Samples*, Space Studies Board, Natl. Acad. Sci., Washington DC, **2002**, 80.
- [2] C. D. Schulze-Makuch, L. N. Irwin, Springer, Berlin, Heidelberg, **2004**, 172.
- [3] A. Litchfield, *Hydrobiologia*, **2001**, 466, 81.
- [4] B. R. T. Simoneit, *Adv. Space Res*, **2004**, 33, 1255.

- [5] J. Jehlicka, H. G. M. Edwards, S. E. J. Villar, O. Frank, *Journal of Raman Spectroscopy*, **2006**, 37,771.
- [6] J. Jehlicka, H. G. M. Edwards, S. E. J. Villar, *Spectrochim. Acta A*, **2006**, 65 ,229.
- [7] J. Jehlicka, H. G. M. Edwards, P. Vitek, *Planetary and space Science*, **2009**, 57, 606.
- [8] J. Jehlicka, H.G.M. Edwards, *Org. Geochem*, **2008**,39, 371.
- [9] J. Parnell, M. Baron, *Int. J. Astrobiology*, **2004**, 3,21.
- [10] D. Gill, R. G. Kilponen , L. Rimai , *Nature*, **1970**, 227, 743.
- [11] J. C. Merlin, *Pure Appl. Chem*, **1985**, 57 , 785.
- [12] C.P. Marshall, S. Leuko, C. M. Coyle, M. R. Walter, B.P. Burns , B.A. Neilan, *Astrobiology*, **2007**, 7, 631.
- [13] R.Withnall , B. Z. Chowdhry, J. Silver, H. G.M. Edwards, L. F.C. de Oliveira, *Spectrochimica Acta Part A*, 2003,59, 2207
- [14] J .Godec , L.Colombo, *Journal of Chemical Physics*, **1976**, 66 (11),4693.
- [15] H. G. M. Edwards, S. E. Jorge Villar, J. Jehlicka, T. Munshi, *Spectrochim Acta A*, **2005**, 61,2273.
- [16] D. Lin-Vien, J. G. Grasselli, N. B. Colthup, W. G. Fateley, *The Handbook of Infrared and Raman Characteristic Frequencies of Organic Molecules*, chapter 11, Academic Press, San Diego, **1991**.
- [17] G. Socrates, *Infrared Characteristic Group Frequencies: Tables and Charts* (Third ed.), John Wiley & Sons Ltd., New York, **2001**.
- [18]J. Jehlicka, H. G. M. Edwards, S. E. JorgeVillar, O. Frank, *Journal of Raman Spectroscopy*, **2006**, 37, 220.
- [19] J. Jehlicka, H. G. M. Edwards. *Org. Geochem*, **2008**, 39, 371.
- [20]Yek Tann Chua , C. Peter. Stair, *Journal of Catalysis*, **2003**, 213,39.

- [21]W. Charles, Jr. Bauschlicher, R. Stephen, Langhoff, S. A. Sandford. J. Phys. Chem. A,**1997**, 101, 2414.
- [22] L. J. Allamandola, in IAU Symposium 135, Interstellar Dust,eds. L. J. Allamandola, A. G. G. M.Tielens (Kluwer, Dordrecht) ,**1989**, 129.
- [23]M. Veronelli, and G.Zerbi, Journal of Raman Spectroscopy, **1995**, 26, 683.
- [24]R. J. Weesie, J. C. Merlin, J. Lugtenburg, G. Britton, F. J. H. M. Jansen, J. P. Cornard, Biospectroscopy, **1999**,5, 19.
- [25]H.G.M. Edwards, E.M. Newton, D.D. Wynn-Williams, J. Mol. Struct, **2003**, 27 , 651.
- [26]ACS Committee on Environmental Improvement, Anal. Chem, **1980**, 52, 2242.
- [27] A. I. Alajtal, H. G. M. Edwards and I. J. Scowen, Anal. Bioanal. Chem.,**2010**, 397,215

CHAPTER 10

Conclusions and Further Work

10.1 Conclusions

Astrobiology is a multidisciplinary science concerning studies into the origins of life in the universe and its evolution; research topics cover the areas of microbiology, biology, palaeontology, geology, astronomy and geochemistry.

Astrobiology is focused on the search for life in extraterrestrial environments, particularly on planetary surfaces [1]. Whether extinct or extant, for survival this life must have adapted to the prevailing extreme environmental conditions, which involves controlling the substratal geology, as is the case for terrestrial analogues [2].

It is evident from previously mentioned studies that Raman spectroscopy has been shown to be a reliable and useful technique of the analysis of organic and inorganic compounds alone and in admixture. It has been possible to identify several pure compounds and compound mixtures of astrobiological relevance using all three Raman instruments available. Raman spectroscopy has also been used to identify organic compounds under crystalline calcite and gypsum using the confocal Renishaw In Via Raman microscope. The RIAS portable instrument has shown promise for offsite analysis although it is recognized that the demand for higher spectral resolution and fluorescence rejection can cause some problems for portable instrumentation.

Powder X-ray diffraction and SEM techniques have also been used to provide a secondary source of analysis for some samples.

The data from previous landers and our own work on Earth, using Martian analogues, provide a basis for understanding the parameters that need to be evaluated for spaceflight. Future explorations of Mars have already been planned using analytical instrumentation and the information from these, and indeed from samples returned as part of a Mars sample return programme, will need to be interpreted. Whether or not life is or has been

present will be indicated by the presence of biomarker molecules. A database of geological samples will help us understand these regions from retrieved spectra; subsequently, any remaining unidentifiable bands in the geological spectra may be attributed to possible life signatures, so a biomolecular database of key Raman spectral signatures is necessary.

The results obtained from this study indicate a clear trend in the quality of spectra obtained from each laser source. The infrared (1064 nm) laser coupled with the Fourier-Transform instrument undoubtedly gave the best spectra. The low energy of the laser irradiation resulted in little or no fluorescence and the high number of scans, made possible by the use of the FT system, resulted in improvements arising from signal-to-noise ratios.

By comparison of these spectra with those collected by the use of higher energy lasers, the near infrared excitation at 785 nm was found to be most successful and provided the clearest and most informative spectra generally avoiding the higher amounts of fluorescence caused by the higher energy lasers working in the visible region

The key factor in determining choice of wavenumber for PAH studies is their propensity to fluoresce strongly under excitation with shorter wavenumber sources.

In this study, the longer wavelength source (785 nm and 1064 nm) used showed the best responses, by minimising fluoresce background.

The portable system used in this study also used a 785 nm laser; although the spectra obtained there-from were informative, the system was not without its problems, the main issue being the quantity of artifact peaks which the instrument introduced to the spectral data. These made the spectra over complicated and hindered the peak identification especially in the low wavenumber region.

In general, the portable system using a 785 nm laser did provide some useful information, however band assignments were necessarily tentative. In addition the spectrometer also could not interrogate the 3500-2500 cm^{-1} wavenumber range, a region with an organic presence exemplified by carbon-hydrogen bond stretching.

Therefore it is logical to conclude that the 1064 and 785 nm lasers in laboratory instrument are better choice for studying organic samples.

10.2 Further Work

- * Application of the RIAS instrument to the analysis of organic compounds under crystalline calcite and gypsum.

- * The use of the 1064 nm laser excitation for organic compounds under crystalline calcite and gypsum which exhibit fluorescence.

- * The use of imaging and mapping techniques for the location and identification of unknown particles and inclusion that could have biogeological relevance

- * Analysis using a combined Raman and SEM system for both molecular and elemental analysis of the same system.

Raman spectroscopy, PXRD and other techniques can be seen as very useful and complementary techniques that have many applications in astrobiology.

- * Investigation of the applicability of the combined techniques to the identification and characterization of larger molecules of polyaromatic hydrocarbons. For example:

Investigate degradation of biomolecules under different Environmental conditions (UV exposure, Oxidation) using Raman spectroscopy, GCMS and LCMS.

10.3 References

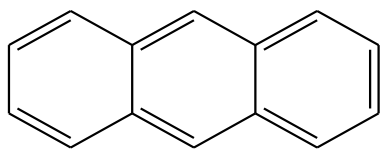
[1] G. Horneck, *Planet Space Sci*, **2000**, 48(11), 1053.

[2] R. Cavicchioli, *Astrobiology*, **2002**, 2(3),281.

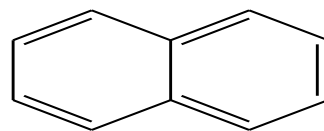
CHAPTER 11

Appendices

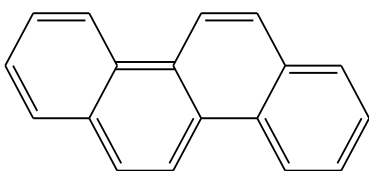
Appendix I: Structural formulae of molecules



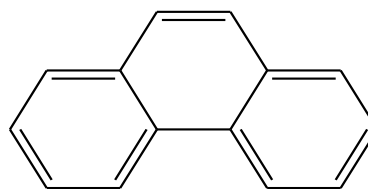
Anthracene



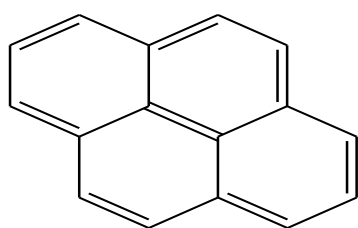
naphthalene



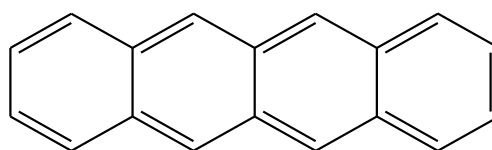
chrysene



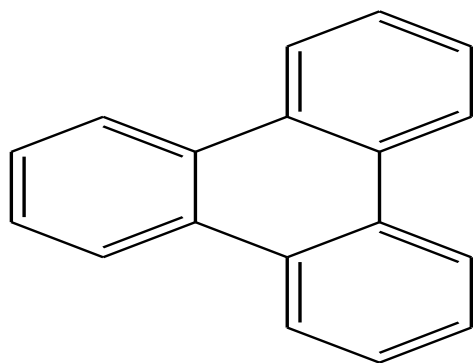
phenanthrene



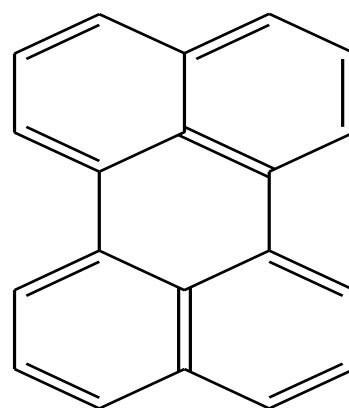
pyrene



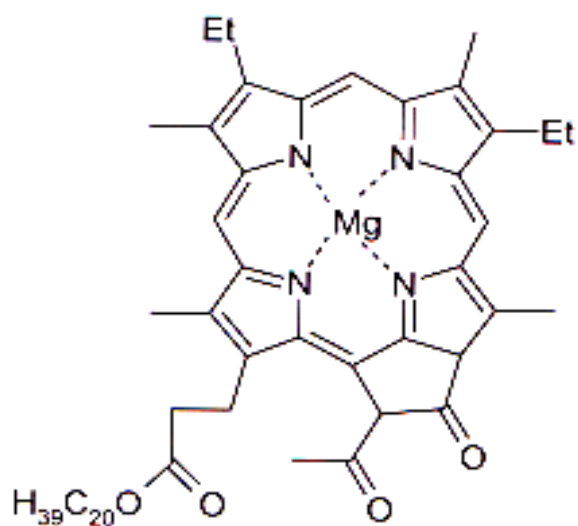
tetracene



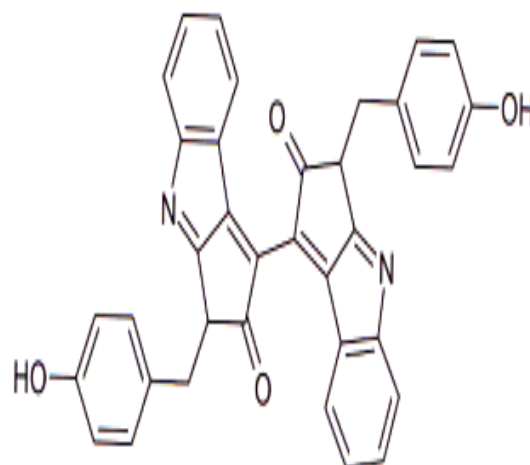
triphenylene



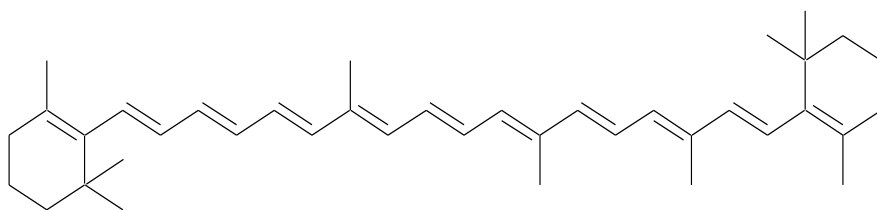
perylene



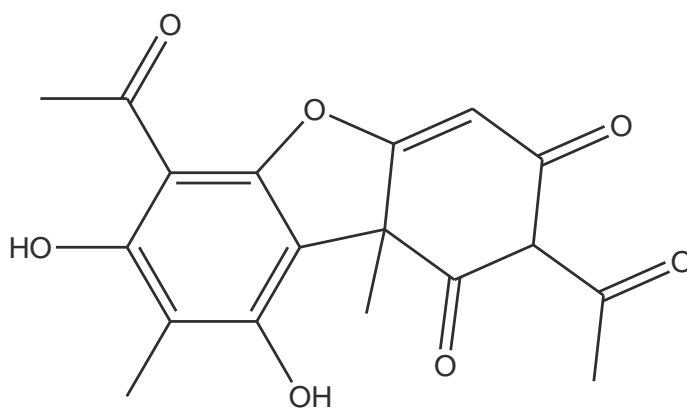
Chlorophyll



Scytonemin



Beta-carotene



Usnic acid

Appendix II: Spectra of the pure compounds on all three instruments.

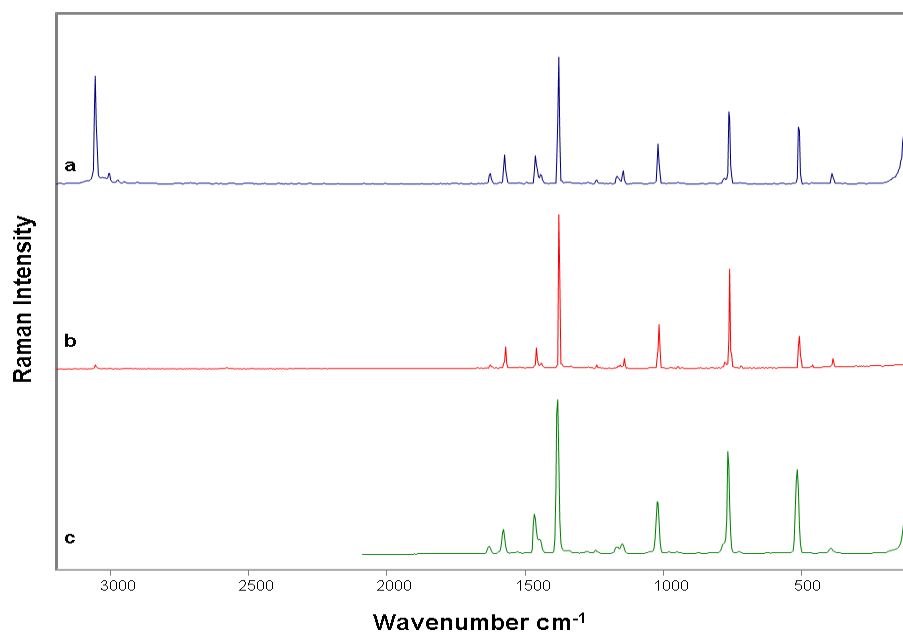


Figure II.1 Naphthalene run on (a) Bruker using 1064 nm (b) Renishaw using 785 nm (c) RIAS using 785 nm .

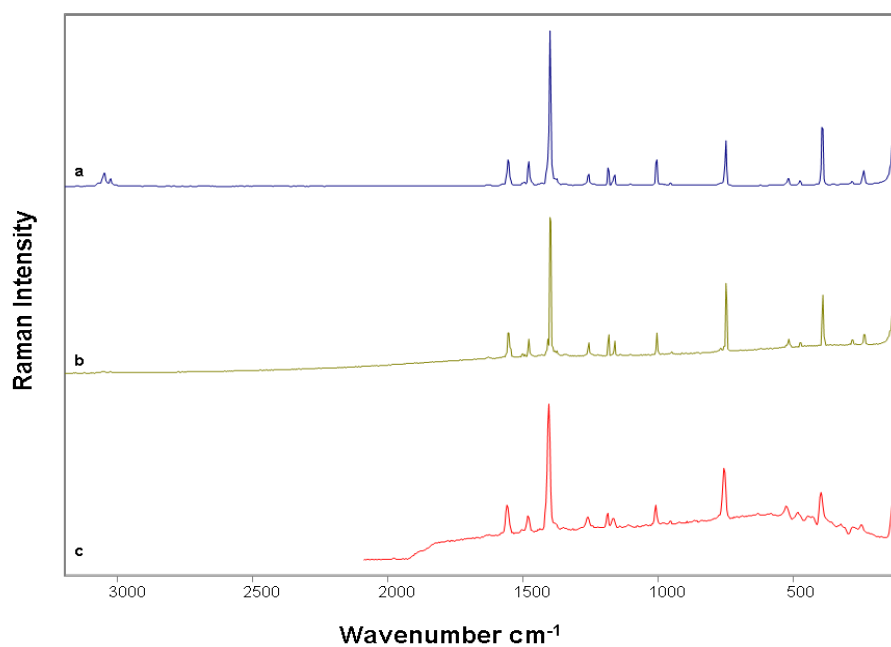


Figure II.2 Anthracene run on (a) Bruker using 1064 nm (b) Renishaw using 785 nm (c) RIAS using 785 nm .

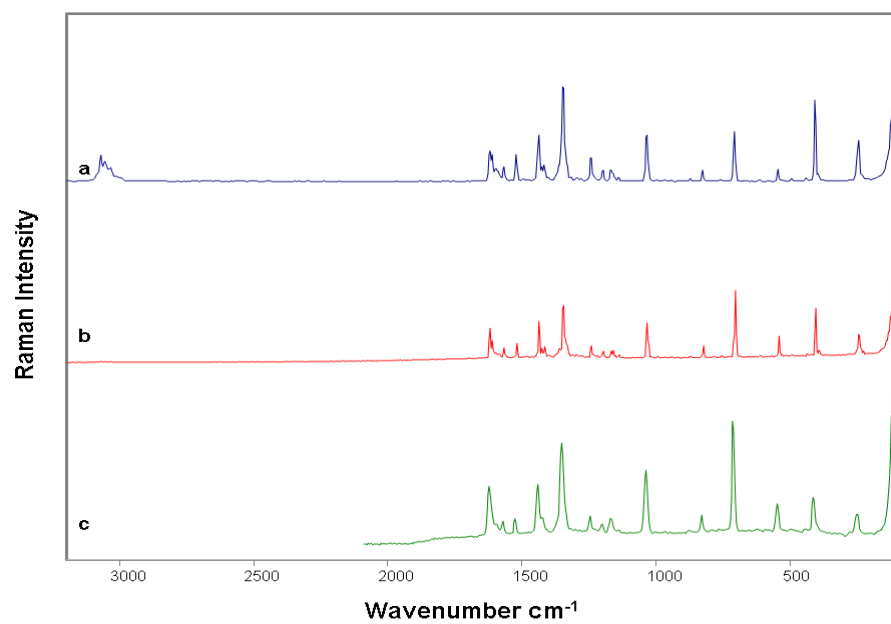


Figure II.3 Phenanthrene run on (a) Bruker using 1064 nm (b) Renishaw using 785 nm (c) RIAS using 785 nm.

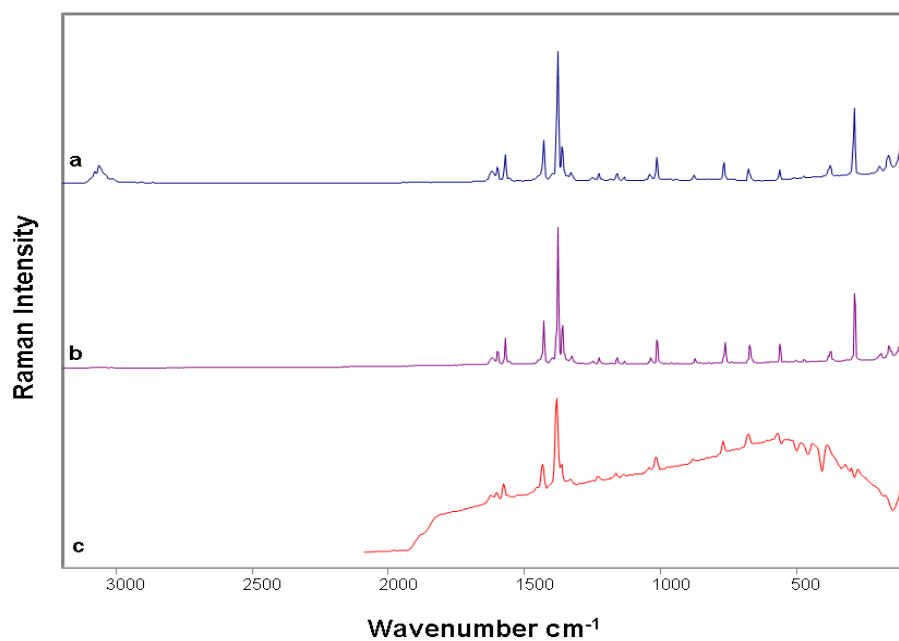


Figure II.4 Chrysene run on (a) Bruker using 1064 nm (b) Renishaw using 785 nm (c) RIAS using 785 nm.

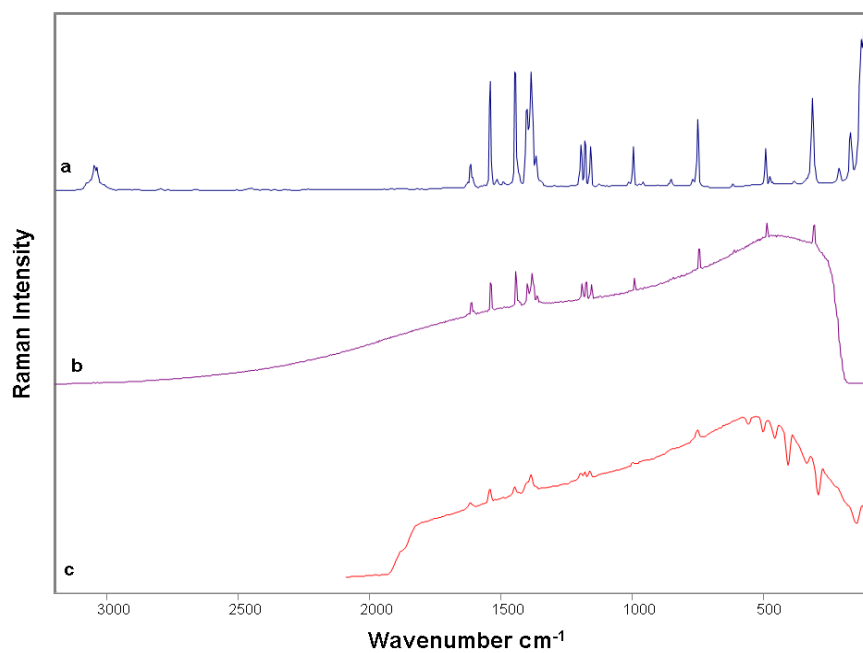


Figure II.5 Tetracene run on (a) Bruker using 1064 nm (b) Renishaw using 785 nm (c) RIAS using 785 nm.

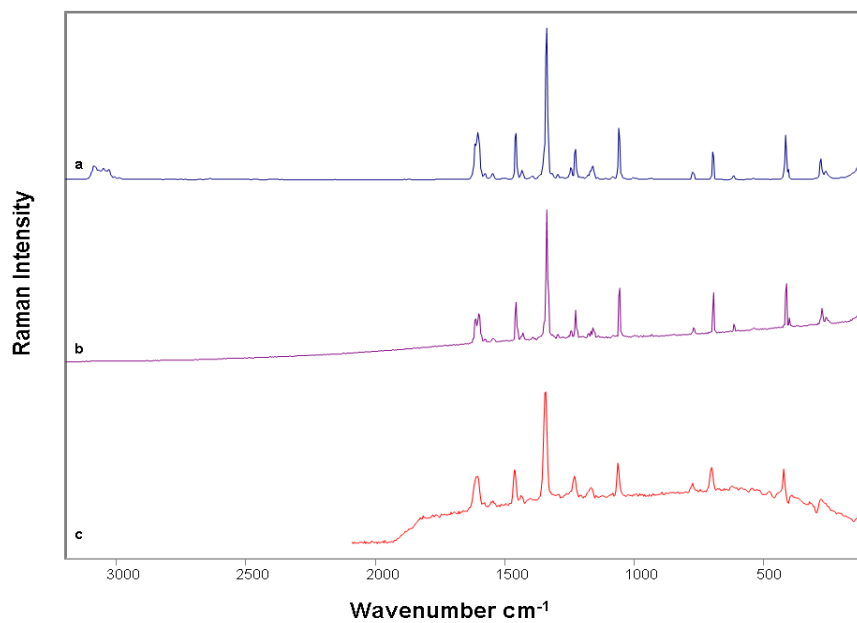


Figure II.6 Triphenylene run on (a) Bruker using 1064 nm (b) Renishaw using 785 nm (c) RIAS using 785 nm.

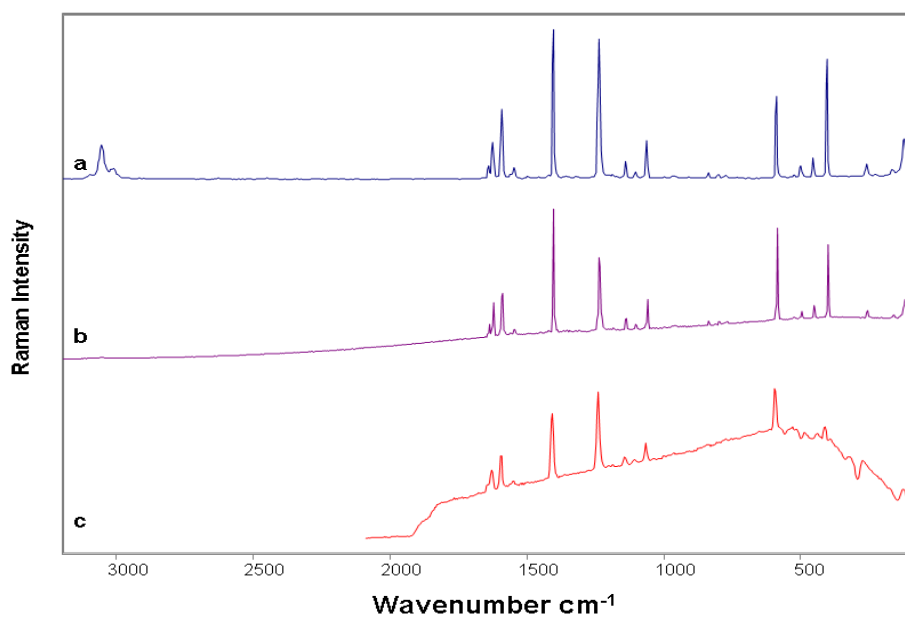


Figure II.7 Pyrene run on (a) Bruker using 1064 nm (b) Renishaw using 785 nm (c) RIAS using 785 nm.

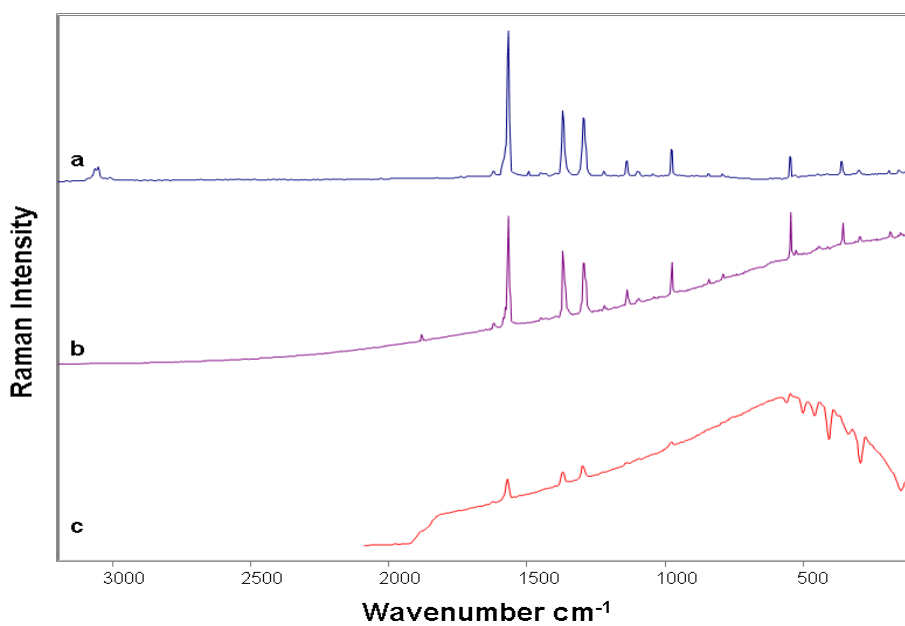


Figure II.8 Perylene run on (a) Bruker using 1064 nm (b) Renishaw using 785 nm (c) RIAS using 785 nm.

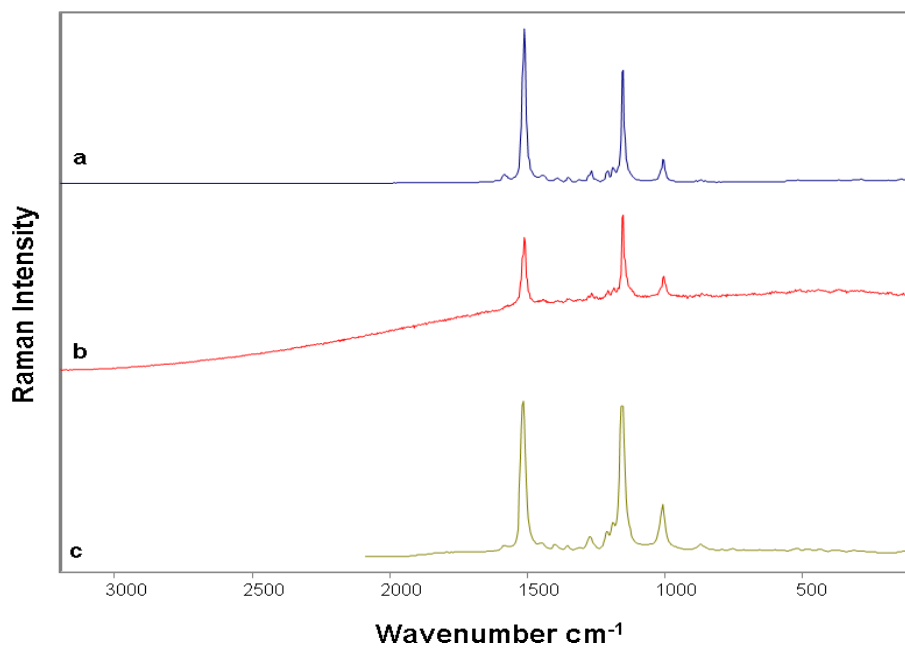


Figure II.9 Beta-carotene run on (a) Bruker using 1064 nm (b) Renishaw using 785 nm (c) RIAS using 785 nm.

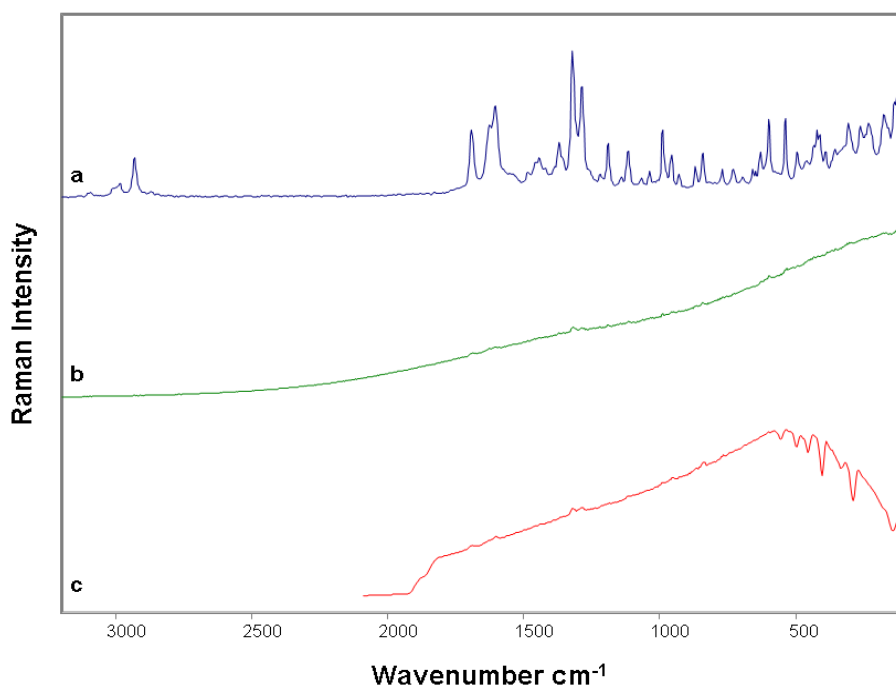


Figure II.10 Usnic acid run on (a) Bruker using 1064 nm (b) Renishaw using 785 nm (c) RIAS using 785 nm.

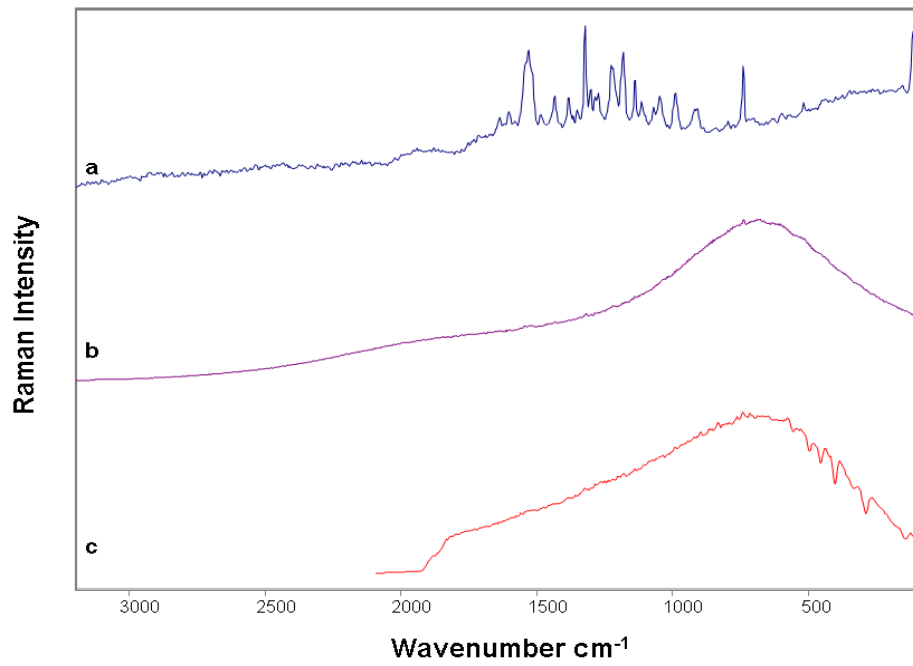


Figure II.11 Chlorophyll a run on (a) Bruker using 1064 nm (b) Renishaw using 785 nm (c) RIAS using 785 nm.

Appendix III: Diffraction patterns of the pure polyaromatic hydrocarbons

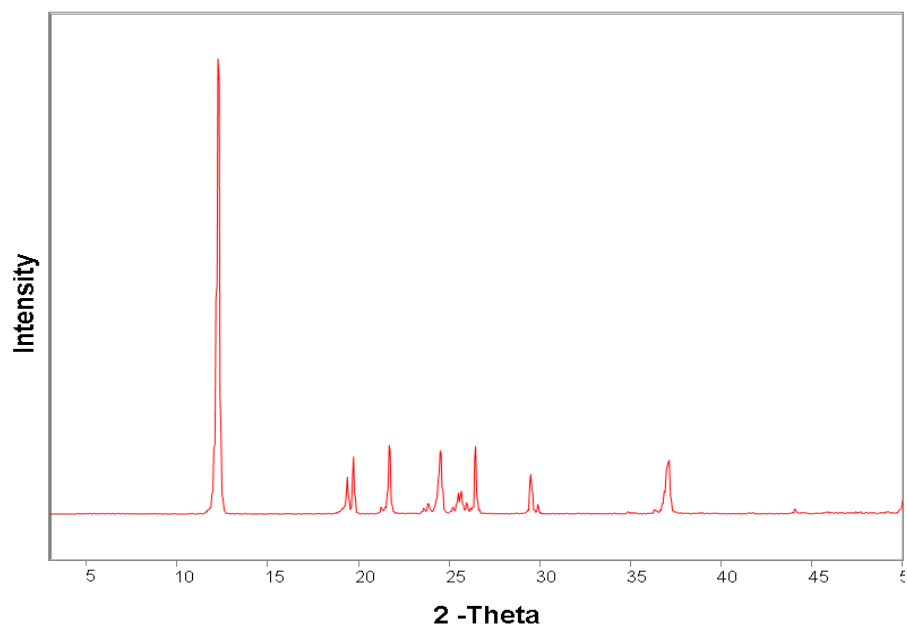


Figure III.1 X-ray powder diffraction pattern of naphthalene

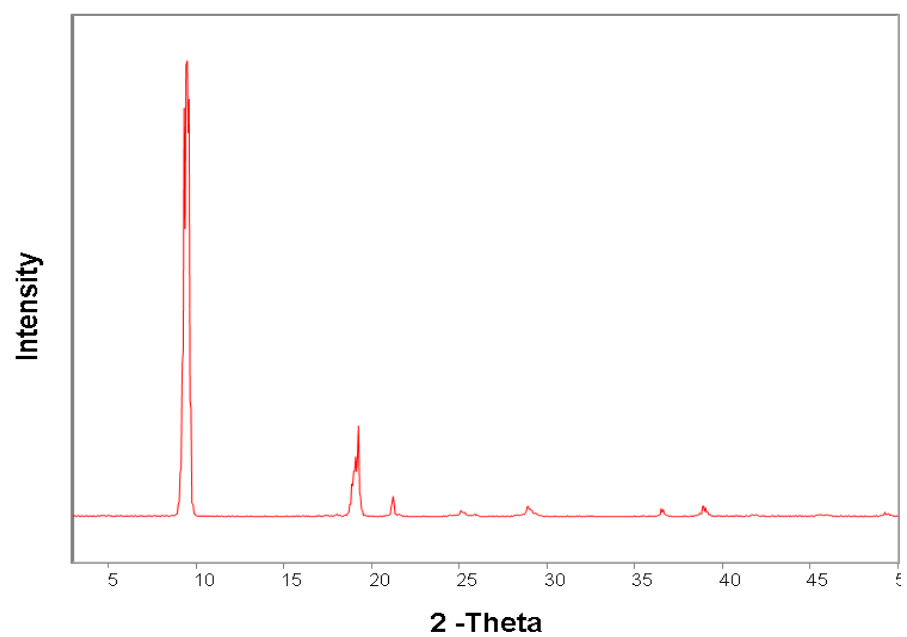


Figure III.2 X-ray powder diffraction pattern of anthracene

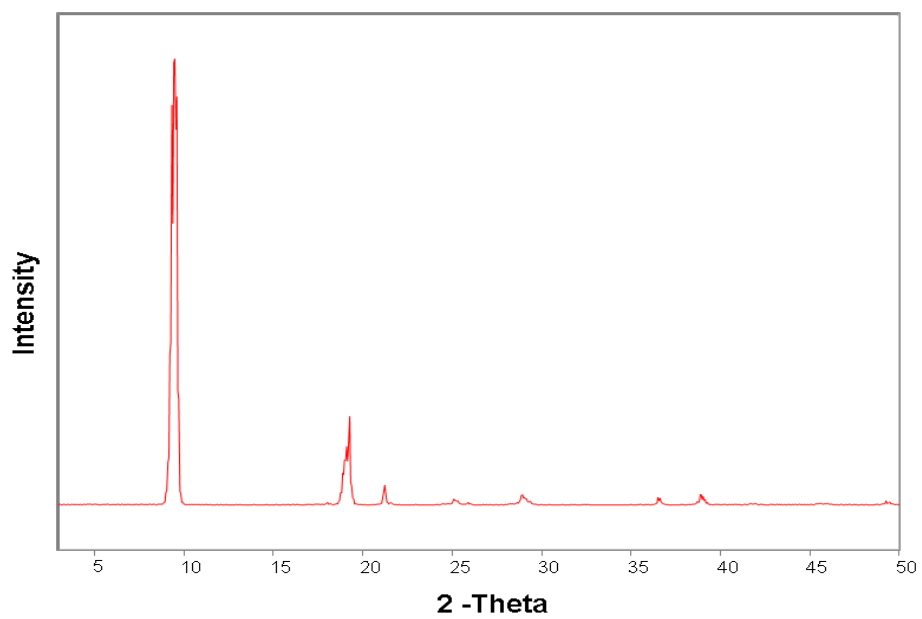


Figure III.3 X-ray powder diffraction pattern of phenanthrene

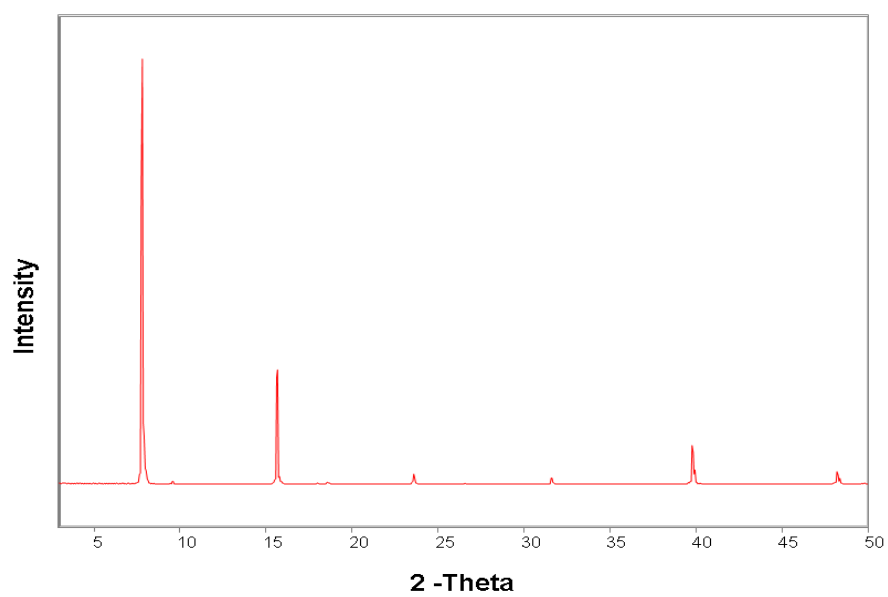


Figure III.4 X-ray powder diffraction pattern of chrysene

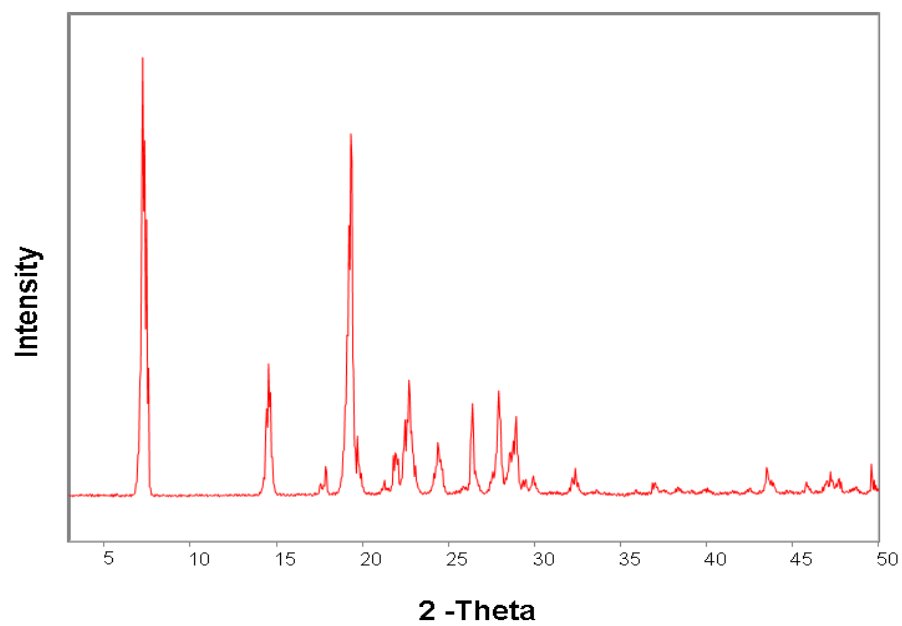


Figure III.5 X-ray powder diffraction pattern of tetracene

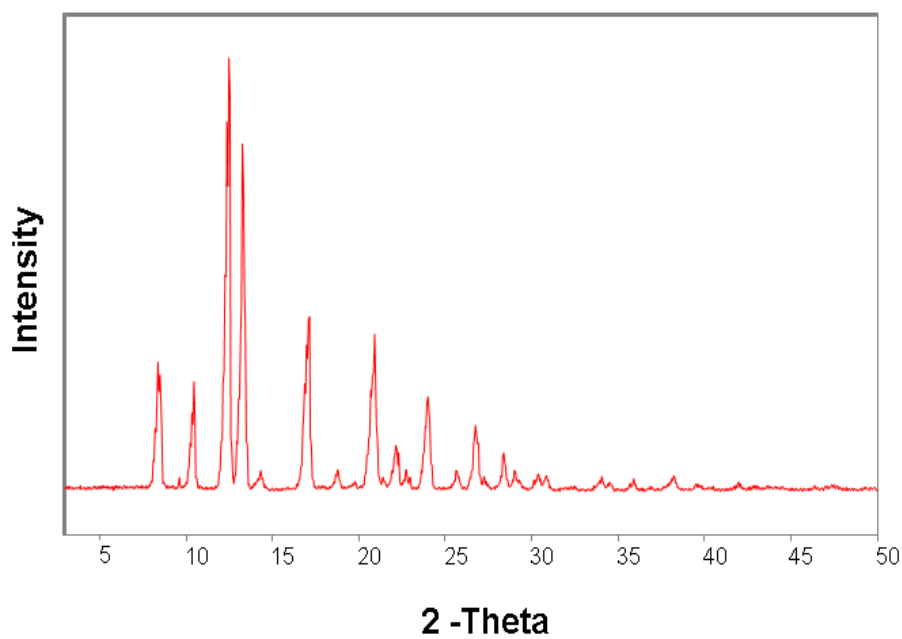


Figure III.6 X-ray powder diffraction pattern of triphenylene

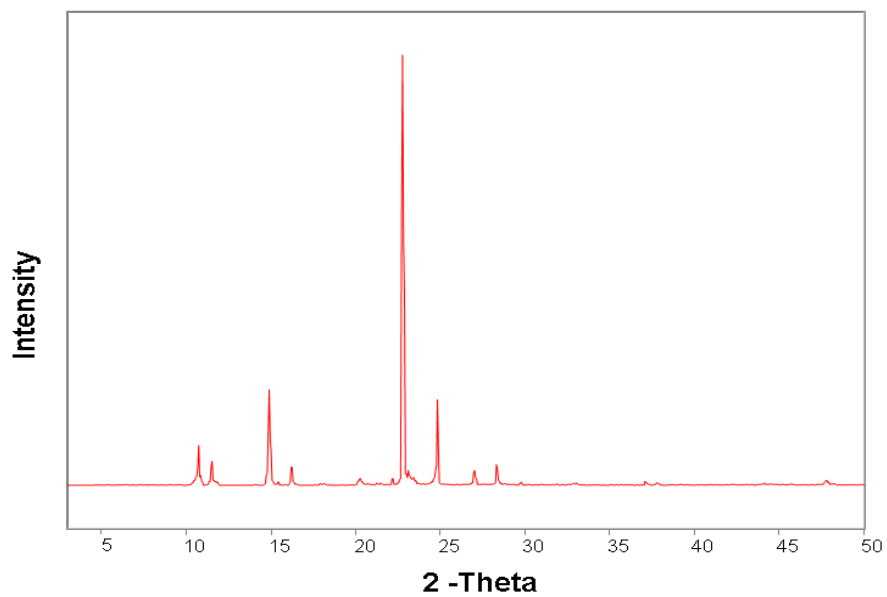


Figure III.7 X-ray powder diffraction pattern of pyrene

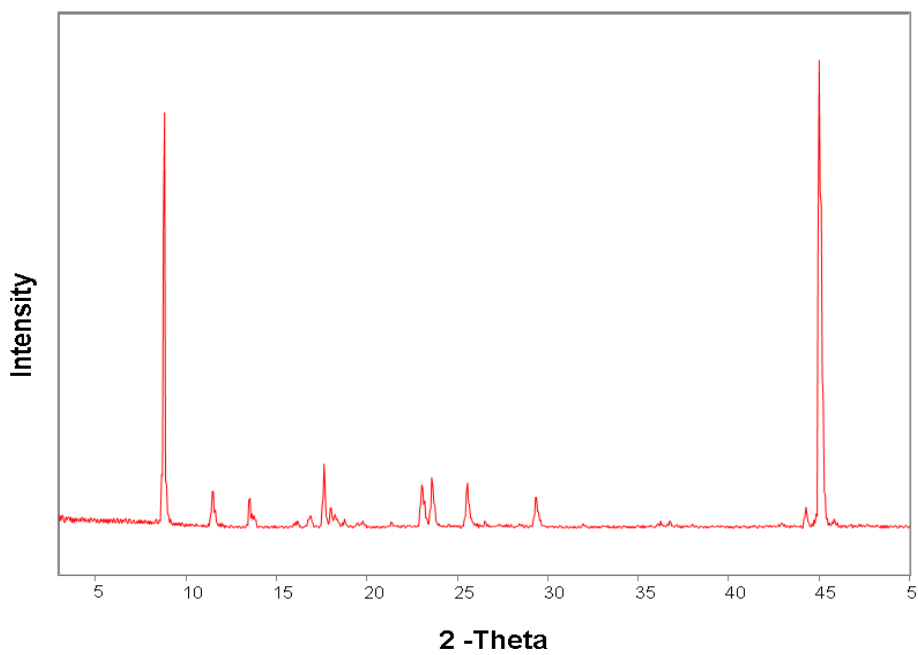


Figure III.8 X-ray powder diffraction pattern of perylene

Appendix IV: SEM of the pure compounds

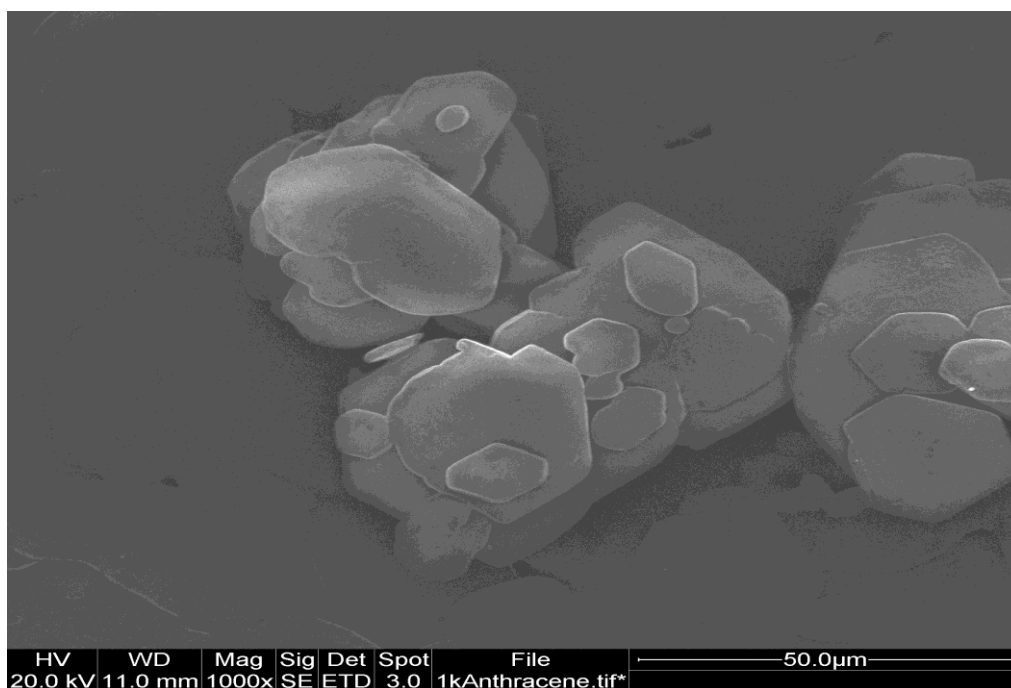


Figure IV.1 SEM of anthracene

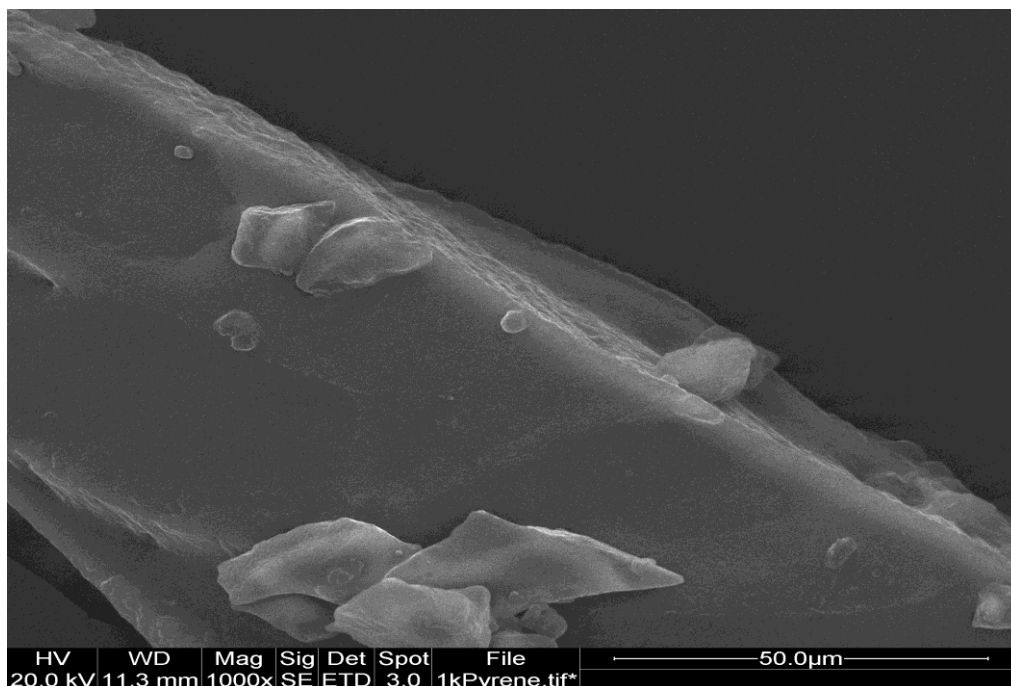


Figure IV.2 SEM of pyrene

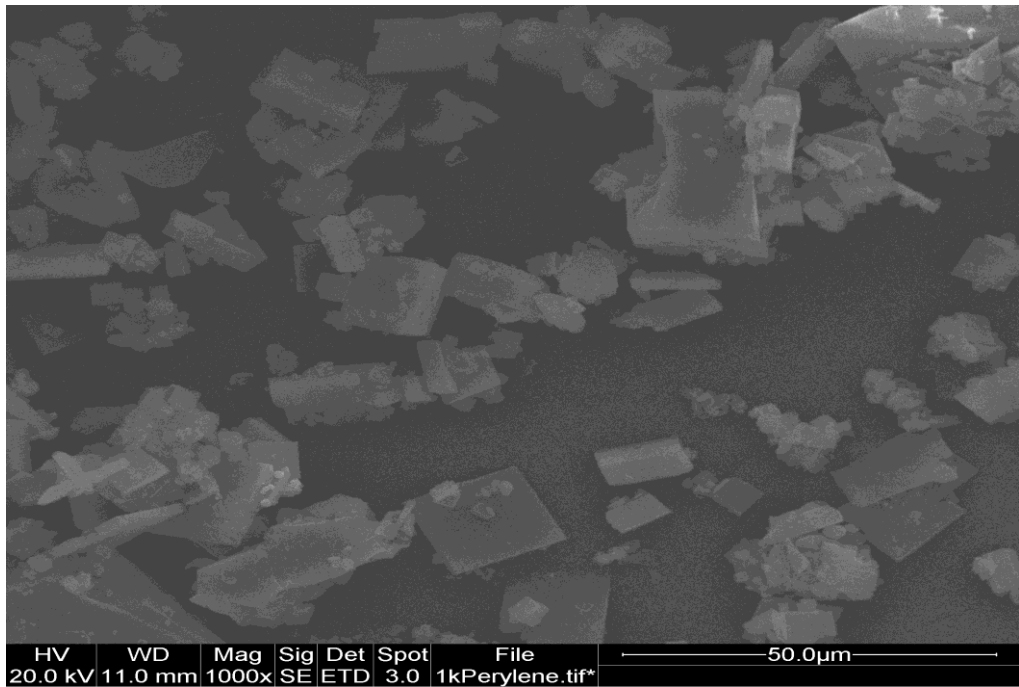


Figure IV.3 SEM of perylene

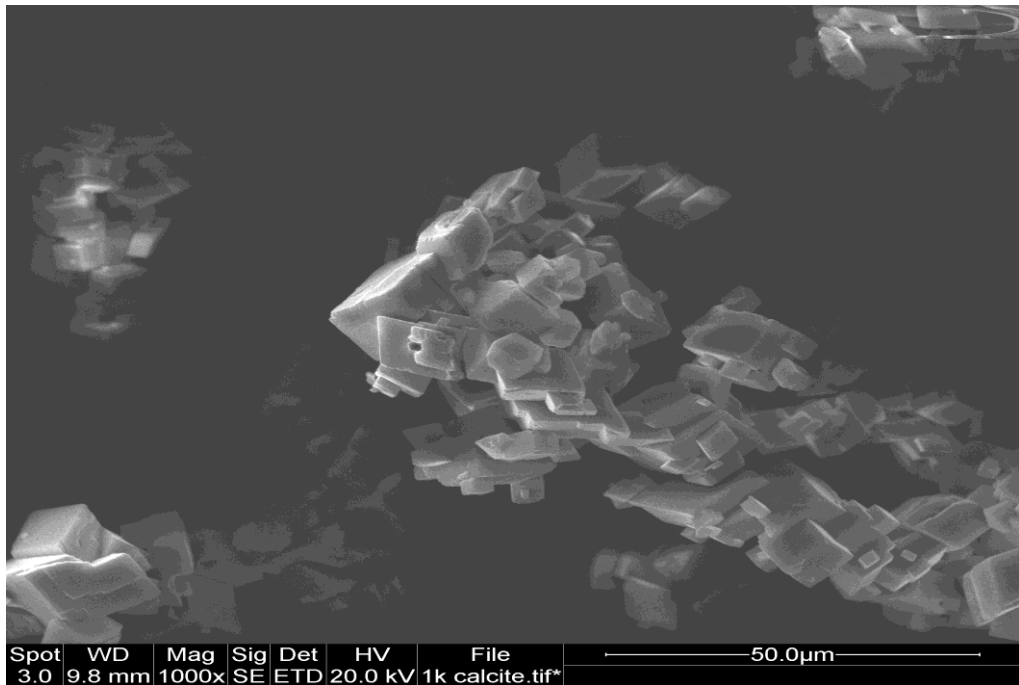


Figure IV.4 SEM of calcite

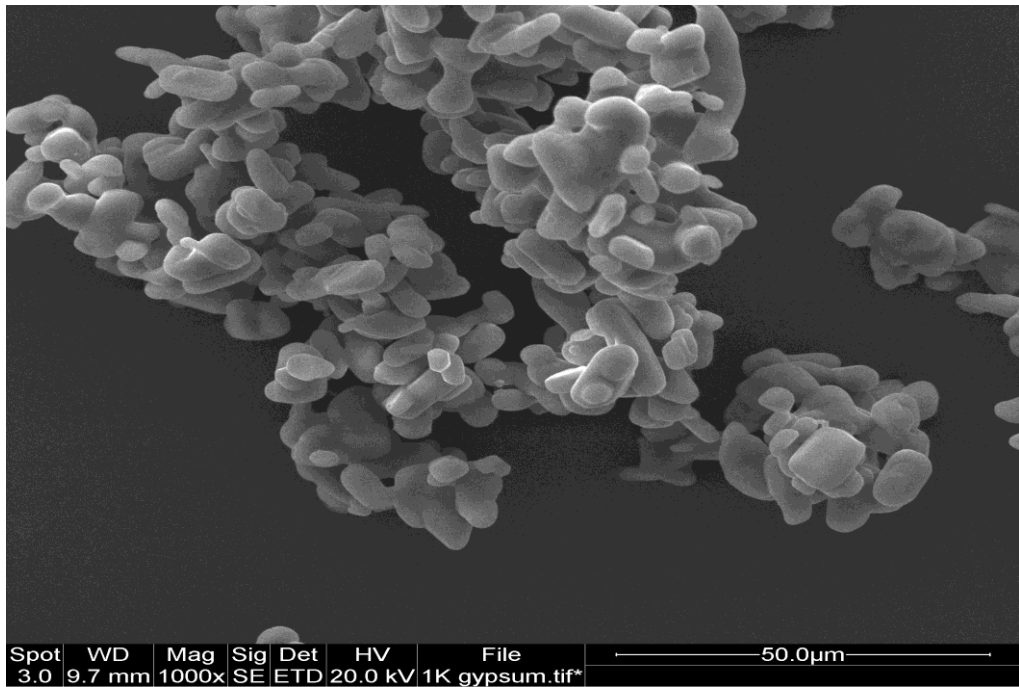


Figure IV.5 SEM of gypsum

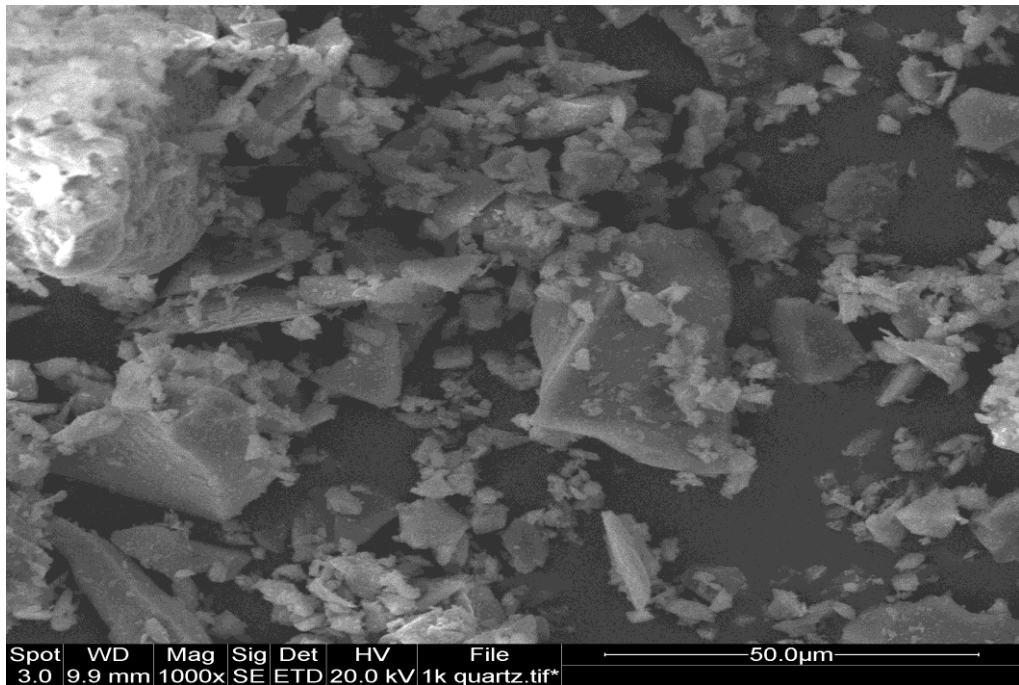


Figure IV.6 SEM of quartz